Stem cell-derived signals in intestinal stem cell homeostasis: investigating the role of SPARC, PLOD, dlp and Timp in the Drosophila midgut

PAULA FERRACES-RIEGAS

Durham University

DEPARTMENT OF BIOSCIENCES

Stem cell-derived signals in intestinal stem cell homeostasis: investigating the role of SPARC, PLOD, dlp and Timp in the *Drosophila* midgut

Paula Ferraces Riegas

Thesis submitted in fulfilment of the
requirements for the degree of
Doctor of Philosophy

March 2024

Stem cell-derived signals in intestinal stem cell homeostasis: investigating the role of SPARC, PLOD, dlp and Timp in the *Drosophila* midgut

Paula Ferraces Riegas

Abstract

Epithelia are constantly turned over as cells are lost from the surface of the tissue and replaced by the proliferation of stem cells. Epithelial stem cells must be tightly regulated to maintain homeostasis and prevent over-proliferation of the tissue, which can lead to hyperplasia and play important roles in disease development and progression. The intestinal stem cells of the *Drosophila* midgut are an ideal model system to identify regulators of intestinal stem fate, and study their function and regulation. We have identified several candidate regulators of *Drosophila* intestinal stem cells that are heavily involved in various aspects of extracellular matrix organization: PLOD, SPARC, dlp and TIMP. The aim of this project is to explore their effects on intestinal stem cell proliferation and on the maintenance of gut homeostasis, using a wide range of genetic manipulation techniques available in the fly. Results suggest that all four proteins play varying roles in the regulation and proliferation of intestinal stem cells in the posterior midgut, which is regulated by a wide range of signalling pathways, including Ras/MAPK, Notch, JNK and Hippo signaling. All 4 proteins are highly conserved in metazoans, and their misregulation has been implicated in disease development, raising the possibility of a conserved role in regulating intestinal stem cells in higher organisms. In vitro analyses of human prostate cancer samples were carried out in order to determine if the findings from the *Drosophila* model system were conserved in human tissues, and explore their translation applications as potential therapeutic targets.

Declaration

I hereby attest that this thesis titled “Stem cell-derived signals in intestinal stem cell homeostasis: investigating the role of SPARC, PLOD, dlp and Timp in the *Drosophila* midgut” here is an original piece of work submitted in fulfilment of the requirements for the degree of Doctor of Philosophy in Biosciences. All the experiments were carried out by me and all the work contained herein is my own except where explicitly stated in the text. Work previously carried out by me as part of my undergraduate MBiol thesis is referenced in Chapter 6 for foundational context, and it has been clearly distinguished from my doctoral work. No part of this thesis has been submitted elsewhere for any other degree or classification.

Section 1.5. “ The stem cell niche” of this thesis has been published as a review article that is product of my own work and is part of this PhD project. The full citation of this work is:

Ferraces-Riegas, P., Galbraith, A. C., & Doupé, D. P. (2022). Epithelial Stem Cells: Making, Shaping and Breaking the Niche. *Advances in experimental medicine and biology*, *1387*, 1–12. https://doi.org/10.1007/5584_2021_686

Funding

My doctoral work was funded by the Academy of Medical Sciences and Durham University.

Statement of Copyright

Acknowledgements

To my supervisor, David, thank you for all your guidance and support throughout my PhD and my undergraduate. You have given me a wonderful platform and environment to grow as a researcher that I will carry with me wherever I go. Thanks to everyone that has been part of the Doupé lab in my time here for creating such a positive and fun working environment. And to Fanila, thanks for keeping me sane through all the ups and downs these last few years - I am not sure I would have got through them (and all the endless hours of microscopy) without you and your entertainment.

A big thank you to everyone that has contributed to this project and has helped me achieve my goals, no matter how ambitious. Thank you to Chieko Itakura at the Electron Microscopy facility for all your patience, and to Dr. Adriana Buskin and everyone at Newcastle University for welcoming me and giving me the opportunity to work with you.

To all of my friends, thanks for keeping me sane and for your constant support throughout these years. You probably heard a lot more about flies than you ever intended to – you are welcome. To the girls, our fun, chaotic adventures have brought me so much joy. You have made me laugh harder than I ever thought possible, and you have got me through some of the toughest times of this PhD. You have truly made England my home away from home. I am so lucky to be a part of such a talented, strong and intelligent group of women. But please don't ask me to go camping again, or put me in charge of dinner.

To DUWRFC and everyone I have had the privilege of sharing the pitch with, thanks for being my escape from work. This sport has given me some of my best friends and many of my favourite memories from my time at Durham, and I will forever be grateful to have been a part of it.

A mis abuelas, por enseñarme que las mujeres siempre hemos sido fuertes e independientes, incluso en las épocas más difíciles. A toda mi familia, porque estar lejos de casa es muy duro, pero siempre hacéis que la distancia no parezca tanta. Y por último y más importante, a mis padres: esto es por vosotros. Gracias por todas las oportunidades que me habéis dado y por todos los sacrificios que habéis hecho para que llegue lejos. Este doctorado es tanto mío como vuestro.

(To my grandmothers, for teaching me that women have always been strong and independent, even during the hardest of times. To all my family, because living far away from home is hard, but you always make the distance seem less daunting. And finally, and most importantly, to my parents: this is for you. Thanks for all the opportunities you have given me and for all the sacrifices you have made for me to get to where I am today. This PhD is as much yours as it is mine.)

Contents

List of Figures

List of Tables

List of Abbreviations

AKT	Ak strain transforming (also known as protein kinase B)
ASC	Adult stem cell
BDSC	Bloomington Drosophila Stock Centre
BM	basement membrane
BMP	bone morphogenetic protein
BM-40	basement membrane-40 protein
BPH	benign prostatic hyperplasia
Brk	brinker
BSA	bovine serum albumin
CAF	cancer-associated fibroblast
cDNA	copy DNA
C. elegans	Caenorhabditis elegans
Cg25C	“collagen at 25C”, collagen IV alpha1 chain (col4a1)
CRIMIC	CRISPR-integrated mediated cassette
CSC	cancer stem cell
DAB	3, 3'-diaminobenzidine
dad	“daughters against Dpp”
DAPI	4',6-diamidino-2-phenylindole
ddH_2O	distilled water
dlp	dally-like protein
DNA	Deoxyribonucleic acid
Dpp	Decapentaplegic
DPX	Dibutylphthalate Polystyrene Xylene
EB	enteroblast
EC	enterocyte
ECM	extracellular matrix
EDTA	Ethylenediaminetetraacetic acid
EE	enteroendocrine
EM	electron microscopy
EMT	epithelial-to-mesenchymal transition
ER	endoplasmic reticulum

ERK1/2	extracellular signal-regulated kinase-1/2
esg	escargot
FCCS	fluorescence cross-correlation microscopy
FFPE	Formalin-fixed paraffin embedded
FLIM	fluorescence live-imaging microscopy
F/O	FlipOut
FOV	Field of View
GAPDH	glyceraldehyde 3-phosphate dehydrogenase
GFP	Green Fluorescent Protein
GPC4	glypican-4
GS	Gene Switch
GT	Gene Trap
HIF-1α	hypoxia-inducible factor 1-alpha
IF	immunofluorescence
IHC	immunohistochemistry
iPSC	induced pluripotent stem cells
ISC	intestinal stem cell
JAK/STAT	Janus kinase/signal transducer activator of transcription proteins
JNK	c-Jun N-terminal kinase
KD	Knockdown
LH	lysyl hydroxylase
LNCaP	lymph node carcinoma of the prostate
MAPK	mitogen-activated protein kinase
MEK	mitogen activated protein kinase kinase (also known as MAPKK or MAP2K)
MMP	matrix metalloproteinase
mRNA	messenger RNA
mTor	mammalian target of rapamycin
M3/5/8/β	muscarinic receptor 3/5/8/Beta
NF-Kβ	nuclear factor Kappa Beta
NGS	normal goat serum
nls	nuclear localization sequence
OE	Overexpression
PBS	phosphate buffered saline

PCR	polymerase chain reaction
PFA	paraformaldehyde
PH3	phospho-histone-3
PLOD	Procollagen-lysine, 2-oxyglutarate, 5-dioxygenase
pnt	pointed, transcriptional activator of RTK
pros	prospero
PTM	post-translational modification
puc	puckered
qPCR	quantitative polymerase chain reaction
RNA	Ribonucleic acid
RNAi	RNA interference
RPL13A	ribosomal protein L13a
RT	room temperature
RTK	receptor tyrosine kinase
RT-qPCR	reverse transcriptase quantitative polymerase chain reaction
RU	mifepristone
RU486	mifepristone
SAPK	stress-activated protein kinase
SHC1	SHC transforming protein-1
SMAD	“small mothers against Dpp”
Soc36e	Suppressor of cytokine signalling 36E
SMOC	secreted modular calcium-binding protein
SPARC	secreted protein acidic rich in cysteine
SPL-1	SPARC-like protein 1
TBS	Tris-buffered saline
TEM	transmission electron microscopy
TF	transcription factor
TGF-B	transforming growth factor beta
TIC	tumour-initiating cell
TIMP	tissue inhibitor of metalloproteinases
TS	temperature sensitive
UAS	Upstream Activator Sequence
Upd	Unpaired

VDRC	Vienna Drosophila Research Centre
VEGF	vascular-endothelial growth factor
Vkg	viking (collagen IV α2 chain, col4a2)
Yki	Yorkie
ZEB1	Zinc finger E-box binding homeobox 1

Chapter 1

Introduction

1.1. Adult stem cells

The presence of stem cells, a subset of cells with regenerative capacities that can divide indefinitely and either self-renew or differentiate to give rise to specialized cells in the tissues (Bongso and Richards, 2004; Li and Xie, 2005), has been known for over a century (Bianco et al., 2008; Casali and Batlle, 2009). Much of the stem cell research carried out in the last half of the 20th century focused on haematopoietic stem cells (Till et al., 1963; Lewis and Trobaugh, 1964; Till and McCulloch, 1980) and embryonic stem cells (Martin, 1981), with many striking breakthroughs along the way. The generation of viable offspring from adult stem cells which demonstrated that there is no detrimental change to the genetic material or the properties between embryonic stem cells and adult stem cells (Wilmut et al., 1997), and the generation of embryonic stem cell lines from a human blastocyst that allowed for the study of embryonic development in vitro (Thomson et al., 1998), revolutionized stem cell research at the end of the 20th century (reviewed by Lovell-Badge, 2001).

Adult stem cells (ASCs), also known as somatic stem cells, are essential for the maintenance of tissue homeostasis and for tissue repair after damage (Yamashita et al., 2005). They have a restricted differentiation capacity and are therefore multipotent or unipotent (Harvey et al. 2019). In adult tissues, stem cells fall under two categories: slow-

cycling stem cells, found in organs made up of long-lived cells, e.g. lung, prostate, that increase their proliferative activity upon damage but are otherwise dividing at slow rates; and fast-cycling stem cells, found in organs with high cellular turnover, such as the intestine, blood tissue or the epidermis (Post and Clevers, 2019). Because of their ability to acquire high proliferative potential, the switch that regulates stem cell division, as well as the decision between self-renewal and differentiation, must be tightly controlled, as its misregulation could have detrimental effects on the tissue and the organism (Yamashita et al., 2005). The renewal and functional abilities of adult stem cells, as well as their potency, have been shown to detrimentally decrease with age and give rise to age-related diseases such as cancer, neurodegenerative disorders, deterioration of bone and muscle tissue, and haematological malignancies (reviewed in Ahmed et al., 2017).

The core characteristics of stem cells, i.e. their potency and abilities to self-renew, differentiate and repair tissue damage, are sometimes referred to as their "stemness" (Bach et al., 2000; Melton, 2014). Besides their two defining properties of self-renewal and differentiation capabilities (McCulloch and Till, 2005), ASCs are also characterized for their longevity, quiescent nature and their asymmetric cell division (reviewed by Barker et al., 2008), key properties which are conserved in *Drosophila* stem cell (Otsuki and Brand, 2018; Easwaran et al., 2022). The concept of stem cell plasticity was introduced in 1999, which described the ability of adult stem cells to adapt to their surrounding microenvironment and having the ability, when relocated to a new niche, to give rise to a different kind of specialized cells which were not present in their previous niche (Poulsom et al., 2002). This ability of ASCs to change cell fate as a response to their microenvironment (Lakshmipathy and Verfaillie, 2005) was first proposed by Petersen et al., who showed that bone marrow cells could give rise to hepatocytes and thus had epithelial lineage capabilities (Petersen et al., 1999), and by Bjornson and colleagues, who demonstrated the ability of neural stem cells to give rise to haematopoietic precursors (Bjorson et al., 1999). Since these original discoveries, stem cell plasticity has been studied in many tissues and model systems, including mammalian epithelia (reviewed by Tetteh et al., 2015). In particular, the ability of intestinal stem cells to respond to microenvironmental changes in both homeostatic and damaged tissue has been heavily documented, where this plasticity can be found at the level of the progenitor cells (reviewed by Beumer and Clevers, 2016; Bankaitis et al., 2018). On the one hand, this plasticity of stem cells has the ability to be exploited for therapeutic purposes (Poulsom et al., 2002), but on the other hand, stem cell plasticity is a major issue in tumour

development, as this ability of cancer stem cells (CSCs) to quickly adapt to their microenvironment promotes the formation of metastatic sites in tissues far from the original tumour site, thus hindering therapeutic approaches (reviewed by Battle and Clevers, 2017; Paul et al., 2022)

1.2. The *Drosophila* intestine

Epithelia are constantly turned over as cells are lost from the surface of the tissue and replaced by the proliferation of stem cells. Therefore, the intestinal epithelium in *Drosophila* is constantly renewed, supported by the intestinal stem cell population (ISCs) (Miccheli and Perrimon, 2006; Ohlsten and Spradling, 2006).

The gastrointestinal (GI) tract of the fruit fly is a simple epithelial tissue with a surrounding network of nerves, visceral muscle and the trachea (Capo et al., 2019), that can be divided into three parts according to morphology and function: the foregut, the midgut and the hindgut (Nászai et al., 2015) (*Figure 1.1*). The extremities of the tissue, the foregut and the hindgut, originate from the ectoderm during fly development, whereas the midgut is of endodermal origin (Capo et al., 2019). These three parts can be subdivided into subregions with specialized functions (Buchon et al., 2013; Marianes and Spradling, 2013) and distinct physicochemical properties, such as pH and oxygen concentration (Miguel-Aliaga et al., 2018). The *Drosophila* midgut is divided into 5 compartments (R1-R5), that can be further divided into 14 different subregions, (Buchon et al., 2013; Buchon and Osman, 2015), each with specialized and distinct morphology, cell characteristics and function. The anterior ends of the midgut are responsible for the breakdown of macromolecules, which carries on to the middle regions of the tissue that are also able to modify these macromolecules before they enter the posterior end of the midgut, which is responsible for their absorption (Marianes and Spradling, 2013). This compartmentalization further enhances the regulatory complexity of the *Drosophila* midgut (Dutta et al., 2015). Independent populations of ISCs are responsible for the maintenance of each of these subregions, only giving rise to cells from their specific subregion, but not to those from other compartments (Buchon et al., 2013). The rate of ISC division is also location-dependent, with ISCs in the posterior end having the highest turnover rates, dividing about once per day, whereas anterior ISCs divide less frequently (Marianes and Spradling, 2013). The morphology and function of ECs is also affected by gut compartmentalization and they vary between different regions of the gut (Marianes

and Spradling, 2013; Capo et al., 2019). Thus, this complex compartmentalization of the gut requires a tight control of ISC regulatory pathways to maintain homeostatic balance within the gastrointestinal tissue.

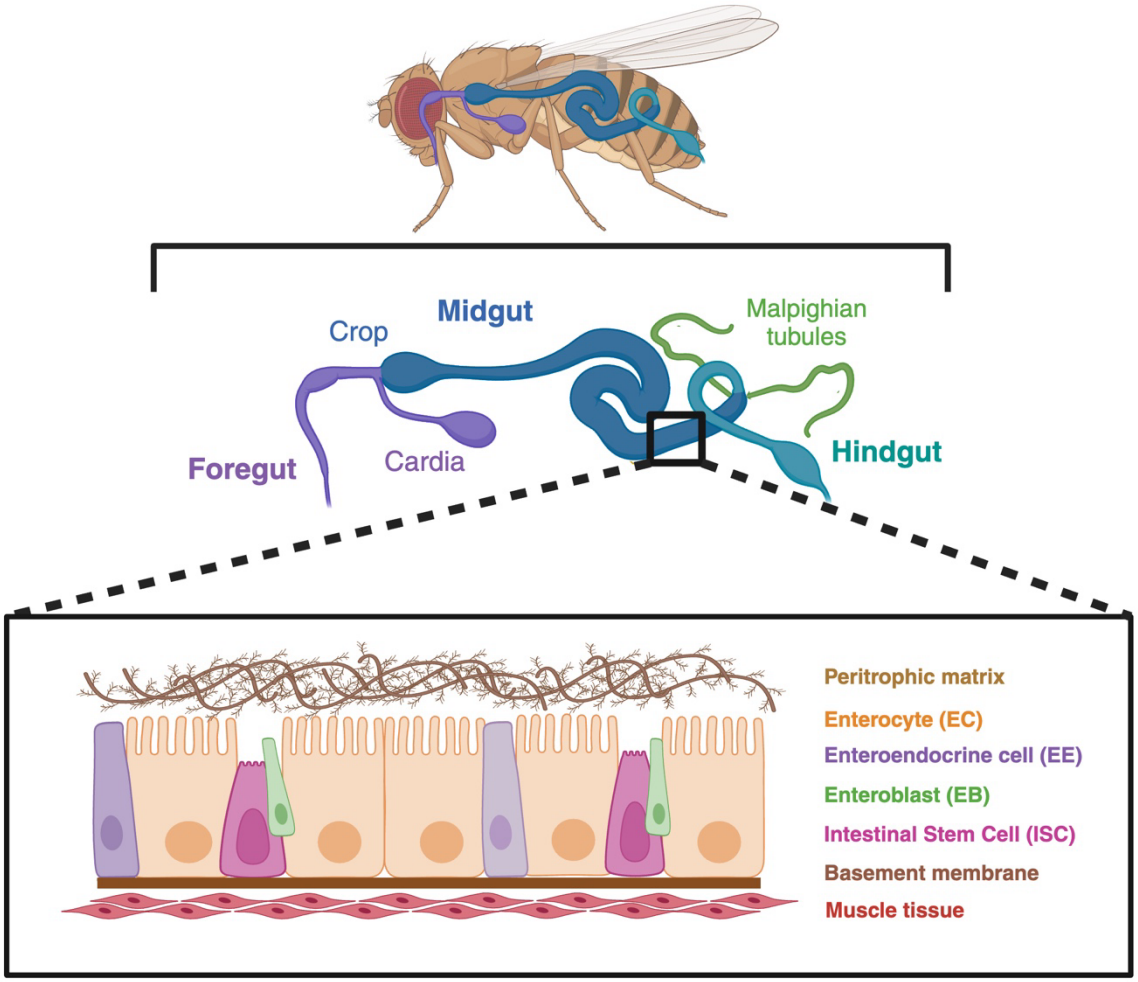

Figure 1.1. The structure of the *Drosophila* gut tissue. The *Drosophila* gut is divided into three main parts: the foregut, the midgut and the hindgut. The intestinal epithelium in the fly is a pseudostratified monolayer made up of four different cell types: the intestinal stem cells (ISCs), progenitor enteroblasts (EBs), and two types of differentiated cells, enterocytes (ECs) and enteroendocrine cells (EEs). ISCs are on the basal side of the tissue, in close contact with the basement membrane and the underlying muscle tissue. The periotrophic matrix on the apical side serves as a barrier to external insults.

The *Drosophila* midgut is functionally equivalent to the mammalian small intestine and is therefore used in most studies to model mammalian intestinal homeostasis (Jiang et al., 2016; Capo et al., 2019). This tissue is made up of 4 different cell types arranged to form monolayer of pseudostratified epithelium (Ohsltein and Spradling, 2006) (*Figure 1.1*). These cells maintain the apical-basal polarity characteristic of epithelial tissues (Miccheli and Perrimon, 2006), with stem cells at the basal surface and the differentiated, specialized daughter cells on the apical surface (Jiang et al., 2016). The absorptive enterocytes (ECs) are large differentiated polyploid cells that make up most of the midgut tissue and are responsible for the maintenance of barrier function (Casali and Battle, 2009). The smaller secretory enteroendocrine cells, EBs and ISCs are interspersed between the ECs (Losick et al., 2011). ISCs at the basal surface of the tissue have a triangular shape and are in close contact with the basement membrane and the underlying muscle tissue (Beebe et al., 2010; Losick et al., 2011), which is thought to resemble a stem cell niche and provide ISCs with the necessary signals for differentiation (Lin et al., 2008; Marianes and Spradling, 2013). Gut compartmentalization also affects ISC morphology: Marianes and colleagues identified different morphological and molecular properties of ISCs in different regions of the midgut, but could not conclude if these were a consequence of other structural changes in the subregion, e.g. EC morphology, or if the differing ISC properties were indeed the catalyst of the compartment characteristics.

1.3. *Drosophila* intestinal stem cells (ISCs)

Although the existence of stem cells and their ability to replace dead or damaged cells to maintain homeostasis and tissue function has been known for over a century (reviewed by Bianco et al., 2008; Casali and Battle, 2009), the existence of such cells within the *Drosophila* intestine was recently discovered (Miccheli and Perrimon, 2006; Ohlsten and Spradling, 2006). *Drosophila* ISCs, which are responsible for tissue turnover to maintain homeostasis and for tissue regeneration after damage (Biteau and Jasper, 2011), have since become an excellent model to study epithelial stem cell homeostasis. Although there are some controversies and a lack of consensus regarding the exact model of ISC differentiation in *Drosophila*, the initial model for ISC fate is based on stem cells undergoing asymmetric cell division, where an ISC self-renews and gives rise to a committed progenitor, known as an enteroblast (EB) (Jiang and Edgar, 2012; Zeng et al., 2015) (*Figure 1.2*). EBs are transient, undifferentiated cells (Choi et al., 2012) that give

rise to two types of differentiated cells: absorptive enterocytes (ECs) and secretory enteroendocrine cells (EEs) (Mirzoyan et al., 2019). Differentiation of EBs into these two cell types is not balanced: differentiation heavily favours absorptive cells, with approximately 90% of progenitors differentiating into ECs, and only 10% into EEs (Amcheslavskly et al., 2009).

Some reports suggest the existence of a pre-EE progenitor (Zheng and Hou, 2015), and the possibility that ISCs directly give rise to EEs without the need for a progenitor EB cell (Biteau and Jasper, 2014; Chen et al., 2018; Korzelius et al., 2019; Ma et al., 2019).

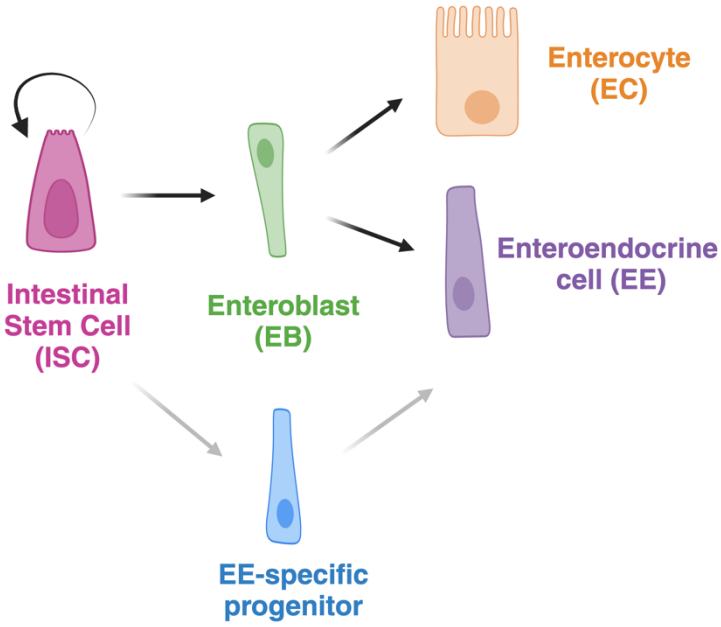

Figure 1.2. The model of *Drosophila* ISC differentiation. *Drosophila* ISCs divide asymmetrically, where the stem cell can either self-renew, or give rise to a progenitor enteroblast (EB) that will immediately differentiate into an absorptive enterocyte (EC) or a secretory enteroendocrine cell (EE). Differentiation is heavily biased towards ECs, which make up the bulk of the tissue.

De Navascués and colleagues demonstrated that the *Drosophila* midgut is maintained by population asymmetry, i.e. that stem cell divisions are symmetric and driven by the loss or differentiation of their neighbouring cells (de Navascués et al., 2012). This competition, known as neutral drift, was later corroborated by other and resembles differentiation models previously established in mammals (reviewed by Jin et al., 2017). Although there are some contradicting conclusions, most reports agree that the majority

of ISC divisions are asymmetric, with symmetric divisions occurring at a lower frequency, and that the switch between these two forms of division is determined by external environmental stimuli (Jiang et al., 2016). This ISC fate model proposed in the fruit fly is conserved in mammalian epithelial stem cells (Doupé et al., 2012), making *Drosophila* a great model organism to study mammalian ISC homeostasis, as well as for the broader study of ASC regulation. This complex model of ISC maintenance is regulated by over 450 genes (Zeng et al., 2016), highlighting the importance of the tightly-regulated cross-talk between the signaling networks that influence ISCs.

1.4. ISC regulation

This complex model of ISC differentiation is accompanied by an equally complex signalling network that regulates ISC fate, i.e. maintenance versus differentiation. The pathways implicated in ISC regulation include Notch, JAK/STAT, Hippo, EGFR/Ras/MAPK, Wnt, JNK, the insulin pathway, and BMP/Dpp (reviewed by Miguel-Aliaga, 2018) (*Figure 1.4*). Additional factors and feedback mechanism from the committed cells also contribute to ISC regulation (Biteau and Jasper, 2014; Chen et al., 2016). Thus, the dynamic interplay between all these signalling pathways and molecules is essential to maintain tissue homeostasis; deregulations or mutations in any of the components implicated in these signalling cascades could give rise to tissue overproliferation or the depletion of the stem cell population (Yamashita et al., 2005; Doupé et al., 2018; Ma et al., 2019). Despite the obvious structural and compositional differences, both *Drosophila* and mammalian ISCs are regulated by conserved signalling pathways, making *Drosophila* ISCs an excellent model that has contributed to our understanding of the regulation of ISCs and epithelial homeostasis in metazoans (Nászai et al., 2015; Doupé et al., 2018).

ISCs regenerate after damage and support the homeostatic maintenance of the midgut tissue (Biteau and Jasper, 2011). Under homeostatic conditions and without the need for previous cellular damage, tissue turnover in the adult *Drosophila* midgut is quick and occurs approximately once a week (Amcheslavsky et al., 2009; Losick et al., 2011). Tissue damage and physiological stress affect tissue homeostasis and turnover rates and can lead to detrimental effects on tissue function (Capo et al., 2019). As mentioned above, deregulation in tissue homeostasis could lead to uncontrolled proliferative activity and tissue dysplasia (Biteau and Jasper, 2011). In humans, these pre-cancerous lesions can

later develop into tumours (Li and Jasper, 2016). Thus, understanding the mechanisms that control stem cell proliferation and maintenance in the intestine is key to enhance our understanding of the development and treatment of human diseases such as cancer (Ma et al., 2019), since ISCs are regulated by a number of conserved signalling pathways that play similar roles in the regulation of mammalian epithelial stem cells.

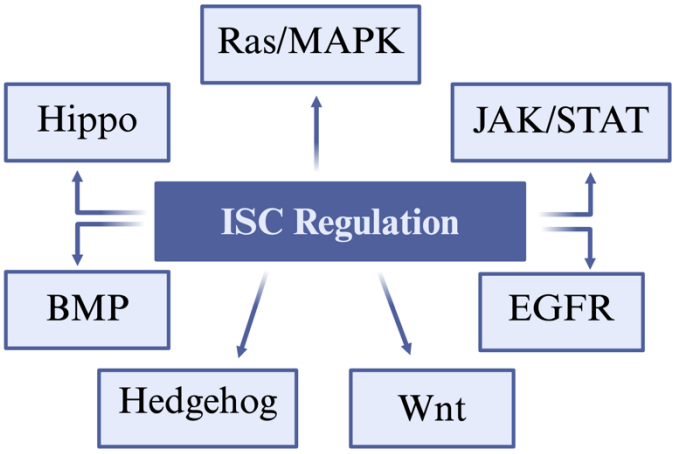

Figure 1.3. A wide range of signalling pathways are responsible for the maintenance of ISCs in the *Drosophila* gut. The pathways implicated in ISC regulation include Notch, JAK/STAT, Hippo, EGFR/Ras/MAPK, Wnt, JNK, the insulin pathway, and BMP/Dpp.

1.4.1. Notch

Notch signalling is the key regulator of *Drosophila* ISC differentiation (Kapuria et al. 2012). Ohsltein and Spradling provided a model of ISC fate in the posterior midgut in which EB daughter cells expressing high levels of the Notch receptor are able to receive strong signals from the Notch signalling pathway that drive differentiation into EC cells. On the contrary, those progenitors exposed to low levels of Dl on their cell surface receive weaker Notch signals and differentiate into secretory enteroendocrine cells (Ohlstein and Spradling, 2007). Delta expression is characteristic and exclusive of ISCs, whereas its receptor is found in both ISCs and EBs (Lu and Li, 2015). ISCs are sometimes referred to as Notch-negative, because they express the ligand Dl, and progenitor EBs are termed Notch-positive (Guisoni et al., 2017). Notch is a negative regulator of ISC proliferation: lower Notch activity promotes ISC division and increases the number of progenitor cells in the tissue, whereas increased level of Notch downregulate the proliferative rates of ISCs (Miccheli and Perrimon, 2006). In other words, absence of Notch prevents

differentiation and triggers uncontrolled proliferation of ISCs (Ohlstein and Spradling, 2006).

Furthermore, de Navascués and colleagues proposed a new ISC division model, whereby ISCs divide symmetrically and the fate of the progeny is determined post-division through the competition for Dl/Notch signalling between sibling cells or other cells in close proximity, leading to population asymmetry in the tissue (de Navascués et al., 2012). This form of tissue maintenance where homeostatic balance between progenitors and differentiated cells is not determined by the stem cell lineage, but rather at the population level, is called neutral competition (Klein and Simmons, 2011; Guisoni et al., 2017). The concept of cell fate determination through neutral competition between cells in close proximity, known as lateral inhibition, was first proposed in Delta/Notch signalling in 1996 by Collier et al. The biased or stochastic variation of Dl/Notch expression in the cell membrane, and the size of the contact area between cells will determine cellular fate (Guisoni et al., 2017). In this model, neighbouring cells expressing similar levels of the Notch receptor and Delta ligand on their cell surface can bind to each other and mutually repress the expression of either the receptor or the ligand, eventually leading to the formation of Notch-expressing cells and a Delta-expressing cell (reviewed by Sancho et al. 2015) (*Figure 1.4*). Thus, Notch signalling in the *Drosophila* midgut is bidirectional and context-dependent (Guo and Ohlstein, 2015). Taken together, all these results demonstrate that ISC fate is a stochastic process dependent on Notch activity, which determines the outcome of ISC division, either symmetrically or asymmetrically, and their differentiation into ECs or EEs.

The regulation of Notch activity is complex and studies have found that there is not a downstream target of Notch that is singularly responsible for its control, but rather it is a collective effort of multiple downstream targets that regulate Notch activity (Lu and Li, 2015). The levels of expression of the protein TSC2, which is found downstream of Notch in ISCs, have been shown to play a role in the regulation of the ISC self-renewal/differentiation switch: high levels of TSC2 in ISCs block differentiation and thus favour ISC self-renewal, whereas decreased expression of the protein in progenitor EBs triggers differentiation into ECs (Kapuria et al., 2012).

Notch has also been found to supress the activity of other ISC regulatory pathways, such as JAK/STAT, by repressing the expression of its activating ligand unpaired (Upd) (Liu et al., 2010). A link between Notch activity and the insulin pathway

(IIS) through microRNAs has also been reported, suggesting that Notch activity could be under nutritional control in the fly (Foronda et al., 2014).

In summary, Notch signalling controls ISC fate in the *Drosophila* gut. Its expression represses EE differentiation and favours the production of enterocyte cells in the posterior midgut, and the regulation of Notch signalling levels is essential in order to maintain a balanced differentiation, and thus tissue function, and to prevent uncontrolled proliferation of ISCs in the tissue.

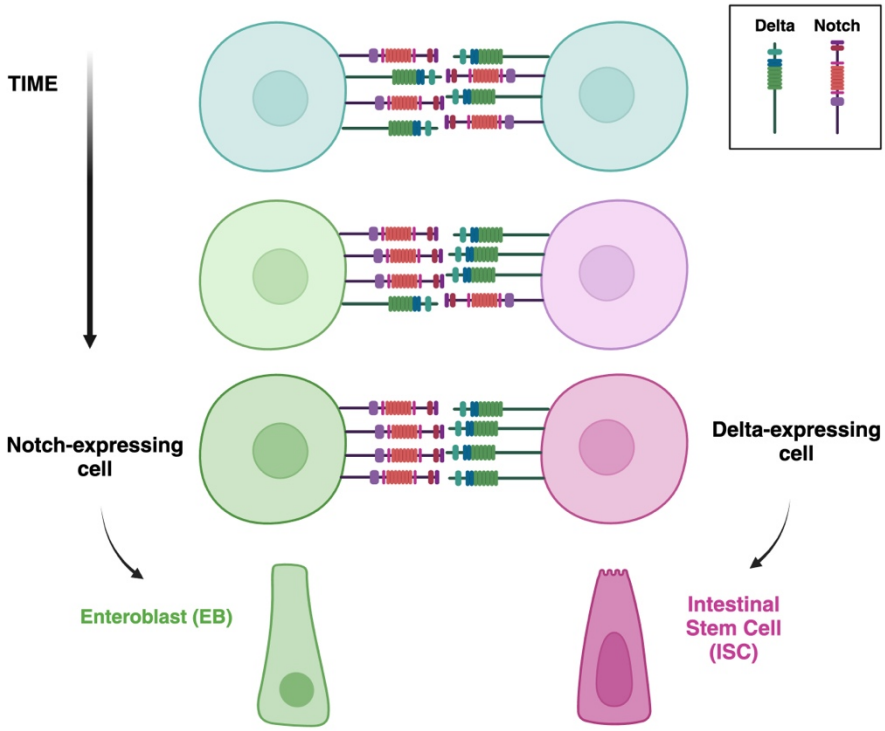

Figure 1.4. Model of lateral inhibition for the determination of cell fate. In this model, progeny express similar levels of the Notch receptor and delta ligand on the cell surface and it is the mutual repression of expression between neighbouring cells that determines cell fate, by eventually determining if a cell with be Notch-expressing (EB) or Delta-expressing (ISC).

1.4.2. JAK/STAT

The Janus Kinase/Signal Transducer and Activator of Transcription (JAK/STAT) is a conserved signaling pathway heavily implicated in many aspects of development and disease (Beebe et al., 2010). In the *Drosophila* gut, it plays roles in the maintenance of tissue homeostasis and it is activated in response to apoptosis, infection and stress (Buchon et al., 2009; Jiang et al., 2009). The JAK/STAT ligand unpaired (upd) is secreted

by the surrounding visceral muscle and activates JAK/STAT signalling in ISCs to control stem cell division (Xu et al., 2011). JAK/STAT signalling is active in ISCs and during the early stages of progeny formation, but it is not present in mature EEs or ECs (Beebe et al., 2010). However, EC-expression of the JAK/STAT Upd ligands has been shown to be induced upon stress and infection (Buchon et al., 2009; Jiang et al., 2009), demonstrating that the midgut tissue possesses endogenous sources of JAK/STAT signaling. Activation of JAK/STAT in damaged ECs is triggered by the JNK-mediated production of unpaired ligands (Karpowicz et al., 2010).

Beebee and colleagues also demonstrated that while JAK/STAT signaling plays roles in ISC proliferation (Liu et al., 2010), it is not a key regulator of self-renewal (Beebee et al., 2010). In the absence of JAK/STAT signalling, midgut ISCs have the ability to divide for up to 5 weeks (Beebe et al., 2010), thanks to the ability of EGFR and Wg signaling to replace low levels of pathway activity and drive ISC proliferation (Xu et al., 2011). This demonstrates a level of functional redundancy in pathway activity within the midgut. Similarly, JAK/STAT has been shown to interact with other signalling cascades in the midgut. Lin and colleagues suggested a double role for JAK/STAT regulation of ISCs: on the one hand, JAK/STAT acts upstream of Notch alongside Wg to regulate ISC division, and, on the other hand, it antagonizes Notch to control stem cell fate (Lin et al., 2010).

Han et al. proposed that, JAK/STAT acts downstream of Hedgehog (Hh) signaling to regulate ISC fate. This, alongside the findings that suggest Notch as another downstream target of JAK/STAT (Lin et al., 2010), starts to build a picture of the complex interactions between ISC regulatory pathways in the *Drosophila* midgut.

1.4.3. Hippo

The Hippo signalling pathway, which plays key roles in the regulation of organ size, cell growth and proliferation, and is fundamental in the development of tumours, is highly conserved between *Drosophila* and higher organisms (Ren et al., 2010). Hippo is essential for the maintenance of midgut homeostasis in the adult fly (Poernbacher et al., 2012). This pathway, originally discovered in the fruit fly, controls the activity of the transcriptional activator Yorkie (Yki), through a kinase signaling cascade (Ren et al., 2010). Thus, regulation of Yki activity occurs through protein phosphorylation: in healthy adult *Drosophila* gut tissue, phosphorylated Yki is repressed and targeted for degradation,

whereas in the absence of phosphorylation, Yki translocates to the nucleus where it interacts with a wide range of target genes that induce cell proliferation (Karpowicz et al., 2010; Hsu et al., 2017). Within the midgut cells, Hippo has been proposed to act as a sensor of cell stress in ECs and EEs (Shaw et al., 2010), where it works in consonance with the JAK/STAT and JNK signaling pathways to maintain homeostasis in the adult *Drosophila* midgut (Karpowicz et al., 2010). Upon injury, stem cell proliferation is driven by the interaction of Yki with target genes that promote ISC division, one of which is the JAK/STAT ligand unpaired (Upd) (Staley and Irvine, 2010). Activation of Yorkie resulted in tissue hyperplasia and an increase in Dl-expressing cells, i.e. ISCs, in the gut, demonstrating that in normal circumstances, Hippo is responsible for maintaining ISC proliferation at low levels by repressing Yki activity (Staley and Irvine, 2010). Moreover, Hippo signalling in the fly gut has been reported to be under the control of microRNAs, which are essential for Hippo-mediated ISC self-renewal, but dispensable in EGFR- and Notch-mediated ISC proliferation (Huang et al., 2014).

In summary, Hippo signalling acts to repress Yki activity in healthy gut tissue to maintain ISC homeostasis. When the Hippo kinase cascade is misregulated, Yki acts as an oncogene by inhibiting cell death and promoting cell growth and ISC proliferation in the *Drosophila* intestine (reviewed by Staley and Irvine, 2012).

1.4.4. EGFR/Ras/MAPK

EGFR/Ras/MAPK (mitogen activated protein kinase) signalling promotes proliferation of adult intestinal stem cells in *Drosophila* (Ragab et al., 2011). The majority of insight into the role of Ras/MAPK in the fruit fly derives from the study of receptor tyrosine kinases (RTKs), which activate the Ras oncogene Ras85D that in turn triggers the phosphorylation of MAPKs (Ragab et al., 2011). In response to damage or stress in the gut epithelium, the EGFR/Ras/MAPK pathway is activated to maintain the ISC pool, and the interplay between EGFR and JAK/STAT signalling alongside it promotes ISC proliferation for gut tissue repair (Jiang et al., 2009; Jiang et al., 2011), thus contributing to the maintenance of tissue homeostasis (Liang et al., 2017). Therefore, as with the other signalling pathways described in this section, EGFR/Ras/MAPK interacts with other signaling pathways to control gut homeostasis in *Drosophila*. Activation of p38-dependent MAPK signalling also plays roles in the regulation of the JAK/STAT ligand unpaired, alongside Hippo, TGF-β and Dpp signaling (Houtz et al., 2017).

One of the three p38 MAPK proteins in *Drosophila*, p38c, plays key roles regulating lipid metabolism, oxidative stress and immune homeostasis in the *Drosophila* intestine (Chakrabarti et al., 2014). Another one of the p38 family members, p38b-MAPK, is a key regulator of age-related changes in ISC proliferation (Park et al., 2018), and has been shown to promote the misdifferentiation of ECs and the growth of EBs and ECs in damaged and aged tissues (Xiang et al., 2017; Park et al., 2018). In the context of tissue damage, increased levels of the Ras protein in the *Drosophila* gut promote hyper-endoreplication of progenitor enteroblasts and differentiated enterocytes (Xiang et al., 2017). However, under normal homeostatic conditions, EGFR/Ras activity is only essential for ISC division and proliferation, but not for EC endoreplication, since mature, fully-differentiated ECs showed a downregulation of MAPK activity and other EGFR pathway components (Xiang et al., 2017).

In a general homeostatic context, components of the EGFR/MAPK/ERK signaling pathway are responsible for maintaining glucose homeostasis in the fly: inhibition of MAPK/ERK lowers the levels of the insulin-like receptor on the surface of eye cells, leading to insulin resistance in the organism (Zhang et al., 2011).

1.4.5. Other contributors to ISC regulation: JNK, Wg, Hedgehog, Slit/Robo, BMP/Dpp and the insulin pathway

Other signaling pathways implicated in the regulation of *Drosophila* ISCs include JNK, Hedgehog (Hh) (Han et al., 2015), Wnt/Wg signaling (Lin et al., 2008), Slit/Robo (Biteau and Jasper, 2014), the insulin pathway (Choi et al., 2011) and BMP/Dpp signaling (Tian and Jiang, 2017).

The exact role of the Jun N-terminal kinase (JNK) pathway in *Drosophila* remains to be elucidated. There is contradicting evidence in the literature, where some groups have identified it as a tumour suppressor that is able to induce apoptosis, whereas others have highlighted its oncogenic properties (Biteau et al., 2008). In the *Drosophila* midgut, JNK is activated in damaged enterocytes (ECs) of the adult tissue as a response to injury (Karpowicz et al., 2010) and stress, where it increases tolerance to insults and mitigates the negative effects of reactive oxygen species (ROS) (Wang et al., 2003). JNK has also been shown to drive ISC misdifferentiation and contribute to loss of tissue homeostasis with age (Biteau et al., 2008). This JNK-mediated increase in ISC proliferation in

response to stress is mediated by the transcription factor FOS, which also controls EGFR-dependent stem cell proliferation (Biteau and Jasper, 2011).

Hedgehog (Hh) signalling is located upstream of JAK/STAT in the intestine and has been shown to promote the differentiation of ISCs into EBs in the posterior midgut (Han et al., 2015). In EBs, Hh activated the expression of Upd2, which in turn promotes ISC proliferation through JAK/STAT (Tian et al., 2015). Hh also interacts with Wingless (Wg) signaling in the hindgut to promote ISC self-renewal, proliferation and differentiation (Takashima et al., 2008). This same study demonstrated that the antagonistic roles of Wg and Hh described in the mammalian intestine are conserved in *Drosophila*, where both high Wg expression and low Hh signaling favour ISC self-renewal and prevent differentiation in the hindgut tissue (Takashima et al., 2008). Initial reports suggested that Wingless was expressed in the surrounding muscle tissue, and thus had a paracrine effect on the regulation of gut ISCs (Lin et al., 2008). A more recent study by Cordero et al. demonstrated that endogenous Wg, produced by the progenitor enteroblasts in the epithelial compartment of the tissue is essential for ISC proliferation and tissue regeneration (Cordero et al., 2012).

In summary, the regulation of the ISCs and *Drosophila* gut homeostasis is tightly controlled by a wide range of signalling pathways that interact and work in tandem to control the adequate proliferation of stem cells and maintain a balance between self-renewal and differentiation.

1.5. The stem cell niche

Adult tissue stem cells play critical roles throughout the body in maintaining normal tissue homeostasis and responding to challenges such as damage. As misregulation of stem cells has major implications for both normal physiology and diseases such as cancer, a great deal of research has focused on understanding the stem cell niche. Classically, the niche has been thought of in terms of signalling from adjacent cells, but more recent work has led to an expanded definition that incorporates not only classical signalling pathways but also mechanical and metabolic inputs (Scadden, 2014; Chacón-Martínez et al., 2018).

Even as understanding of what constitutes the niche has broadened, most studies have focused on the cells and tissues surrounding the stem cells and their role in creating the microenvironment. In this context, stem cells are viewed primarily as the recipients

of chemical and mechanical cues. However, work in a range of systems has shown that stem cells themselves contribute substantially to the niche (*Figure 1.5*).

While niche signals often originate from surrounding tissues, such as the underlying mesenchyme for many epithelial stem cells, an increasing number of examples have emerged of epithelial stem cell progeny playing a major role as sources of niche signals (*Figure 1.5A*). In the mammalian intestine, for example, both mesenchymal- and stem cell-derived epithelial cells supply signals to regulate the intestinal stem cells (ISCs) (Santos et al., 2018).

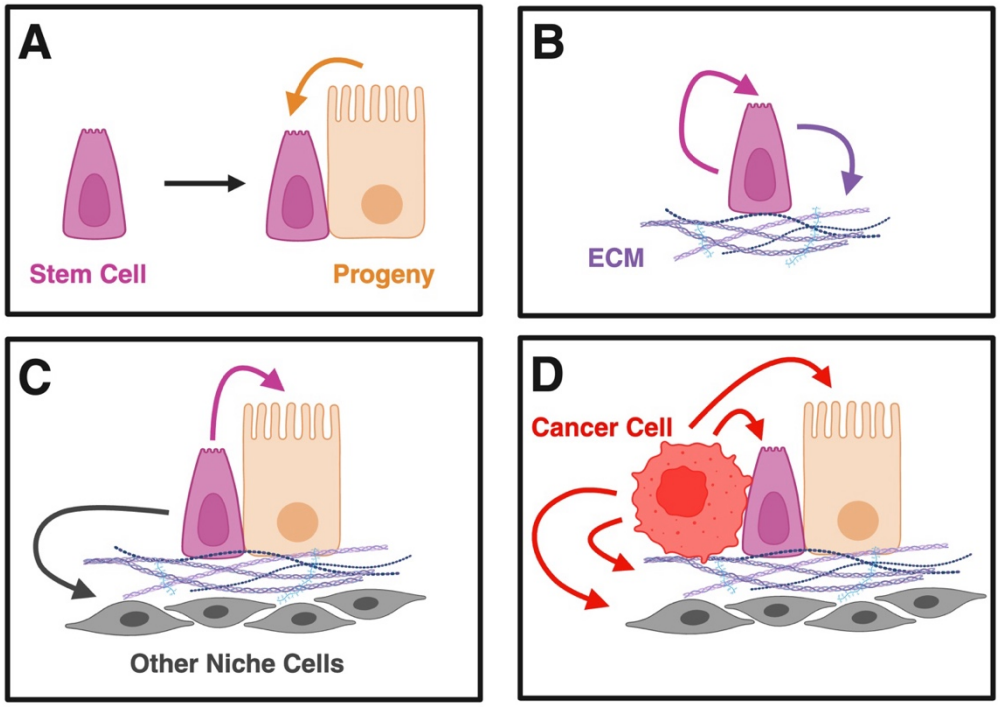

Figure 1.5. Contributions to the stem cell niche. Stem cells may generate progeny that act as niche components and regulate their own progenitors (***A***). Stem cells may act as their own niche cells producing autocrine signals or ECM components (***B***). Stem cells may regulate both epithelial and non-epithelial niche cells, or the ECM to influence the microenvironment (***C***). Cancer cells may subvert the niche, exploiting all the niche signals and creating a new microenvironment that supports their growth (***D***). Figure adapted from Ferraces-Riegas et al., 2022.

The *Drosophila* gut cells have also been shown to heavily contribute to the establishment and maintenance of the stem cell niche. Slit-Robo signalling from EEs to ISCs has been reported to act as a negative feedback loop to regulate EE production (Biteau and Jasper, 2014), but contradicting reports have demonstrated that Slit does not modulate EE production in epithelial tissues (Sallé et al., 2017). EEs may also indirectly regulate ISCs via the secretion of tachykinin to regulate Dilp3 production by smooth

muscle, which in turn promotes ISC maintenance (Amcheslavsky et al., 2014). Differentiated ECs are sources of BMP ligands that promote ISC maintenance and self-renewal (Tian and Jiang, 2014), Hippo regulators (Karpowicz et al., 2010) and cytokine ligands that activate JAK/STAT signalling to promote tissue turnover (Jiang et al. 2009; Zhou et al. 2013). Differentiating progeny also contribute to the niche in the form of Wingless signals from enteroblast (EB) progenitors, which are required for ISC proliferation in regenerating midguts (Cordero et al., 2012). Regulated secretion of EGF ligands from ECs is instrumental in driving turnover and ISC proliferation (Liang et al., 2017) demonstrating the utility of feedback from progeny to the stem cells in coupling cell loss and replacement to maintain balance.

Given the importance of coupling cell loss to new cell production, both in normal homeostasis and in response to challenges, it is perhaps not surprising that progeny should feed back to the stem cells. This form of coupling would allow the status of the epithelium to be communicated continuously to the stem cells, enabling them in turn to tune the production of new cells according to demand. The importance of stem cell progeny in the niche shifts our understanding from that of a fixed, clearly defined anatomical niche to that of a niche in continuous flux, able to act as rheostat, dynamically adapting to challenges and maintaining balance (Hsu and Fuchs, 2012).

In addition to producing differentiated progeny that comprises part of the stem cell niche, there are an increasing number of examples of stem cells expressing their own niche components (*Figure 1.5B*). In some cases, these act as autocrine signals; in others, they may contribute to the local environment, shaping the extracellular matrix (ECM) and modulating paracrine signals. As in mammalian epidermis, there is some evidence that autocrine Wg signalling may contribute to stem cell regulation in the *Drosophila* midgut, particularly in anterior regions that may be further from a source of paracrine Wingless signals (Fang et al., 2016).

The role of stem cells in secreting their own niche proteins is not limited to signalling pathway ligands but also includes the contribution of stem cells to ECM composition. Given that integrin expression and adhesive properties are well-established markers of epidermal stem cells and that Ilk signalling in epidermal progenitor cells has been linked to the composition of the ECM, this may in effect represent an autocrine signalling mechanism with stem cells secreting their own ECM substrate to promote their maintenance (Jones and Watt, 1993; Jones et al., 1995; Morgner et al., 2015). This may be a conserved principle of epithelial stem cell niches as *Drosophila* midgut ISCs are also

maintained by integrin signalling and express the ECM component laminin as an integrin ligand (Lin et al., 2013).

Autocrine signalling from stem cells may be broadly associated with positive feedback mechanisms, serving to keep stem cells in a primed state where the removal of inhibitory factors could lead to rapid proliferation, for example, in the context of repairing tissue damage. However, such mechanisms pose risks for unregulated proliferation.

In addition to autocrine signals, stem cells also express a range of paracrine signals that play important roles in the regulation of their environment (*Figure 1.5C*). Stem cell progeny in many cases constitute a critical niche component regulating their parental stem cells; in turn, it is perhaps not surprising that stem cells also regulate their progeny. As explained previously, *Drosophila* ISCs express the Notch ligand Delta, which signals to differentiating EBs to promote enterocyte fate (Micchelli and Perrimon, 2006; Ohlstein and Spradling, 2006, 2007). Expression profiling has also identified a number of secreted proteins expressed by *Drosophila* ISCs that may act to regulate the local microenvironment (Doupé et al., 2018), including SPARC, PLOD, dlp and TIMP, the four proteins studied in this project.

Given the dynamic nature of epithelial turnover in homeostasis and the need to closely coordinate cell loss, differentiation and proliferation, it is perhaps not surprising that stem cells communicate their status to the niche, including their own progeny. In effect, this allows stem cells to answer back to the microenvironment, allowing a precise two-way feedback with the niche to offer a range of mechanisms that support balanced turnover.

The ability of stem cells to form, regulate or act as niche cells can be a double-edged sword. The potency that enables precise coordinated regulation in homeostasis and repair can be subverted in diseases such as cancers. Mutations not only trigger autonomous effects in the tumour itself but also impact the ability of the cancer stem cells (CSCs) or tumour-initiating cells (TICs) to communicate to and regulate their surroundings. The importance of cancer cell progeny as components of the niche that drive proliferation has been explored in the *Drosophila* midgut epithelium (*Figure 1.5D*). In a *Drosophila* intestinal tumour model driven by loss of Notch function, which blocks differentiation, both autocrine and paracrine signals are responsible for tumour growth (Patel et al., 2015). CSC- or TIC-derived signals play critical roles in regulating their own niche through recruitment or induction of cells in the microenvironment to express niche signals that promote tumour properties. In the *Drosophila* midgut, Apc mutant cells

subvert the normal EGF-driven feedback circuit that acts to couple cell loss to ISC proliferation by inducing rhomboid in adjacent cells to drive constitutive secretion of active EGF ligands (Ngo et al., 2020). Remodelling of the ECM elements of the niche is also critical in tumour development and progression, with contributions from both tumour cells themselves expressing ECM components or regulators such as MMPs and from tumour-associated cells, particularly cancer-associated fibroblast (CAFs) (Winkler et al., 2020).

In summary, coupling both at the level of two-way signalling between stem cells and the niche, and between cell production and loss through niche roles of stem cell progeny provides mechanisms to maintain balance. Many of the known mechanisms appear to be conserved from the relatively simple invertebrate model of the *Drosophila* midgut to mammalian systems, suggesting that complementary studies in both basic model organisms and more complex mammalian systems will be key to elucidating the full logic of these complex interactions.

1.6. *Drosophila* as a model organism

The fruit fly *Drosophila* melanogaster has been used as a model organism in research for over a century. The first documented use of *Drosophila* melanogaster in research dates back to 1901, in William Castle's laboratory at Harvard University (Jennings, 2011). Initial breakthrough work by Thomas Hunt Morgan in the 1910s, where he demonstrated the sex linkage for the white-eye gene in the fruit fly (Hunt-Morgan, 1910) and established the linear arrangement of genes in chromosomes (Hunt-Morgan, 1910b; Hunt-Morgan, 1917) using *Drosophila* melanogaster as a model system, shed a spotlight on the value of this organism for genetic analysis.

Since then, it has become one of the best-characterized and widely-used genetic models in biomedical research to study developmental processes and ageing (Casas-Vila et al., 2017). Many efforts have been focused on the characterization of this model organism. Adams and colleagues provided the full genome sequence of *Drosophila* and revealed that despite being smaller than other commonly used model organisms like *C. elegans*, its ~13,600 genes, divided across 4 chromosomes (Prüßing et al., 2013) still retain the wide scope of functional diversity of other models (Adams et al., 2000). Updated genomic analyses have increased the number of protein-coding genes in the *Drosophila* genome to 13,903, and established ~ 3,719 non-coding genes (Hu et al.,

2015). Its compact genome, low genetic redundancy, and functional simplicity are some of the key features of *D. melanogaster* (Nichols, 2006; Mirzoyan et al., 2019) (*Figure 1.6*). These are accompanied by its low cost of maintenance, high reproductive rates and rapid regeneration times, which further contribute to its extensive use in research (Lee and Min, 2019). Despite the obvious complexity, anatomical and physiological differences between the fly and humans, the pathways that regulate key developmental processes, as well as the regulation of genetic expression and other fundamental aspects of cell biology, are conserved between *Drosophila* and higher organisms (Koon and Chan, 2017). Moreover, comparisons between the annotated genomes of the fly and humans showed ~60% homology between them (Mirzoyan et al., 2019), with ~75% of the genes implicated in the development of human disorders having orthologs in the fly (Koon and Chan, 2017). Many resources and databases have been created with readily available and updatable information about fly genes and proteins, such as the GLAD (Gene List Annotation for *Drosophila*) developed by Hu and colleagues.

With all this, the fly has emerged as a powerful model system for the study *in vivo* of many biological processes, as well as to study the underlying mechanisms that drive disease. Such examples include its use in the study of the biology of ageing (Lee and Min, 2019), neurodegenerative diseases (reviewed in Prüßing et al., 2013; Koon and Chan, 2017), and cancer (reviewed in Mirzoyan et al., 2019).

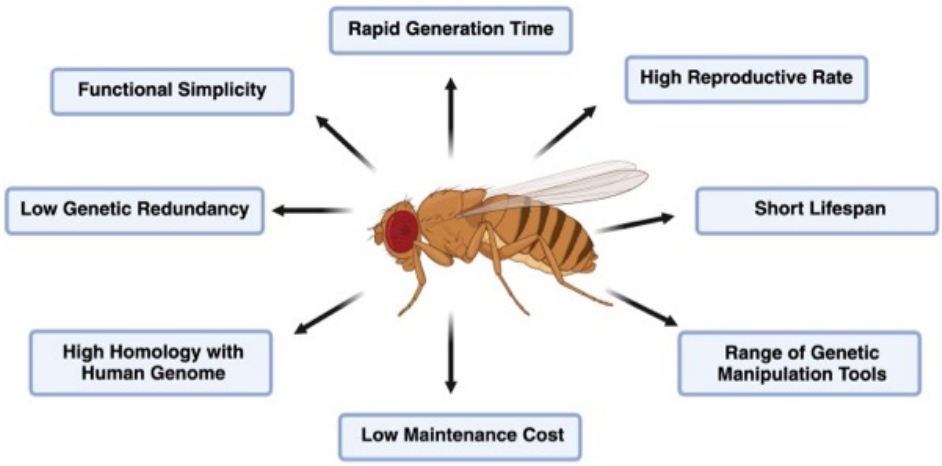

Figure 1.6. The benefits of the use of *Drosophila* as a model organism. Some of the advantages of the use of the fruit fly in research include its compact genome, low genetic redundancy, and functional simplicity, as well as the wide range of genetic manipulation tools available in *Drosophila*. Flies and humans have a ~60% homology between their genomes, with ~75% of genes implicated in human diseases having an ortholog in the fly. All of this makes *Drosophila* a powerful system to study many biological processes *in vivo*.

1.6.1. Genetic manipulation techniques

During its century-long stint as a key model organism in biomedical research, a wide range of genetic manipulation tools for the *Drosophila* genome have become available, making it the key feature of its advantage as a model organism. Many tools allow for the controlled manipulation of gene expression in specific cells and tissues (del Valle-Rodríguez et al., 2012).

The GAL4-UAS system is one of the most widely-used genetic manipulation tools in *Drosophila* research. It is a two-component gene expression system that allows for temporal and spatial regulation of genetic function, and it was developed as a tool for targeted gene expression in *Drosophila* by Brand and Perrimon in 1993 (Brand and Perrimon, 1993). The GAL4 protein was initially identified as a genetic regulator in the yeast *Saccharomyces cerevisiae* (Duffy, 2002), and it was first demonstrated to work in *Drosophila* by Fischer et al. in 1988. In the GAL4/UAS system, the GAL4 transcriptional activator, which is under the control of a cell-type specific promoter, binds its target, Upstream Activator Sequence (UAS), which in turn drives the expression of an RNAi construct, an open reading frame (ORF) of the gene of interest or a reporter gene. Thus, this system allows the overexpression and downregulation of a gene of interest in a specific cell or tissue type. This tool represents the basis of the genetic manipulations that will be used in this project, allowing us to assess the effects that our genes of interest have on ISC homeostasis. Many of these genetically-modified *Drosophila* GAL4 lines are readily available from stock centres, making the GAL4-UAS system the most widely used in *Drosophila* research (Poirier et al., 2008). Therefore, without temporal control to keep gene expression off during development, this could have deleterious effects stopping adult phenotypes from being seen. It is possible to temporally restrict the GAL4 transcriptional activator using the temperature-sensitive Gal80 protein (del Valle-Rodríguez et al., 2012), but some of the enhancers and promoters used in these lines are expressed in multiple developmental stages of the fruit fly, making the lack of temporal control of genetic expression a limitation to consider in the GAL4 system (Poirier et al., 2008). The temperature shifts necessary for this control could also affect intestinal physiology and therefore influence the phenotypes observed as a result of genetic manipulation. Osterwalder and colleagues developed a variation of the GAL4 system that sidesteps this limitation: they demonstrated that the mifepristone-dependent GAL4-progesterone-receptor fusion protein, commonly known as Gene Switch, allows

for tight temporal and spatial controls of transgene expression (Osterwalder et al., 2001) (*Figure 1.7*). In this Gene Switch system, expression of the gene of interest is only driven in the presence of the drug mifespristone (also referred to as RU486 or RU), allowing genetic expression to be induced at specific stages of development or adulthood (McGuire et al., 2004). This Gene Switch system provides an identical genetic background in the control and experimental groups, sidestepping another potential source of variation.

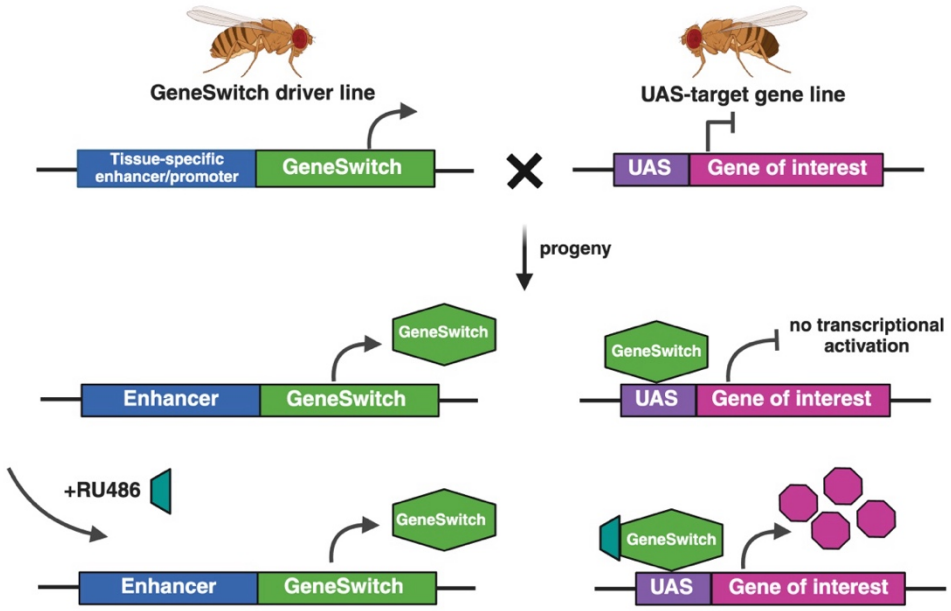

Figure 1.7. The Gene Switch system allows for spatial and temporal control of gene expression. In this variation of the GAL4/UAS system, the GAL4 is under the control of a cell type-specific promoter, which binds to the upstream activator sequence to drive the expression of the gene of interest. However, in this system, expression of the gene of interest is only driven in the presence of the drug mifespristone (RU486 or RU), allowing for genetic expression to be induced at specific stages of development of during adulthood.

Although the GAL4/UAS expression system and its Gene Switch variant represent the basis of the genetic manipulation techniques in *Drosophila*, other genetic manipulation techniques which are relevant to the experimental approaches used in this project include the "Flp-Out" system, the generation of protein traps, CRIMIC lines and the use of GFP-tagged nuclear localization sequences.

The "FLP-OUT" system, developed by Golic and Lindquist in 1989, is a binary system, like Gene Switch, that allows for the temporal and spatial control of genetic expression, but expression of Gal4 is induced by heat-shock rather than addition of a drug

(Phipps et al., 2023). The novel feature of this system is that the UAS promoter also controls the expression of a fluorescent reporter that labels any cells where recombination has occurred, as well as all the clones produced from that cell (Phipps et al., 2023). Using this system, all cells expressing the protein of interest are tagged with fluorescent protein markers, such as green fluorescent protein (GFP) or red fluorescent protein (RFP).

By the start of the 21st century, genetic manipulation of the *Drosophila* genome had yielded three types of gene traps: enhancer traps, promoter traps and gene traps, all relying on the ability of the reporter gene to respond to regulatory sequences at the insertion site (reviewed by Springer, 2000) (*Figure 1.8*). Enhancer traps drive the expression of the reporter gene by activation of the gene promotor by an enhancer; in a promoter trap, the reporter is inserted in an exon and therefore drives transcriptional fusion; and in a gene trap, the reporter is inserted into an intron and transcriptional fusion occurs after gene splicing (reviewed by Springer, 2000). Morin et al. developed a protein trap in *Drosophila* for the first time, in which the full-length endogenous protein is fused with green fluorescent protein (GFP) to allow for the observation of cellular and subcellular protein localization and distribution (Morin et al., 2001). Using this approach, the GFP marker enables the study of protein dynamics within the organism and provides more accurate information than the previously-used enhancer traps. The commercially available antibodies for fly proteins only account for a small proportion of the genes expressed in *Drosophila* (Casas-Vila et al., 2017), and therefore, this protein trap approach allows for the visualization of proteins for which reagents are limited.

The development of CRIMIC (CRISPR-Mediated Integration Cassette) lines by Lee and colleagues in 2018 provided a potent resource to study gene function in *Drosophila*. Here, a construct is inserted into the intron of the gene of interest, maintaining the promoter-specific expression of the Gal4 protein while arresting transcription. Thus, this technique generated powerful lines to study the effect of loss-of-function mutations of fly proteins (Lee et al., 2018). These CRIMIC lines can then be easily converted to express a fluorescent tag (Avellaneda and Schnorrer, 2018).

In eukaryotic cells, transport of proteins from the cytoplasm to the nucleus is mediated by a nuclear localization sequence (NLS) (Böhm et al., 2017). GFP can be translationally fused to a NLS in order to study the expression pattern of the reporter gene (Lyssenko et al., 2007) and determine if its expression is restricted to the nuclear compartment. This technique is useful to elucidate if the expression of a protein of interest is exclusively nuclear or limited to the cytoplasm.

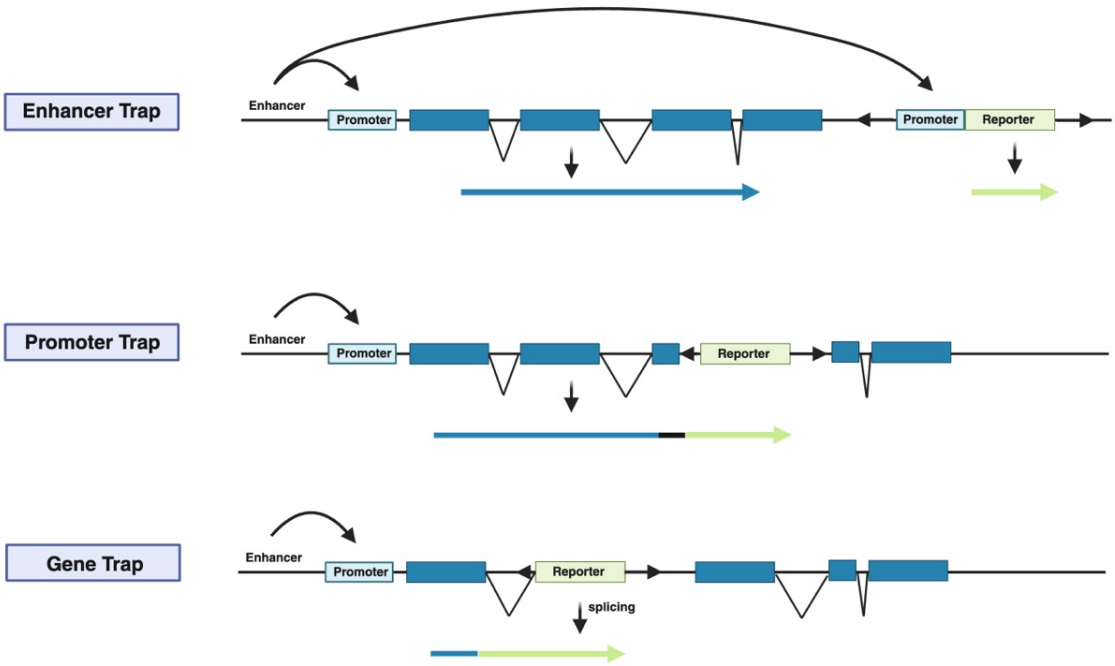

Figure 1.8. Comparison between enhancer traps, promoter traps and gene traps in *Drosophila*. Enhancer traps drive the expression of a reporter gene by the activation of a gene promoter by an enhancer. In promoter traps, the reporter is inserted in an exon and drives transcriptional fusion. And in a gene trap, the reporter is inserted in an intron, and transcriptional fusion occurs after splicing. Figure adapted from Springer, 2000.

1.7. Thesis aims and objectives

Previous work from the Doupé group has identified 49 secreted proteins specifically expressed or enriched in *Drosophila* ISCs and EBs compared to differentiated ECs (Doupé et al., 2018). Using an ortholog predicting tool that compares gene-pair relationships across species, known as DIOPT (Hu et al., 2011), Doupé et al. demonstrated that 29 of these proteins have high-confidence human orthologs. This project aims to characterize the roles of some of these candidate genes of interest and explore their roles in the maintenance of ISC homeostasis and their contributions to the niche, as well as their potential roles in disease development. Considering preliminary data, DIOPT scores and findings from published literature, the strongest candidates that will be the focus of this PhD project include BM-40/SPARC (Basement membrane-40/secreted protein acidic and rich in cysteine), PLOD (procollagen-lysing, 2-oxoglutarate 5 deoxygenase), dlp (Dally-like protein), and TIMP (Tissue inhibitor of metalloproteinases). Previous examples in the literature have demonstrated that these proteins or their orthologs contribute to ISC homeostasis, and that their misregulation

leads to altered tissue structure and function (Godenschewege et al., 2000; Gallet et al., 2008; Wang and Page-McCaw, 2014; Zhu et al., 2016; Shilts and Broadie, 2017; Vaughan et al., 2018; Khetan et al., 2019). SPARC is a calcium-binding protein with a wide range of roles in the tissue, including cell cycle control, cell proliferation, differentiation, migration, adhesion and signalling (Liu et al., 2020; Zhu et al., 2020). Moreover, it plays non-structural roles in the ECM and facilitates the cross-talk between different ECM molecules (Ehninger et al., 2014; Hu et al., 2020), and it has both oncogenic and tumour-suppressor roles in a tissue- and context-dependent manner (reviewed by Ghanemi et al., 2020). PLOD is a collagen-binding protein responsible for the post-translational modifications of collagen and for its correct deposition and distribution across the tissue (Yamada et al., 2019; Zhang et al., 2021), and overexpression of PLOD promotes the acquisition of stem cell phenotypes in tumour cells (Song et al., 2022). Increased levels of TIMP (Tissue Inhibitor of Metalloproteinases) in the midgut of the fly have been shown to correlate with higher proliferation rates of ISCs (Lee et al., 2012), whereas downregulation of GPC4, one of the mammalian orthologs of dlp, facilitates proliferation in tumour cells (Munir et al., 2020), but its roles within the adult midgut have yet to be elucidated.

The two main hypotheses of this project are: (1) that stem cell-secreted factors play key roles in the regulation of stem cell homeostasis, and (2) that understanding the functions of said factors will provide insights into ISC dysregulation in disease, particularly in cancer development. In order to determine the validity of these hypothesis, three main aims have been established:

1. To characterize the mechanism of secreted protein function and their target cell type(s).
2. To characterize the regulation of secreted protein expression.
3. To characterize how the expression of said secreted factors is conserved in human intestinal tissue.

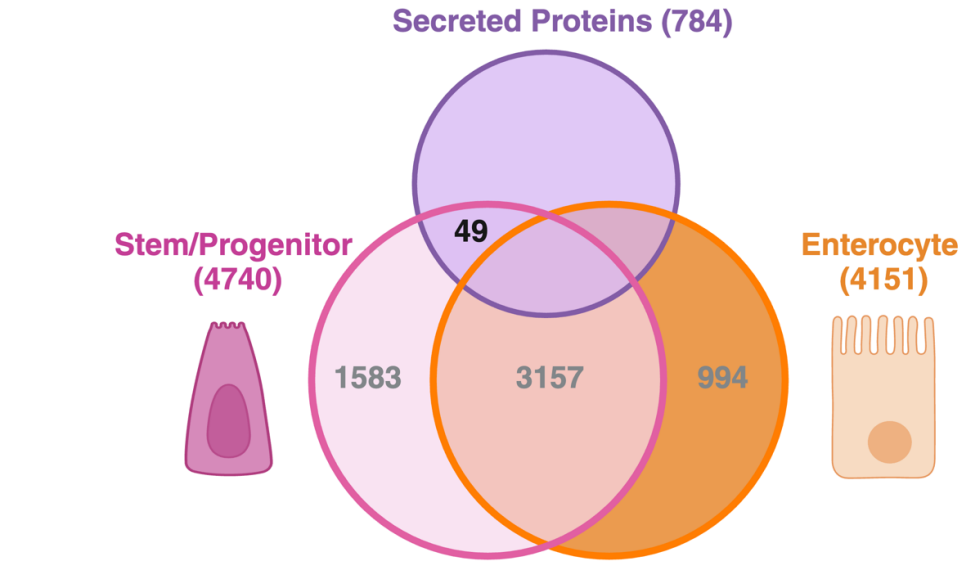

Gene	Description	DIOPT Human	DIOPT 7.1 Score
Tsf2	transferrin2, septate junction assembly	MELTF	15
sli	slit glycoprotein	SLIT3	14
LanB1	laminin	LAMB2	14
dlp	dally-like glypican	GPC4	14
Plod	procollagen lysyl hydroxylase	PLOD3	14
BM-40-SPARC	involved in basal lamina assembly	SPARC	14
gbb	TGFB ligand	BMP7	14
Dl	Delta, Notch ligand	DLL1	13
dally	proteoglycan co-receptor (for FGFs)	GPC5	13
LanA	laminin	LAMA5	12
LanB2	laminin	LAMC1	12
mfas	midline fascilin	TGFBI	12
Timp	tissue inhibitor of metalloproteases	TIMP3	12
Tep4	thioester-containing protein 4, macroglobulin	CD109	11
Npc2a	Nieman Pick gene involved in sterol homeostasis	NPC2	11
magu / pent	secrted protein, binds glypicans, regulates BMP signaling	SMOC2	10
trol	laminin	HSPG2	9
RNaseX25	ribonuclease	RNASET2	9
PGRP-SA	peptidoglycan recognition protein	PGLYRP3	8
brn	braniac	B3GNT6	8
Phm	secretory peptide biosynthesis role	PAM	7
Adgf-A2	adenosine deaminase related growth factor	ADA2	7
CG8642	fibrinogen motifs	FIBCD1	6
BthD	selenoprotein	SELENOH	6
Wnt5	Wnt ligand	WNT5B	5
PGRP-SD	peptidoglycan recognition protein	PGLYRP1	5
egr	eiger, TNF ligand	EDA	5
vn	vein, EGF ligand	NRG2	4
Egm	enigma	ACAD9	3

Figure 1.9. Identification of stem cell-derived secreted proteins through expression profiling. Schematic diagram summarizing the initial screen carried out by Doupé et al., 2018, which identified 49 secreted proteins specifically expressed by the stem and progenitor cells. Using an ortholog predicting tool that compares gene-pair relationships across species, known as DIOPT (Hu et al., 2011) , they were able to identify that 29 of these hits had human orthologs. Adapted from Doupé et al., 2018.

Chapter 2

Materials and Methods

This section outlines all the materials and methods used throughout this study. A full list of reagents can be found in the appendix.

2.1. Fly maintenance

Fly stocks were kept in temperature- and humidity-controlled incubators at 18ºC and on 12-hour light/dark cycles and 60% humidity that allow constant maintenance of circadian rhythms. This helps minimize variabilities in our data. All stocks were flipped onto fresh cornmeal food (See Fly Media section) once every 4 weeks. Some frequently-used stocks were kept at room temperature and flipped onto fresh food every 2 weeks.

2.2. Virgin collection and fly sorting

Appropriate fly lines were expanded, as needed, from stock vials onto bottles to facilitate experimental set up. Virgin females were collected upon eclosion and kept in separate vials until needed. All virgins were used within 96 hours of collection, to ensure flies in each experiment were age-matched.

2.3. Fly genetics and husbandry

A complete list of all the *Drosophila* stock lines used in this study can be found in Table 1.

Crosses were set up in vials containing 15-20 female virgin flies of the driver line and 7-10 males of the target gene line, maintaining a consistent ratio of 2:1 female:male. All crosses with the Gene Switch driver line were set up at 25°C and flies were allowed to mate for 3-4 days before the parents were cleared. The first progeny was collected on day 10, with a second progeny collection 48-72h later. Both sets of progeny were kept in separate vials and allowed to age for one week before dissection. Thus, all flies used in this study are age matched within 72 hours.

Temperature-inducible experiments with the TubGal80^{TS} driver line were set up at 18°C and the flies were allowed to mate for 5-7 days prior to clearing parents. The first progeny collection was done at day 18, with a second collection on day 21. Flies were then allowed to age for 7 days and then moved to a 29°C incubator for a further 7 days in order to allow for the induction of expression of the genes of interest. Therefore, for temperature-sensitive experiments, flies were dissected at age 14-17 days.

2.4. Lifespan Analysis

For lifespan survival curves, experimental set up was carried out at 25°C. For each lifespan, 10 control vials and 10 experimental vials were set up. If the target line contained genetic balancers, an extra 25% of vials, i.e. 25 vials, were set up to ensure enough progeny. Pupae eclosion occurred after 10 days, and flies were collected in 4ml food vials around 12 days after experimental set up. Upon collection, 30 female flies were sorted into each vial, with 10 vials for the control and another 10 vials for the experimental set up, making n = 300 for each condition. All flies were age-matched to ensure reliability of the results. Flies were flipped 3 times a week (Monday/Wednesday/Friday) onto fresh food and deaths were recorded. Censored flies include any dead flies accidentally transferred over, or any flies that escaped or got stuck on the food during the flipping process.

2.5. Fly media

2.5.1. Standard cornmeal media

Standard cornmeal media contained: 1% agar, 3% yeast, 1.9% sucrose, 3.8% dextrose and 9.1% cornmeal, in 90% distilled water to make up the final volume. 10% Nipagin dissolved in ethanol and an acid mix were added at the end. The acid mix is made up of 0.8M phosphoric acid and 5.6M propionic acid, e.g. 1000ml of acid mix contains 41.5ml of phosphoric acid and 418ml of propionic acid in distilled water.

All dry ingredients were carefully weighed and mixed together, along with the water, and heated in a microwave, at full power (800W). The mixture was taken out every 30 seconds and stirred until dense. The 10% Nipagin and the acid mix, stored separately in appropriate chemical storage cupboards, were then added to the mixture in the fume hood, and the entire mixture was thoroughly stirred before individually pipetting the appropriate amount of food into each vial or bottle. Vials contained either 4ml (for short term use in lifespans) or 8ml of food (for crosses and stocks) and bottles contained 75ml.

All products used in this procedure were kept at room temperature, with the nipagen and acid mix kept in their appropriate safety cupboards.

A list of reagents used can be found at the end of this section in Table 2.

2.5.2. Mifepristone media

The preparation process for food containing mifespristone (or RU486) is as stated above for standard cornmeal media, with the addition of the drug at the end of the cooking process, after the acid mix and Nipagin. From here onwards, this will be referred to as RU food. The mixture must be allowed to cool down slightly prior to addition of mifepristone. 250µl of RU486 (20mg/ml stock solution in ethanol) were added per 1000ml of food; ethanol was used as the control in the same proportion as mifepristone, and both mixtures are referred to as RU50 and RU0 (Control), respectively. Mifepristone and ethanol are stored at -20°C.

2.6. *Drosophila* samples

2.6.1. Immunofluorescence of *Drosophila* samples

Guts were dissected with fine forceps in 9-well glass spot-plates containing 150ul of Phosphate Buffered Saline (PBS) per well. Dissection plates and PBS were kept at 4ºC and put on ice prior to dissection. Guts were then fixed in 4% paraformaldehyde (PFA) at room temperature for 30 minutes. The dissection plates were covered with parafilm to prevent evaporation and aluminum foil to prevent evaporation and to diminish light exposure of the samples, and placed on a shaker for fixation. Samples were washed in PBS 3 times and blocked in 0.5% Triton X-100, 0.5% BSA, 5% NGS in PBS for a further 30 minutes. Guts were then placed in a shaker and incubated overnight in a cold room at 2ºC with primary antibodies diluted in PBS 0.5% Triton X-100. Samples were washed 3 times in PBS for 10 minutes before a 2-hour incubation in the corresponding secondary antibody, diluted in PBS 0.5% Triton X-100 to make a final concentration of 1:500. DAPI staining was carried out for 10 minutes before a final washing step (3 10-minute washes in PBS) of the samples prior to mounting. Guts were mounted on a microscope slide in Vectashield mounting medium and coverslips were sealed using commercial nail polish. All slides were stored in a dark box at 4ºC.

Blocking buffer was made by mixing 50mg of Bovine Serum Albumin (BSA) and 50ul of Triton X-100 to 10ml of PBS. This mixture can be stored at 4ºC for up to 2 weeks. The necessary volume of blocking buffer is aliquoted before each use and 5% Normal goat serum (NGS) (50ul for 1ml of blocking buffer) is added to it.

In the cases where α-phospho-MAPK, α-phospho-SMAD and α-phospho-SAPK/JNK antibodies were used, PhosSTOP (inhibitor tablets of phosphatase) was added to the PBS during dissections, the blocking buffer and the primary antibody dilution at a concentration of 1:10.

A list of antibodies used can be found at the end of this section in Table 3.

2.6.2. RNA extraction and cDNA synthesis from *Drosophila* samples

Initially, isolation of RNA from samples for qRT-PCR was carried out using TRIZol reagent. 10 whole guts per sample were dissected and transferred to 100µl of

TRIzol for homogenization for 10 minutes at room temperature (RT). At this stage, samples were either stored at -80ºC or continued directly to phase separation at a later stage. If starting with a frozen sample, they were left at RT for 10 minutes before adding 20µl of chloroform. The samples were left to incubate at RT for 3 minutes and were then spun at 12000g in a pre-cooled centrifuged at 4ºC for 15 minutes. 45µl of the aqueous phase after centrifugation were transferred to a clean Eppendorf tube, where 4.5µl of 3M sodium acetate (10% volume, RNA grade) and 2µl 20mg/ml Glycogen (RNA grade) were added to the aqueous phase, with vigorous mixing between steps. The samples were left at RT for 10 minutes and then spun once again at 12000g at 4ºC for 5 minutes. The resulting supernatant was then removed and 200µl of 75% ethanol (RNA grade) were added to resuspend the pellet before being centrifuged for a further 5 minutes. At this stage, samples can be stored at -80°C.

For cDNA synthesis, samples were spun for 5 minutes at 12000g and 4°C, the supernatant was removed, and the pellet was allowed to air dry for about 5 minutes. 20µl of distilled water were added to the pellet, with gentle pipette mixing and samples were heated at 55ºC for 10 minutes. 8.5µl of RNA were then transferred to a clean labelled Eppendorf and 1µl of DNase buffer and 0.5µl of DNase I were added to make a 10µl reaction. Samples were then incubated at 37°C for 30 minutes, followed by the addition of 0.5µl of EDTA (1U/µl) and a further 10-minute incubation at 65ºC. After a brief spin, 1µl of 20X random hexamer primers was added. After a 5-minute incubation at 70ºC, samples were immediate cooled on ice and spun down, before adding 9µl of master mix. This master mix contains 4µl of 5X first strand buffer, 0.5µl of RIbolock RNase inhibitor, 2µl of 10nM dNTPs, 0.2µl of reverse transcriptase and 2.3µl of ddH2O per sample. Samples were then incubated at room temperature for 10 minutes, at 37ºC for 1 hour and at 70ºC for 10 minutes. All undiluted and diluted samples were kept at -20°C.

To optimize qRT-PCR conditions, the primers used were tested beforehand, to validate their sensitivity and to exclude the possibility of primer dimer formation. Standard curve and melt curve analysis were used to determine the specificity of the primers (data not shown).

Because of the variability in some results, commercial RNA extraction and cDNA synthesis kits were used for the final year of this project to see if this would increase the reliability of the data. The Monarch® Total RNA Miniprep Kit from NEB and

UltraScript™ 2.0 cDNA Synthesis Kit from PCR Biosystems were used, following the protocols as specified by the companies.

2.6.3. qRT-PCR (quantitative reverse transcriptase polymerase chain reaction) of *Drosophila* samples

qRT-PRCs were run using a CFX Connect Real-Time PCR Detection System from Bio-Rad Laboratories. Samples were loaded onto MicroAmp® Fast 96-Well reaction plates, with each well containing 1μl of the sample, 5μl of Power SYBR™ Green PCR Master Mix and 3.5μl of ddH_2O, and the plate was tightly sealed using and optically clear adhesive seal sheets. Cycle conditions were as follows: 95ºC for 10 minutes, and 40 cycles of 95ºC for 15 seconds followed by 60ºC for 60 seconds. Gene expression was calculated using two different methods, depending on the intended purpose of the analysis. ΔΔCT method or Sq value analysis. All expression results were normalized against a housekeeping gene and standards were run alongside each sample to validate primer function. The primer sequences can be found at the end of this chapter in Table 4.

2.6.4. Sample preparation for transmission electron microscopy (TEM) of *Drosophila* samples

Whole *Drosophila* guts were dissected in PBS and transferred directly to 4% formaldehyde in 0.1M sodium cacodylate buffer for 15-30 minutes on ice. Guts were then transferred to Karnovsky's fix (3% glutaraldehyde and 2% formaldehyde in 0.1M sodium cacodylate buffer) for 20-120 minutes at 4ºC, followed by 3-5 10-minute washes in 0.1M sodium cacodylate buffer to wash out Karnovsky's fixative solution. Samples were transferred to 2% osmium tetroxide in 0.1M sodium cacodylate buffer for 1-2 hours at 4ºC. Guts were then dehydrated through an ethanol series: 30% ethanol, 50% ethanol, 70% ethanol, 80% ethanol, 90% ethanol and 95% ethanol, for 5-10 minutes in each at 4ºC. For the final step of sample dehydration, samples were placed in 100% ethanol for 10 minutes at room temperature, and repeated 3 times before being transferred to propylene oxide for 15 minutes and repeated twice. A mix of agar 100 resin was prepared in the fume hood, and samples were transferred to a series of propylene oxide:agar 100 resine mixture at different concentrations: first, on a 3:1 ratio for 1-2 hours, followed by

a 1:1 ratio for 1-2 hours, 1:3 ratio for 2-10 hours, and finally transferred to pure agar 100 resin for 2-5 hours. Samples were then left in a 60ºC oven for 3 days. The polymerized resin blocks were taken out of the oven, trimmed and thin sections were made using a Leica ARTOS 3D ultra-microtome. These sections were placed on 200-mesh copper grids and stained with 3% uranyl acetate in aqueous solution. Samples were then washed with MQ water before staining with lead citrate and washed again. Samples were left to dry before visualizing them by TEM.

In order to optimize the protocol and increase the quality of the sample images, an alternative dissection and fixation method was used on one of the samples for comparison. In this instance, anesthetized flies had their heads and rear-ends removed with a razor blade and the whole thorax was immediately transferred to 4% paraformaldehyde solution on ice for 30 minutes to fix the tissue. Karnovsky's fix was then added for 20-30 minutes and samples were washed 3 times in 0.1M cacodylate buffer for 3 minutes, before the guts were extracted. The dissected guts were then transferred to Karnovsky's fix again and the protocol was followed as stated above. This was done in order to prevent separation of cells within the tissue at the point of dissection, improving the preservation of tissue structure.

2.6.5. Imaging of IF *Drosophila* samples

Immunofluorescence samples were observed using a Leica SP5 confocal laser scanning microscope with fluorescence live-imaging microscopy (FLIM) and fluorescence cross-correlation microscopy (FCCS). Z-stacks of the stained midguts were taken using the 63x oil lens with the zoom factor set to 1, keeping the acquisition and laser characteristics consistent across all samples for each experiment. Slice thickness was 0.8μm.

2.6.6. Data analysis of *Drosophila* samples

Confocal data was analyzed using ImageJ. Z-stacks were converted into single maximum projected images for further analysis and cell counts were performed with the Cell Counter plug-in. For the Z-stacks of the stained guts, the maximum intensity image was used to perform cell counts.

Quantitative and statistical analysis was performed using Prism10 (GraphPad), and all graphs were created using this same software. Data sets were analyzed to identify outliers, and normality tests were performed on the clean data to determine the appropriate statistical test. Normality was analyzed using the Shapiro-Wilk test for data sets of <40 data points, and the Kolmogorov-Smirnov test for data sets with >40 data points. For normally distributed data, unpaired t-tests were used, whereas if the data was did not present a normal distribution, a Mann-Whitney U test was performed. The statistical analysis used in each instance is stated in the corresponding figure legends. Results were deemed statistically significant if $p < 0.05$. Statistical significance is represented using the following symbols: * if $p \leq 0.05$; ** if $p \leq 0.01$; *** if $p \leq 0.001$; and **** if $p \leq 0.0001$. Not significant (ns) pairwise comparisons were only added to those graphs were, at first instance, the trends might suggest a significant change. Graphs with no pairwise comparisons are not statistically significant. Data points represent individual guts, and all the individual values presented for DAPI, GFP and prospero counts represent the mean number of cells observed per field of view. To determine mitotic activity, whole-gut PH3 counts were performed for accurate quantification of mitoses as the quantification per FOV was too low for robust scoring. Each experiment consists of a minimum of 3 independent replicates with each replicate consisting of at least 5 guts.

All images presented in the introduction of this thesis were made using BioRender.

2.6.7. Validation of the Gene Switch stock line

Initial experiments focused on validating the 5961-Gene Switch (*5961^{GS}*) driver line to confirm that: (1) in the absence of the RU486 drug there is no expression of the responder gene; (2) that addition of RU486 to the food induces gene expression; and (3) that the induced expression is in stem and progenitor cells. To do this, 596^{GS} female virgins were crossed to males carrying an enhanced green fluorescent protein, eGFP, downstream of Gal4-UAS sites. Addition of the RU468 drug induced expression of GFP in the small nuclei of the *Drosophila* gut representing ISCs and EBs, whereas control guts treated with EtOH did not show any GFP expression (*Figure 2.1*). This difference in GFP expression between RU-treated and untreated guts was statistically significant (*Figure 2.1B*), thus proving that the Gene Switch system is working adequately in the 5961^{GS} line.

There was no significant change in the total number of cells observed per field of view between the control and RU- treated guts (*Figure 2.1B*), which indicates that addition of the drug does not have a significant effect on gut tissue and structure. This simple experiment provided robust data about the reliability of this line, so that inadequate expression or inconsistencies in future experiments cannot be attributed to incorrect induction of gene expression.

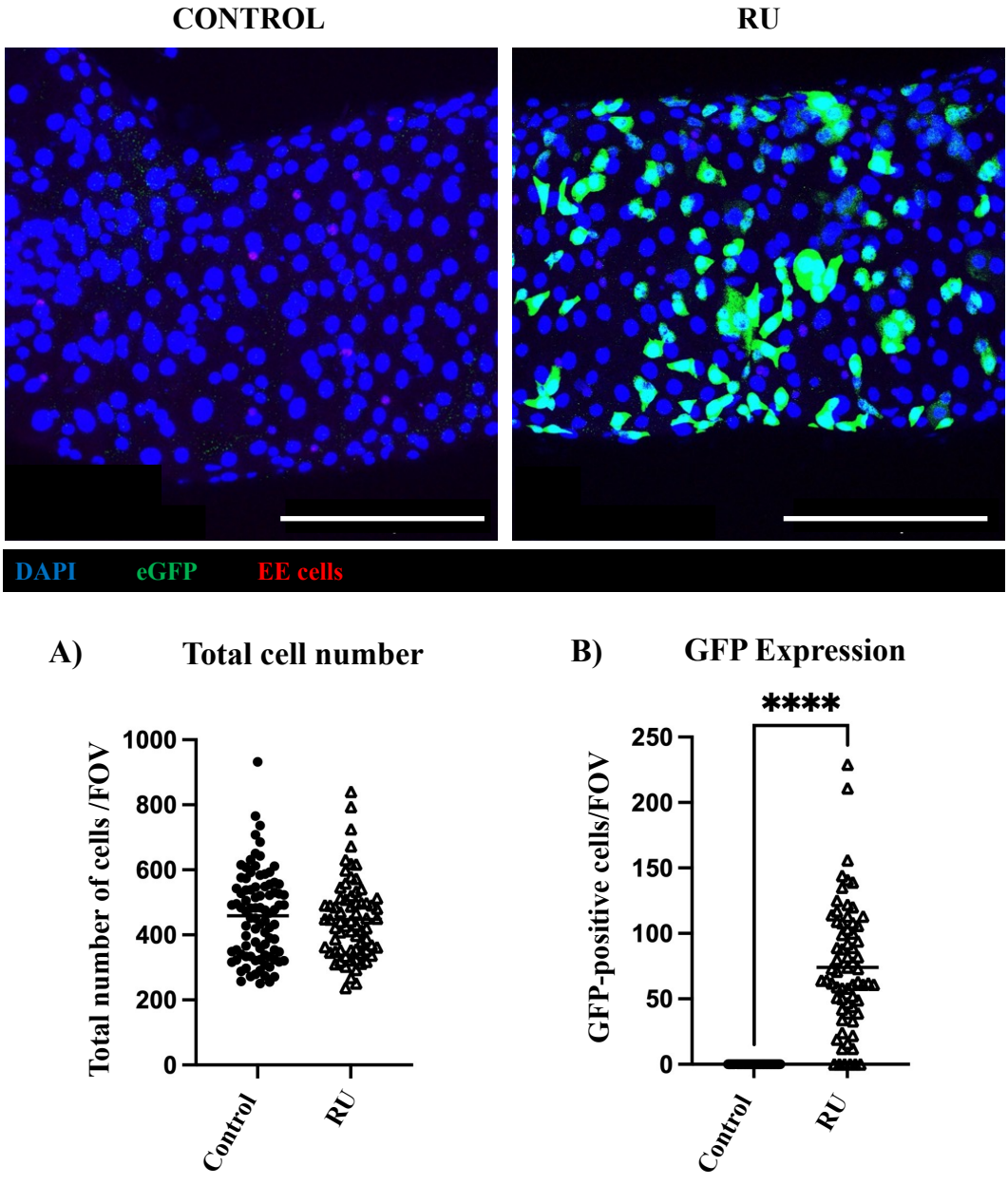

Figure 2.1. Validation of the GeneSwitch (5961^{GS}) driver line. *5961^{GS} > UAS eGFP* female fly midguts were dissected and stained with α-prospero (1:100), α-GFP (1:2000) and DAPI. Results demonstrate that the addition of the mifesprisone drug (RU) induces responder gene expression and does not affect the morphology of the posterior midgut. This is proven by the statistically significant increase in GFP expression in RU-positive guts compared to control guts ($p < 0.0001$) and the lack of GFP expression in RU-negative guts (control). Scale bars in the bottom right corner represent 100μm.

2.7. Mammalian Samples

2.7.1. Cell culture

Human induced pluripotent stem cells (iPSCs) were cultured for spheroid formation. The generation of iPSCs is described in Hepburn et al., 2020. Cells were treated with dissociation media to break down the colonies and generate a single cell suspension. Cells were centrifuged at 300g for 5 minutes, the supernatant was discarded and ROCK inhibitor (10ug/ml) was added to prevent apoptosis. 10ul of Triton-blue were added to visualize dead cells and calculate the concentration of cells in the suspension. Calculations were done to work out the volume of cell suspension to be added to the media so that an average of 1000 cells were plated in each well. ROCK inhibitor was also added at this stage, alongside the cell media and the cell suspension to further ensure cell survival. 100ul of the iPSC mix were added in each well and the plate was centrifuged at 300g for 10 minutes. For spheroid formation, round bottom wells were used to prevent cellular attachment to the bottom of the well and facilitate spheroid formation. The plate containing the iPSCs was then incubated overnight at 37ºC. Spheroids formed overnight and were treated with Activin A (100ng/ml) to drive definite endoderm differentiation, as well as B27, and this was diluted in RPMI 1640 media. 50ul of media were removed from each well containing a formed spheroid, and 100ul of treatment were added. This is considered day 0. For the control, 100ul of the stem cell-specific mTesR media were used. Spheroids were then left to incubate at 37ºC and samples were taken on day 1, 3 and 5. All samples were processed for qPCR, immunofluorescence (IF) analysis and immunohistochemistry (IHC).

2.7.2. Immunohistochemistry of hiPSC spheroid and human tissue samples

Formalin-fixed paraffin embedded (FFPE) tissues slides of human samples were prepared for immunohistochemistry (IHC). All surgical specimens were collected according to local ethical and regulatory guidelines and included written, informed patient consent (Newcastle REC 2003/11 and Human Tissue Authority License 12 534, Freeman Hospital, Newcastle upon Tyne, United Kingdom). Tissue sections of 3 separate samples were prepared: a non-cancerous sample (#11972) and two cancerous samples of localized prostate cancer (#12782 and #12910). Coated slides were baked at 50ºC overnight to

remove any moisture in the samples. De-paraffinisation of samples was done by placing the slides in xylene for 5 minutes and then dipping them in the same chemical 15 times. Samples were then hydrated by dipping them in a series of different ethanol concentrations (100% > 95% > 70% > 50%) and rinsed in running tap water. Antigen retrieval was carried out using a decloaking chamber and using a citrate retrieval solution. Dewaxed and dehydrated samples were placed in the retrieval solution in the decloaking chamber until it reached a temperature of 121ºC. Slides were immediately placed in cool running water before being transferred to a 3% H_2O_2 solution for 10 minutes to remove any endogenous peroxidise activity. Any excess peroxide solution was removed and slides were rinsed in running tap water for 5 minutes and placed into TBS/Tween. The outline of the tissue sections was marked using a hydrophobic marker and slides were placed in a slide tray lined with damp tissue, to prevent them from drying out. Tissue sections were covered in anti-mouse or anti-rabbit serum (depending on the species the secondary antibody was raised in) and left for 20 minutes. Samples were rinsed in running water for 5 minutes and placed in TBS/Tween. 100ul of the appropriate primary antibody diluted in TBS were added to cover the sample and slides were left to incubate overnight at 4ºC. After incubation with primary antibody, slides were washed in TBS/Tween twice for 5 minutes and anti-rabbit IgG or anti-mouse IgG was applied for 30 minutes at room temperature. Slides were then rinsed in running tap water for 5 minutes and placed in TBS/Tween. In the fume hood, a DAB solution was prepared adding 1 drop of chromogen to 1ml of DAB diluent, and added to the slides, covering the entire tissue section, and left to incubate for 5 minutes. Any excess DAB was tipped into sodium hypochlorite solution to neutralise and slides were rinsed in running tap water for 5 minutes. Tissue sections were counter-stained using Gills II Haematoxylin for 15 seconds, slides were rinsed in running tap water until this runs clear and then placed in blue in Scotts tap-water for 30 seconds. A final dehydration step was carried out, where slides were placed in a series of ethanol concentrations, in increasing order (50% > 70% > 95% > 100%), followed by 3 separate dips in xylene. The slides were left in xylene until they were ready to mount. Mounting was carried out in the fume hood, using a Pasteur pipette to apply DPX to an appropriate-size coverslip. Tissue slides were removed from the xylene solution and any excess was removed using tissue paper. Slides were carefully placed onto the coverslip, face down, to avoid the formation of air bubbles. Slides were left to dry overnight before scanning them in an Aperio Virtual Pathology System (Leica BioSystems). Images obtained were then analyzed using the Aperio ImageScope software system.

2.7.3. Immunofluorescence of spheroid and human tissue samples

FFPE tissue sections of spheroid samples were dewaxed and dehydrated, and antigen retrieval was carried out as stated in the immunohistochemistry section. Sections were then rinsed in PBS for 5 minutes, in PBS containing 0.5% Triton X-100 for 30 minutes, and a further 5 minutes in PBS in order to permeabilize the tissue. Slides were dried by dabbing into tissue paper and, using a hydrophobic marker, an area was drawn around the sections. These sections were blocked in PBS containing 0.5% BSA, 0.5% Triton X-100 and 5% NGS for 30 minutes before adding the primary antibody at the appropriate concentration. All antibodies and reagents are diluted in PBS + 0.5% Triton X-100. Slides were left to incubate with the primary antibody overnight at 4ºC in a dark room. All incubation times from this point onwards were carried out in the dark to preserve the fluorescence. Tissue sections were washed in PBS three times for 10 minutes to get rid of any excess antibody before adding the secondary antibody raised against the appropriate species. This was left to incubate at room temperature for 2 hours and DAPI was added for 10 minutes. Three final PBS washes were done and slides were mounted using Vectashield mounting medium. They were left to dry overnight before imaging them using a Leica MD6 microscope.

The list of antibodies used can be found at the end of this chapter in Table 3.

2.7.4. Imaging of IF and IHC spheroid and human tissue samples

Immunohistochemistry images were analyzed using the Aperio ImageScope software (v.12.4.6.5003). Immunofluorescence samples were imaged using the Leica SP5 confocal laser scanning microscope with fluorescence live-imaging microscopy (FLIM) and fluorescence cross-correlation microscopy (FCCS) at Durham University. No data from the immunofluorescence experiments was available for analysis due to a technical issues during sample preparation.

2.7.5. RNA extraction and cDNA synthesis of spheroid samples

RNA extraction of spheroid samples was done using the GenElute^{TM} Mammalian Total RNA Miniprep Kit (RTN350) from Sigma Aldrich. The protocol followed was as

stated by the manufacturer, and samples were stored at -80°C. cDNA synthesis was kindly carried out by Dr. Adriana Buskin at Newcastle University and cDNA.

2.7.6. RT-qPCR of spheroid samples

Samples were analyzed using RT-qPCR analysis to determine the expression levels of the genes of interest in a mammalian in vitro system. cDNA from LNCaP cells (kindly gifted by Prof. Craig Robson), which show high expression of all four genes of interest, was used to test the primers beforehand. RT-qPRCs were run using a CFX Connect Real-Time PCR Detection System from Bio-Rad Laboratories. Plate preparation and cycle conditions were as stated for *Drosophila* samples. Gene expression was calculated using the ΔΔCT method. All expression results were normalized against the housekeeping gene RPL13a and LNCaP cell samples were run alongside each spheroid sample to validate primer function. The primer sequences can be found at the end of this chapter in Table 6.

2.7.7. Statistical analysis of mammalian samples

Quantitative and statistical analysis was performed using Prism10 (GraphPad), and all graphs were created using this same software. Data sets were analyzed to identify outliers, and normality tests were performed on the clean data to determine the appropriate statistical test. Normality was analyzed using the Shapiro-Wilk test for data sets of <40 data points, and the Kolmogorov-Smirnov test for data sets with >40 data points. For normally distributed data, unpaired t-tests were used, whereas if the data was did not present a normal distribution, a Mann-Whitney U test was performed. The statistical analysis used in each instance is stated in the corresponding figure legends. Results were deemed statistically significant if $p < 0.05$. Statistical significance is represented using the following symbols: * if $p \leq 0.05$; ** if $p \leq 0.01$; *** if $p \leq 0.001$; and **** if $p \leq 0.0001$. Not significant (ns) pairwise comparisons were only added to those graphs were, at first instance, the trends might suggest a significant change. Graphs with no pairwise comparisons are not statistically significant.

Table 1. List of *Drosophila* stocks.

Line	Stock Centre & Number	Genotype
UAS-eGFP	BDSC_6874	*w[*]; P{w[+mC]=UAS-2xEGFP}AH2*
UAS-RasV12	BDSC_64195	*w[*]; P{w[+mC]=UAS-Ras85D.V12}TL1*
UAS-yki.28816	BDSC_28816	*y[1] w[*]; P{w[+mC]=UAS-yki.S168A.GFP.HA}10-7-Y*
UAS-yki.28817	BDSC_28817	*w[*]; P{y[+t7.7] w[+mC]=UAS-yki.S111A.S168A.S250A.V5}attP2*
UAS-yki.28818	BDSC_28818	*w[*]; P{y[+t7.7] w[+mC]=UAS-yki.S168A.V5}attP2*
vkg::GFP	BDSC_98343	*y[1] w[*]; P{w[+mC]=PTT-un}vkg[G00454]*
UAS-dlp	BDSC_9160	*w[1118]; P{w[+mC]=UAS-dlp.WT}3*
UAS-dlp-RNAi 34089	BDSC_34089	*y[1] sc[*] v[1] sev[21]; P{y[+t7.7] v[+t1.8]=TRiP.HMS00875}attP2*
UAS-dlp-RNAi 34091	BDSC_34091	*No longer available on BDSC*
UAS-dlp-RNAi 50540	BDSC_50540	*y[1] v[1]; P{y[+t7.7] v[+t1.8]=TRiP.GLC01658}attP40*
UAS-dlp-RNAi	VDRC_10299	*w; dlp^{RNAi}*
dlp Mi{MIC}	BDSC_60540	*y[1] w[*]; Mi{PT-GFSTF.1}dlp[MI04217-GFSTF.1]/TM3, Sb[1] Ser[1]*
UAS-Timp 58707	BDSC_58707	*P{w[+mC]=UAS-Timp.P}1, w[*]*
UAS-Timp58708	BDSC_58708	*w[*]; P{w[+mC]=UAS-Timp.P}3*
UAS-Timp-RNAi 61294	BDSC_61294	*y[1] v[1]; P{y[+t7.7] v[+t1.8]=TRiP.HMJ23126}attP40*
UAS-Timp-RNAi	VDRC_15372	*w; $TIMP^{RNAi}$*
UAS-SPARC 77924	BDSC_77924	*y[1] w[*]; P{w[+mC]=UASp-SPARC.HA}2/CyO*
UAS-SPARC-RNAi 40885	BDSC_40885	*y[1] v[1]; P{y[+t7.7] v[+t1.8]=TRiP.HMS02133}attP40*
UAS-SPARC RNAi 16677	VDRC_16677	*w; $SPARC^{RNAi}$*
SPARC GFP FlyFos	VDRC_318015	*FlyFos016090(pRedFlp-Hgr)(BM-40-SPARC[36820]::2XTY1-SGFP-V5-preTEV-BLRP-3XFLAG)dFRT*
SPARC GT-GAL4	BDSC_77473	*y[1] w[*]; Mi{GT-GAL4}SPARC[MI00329-GAL4]/TM6B, Tb[1]*
UAS-PLOD-RNAi 67935	BDSC_67935	*y[1] sc[*] v[1] sev[21]; P{y[+t7.7] v[+t1.8]=TRiP.HMS05720}attP40/CyO*
UAS-PLOD-RNAi 34911	BDSC_34911	*y[1] sc[*] v[1] sev[21]; P{y[+t7.7] v[+t1.8]=TRiP.HMS01259}attP2*
UAS-PLOD-RNAi 45484	VDRC_45484	*w; $PLOD^{RNAi}$*
PLOD Gal4 CRIMIC	BDSC_79241	*y[1] w[*]; TI{GFP[3xP3.cLa]=CRIMIC.TG4.2}Plod[CR00348-TG4.2]/TM3, Sb[1] Ser[1]*
UAS vkg RNAi	BDSC_50895	*y[1] v[1]; P{y[+t7.7] v[+t1.8]=TRiP.HMC02400}attP2*
Vkg Gal4 CRIMIC	BDSC_83258	*y[1] w[*]; TI{GFP[3xP3.cLa]=CRIMIC.TG4.0}vkg[CR01302-TG4.0]*
UAS Upd3	From Bruce Edgar Lab	*w;UAS-Upd3*
UAS-GFP-nls 4775	BDSC_4775	*w[1118]; P{w[+mC]=UAS-GFP.nls}14*

UAS-GFP-nls 4776	BDSC_4776	*w[1118]; P{w[+mC]=UAS-GFP.nls}8*
TubGal80^{TS}		*y w; tub-Gal80^{ts}; tub-Gal4/TM6B*
5961 GeneSwitch	5961	*5961-GeneSwitch-Gal4*
esgTSFlip		*esg^{TS}-GFP-Flp-Out*
ProsG4TS	FJ332	*w;tub-Gal80ts;UAS-GFP/Cyo,wgLacZ;Prosv1-Gal4/TM6B*
esgLacZ	K6D6	*esgLacZ*
Su(H)LacZ		*Su(H)LacZ*
DlLacZ		If/Cyo;DlLacZ
Luciferase	31603	*y[1] v[1]; P{y[+t7.7] v[+t1.8]=TRiP.JF01355}attP2*
CantonS		wild-type

Table 2. List of reagents.

Product	Supplier	Catalog Number
Phosphate Buffered Saline Tablets 0.01M	Fisher Bioreagents	BP2944100
Bovine Serum Albumin	Fisher Scientific	BP-1600-100
Trizol™ Reagent (Ref: 15596026)	ThermoFisher	15596026
Vectashield Antifade Mounting Medim	2BScientific	H-1000
Triton X-100	Sigma Aldrich	9002-93-1
Apex Drosophila Agar Type II (pH = 6.13)	SLS	#AN-171047,
Inactive Dry Yeast)	SLS	FLY#62-106
Sucrose Crystallized	Duchefa Biochemie	S0809.5000
D-(+)-Glucose Anhydrous (MW = 180.16)	Melford	G32040, Lot. 42613-42844
Cornmeal Yellow	SLS	FLY#62-100
Mifepristone – Cayman Chemicals	Cambridge Bioscience	CAY10006317
Phosphoric acid	VWR	20624.262
Propionic acid	Sigma	P5561
Nipagin	SLS	FLY1136
Dextran Sulfate Sodium (DSS) Salt Colitis Grade (36,000 to 50,000)	MP Biomedicals	0216011010
D-Sucrose	Fisher Bioreagents	BP220-1, Lot. 215025
MicroAmp® Fast 96-Well Reaction Plate (0.1mL)	Life Technologies	4346907
Optically Clear Adhesive Seal Sheets	ThermoFisher Scientific	AB-1170
Grace's Insect Medium (1X) Unsupplemented	Gibco	11595-030
Schneider's Drosophila Medium (1X)	Gibco	21720-024
Water (for RNA work), DEPC-treated and nuclease free, autoclave	Fisher Bioreagents	BP561-1, Lot. 207040
Chlorophorm	Sigma	C0549
RNA grade Isopropanol	Sigma	I9516
Sodium acetate solution (3M, pH5.2)	Thermofisher	R1181
Glycogen, RNA grade (20mg/mL)	Thermofisher	R0551
Ethanol (75%, RNA grade)	Sigma	51976
DNase buffer	Thermofisher	EN0521
DNase I, RNase free (1U/μl)	Thermofisher	EN0521
EDTA	Thermofisher	EN0521
Random Hexamer Primers	Thermofisher	SO142

5X First Strand Buffer	Thermofisher	EPO442
ThermoScientific™ RIbolock RNase Inhibitor	Thermofisher	EO0382
dNTP Set 100mM Solutions	Thermofisher	R0181
ThermoScientific™ RevertAid™ Reverse transcriptase	Thermofisher	EPO442
Power SYBR™ Green PCR Master Mix	Fisher	10219284
Paraformaldehyde (PFA), 16%, 2x10mL	Fisher	11490570
Normal Goat Serum (NGS), 2mL	Gibco	PCN5000
Invitrogen™ DAPI (4',6- Diamidino-2-Phenylindole, Dihydrochloride)	Fisher Scientific	10184322
PhoSTOP™	Merck Life Science	4906837001
Parafilm M Sealing Film	SLS	FIL1024
KITS		
UltraScript 2.0 cDNA synthesis kit	PCR BioSystems	PB30.31-10
Monarch® Total RNA Miniprep Kit	New England Biosystems	T2010S
ImmPRESS[R] HRP Horse Anti-Mouse IgG Polymer Detection Kit, Peroxidase	2bScientific	MP-7402-15ML
ImmPRESS[R] HRP Horse Anti-Rabbit IgG Polymer Detection Kit, Peroxidase	2bScientific	MP-7401-50ML

Table 3. List of antibodies.

Type	Species	Antibody	Concentration	Supplier	Reference
Primary					
Primary	*Drosophila*	Anti-prospero Mouse IgG Monoclonal Antibody	1:100	Developmental Studies Hybridoma Bank (DSHB)	MR1A
Primary	*Drosophila*	Anti-phospho-histone-H3 (Ser10), Mitosis Marker Rabbit Polyclonal Antibody	1:1000	Merck Life Science	06-570
Primary	*Drosophila*	Anti-Green Fluorescent Protein (GFP) Chicken IgY Polyclonal Antibody	1:2000	Abcam	ab13970
Primary	*Drosophila*	Anti-β-galactosidase rabbit IgG Polyclonal Antibody	1:500	Invitrogen	A11132
Primary	*Drosophila*	Anti-Dally-like protein (Dlp) (13G8) mouse IgG Monoclonal Antibody	1:5	Developmental Studies Hybridoma Bank (DSHB)	
Primary	*Drosophila*	Anti-Phospho-SAPK/JNK (Thr183/Tyr185) (81E11) Rabbit IgG Monoclonal Antibody	1:100	Cell Signaling Technologies	4886S
Primary	*Drosophila*	Anti-Phospho-p44/42 MAPK (Erk1/2) (Thr202/Tyr204) Rabbit IgG Monoclonal Antibody	1:200	Cell Signaling Technologies	4370S
Primary	*Drosophila*	Anti-Smad3 (phospho S423 + S425) Rabbit IgG Monoclonal antibody [EP823Y]	1:100	Abcam:	ab52903
Primary	*Drosophila*	Anti-Collagen IV Rabbit IgG Polyclonal Antibody	1:400	Abcam	ab6586
Primary	*Drosophila*	Anti-TIMP	1:100	Dear et al., 2016	
Primary	Human	Glypican 4 Rabbit IgG Polyclonal Antibody	1:50 (IHC) 1:100 (IF)	Invitrogen	PA5-97801
Primary	Human	TIMP1 Monoclonal Antibody (102D1), Mouse IgG1	1:50 (IHC) 1:100 (IF)	Invitrogen	MA5-13688
Primary	Human	PLOD3 Polyclonal Antibody, Rabbit IgG	1:50 (IHC) 1:100 (IF)	ProteinTech	11027-1-AP
Primary	Human	SPARC Monoclonal Antibody (ON1-1) ,Mouse IgG1	1:50 (IHC) 1:100 (IF)	Invitrogen	335500

Secondary					
Secondary	*Drosophila* & Human	Alexa Fluor 488 goat anti-rabbit IgG (H+L)	1:500	Invitrogen	A11008
Secondary	*Drosophila* & Human	Alexa Fluor 555 goat anti-rabbit IgG (H&L)	1:500	Invitrogen	A21428
Secondary	*Drosophila* & Human	Alexa Fluor 488 goat-anti chicken IgG (H+L)	1:500	Invitrogen	A11039
Secondary	*Drosophila* & Human	Alexa Fluor 488 goat-anti mouse IgG (H+L)	1:500	Invitrogen	A11001
Secondary	*Drosophila* & Human	Alexa Fluor 546 goat-anti mouse IgG1	1:500	Invitrogen	A21123
Stain					
	Drosophila & Human	Invitrogen™ DAPI (4',6-Diamidino-2-Phenylindole, Dihydrochloride)	1:2000	Fisher Scientific	10184322
	Drosophila	Alexa Fluor 555 Phalloidin	1:100	Invitrogen	10389132

Table 4. List of *Drosophila* primers.

Gene	Primer Type	Primer Sequence	Reference
GAPDH	Forward Primer	5’ CCA ATG TCT CCG TTG TGG A 3’	This study (FlyPrimerBank)
	Reverse Primer	5’ TCG GTG TAG CCC AGG ATT 3’	
α-tubulin	Forward Primer	5’ GCT GTT CCA CCC CGA GCA GCT GAT C 3’	This study (FlyPrimerBank)
	Reverse Primer	5’ GGC GAA CTC CAG CTT GGA CTT CTT GC 3’	
Rp49	Forward Primer	5’ ATC GGT TAC GGA TCG AAC AA 3’	This study (FlyPrimerBank)
	Reverse Primer	5’ GAC AAT CTC CTT GCG CTT CT 3’	
SPARC	Forward Primer	5’ CCA GGC CTC TAC GGA GTT TT 3’	This study (FlyPrimerBank)
	Reverse Primer	5’ CAT CGA TGT CGG ACA GGT CG 3’	
Timp	Forward Primer	5’ GAG TCC TTC GCA AAT CGG ATA C 3’	This study (FlyPrimerBank)
	Reverse Primer	5’ GCT TCG GAT GTA GCC TTG TAG G 3’	
Dlp	Forward Primer	5’ TTC GAG CAG GGC CGT GAA AA 3’	This study (FlyPrimerBank)
	Reverse Primer	5’ AAC CCA GTA ACG AAC GAG TCC 5’	
Dlp_2	Forward Primer	5’ TGC AGT GCT GTG ACA CAC ATT 3’	This study (FlyPrimerBank)
	Reverse Primer	5’ ACT CTT CGT TAC TGG GTT TTT 3’	
Dlp_3	Forward Primer	5’ AGC AAA ACA ATC GCG ACG 3’	This study (FlyPrimerBank)
	Reverse Primer	5’ GCC ATT TGA GCT GTT TGC 3’	
PLOD	Forward Primer	5’ AAA ATC AAA GTG TTC ACT GTG GC 3’	This study (FlyPrimerBank)
	Reverse Primer	5’ AGG GTG GTT ACC TCA ATA TCG T 3’	
Actin5C	Forward Primer	5’ TTG TCT GGG CAA GAG GAT CAG 3’	This study (FlyPrimerBank)
	Reverse Primer	5’ CGT GGA CGA CTG TCT TCA CC 3’	
Npc2a	Forward Primer	5’ GGC GGA GTG CAT CCT CAA G 3’	This study (FlyPrimerBank)
	Reverse Primer	5’ CGT GGA CGA CTG TCT TCA CC 3’	
brn	Forward Primer	5’ AAG TTC GCC TAC CTG CGA G 3’	This study (FlyPrimerBank)
	Reverse Primer	5’ CGC GCT CTT TAT GAG CAT CG 3’	
BthD	Forward Primer	5’ GAG CGT GGT CTC CAA CAG C 3’	This study (FlyPrimerBank)
	Reverse Primer	5’ ACT TAA CTC GAA GGC TTC TCG 3’	

CG8642	Forward Primer	5’ CGG TGG AAT CTC CTT CAC GG 3’	This study (FlyPrimerBank)
	Reverse Primer	5’ CTG ATC CTC ATA ATG CTG CCG 3’	
Adgf-A2	Forward Primer	5’ AGC CGT CAT GCT TTG TGT AAT 3’	This study (FlyPrimerBank)
	Reverse Primer	5’ CCT CGG ACG TAA GAT TGG ACA 3’	
PGRP-SA	Forward Primer	5’ ACG GGC ATA GCC TTA ATC GG 3’	This study (FlyPrimerBank)
	Reverse Primer	5’ TAA TCC TCG CTC AGC TCA CC 3’	
Tep4	Forward Primer	5’ AAA AGC CGA GGG CAA GTA CAC 3’	This study (FlyPrimerBank)
	Reverse Primer	5’ TTT CAG GGT GAC TGG CTC CT 3’	
Miple1	Forward Primer	5’ ATC CGT GGA CTG AGT GTG ACA 3’	This study (FlyPrimerBank)
	Reverse Primer	5’ TTC TGA ATG GTT GCG GTT TGG 3’	
LanA	Forward Primer	5’ GGG CTC TGC TAG TAA TCC TGG 3’	This study (FlyPrimerBank)
	Reverse Primer	5’ CAC ACG TAG CTG TGG CAT AAA T 3’	
LanB2	Forward Primer	5’ GGC CAC AGA AAT GTC TGC CA 3’	This study (FlyPrimerBank)
	Reverse Primer	5’ CTG CTC ACC ACA GGT ATT AGT TG 3’	
Tsf2	Forward Primer	5’ AGC CTC GTT TTT GTG GCT CTA 3’	This study (FlyPrimerBank)
	Reverse Primer	5’ TGT GCT CAT GCT AGT GAT GTT G 3’	
Miple2	Forward Primer	5’ ATA CTG GCT TTA ACC ACG GCT 3’	This study (FlyPrimerBank)
	Reverse Primer	5’ ACG TAT GCC ATC AGA AAG GCT 3’	
LanB1	Forward Primer	5’ CTC GCC GGA GAG ATT CTG C 3’	This study (FlyPrimerBank)
	Reverse Primer	5’ ACG TAT GCC ATC AGA AAG GCT 3’	
Tsf1	Forward Primer	5’ CGG AGG AAC CCA TTT ATC GCC 3’	This study (FlyPrimerBank)
	Reverse Primer	5’ GCT GCG TTC GGA TCT CAG A 3’	
Trol	Forward Primer	5’ CGC CGA TAG TAA TGA TCG CAG 3’	This study (FlyPrimerBank)
	Reverse Primer	5’ ACC CTA ATG TTG GGA ATC TCC A 3’	
Magu	Forward Primer	5’ GGC GAG ATG TGT TTT GTT CGT 3’	This study (FlyPrimerBank)
	Reverse Primer	5’ TCA TCG CAC TCT CCC TGT TTG 3’	

Table 5. List of mammalian primers.

Gene	Primer Type	Primer Sequence	Reference
RPL13a	Forward Primer	5' CAT AGG AAG CTG GGA GCA AG 3'	Köllmer et al., 2013
	Reverse Primer	5' GCC CTC CAA TCA GTC TTC TG 3'	
SPARC	Forward Primer	5’ GAC CCG GTC AAC CCA GAG A 3’	Chen et al., 2022
	Reverse Primer	5’ GAC CCG GTC AAC CCA GAG A 3’	
SPARC	Forward Primer	5′ TCA ACT ACA CTG TGC GGA CC 3′	Xie et al., 2020
	Reverse Primer	5′ GTG GAT GGT GGT GGC AAA AC 3’	
PLOD3	Forward Primer	5’ GCT GTT GGA AAC GGA GTT G 3’	Zou et al., 2021
	Reverse Primer	5’ CTT GCC ATG TGG GTT CTG ACT 3’	
PLOD3	Forward Primer	5’ ATG AGG GCC TGG ATC TTC TTT CTC CTT T 3’	Hatori et al. 2023
	Reverse Primer	5’ TTA GAT CAC CAG ATC CTT GTT GAT GTC CTG 3’	
TIMP1	Forward Primer	5′ CAC CTT ATA CCA GCG TTA TG 3’	Oszajca and Szemraj, 2021
	Reverse Primer	5′ TTT CCA GCA ATG AGA AAC TC 3’	
TIMP1	Forward Primer	5′ GAC GGC CTT CTG CAA TTC C 3’	Pan et al., 2019
	Reverse Primer	5′ GTA TAA GGT GGT CTG GTT GAC TTC TG 3′	
GPC4	Forward Primer	5’ GTC AGC GAA CAG TGC AAT CAT 3’	Legier et al., 2023
	Reverse Primer	5’ ACA TTT CCC ACC ACG TAG TAA C 3’	
GPC4	Forward Primer	5’ TCC CTC GCA AAT TGA AGC TCC 3’	Munir et al., 2020
	Reverse Primer	5’ GCA ACC GCT AAG CCT TGA G 3’	

Chapter 3

SPARC as a regulator of intestinal stem cell homeostasis

3.1. Introduction

Secreted protein acidic and rich in cysteine (SPARC), also known as osteonectin or basement membrane-40 (BM-40) is an extracellular, calcium-binding, matricellular glycoprotein (Ma et al., 2017; Hu et al., 2020) that plays non-structural roles in the extracellular matrix (ECM). Originally identified in bone tissue by Termine et al. (1981) as a 32kDa collagen-protein found in the ECM that played key roles in bone mineralization, studies since have shown that the molecular weight of the protein can actually slightly differ, and it ranges between 30-35kDa as a result of differences in protein structure (Martinek et al., 2002).

The mammalian SPARC-family of proteins is composed of 8 members, each with a characteristic calcium-binding domain with unique motifs: SPARC, SPARC-like 1 (SPL-1 or hevin), SMOC (secreted modular calcium-binding protein) 1/2, testican 1/2/3 and follistatin-like 1 (Bradshaw, 2012). *Drosophila melanogaster* only has a single SPARC gene (Martinek et al., 2002), and it is a homolog for 3 of the mammalian

counterparts: SPARC, SPL-1 and follistatin-like 1 (Portela et al., 2010). One of the important features of SPARC structure is that it contains specific low-affinity and high-affinity Ca^{2+} binding sites (Martinek et al., 2002), which differ in their ability to bind to different collagen molecules (Giudici et al., 2008) and therefore affect basement membrane composition in epithelial tissues (Duncan et al., 2020)

SPARC is a well-characterized protein that has been highly conserved between vertebrates and invertebrate organism during evolution (Martinek et al., 2002; Vaughan et al., 2018). Despite the differences in complexity between the *Drosophila* SPARC protein and its mammalian orthologs, and the fact that the conservation of the primary amino acid sequence between them is only about 30%, this homology is high in the gene regions responsible for the maintenance of protein structure, which confers a high conservation of functionality between the fly and mammalian proteins (Martinek et al., 2002). Most importantly, the conformation of the calcium-binding sites is conserved, thus maintaining the ability of SPARC to bind to collagen IV and its affinity for the structural protein (Martinek et al., 2002). Thus, *Drosophila* is an excellent model system to characterize SPARC function and its relationship with collagen in a variety of tissues and how this affects the maintenance of tissue homeostasis.

SPARC has a wide range of roles that are cell-, tissue- and context-dependent (Zhong et al., 2019). Some of these include cell cycle control, cell proliferation, differentiation, migration, adhesion and signalling (Zhu et al., 2019; Liu et al., 2020). Because of its important links to the extracellular matrix and its assembly, SPARC functions revolve around tissue development, repair and remodelling, as well as cross-talk between different ECM components (Ehninger et al., 2014; Hu et al., 2020). It is also involved in cell migration and differentiation (Jiang et al., 2019) and in modulating cell-to-cell interactions as well as their interactions with the microenvironment (López-Mancada et al., 2022). Other functions include its involvement in osteoblast maturation in the bone tissue (Wang et al., 2019), its role in the development of tissue fibrosis (Vaughan et al., 2018) and its control over immune cell recruitment to tissues (Bellenghi et al., 2022). Liang et al. suggested that these differential properties of SPARC could be due to a slight variation of the biochemical properties of the protein, depending on whether the source of SPARC is endogenous or exogenous. In epithelial tissues, high concentrations of SPARC can be found between the cells and the basement membrane, with lower levels associated with the plasma membrane, where it binds to growth factor receptors as a competitive inhibitor in order to modulate cell signalling (Martinek et al.,

2008). In *Drosophila*, the association between SPARC and the basement membrane of epithelial tissues has been documented from early stages of development all the way to adult tissues (Martinek et al., 2002). Overall, SPARC is a tightly-regulated protein with a wide range of functions that works to maintain tissue homeostasis in adult organisms (Ehninger et al., 2014).

Although SPARC has been demonstrated to play roles in ageing, cardiomyopathies (Vaughan et al., 2018) and haematological malignancies (Ehninger et al., 2014), most studies have focused on SPARC functions in tumour development and cancer progression. Following the context-dependent variation in SPARC functions, studies have found SPARC to have oncogenic or tumour suppressor properties depending on the tissue type and stage of the disease (reviewed by Ghanemi et al., 2020). As part of its tumour suppressive activity, SPARC has been shown to inhibit migration and invasion of breast cancer cells (Ma et al., 2017) and reduce angiogenesis in colon cancer (Liang et al., 2010) and is thus associated with lower incidence of metastasis in these tumour types. On the contrary, in the context where SPARC has oncogenic properties, some studies have shown that the presence of SPARC promotes the survival of malignant cells through the acquisition of stem cell properties that facilitates the proliferation and migration capabilities of the tumour cells in the liver (Liu et al., 2020; Gao et al. 2021). In this tumorigenic context, SPARC has also been shown to affect patient response to drugs and therapeutic treatment (reviewed in Vaz et al., 2015 and Jiang et al., 2023; Zhong et al., 2019).

Most importantly, SPARC has been shown to promote epithelial to mesenchymal transition (EMT) and the regulation of EMT-related genes, e.g. E-cadherin, N-cadherin and vimentin (Zhong et al., 2019). EMT is a physiological process whereby epithelial cells acquire mesenchymal characteristics, including the loss of their distinctive apico-basal polarity and tight junctions, and cytoskeletal reorganisation (Carriere et al., 2021). EMT is key in a pathological context for tumour progression and one of the fundamental characteristics of advanced cancer tissues. Some studies suggest that the SPARC could have autocrine or paracrine roles within the tumour microenvironment and that these would be responsible for the context-dependent roles of the protein in EMT (Carriere et al., 2021).

With this wide range of functions and the varying degrees of importance SPARC has based on cell and tissue type comes an equally wide range of regulatory mechanism that control SPARC expression and function. Evidence in the literature suggests MAPK

signalling as an important regulator of SPARC expression. Silencing of SPARC in bone tissue inhibits MAPK signalling, where SPARC increases the levels of phosphorylated, i.e. active, p38 MAPK (Wang et al., 2019). This link between SPARC and p38 MAPK has also been shown in prostate cancer (Wang et al., 2019); in glioma (Golembieski et al., 2008; Alam et al., 2013); and in the regulation of limbal epithelial stem cells (Zhu et al. 2019), where p38 MAPK works alongside JNK to promote stem cell proliferation. ERK1/2, another member of the MAPK signalling cascade, has also been extensive demonstrated to regulate SPARC. Liu et al. demonstrated a link between ERK1/2 and MMP expression in liver cells, and both Ma et al. and Hu et al. showed that ERK1/2 is a key regulator of the angiogenic properties of SPARC, whereby SPARC sequesters vascular-endothelial growth factor (VEGF), limiting the activation of its receptor and thus hindering the ability of tumour cells to proliferate and metastasize. SPARC also activates the expression of ZEB1 (López-Mancada et al., 2022), a critical regulator of the EMT (Pérez-Oquendo and Gibbons, 2022), which has been shown to negatively regulate MAPK signalling in human lung tumours, i.e. high ZEB1 expression correlates with low MAPK signalling (Peng et al., 2019). Upregulation of SPARC in early stages of tumour development has been shown to occur downstream of Dpp signalling while at the same time being independent of JNK signaling (Portela et al., 2010). It has long been known that JNK and p38 MAP kinases are involved in NF-Kβ activation (as reviewed by Schulze-Osthoff et al., 1997), and this transcription factor has also been proposed as a regulator of SPARC levels in adipocytes (John et al., 2019).

While SPARC has been shown to regulate a range of signaling pathways in the contexts of tumours, it was originally identified as a collagen I-binding protein in bone tissue, and Termine and colleagues hypothesized its possible role in mediating bone mineralization. Since then, many studies have tried to characterize the interaction between these two molecules in a wide range of tissues, in order to establish the nature of their relationship and the resulting functions. Studies have shown collagen IV to be the most abundant SPARC-binding molecule in the ECM. Martinek et al. demonstrated that this interaction between collagen IV fibrils and SPARC in the basement membrane is conserved in metazoans and that it is essential for the development of the basal lamina in early stages of *Drosophila* development (Martinek et al., 2008).

It has been shown to act as a chaperone for collagen IV (Shahab et al., 2015), where intracellular association between these two proteins prevents collagen IV from binding to integrins and maintains collagen homeostasis in the cell (Duncan et al., 2020).

SPARC and collagen IV form a complex in the endoplasmic reticulum, and this interaction allows for correct folding, assembly, secretion and solubility of the collagen fibrils (Pastor-Pareja and Xu, 2011; Morrissey et al., 2016; Bellenghi et al., 2022). Moreover, SPARC is responsible for transporting collagen molecules from their synthesis site to other tissues that do not express the fibrils, and for maintaining collagen levels in the basement membrane (Morrissey et al., 2016). The maintenance of a homeostatic balance between these two molecules is essential to maintain basement membrane integrity: Morrissey et al. demonstrated that in situations where there is a surplus of SPARC, the rate of incorporation of collagen IV fibrils to the basement membrane is decreased, thus weakening the barrier and facilitating invasion.

Its localization in the ECM means SPARC has the ability to bind to a variety of other molecules besides collagen, including actin, laminin and perlecan (Martinek et al., 2008). However, not many studies have focused on establishing a role between SPARC and other ECM molecules, and those that have, have found that SPARC does not directly affect their levels, e.g. laminin (Morrissey et al. 2016).

3.2. Aims and objectives

Previous work from the Doupé group had identified a small group of proteins that are specifically secreted in stem and progenitor cells of the *Drosophila* midgut, but not by the differentiated cells of the tissue. SPARC was identified as a hit in this study, and subsequent follow-up experiments showed that knockdown of SPARC did not significantly affect the ratio of ISC and EB cells in the tissue (Galbraith, unpublished). With this, the aim of this project is to identify the role of intestinal stem cell derived SPARC in the *Drosophila* midgut, and elucidating its function, expression and regulation, as well as trying to establish the relationship of SPARC with other interacting partners within the gut tissue.

3.3. Results

3.3.1. Manipulation of SPARC expression levels in the stem and progenitor cells of the *Drosophila* midgut affects homeostasis in the tissue

In order to determine the role of SPARC in the midgut tissue, the gene was overexpressed and knocked down in the stem and progenitor cells of the *Drosophila* gut using a Gene Switch driver, which specifically overexpressed or knocked down SPARC in stem and progenitor cells (ISCs and EBs). Overexpression of SPARC (*Figure 3.1*) showed a significant decrease in the total number of cells observed per field of view. This result demonstrates an increase in cells in the midgut tissue when levels of SPARC are elevated. However, gut measurements showed no significant change in mean gut width or mean gut area observed per field of view between control and SPARC-overexpressing guts. Since there is no change in overall size of the fly gut when SPARC levels are increased, but the total number of cells is reduced, overexpression of SPARC leads to a decrease in cell density in the tissue, as shown in *Figure 3.2*.

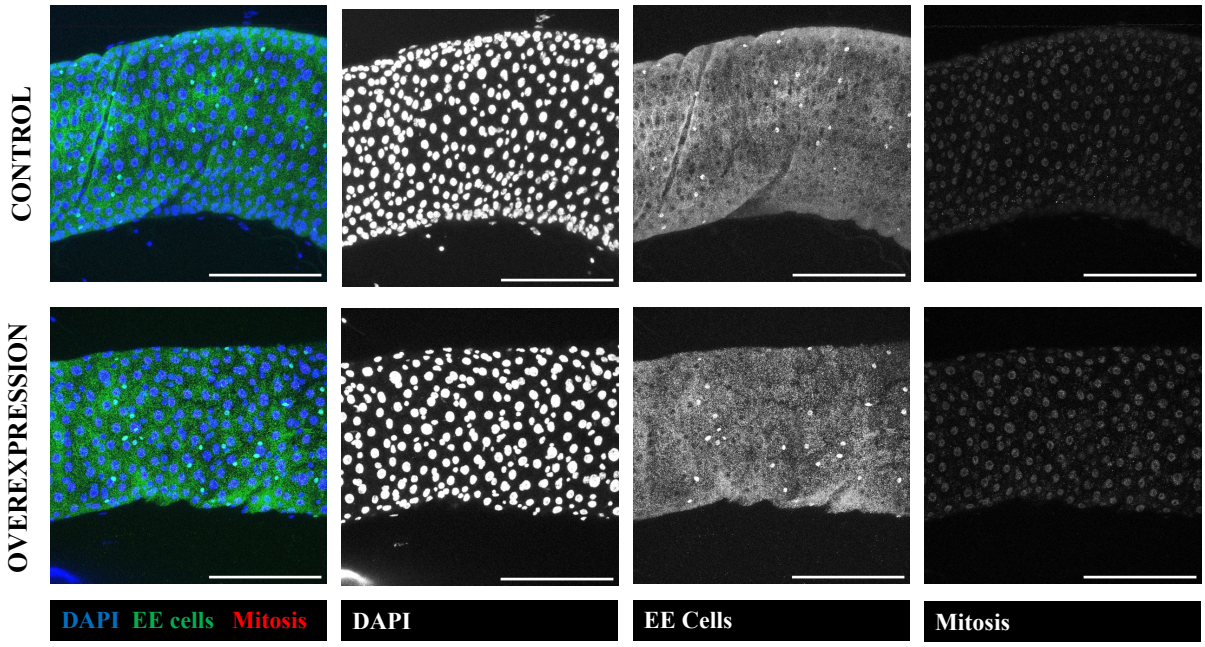

Figure 3.1. The effects of SPARC overexpression in ISCs and EBs of the *Drosophila* midgut. SPARC overexpression causes a decrease in the total number of cells and EEs observed per field of view. Guts were stained with α-prospero (1:100), α-PH3 (1:1000) and DAPI. Scale bars in the bottom right corner represent 100μm.

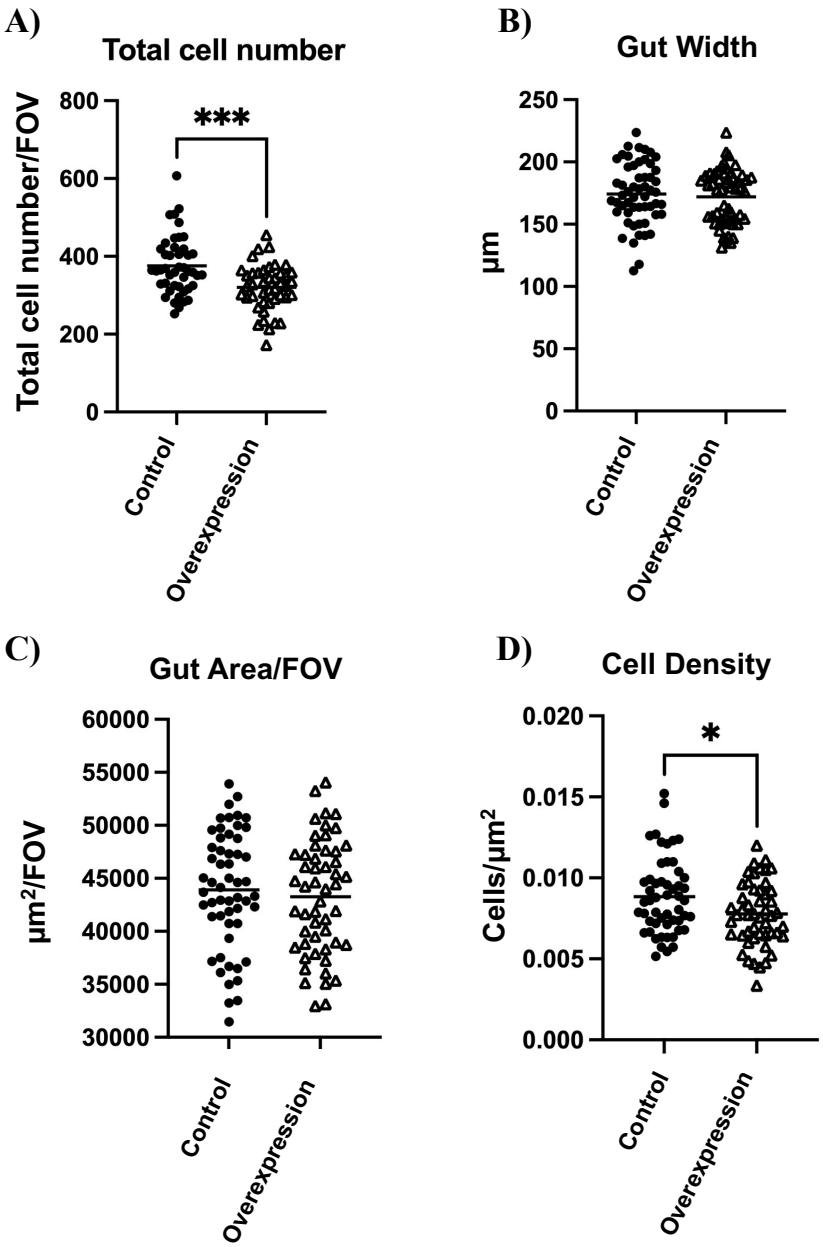

Figure 3.2. The effects of SPARC overexpression in ISCs and EBs. Overexpression of SPARC leads to a significant decrease in the number of cells per field of view ($p = 0.0002$) (control n = 45, OE n = 43) (***A***), but no changes in gut width (control n = 55, OE n = 54) (***B***) or gut area/FOV (control n = 55, OE n = 52) (***C***) between overexpression and control guts. This leads to a significant decrease in cell density in the posterior midgut ($p = 0.01$) (control n = 53, OE n = 50) (***D***).Unpaired t-tests were used for normally distributed data (A,C,D), and non-parametric Mann Whitney-U tests for non-normally distributed data (B) .

In order to characterize this decrease in cells, quantification of the specific cells within the midgut was carried out using the EE-specific marker prospero. Results showed there is a significant decrease in the number of enteroendocrine cells observed per field of view in the posterior midgut (*Figure 3.3*). Interestingly, the proportion of enteroendocrine cells in relation to total cell number is maintained consistent between the control and the overexpression line, suggesting that despite the changes, balanced differentiation in the gut is maintained and the proportion of each cell type is constant. A reduction in cell number could be caused by either an increase in cell loss or increase in cell production. To distinguish these possibilities guts were stained for the mitotic marker phosphor-histone H3, and data showed there is a significant decrease in the number of mitoses in the gut tissue upon SPARC overexpression.

Taken together, these results show that overexpressing SPARC in the stem and progenitor cells of the *Drosophila* gut slows down the proliferation rates of the gut and therefore leads to a lower number of cells in the tissue and decreased cell density. These results strongly suggests that SPARC contributes, in some capacity, to maintaining homeostasis in the gut, as manipulating the levels of genetic expression alters the number of cells in the gut, their proliferation rates and cell density in the tissue.

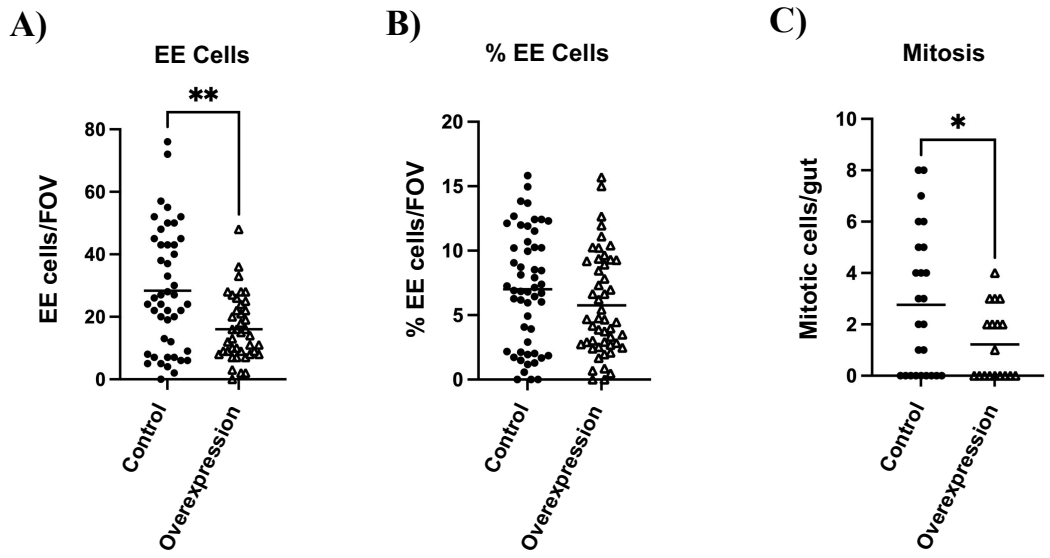

Figure 3.3. SPARC overexpression in ISC and EBs decreases the proliferation rate of ISCs and the number of EE cells in the posterior midgut. Overexpression of SPARC in the stem and progenitor cells of the posterior midgut significantly decreases the number of EE cells observed per field of view ($p = 0.005$) ($n = 41$) (***A***), but the ratio of EE cells normalized to total number of cells observed per FOV remains constant between control and overexpression guts ($n = 49$) (***B***). SPARC overexpression significantly decreases the number of proliferating ISCs in the whole *Drosophila* gut ($p = 0.05$) ($n = 25$) (***C***). Data was not normally distributed, non-parametric Mann Whitney U-tests were used for statistical analysis.

To establish if downregulation of SPARC has the opposite effect on the midgut as its overexpression, two different RNAi knockdown lines were used. The rationale behind this is that one RNAi knockdown line may have a stronger phenotype than the other depending on the strength of the knockdown, and it also rules out the possibility of phenotypes being due to off-target effects resulting from the genetic manipulation. The SPARC RNAi lines used were *UAS-SPARC-RNAi 40885* and *UAS-SPARC-RNAi 16677*, which will be referred to from here onwards as SPARC RNAi-1 and SPARC-RNAi-2, respectively, for ease of understanding. The numbers provided above represent the stock number of each RNAi line.

Varying effects were observed when comparing the RNAi lines. Knockdown of SPARC using *SPARC-RNAi-1* (*Figure 3.*4) showed a significant decrease in the total number of cells observed per field of view, but no changes in gut width or area (*Figure 3.5A-C*). Cell density analysis suggests a possible reduction in knockdown guts compared to controls, but this change was not statistically significant. (*Figure 3.5D*). This same line showed a pronounced decrease in the number of mitosis in the tissue (*Figure 3.6C*), but no significant changes in EE cells or their proportion in the tissue (*Figure 3.6A-B*). From this, we concluded that knockdown of SPARC perhaps has a similar effect on the tissue as overexpression, where the proliferating capacity of the tissue is diminished, leading to a decrease in total cell number.

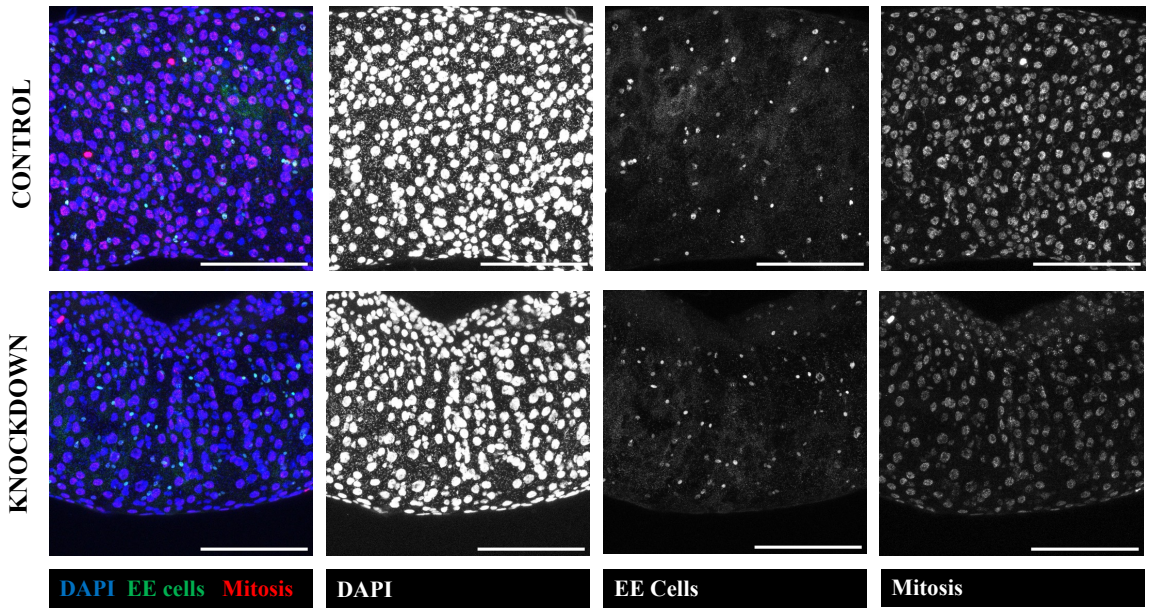

Figure 3.4. The effect of SPARC knockdown in the ISCs and EBs of the *Drosophila* midgut using *SPARC-RNAi-1*. Knockdown of SPARC (*5961^{GS} > UAS-SPARC RNAi-1*) reduces the number total cells observed per field of view in the posterior midgut and decreases the number of proliferating cells in the tissue. Guts were stained with α-prospero (1:100), α-PH3 (1:1000) and DAPI. Scale bars in the bottom right corner represent 100μm.

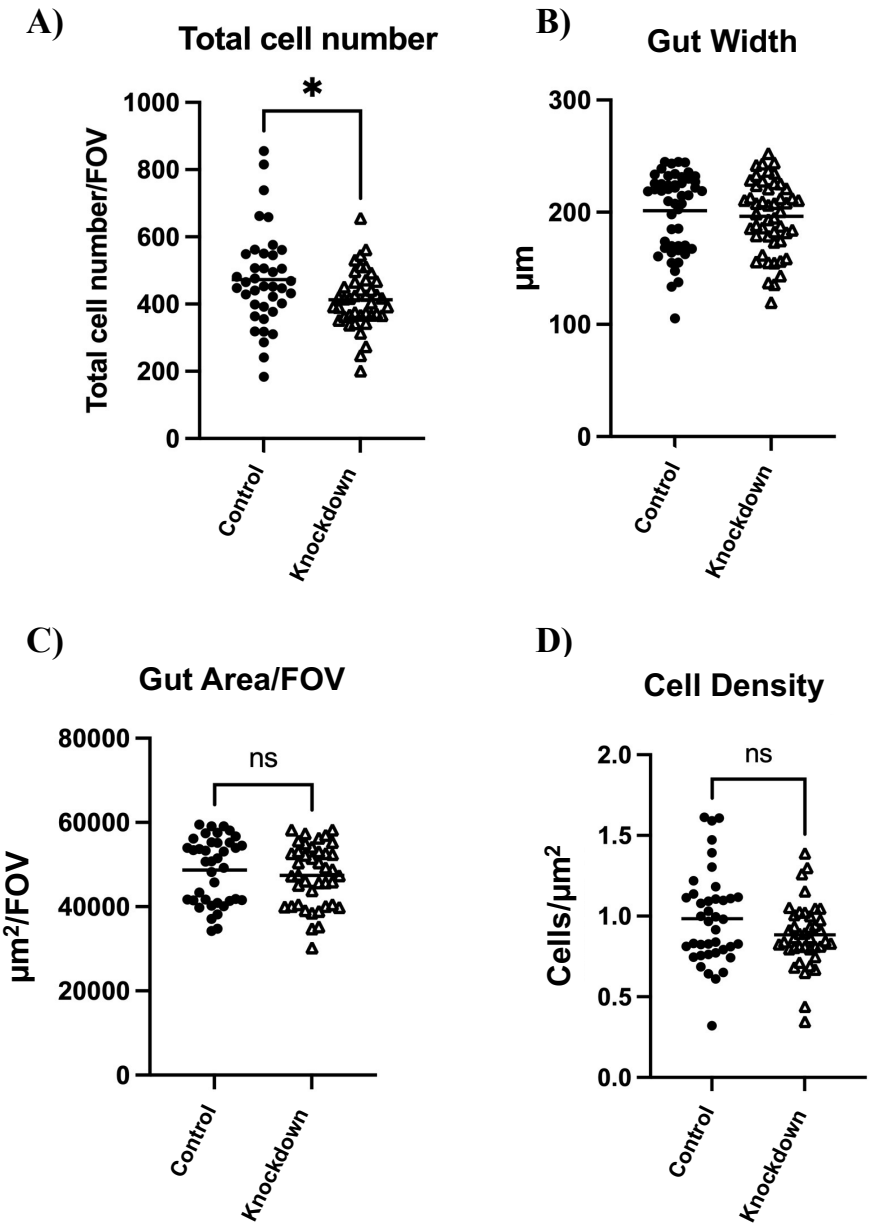

Figure 3.5. Knockdown of SPARC with SPARC-RNAi-1 significantly reduces the number of cells in the posterior midgut. *5961^{GS} > UAS-SPARC RNAi-1* leads to a significant decrease in the total number of cell observed per field of view (p = 0.02) (Control n = 39, KD n = 41) (***A***), but no significant changes were found between control and knockdown guts in regards to gut width (Control n = 50, KD n = 49) (***B***), gut area observed per field of view (Control n = 39, KD n = 41) (***C***) or cellular density (Control n = 40, KD n = 40) (***D***). Unpaired t-tests were used to analyze normally-distributed data (A, D), and non-parametric Mann Whitney U-tests for non-normally distributed data (B, C).

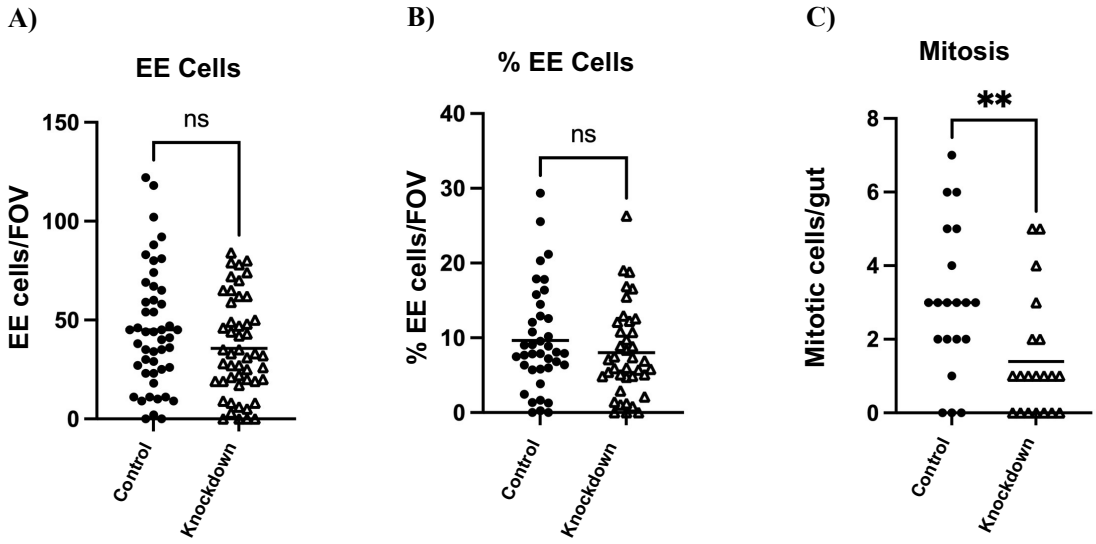

Figure 3.6. SPARC knockdown using *SPARC RNAi line 1* significantly reduces ISC proliferation rates in the posterior midgut. The number of EE cells observed per field of view (***A***), as well as the proportion of EE cells normalized to the total number of cells per FOV (***B***) in the posterior end of the midgut remained unchanged between control and SPARC knockdown guts (*5961^{GS} > UAS SPARC RNAi 1*) (control n = 48, KD n = 49 ,and control n = 39, KD n = 39, respectively). However, SPARC knockdown significantly decreased the number of mitoses observed across the entire gut (p = 0.007) (control n = 20, KD n = 20) (***C***), indicating a reduction in the proliferation rates in the tissue. Data was not normally distributed and non-parametric Mann-Whitney U-tests were used for statistical analysis.

On the contrary, analysis of SPARC knockdown using *SPARC-RNAi-2* showed contradicting results (*Figure 3.7*). This line showed that knock down of SPARC in the stem and progenitor cells of the tissue does not affect total cell number, EE cells observed per field of view or gut width, but it does cause a significant decrease in the gut area compared to control guts (*Figures 3.8* and *3.9*). Interestingly, this decrease in area is accompanied by an increased number of mitosis in the tissue (*Figure 3.9C*), demonstrating that knockdown of SPARC could accelerate tissue turnover, where an increased loss of cells in the tissue is matched by an increase in proliferation.

Qualitatively, knockdown of SPARC using RNAi line 2 showed a very striking phenotype. We observed a loss of distribution of cells within the tissue, where cells are often clumped and nuclei have increased irregular shapes (*Figure 3.7)*. This fits in with the quantification results showed above, where we show that the same number of cells as in control guts are now found in a smaller area. Interestingly, we found no changes in cell density. This could be explained due to the fact that the disorganization of cells within the

tissue made quantification harder, i.e. multiple nuclei in close proximity may have been scored a single, larger nucleus, allowing room for error within these results.

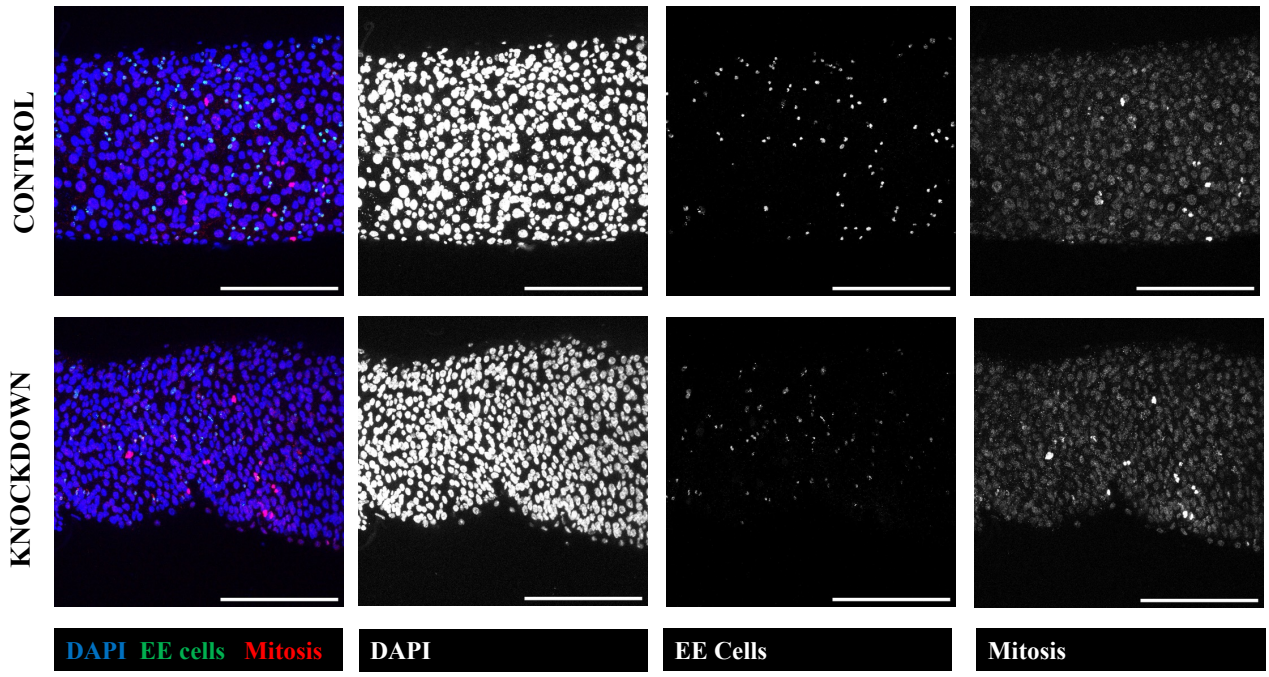

Figure 3.7. Knockdown of SPARC using *SPARC-RNAi-2* increases the number of proliferative cells in the gut and causes a loss of distribution of cell in the posterior midgut. *5961^{GS} > SPARC-RNAi-2* affects the homeostatic balance of the posterior midgut and induces changes to cell distribution in the tissue. Guts were stained with α-prospero (1:100), α-PH3 (1:1000) and DAPI. Scale bars in the bottom right corner represent 100μm.

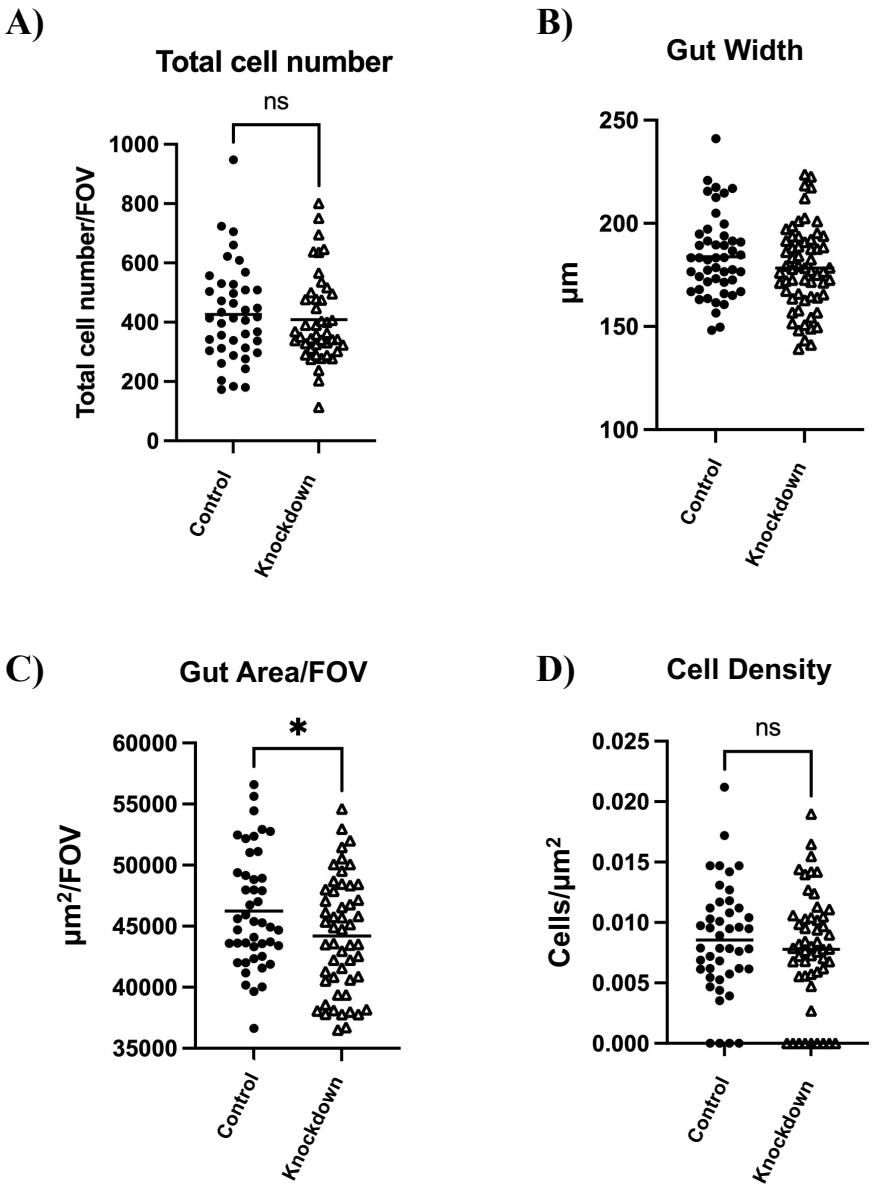

Figure 3.8. Knockdown of SPARC with *SPARC-RNAi-2* significantly decreases the area of the gut observed per field of view. *5961^{GS}> SPARC-RNAi-2* does not change the total number of cells observed per field of view (control n = 42, KD n = 44) (***A***), gut width (control n = 48, KD n = 61) (***B***) or cell density (control n = 45, KD n = 52) (***D***), but significantly decreases the area of the gut observed per FOV (p = 0.03) (control n = 45, KD n = 52) (***C***). Unpaired t-tests were used for statistical analysis of normally distributed data (B, C), and Mann Whitney U-tests for non-normally distributed data sets (A, D).

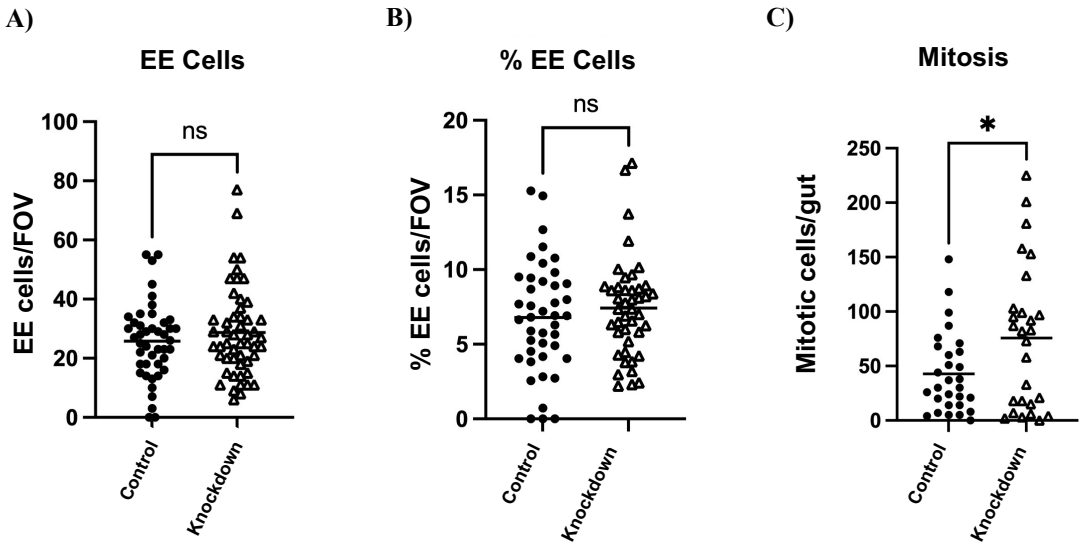

Figure 3.9. Knockdown of SPARC with *SPARC-RNAi-2* significantly increases the mitotic rates in the *Drosophila* gut. *5961^{GS} > SPARC-RNAi-2* does not change the number of EE cells observed per field of view (control n = 44, KD n = 51) (***A***), or the % of EE cells normalized to total cell number in the posterior midgut (control n = 42, KD n = 43) (***B***), but significantly increases the number of mitoses across the whole gut tissue (p = 0.02) (control n = 29, KD n = 27) (***C***). Unpaired t-tests were used for statistical analysis of normally distributed data (C), and Mann Whitney U-tests for non-normally distributed data sets (A, B).

3.3.2. Validation of SPARC RNAi lines

Because of the varying results obtained in the initial immunofluorescence experiments, qPCR analysis was carried out to validate the extent of the knockdowns and to test whether the differing phenotypes may reflect differences in knockdown efficiency (*Figure 3.10*). SPARC was knocked down in the whole gut tissue (*$TubGal80^{TS}$ > SPARC RNAi 40885* and *$TubGal80^{TS}$ > SPARC RNAi 16677)* and qPCR analysis showed that both lines knocked down SPARC expression in the tissue. The percentage knockdown compared to the control flies was 50% in both. Thus, we can confidently assume that the RNAi lines used here are, to a certain degree, knocking down SPARC expression in the *Drosophila* midgut, and that results obtained and the phenotypes observed are likely a direct consequence of SPARC knockdown and not due to off-target effects or incorrect genetic manipulation.

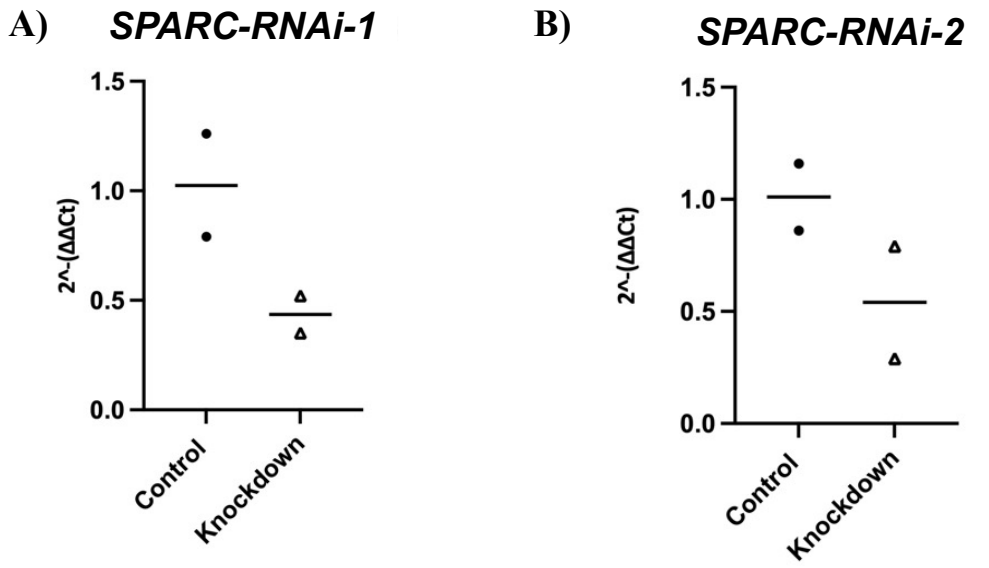

Figure 3.10. *SPARC-RNAi-1* and *SPARC RNAi-2* accurately knock down SPARC expression in the *Drosophila* gut. Both *TubGal80^{TS} > SPARC-RNAi-1* (***A***) and *TubGal80^{TS} > SPARC-RNAi-2* (***B***) appropriately reduce the levels of SPARC expression in whole-gut *Drosophila* samples. Results calculated using the ΔΔCt method. Each data point represents a sample, and each sample contains 10 whole guts.

3.3.3. Overexpression or knockdown of SPARC in the ISCs and EBs does not affect the lifespan of the fly

In order to determine if the changes to gut physiology observed in the immunofluorescence experiments have a long-term effect on the survival of the organism (Li et al., 2016; Akagi et al., 2018), lifespan survival experiments were carried out. Two replicates of each lifespan were carried out, containing 300 flies each, and their survival was monitored. Consistently with the immunofluorescence data, overexpression or knockdown of SPARC was induced at day 10, to maintain the same experimental conditions throughout all approaches. Results show that overexpressing SPARC in the ISCs and EBs in the *Drosophila* gut does not affect the life expectancy of the fly, as both control and overexpression flies had similar survival curves (*Figure 3.11*). Similarly, neither of the two SPARC RNAi lines showed a consistent effect on lifespan (*Figures 3.12 and 3.13*). Knockdown of SPARC seems to reduce lifespan in early stages of adulthood (< 50 days), but at later stages, survival between knockdown and control levelled out.

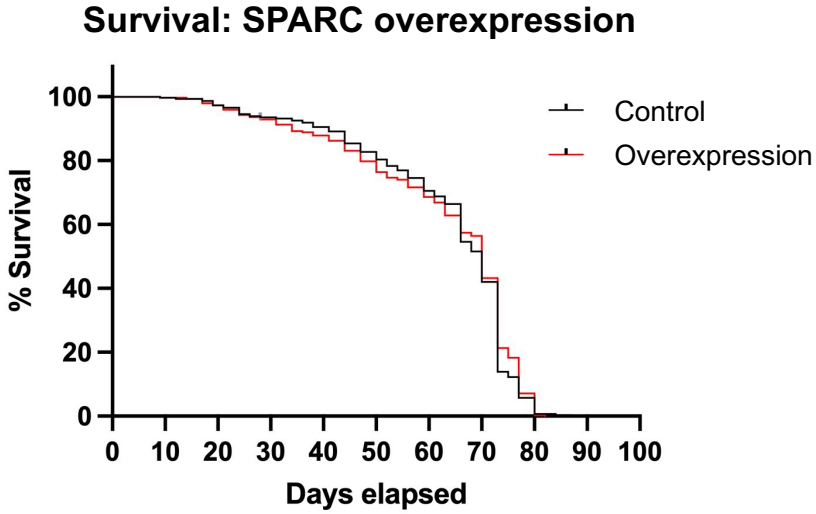

Figure 3.11. Overexpression of SPARC in the ISCs and EBs of the *Drosophila* gut has no effect on the lifespan of the fly. Overexpression of SPARC is induced at day 10 of the experiment, when flies are swapped to food containing the mifespristone drug that triggers the overexpression of SPARC (n = 300).

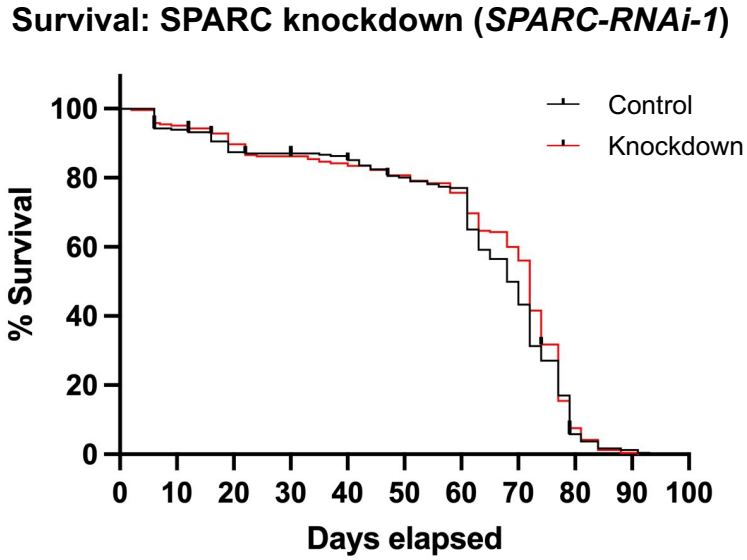

Figure 3.12. Knockdown of SPARC with *SPARC-RNAi-1* in the ISCs and EBs of the *Drosophila* gut has no effect on the lifespan of the fly. Knockdown of SPARC (*5961^{GS} > SPARC-RNAi-1*) is induced at day 10 of the experiment, when flies are swapped to food containing the mifespristone drug that triggers the expression of the SPARC RNAi construct (n = 300).

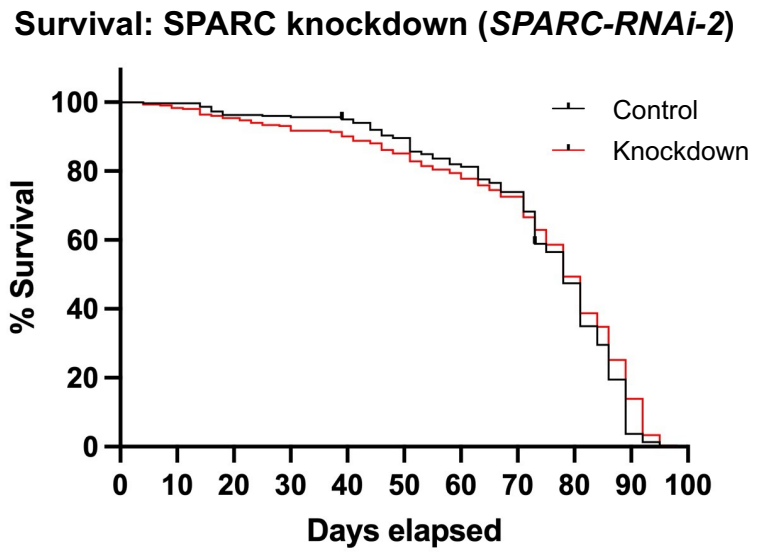

Figure 3.13. Knockdown of SPARC with S*PARC-RNAi-2* in the ISCs and EBs of the *Drosophila* gut significantly reduces the lifespan of the fly in the early stages of adulthood. Knockdown of SPARC (*5961^{GS} > SPARC-RNAi-2)* is induced at day 10 of the experiment, when flies are swapped to food containing the mifespristone drug that triggers the expression of the SPARC RNAi construct. Statistical analysis revealed that the increased mortality observed in the early stages upon SPARC knockdown from days 10 to 55 is statistically significant (Mantel-Cox Chi-squared test, p = 0.04) (n = 300).

3.3.4. Manipulation of SPARC levels using the Flp-Out system

As mentioned above, the Gene Switch driver allows for the temporal and spatial manipulation of gene expression while maintaining an identical genetic background between the experimental and control groups. In the results presented so far, overexpression of SPARC was specifically carried out in stem and progenitor cells in the adult gut of *Drosophila* females, where expression is not induced until the flies have reached "adulthood", rather than at early stages of development.

In order to see if the manipulation of SPARC using different gene expression systems yielded similar results, we used a "FLP-OUT" system, developed by Golic and Lindquist in 1989, that allows for lineage tracing. This binary system, like Gene Switch, also allows for the temporal and spatial control of genetic expression, but expression of Gal4 is induced by a shift in temperature rather than addition of a drug (Phipps et al.,

2023). The novel feature of this system is that the UAS promoter also controls the expression of a fluorescent reporter (GFP) that labels any cells where recombination has occurred, as well as all the clones produced from that cell (Phipps et al., 2023). Immunofluorescence experiments of SPARC overexpression driven by esg^{TS}Flip (*esg^{TS}Flip > UAS SPARC*) were carried out (*Figure 3.14*) and results showed no significant increase in the total number of cells per field of view expressing GFP in the overexpression compared to the control (*Figure 3.15*). In order to establish a relationship between the number of cells observed in the gut per field of view and the number of cells expressing SPARC, the percentage of labelled cells was calculated. Similarly, there was no significant change in labelled cells between the control and knockdown using *SPARC-RNAi-1* (*Figures 3.16 and 3.17*). On the contrary, there was a significant reduction of GFP labelled cells and clones when knockdown was induced by *SPARC RNAi- 2* (*Figure 3.18 and 3.19*) .

The use of this expression system has not yielded any conclusive evidence that overexpressing SPARC affects the *Drosophila* gut. Similarly to the SPARC overexpression data, *esg^{TS}Flip > SPARC RNAi* lines did not yield any significant results. We cannot conclude that SPARC knockdown has any effect on tissue homeostasis using this expression system. There were no significant changes in the number of GFP-positive cells observed per field of view, or in the percentage of GFP-expressing cells for either of the two RNAi lines used.

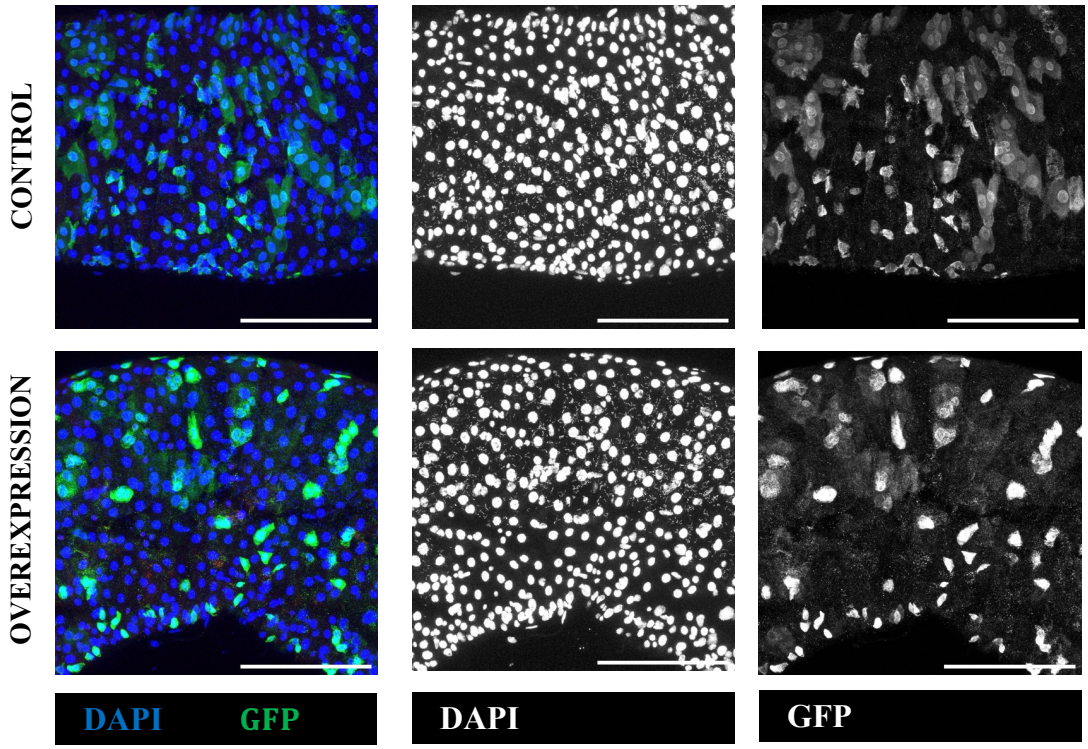

Figure 3.14. Overexpression of SPARC driven by *esg^{TS}Flip* does not show any changes in SPARC expression between control and SPARC-overexpressing guts. SPARC overexpression (*esg^{TS}Flip > UAS-SPARC)* does not show any differences in GFP levels compared to control guts (*esg^{TS}Flip > Luciferase).* GFP tags SPARC-expressing cells and its clones. Guts were stained with α-GFP (1:2000) and DAPI. Scale bars in the bottom right corner represent 100μm.

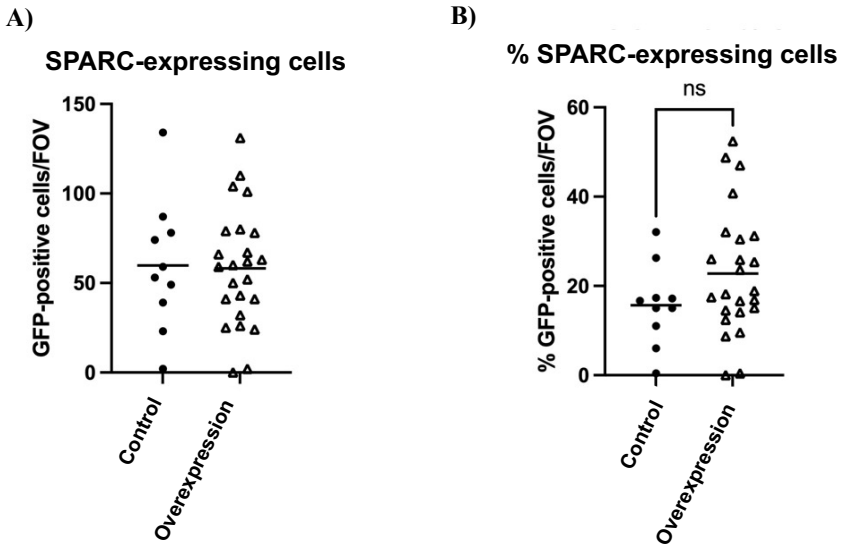

Figure 3.15. Quantification of the overexpression of SPARC driven by *esg^{TS}Flip* does not show any changes in SPARC expression between control and SPARC-overexpressing guts. SPARC overexpression (*esg^{TS}Flip > UAS-SPARC)* does not show any differences in GFP levels compared to control guts (*esg^{TS}Flip > Luciferase),* both in terms of total number of GFP-positive cells (Control n = 10, OE n = 24) (***A***) and % of GFP-positive cells normalized to the total cell number/FOV (Control n = 10, OE n = 24) (***B***). Data is normally distributed so unpaired t-tests were used for statistical analysis.

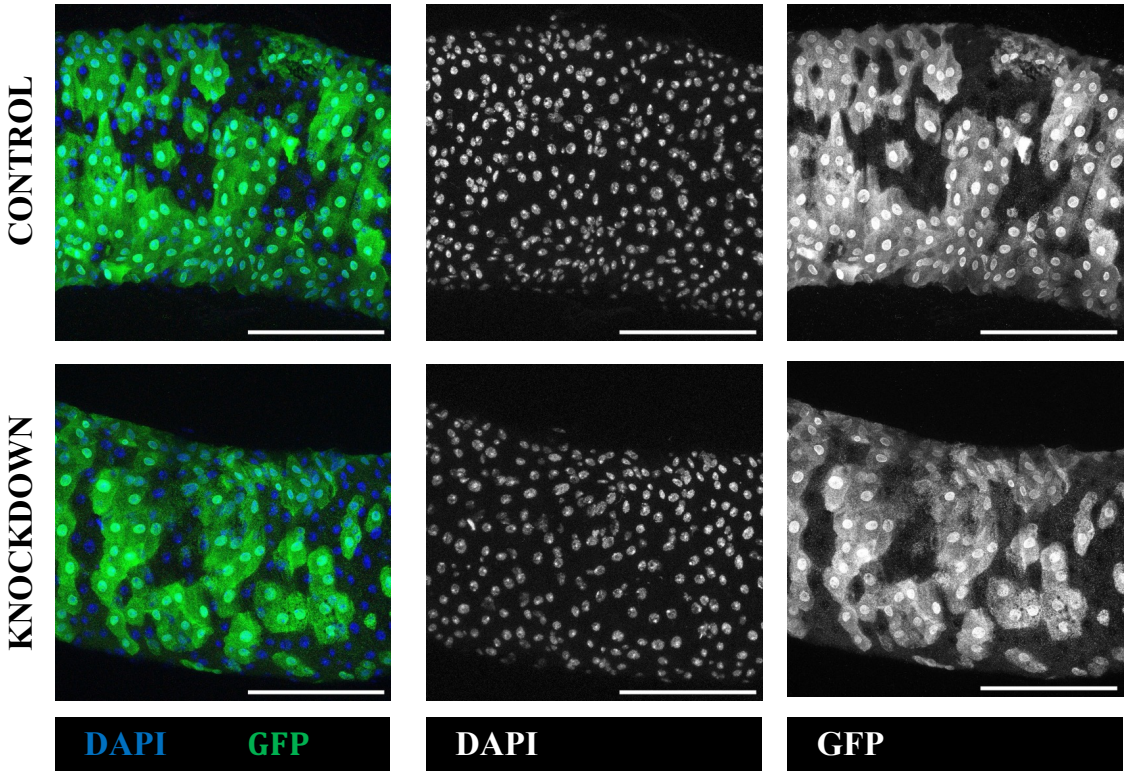

Figure 3.16. Knockdown of *SPARC-RNAi-1* driven by *esg^{TS}Flip* does not show any changes in SPARC expression between control and SPARC knockdown guts. SPARC knockdown (*esg^{TS}Flip > UAS-SPARC-RNAi-1)* does not show any differences in GFP levels compared to control guts (*esg^{TS}Flip > Luciferase).* GFP tags SPARC-expressing cells and its clones. Guts were stained with α-GFP (1:2000) and DAPI. Scale bars in the bottom right corner represent 100μm.

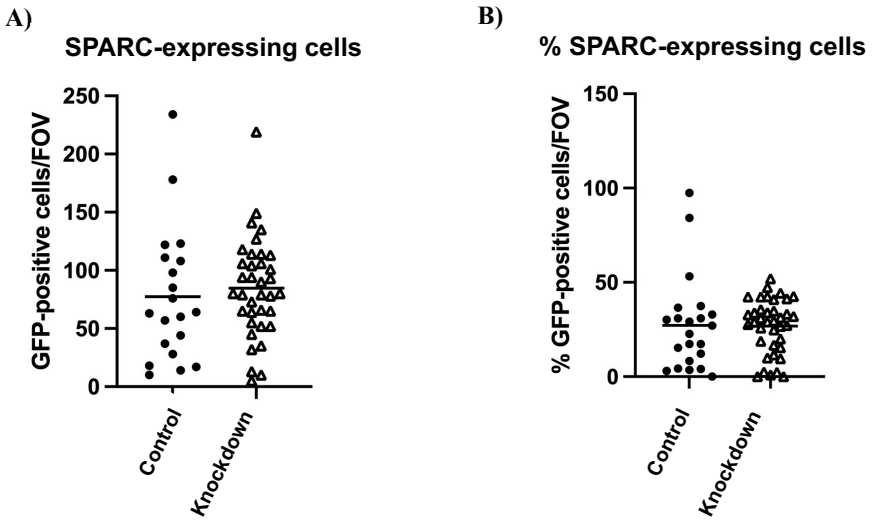

Figure 3.17. Quantification of the knockdown of SPARC using *SPARC-RNAi-1* driven by *esg^{TS}Flip* does not show any changes in SPARC expression between control and SPARC-knockdown guts. SPARC knockdown (*esg^{TS}Flip > UAS-SPARC-RNAi-1)* does not show any differences in GFP levels compared to control guts (*esg^{TS}Flip > Luciferase),* both in terms of total number of GFP-positive cells (Control n = 20, KD n = 36) (***A***) and % of GFP-positive cells normalized to the total cell number/FOV (Control n = 22, KD n = 36) (***B***) . Data is not normally distributed so Mann- Whitney U-tests were used for statistical analysis.

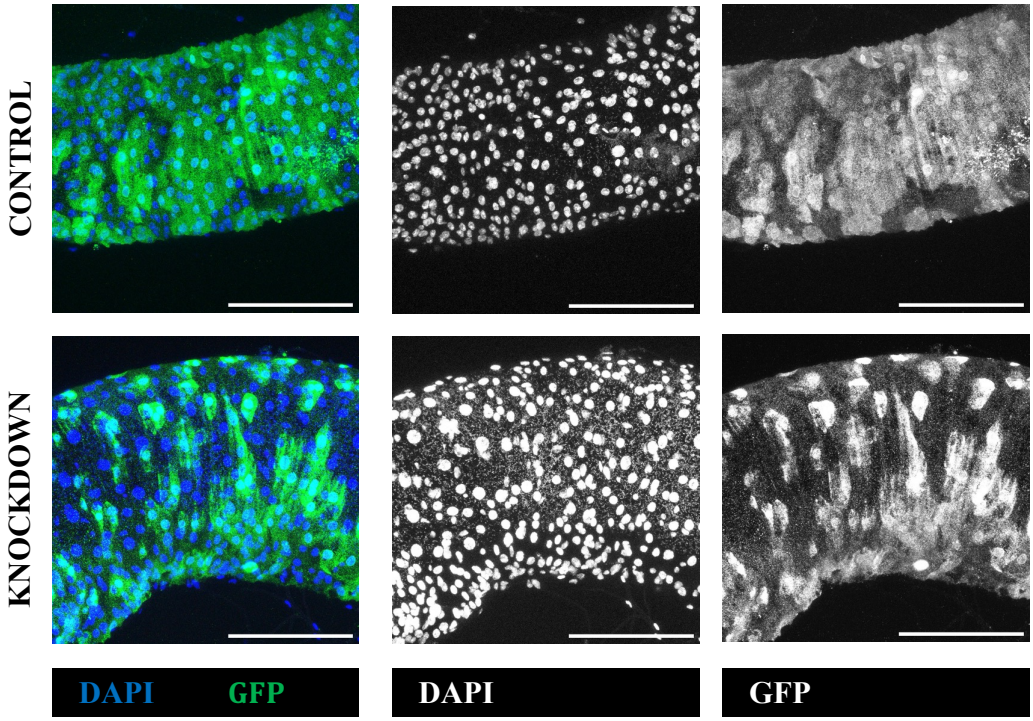

Figure 3.18. Knockdown of *SPARC-RNAi-2* driven by *esg^{TS}Flip* decreases the number GFP-positive cells in SPARC knockdown. SPARC knockdown (*esg^{TS}Flip > UAS-SPARC-RNAi-2)* decreases GFP expression compared to control guts (*esg^{TS}Flip > Luciferase)*. GFP tags SPARC-expressing cells and its clones. Guts were stained with α-GFP (1:2000) and DAPI. Scale bars in the bottom right corner represent 100μm.

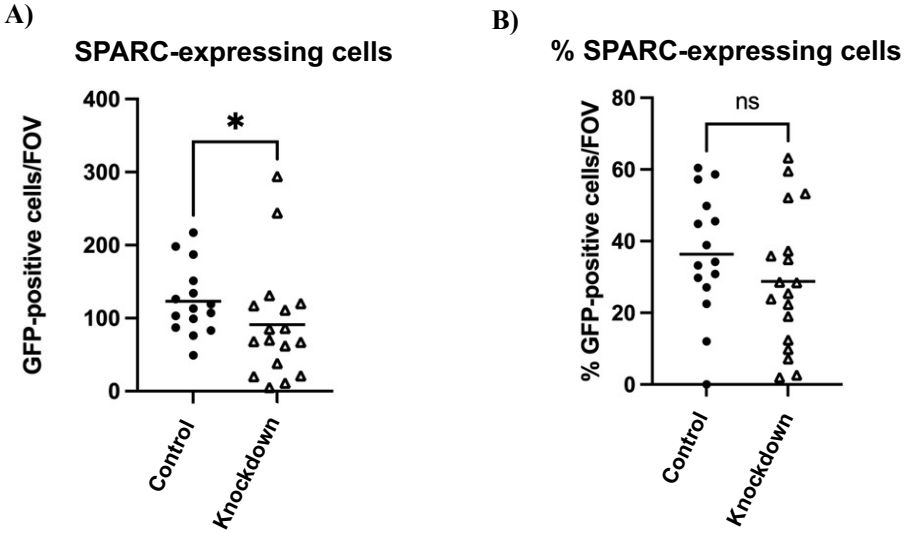

Figure 3.19. Quantification of the knockdown of SPARC using *SPARC-RNAi-2* driven by *esg^{TS}Flip* shows a significant decrease in GFP-positive cells in SPARC-knockdown guts compared to controls. SPARC knockdown (*esg^{TS}Flip > UAS-SPARC-RNAi-2)* significantly decreases the number of GFP-positive cells in SPARC knockdown guts compared to control guts (*esg^{TS}Flip > Luciferase)* (p = 0.04) (A) (Control n = 15, KD n = 17) (***A***), but the % of GFP-positive cells normalized to the total cell number/FOV remains unchanged (Control n = 15, KD n = 18) (***B***). Unpaired t-tests were used for the stastistical analysis of normally-distributed data (B), and Mann-Whitney U-tests for non-normally distributed data (A).

3.3.5. SPARC is not expressed in stem and progenitor cells

After concluding that alteration of SPARC levels in stem and progenitor cells affects, in some capacity, the homeostasis of the gut tissue, the next step was to characterize the expression pattern of SPARC within the different cells of the gut. Morin et al. (2001) developed a protein trap system whereby GFP tags the endogenous protein and allows the visualization of protein localization within the cell and the dynamics of their distribution. Using an *UAS-eGFP reporter line > SPARC GeneTrap 77473*, we observed that SPARC-positive cells colocalize with prospero staining, which tags enteroendocrine cells (*Figure 3.20*). Interestingly, some SPARC-positive cells did not colocalize with prospero. This distinction of two different SPARC-expressing cell populations could be explained by the theory that the *Drosophila* gut has an EE-specific progenitor that bypasses the need for enteroblast cells, whereby the EE cells that arise from EBs and those that arise from the EE-specific progenitor have different SPARC expression patterns.

To further investigate this expression pattern, adult *esgLacZ* female flies were stained with a SPARC antibody (*Figure 3.21*). We observed no colocalization between stem and progenitor cells, stained with β-gal, and SPARC-positive cells. This shows that ISCs/EBs do not express SPARC. Interestingly, SPARC staining seems to be concentrated in the cytoplasm of cells containing larger nuclei. This hints to the possibility that SPARC could be expressed in absorptive enterocytes, the other type of differentiated cells in the tissue, rather than EEs, as suggested by the protein trap data.

The use of a GFP reporter line with a nuclear-localization sequence (*SPARC GeneTrap > UAS-GFP* nls) which expresses nuclear GFP in SPARC-expressing cells, also supported these findings, showing that SPARC staining is in a clear subset of EC nuclei. Only a few cells express SPARC, but these ECs seem to be arranged in a linear manner on the tissue (*Figure 3.22*), suggesting SPARC expression in the visceral muscle that surrounds the epithelium.

To test whether the manipulation of SPARC in the EEs plays a role in the homeostastic balance of the tissue, a specific EE-driver line, *prosGal4^{TS}* (kindly gifted by the O'Brien lab) was used to drive SPARC overexpression and knockdown (*Figure 3.23*), and changes to the tissue were quantified (*Figure 3.24*). There were no significant changes to the total number of cells observed per field of view, to the number of GFP-positive cells per FOV or the % of GFP-positive cells observed between the control and the

overexpression and knockdowns. From this, we concluded that EE-specific manipulation of SPARC expression levels has no effect on the midgut tissue.

Taken together, these results suggest that SPARC is not expressed by the stem and progenitor cells of the tissue. The main source of SPARC in the midgut could be the differentiated cells, either the enterocytes or a specific subset of enteroendocrine cells, but the data obtained does not allow for a conclusive expression pattern of this gene.

Since EE-specific manipulation has no effect on SPARC expression, one theory could be that the main source of SPARC in the midgut tissue are a specific subset of ECs, and that this SPARC is then transported to another specific subset of EE cells. Regardless, SPARC expression in the midgut is restricted to a very small subset of differentiated cells and is not expressed evenly across the tissue.

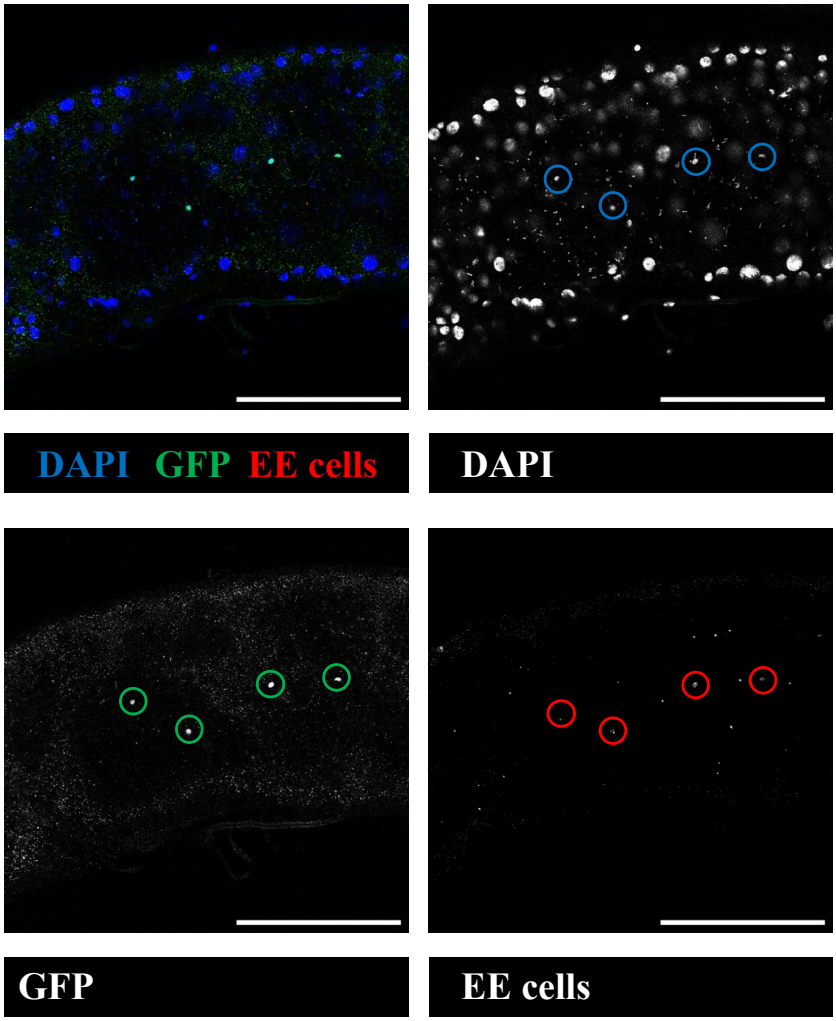

Figure 3.20. SPARC is expressed in EE cells in the posterior midgut. *SPARC Gal4 GeneTrap > UAS eGFP* showed colocalization between GFP, which tags SPARC-expressing cells, and the EE marker prospero. Guts were stained with α-GFP (1:2000), α-prospero (1:100), and DAPI. Scale bars in the bottom right corner represent 100μm.

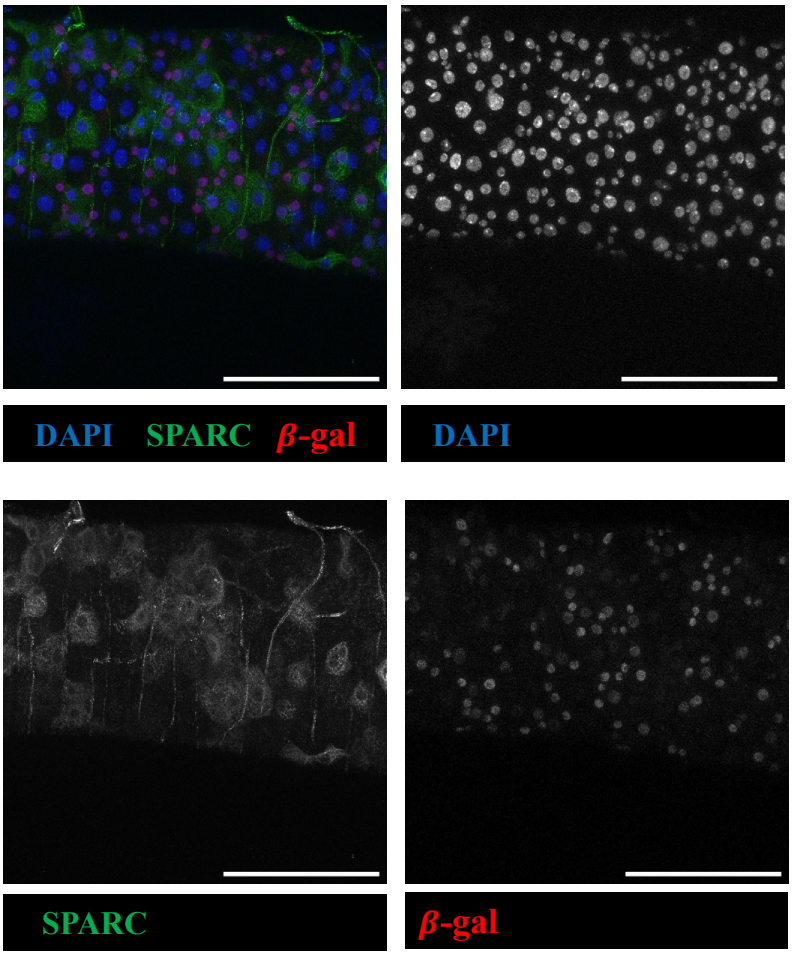

Figure 3.21. SPARC is not expressed in the stem and progenitor cells in the posterior midgut. *esgLacZ* female guts were stained with α-SPARC (1:100), α-β-galactosidase (1:500), and DAPI. β-galactosidase tags stem and progenitor cells and results showed no colocalization with SPARC, indicating that SPARC is not expressed in ISCs and EBs. Scale bars in the bottom right corner represent 100μm.

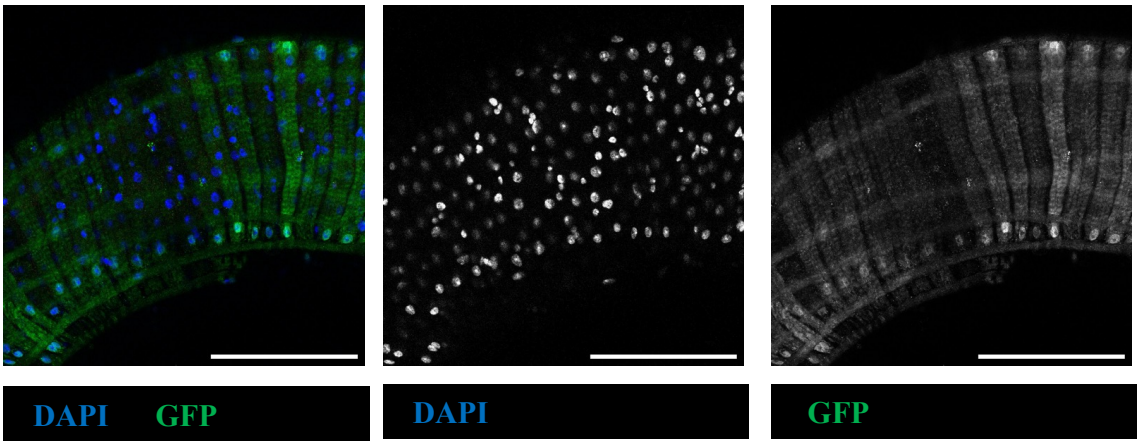

Figure 3.22. A nuclear localization sequence suggest SPARC is expressed in the larger cells of the tissue. *SPARC Gal4 GeneTrap > UAS-GFP-nls* guts were stained with α-GFP (1:2000), and DAPI, where GFP tags SPARC-expressing cells, and results suggested that SPARC is expressed in the larger nuclei of the epithelial tissue, i.e. in the ECs. Scale bars in the bottom right corner represent 100μm.

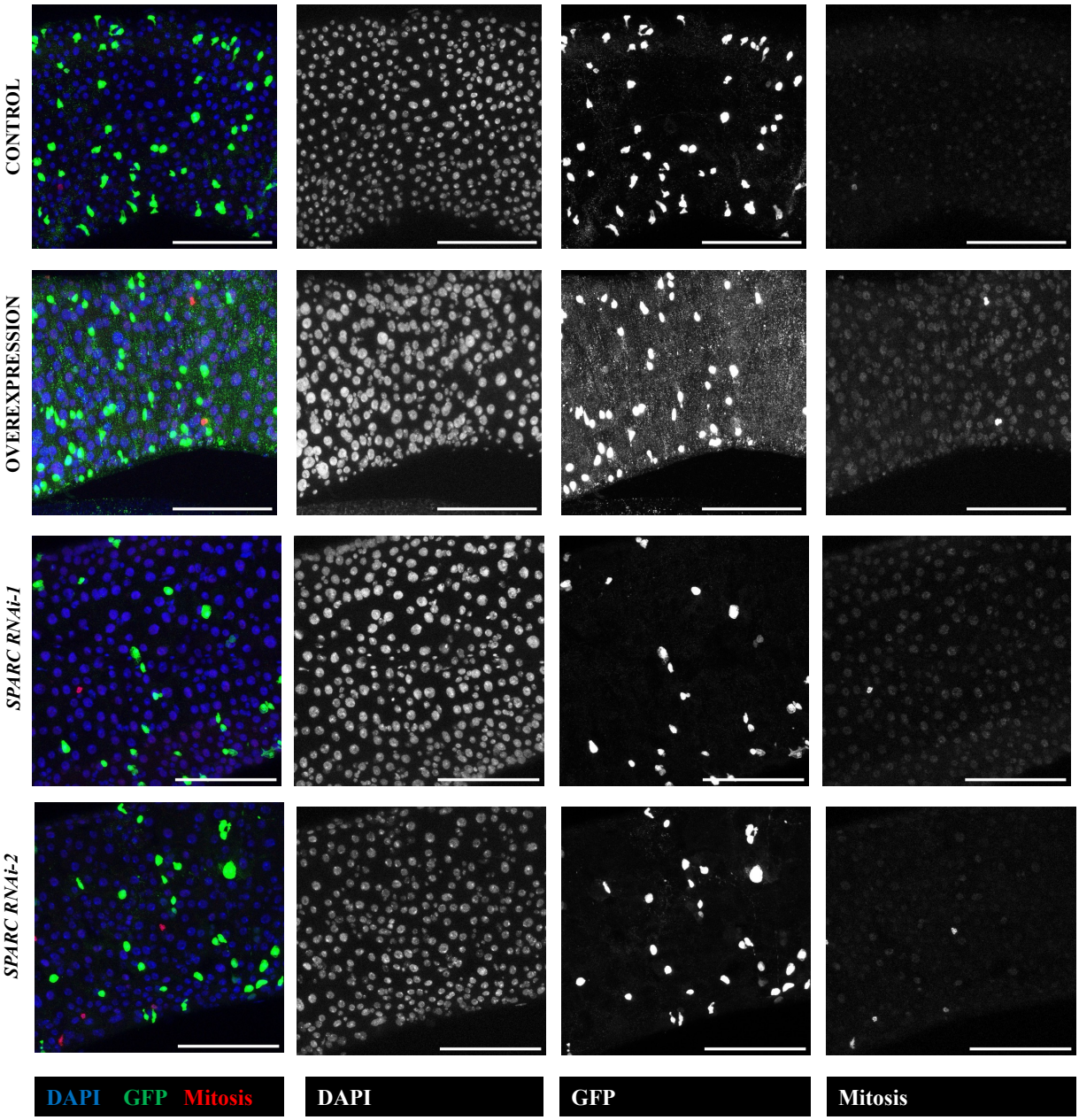

Figure 3.23. SPARC overexpression and knockdown driven by an EE-specific driver shown no changes compared to control guts. *ProsGal4^{TS}> UAS SPARC, prosGal4^{TS} > SPARC-RNAi-1, and prosGal4^{TS}> SPARC-RNAi-2* showed no changes in GFP-positive cells in the posterior midgut, or in the number of mitoses observed across the whole gut. Guts were stained with α-GFP (1:2000), α-PH3 (1:1000), and DAPI. Scale bars in the bottom right corner represent 100μm.

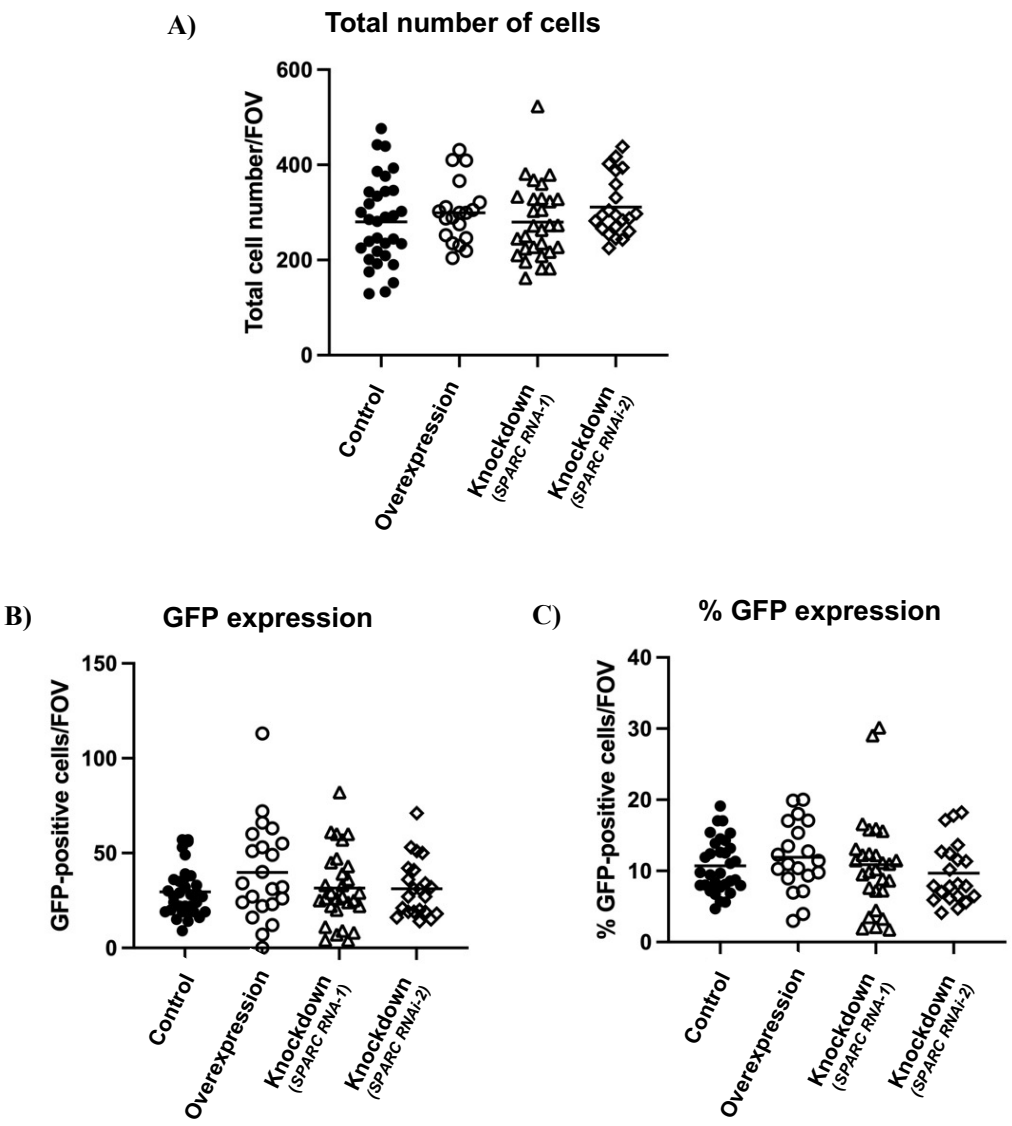

Figure 3.24. Quantification of SPARC overexpression and knockdown driven by an EE-specific driver shown no significant changes compared to control guts. *ProsGal4^{TS} > UAS SPARC, prosGal4^{TS}> SPARC-RNAi-1, and prosGal4^{TS}> SPARC-RNAi-2* showed no significant changes in the total number of cells in the gut (Control n = 32, OE n = 19, KD-1 n = 29, KD-2 n = 21) (***A***), the number of GFP-positive cells in the posterior midgut (Control n = 33, OE n = 22, KD-1 n = 29, KD-2 n = 22) (***B***), or in the % of GFP positive cells normalized to total cell number Control n = 32, OE n = 20, KD-1 n = 28, KD-2 n = 21) (***C***). or in the number of mitoses observed across the whole gut. Unpaired t-tests were used for the statistical analysis of normally-distributed data (OE DAPI, KD-1 DAPI, OE % GFP), and Mann- Whitney U-tests for non-normally distributed data. OE = overexpression, KD-1 = *SPARC-RNAi-1* and KD-2 = *SPARC-RNAi-2*.

3.3.6. The interactions of SPARC with collagen (vkg) and other ECM molecules

Since initial results had demonstrated a degree of tissue disorganization when SPARC levels were altered in the midgut, the next step was to determine the cause of this. SPARC and its interaction with collagen IV chains has been well documented in the literature in a variety of tissues and cellular contexts. We wanted to characterize the interaction between SPARC and collagen in the *Drosophila* midgut. There are two collagen IV genes in *Drosophila*, Viking (*Vkg*) and Cg25c (Shahab et al., 2015), which encode for collagen α-chain 2 and 1, respectively (Vaughan et al., 2018). *5961^{GS} > UAS SPARC, 5961^{GS} > UAS-SPARC RNAi 1* and *5961^{GS} > UAS-SPARC RNAi-2* female guts were analyzed using immunofluorescence and stained with an antibody raised against *Drosophila vkg*. There was a significant increase in the number of collagen-expressing cells per field of view in midguts with SPARC overexpression (*Figures 3.25 and 3.26A*). Similarly, a significant increase in vkg levels was observed in SPARC RNAi midguts but interestingly (*Figures 3.27 and 3.28A*), the proportion of vkg-positive cells in relation to total cell number, although higher in both cases, was not statistically significant (*Figures 3.26B and 3.28B*). On the contrary, knockdown of SPARC with *SPARC-RNAi-2* did not affect collagen levels in the midgut (*Figures 3.29 and 3.30*). Taken together, these results show that despite the close relationship between the two proteins in the ECM, collagen cannot be the only ECM components responsible for the disorganization of the tissue upon SPARC manipulation.

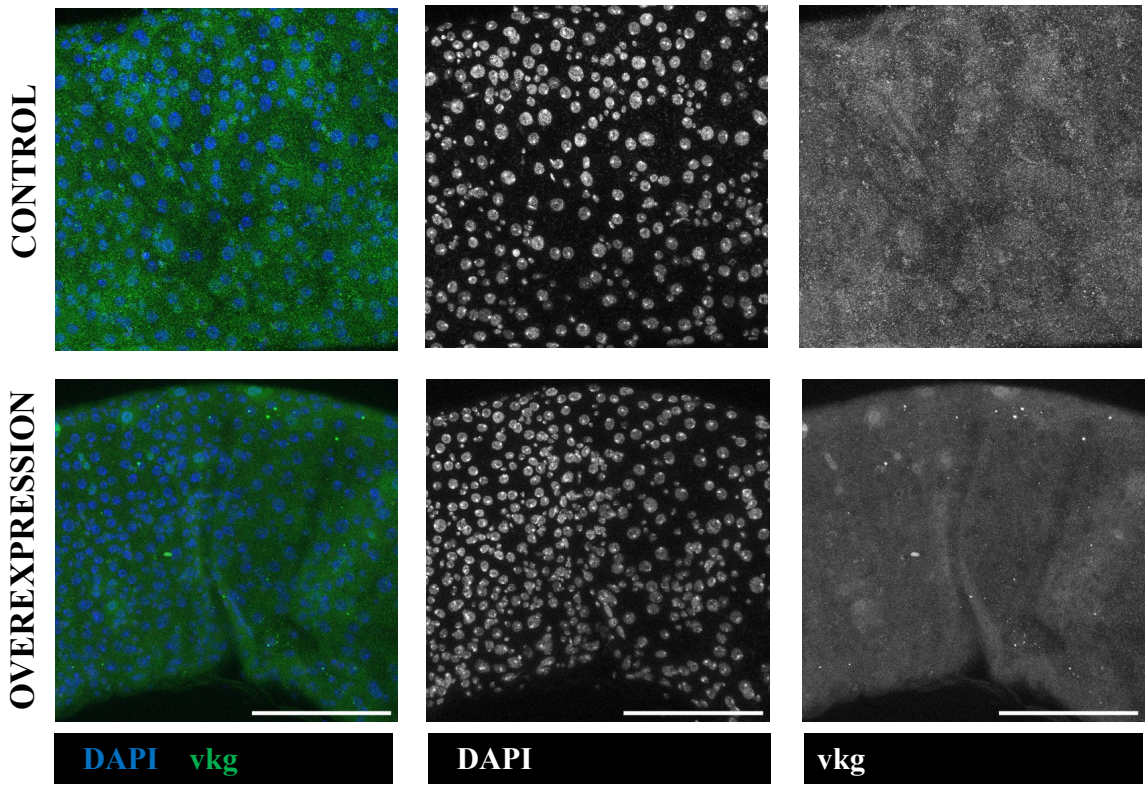

Figure 3.25. Collagen expression in SPARC-overexpressing guts. Overexpression of SPARC (*5961^{GS} > UAS SPARC*) seems to increase collagen (vkg) staining in the posterior midgut. Guts were stained with α- vkg (1:100) and DAPI. Scale bars in the bottom right corner represent 100μm.

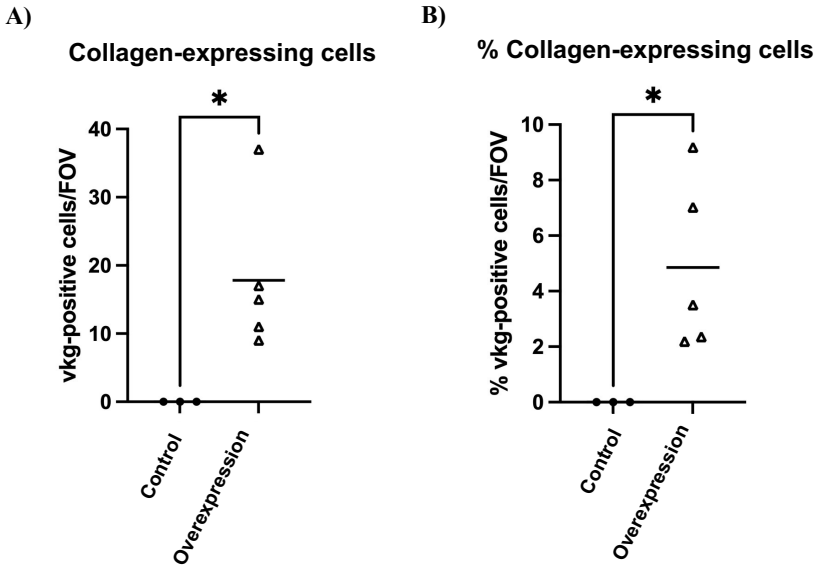

Figure 3.26. SPARC overexpression significantly increases the number of vkg-positive cells in the posterior midgut. Overexpression of SPARC (*5961^{GS} > UAS SPARC*) significantly increases both the total number of vkg-positive cells observed per FOV (p = 0.03) (control n = 3, OE n = 5) (***A***), as well as the proportion of vkg-positive cells normalized to total cell number/FOV (p = 0.03) (control n = 3, OE n = 5) (***B***). Data was normally distributed to unpaired t-tests were used for the statistical analysis. Each data point represents a gut.

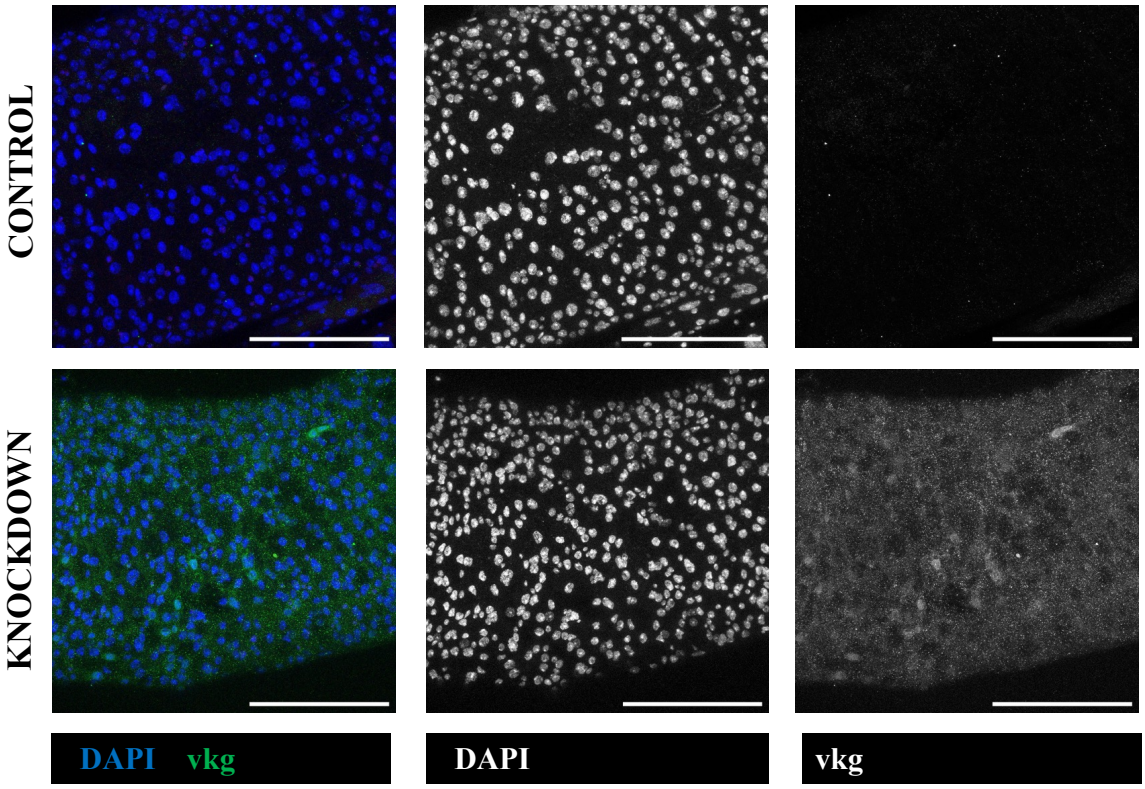

Figure 3.27. Collagen levels increase in *SPARC-RNAi-1* knockdown guts. Knockdown of SPARC (*5961^{GS} > SPARC-RNAi-1*) seems to increase collagen (vkg) staining in the posterior midgut. Guts were stained with α-vkg (1:100) and DAPI. Scale bars in the bottom right corner represent 100μm.

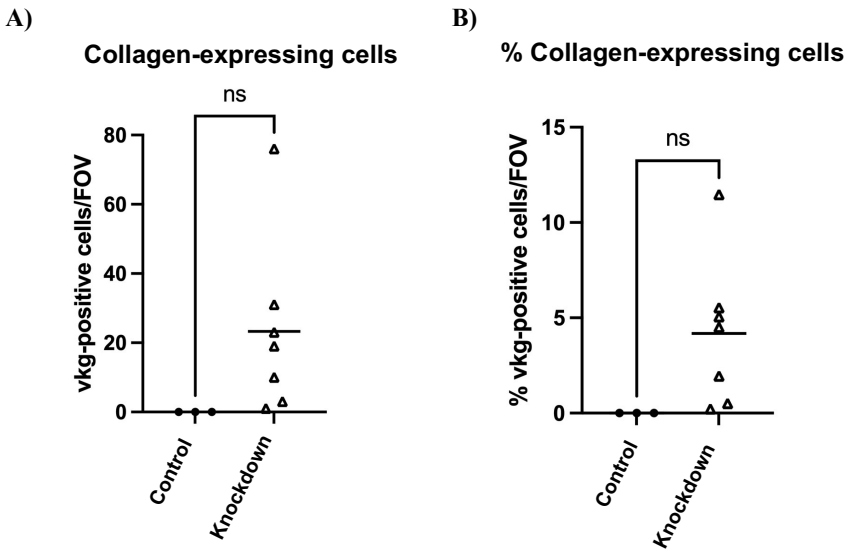

Figure 3.28. SPARC knockdown with *SPARC-RNAi-1* increases vkg expression in the posterior midgut. Knockdown of SPARC (*5961^{GS} > SPARC-RNAi-1*) increases both the total number of vkg-positive cells observed per FOV (***A***), as well as the proportion of vkg-positive cells normalized to total cell number/FOV (***B***), but statistical analysis did not deem these changes significant (p =0.1) (control n = 3, OE n = 7). Data was normally distributed to unpaired t-tests were used for the statistical analysis. Each data point represents a gut.

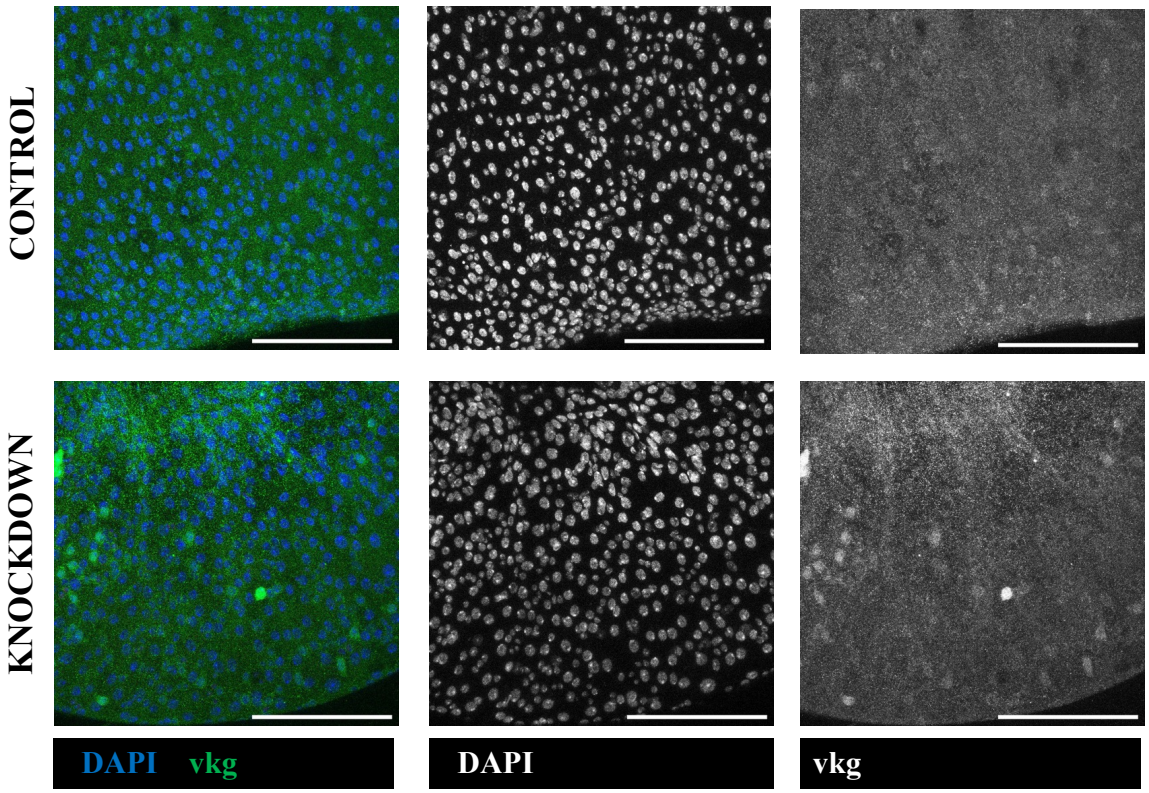

Figure 3.29. Collagen levels increase in *SPARC-RNAi-2* knockdown guts. Knockdown of SPARC (*5961^{GS} > SPARC-RNAi-2*) seems to increase collagen (vkg) staining in the posterior midgut. Guts were stained with α-vkg (1:100) and DAPI. Scale bars in the bottom right corner represent 100μm.

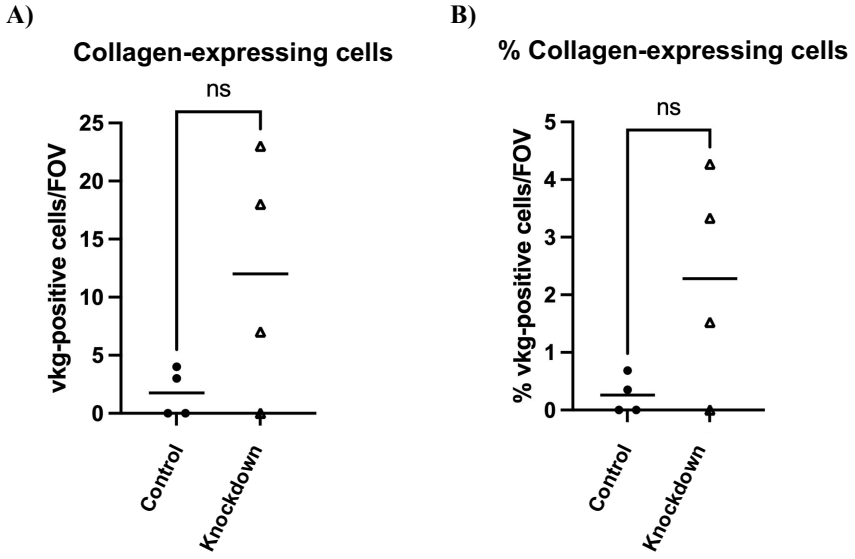

Figure 3.30. SPARC knockdown with *SPARC-RNAi-2* increases vkg expression in the posterior midgut. Knockdown of SPARC (*5961^{GS} > SPARC-RNAi-2*) increases both the total number of vkg-positive cells observed per FOV (***A***), as well as the proportion of vkg-positive cells normalized to total cell number/FOV (***B***), but statistical analysis did not deem these changes significant (p = 0.1) and (p = 0.08), respectively (n = 4). Data was normally distributed to unpaired t-tests were used for the statistical analysis. Each data point represents a gut.

We then wanted to establish if perhaps actin, one of the most important cytoskeletal components of the cell which closely interacts with ECM molecules, could play a role in maintaining tissue homeostasis. *5961^{GS} > UAS SPARC, 5961^{GS} > UAS-SPARC RNAi-1* and *5961^{GS} > UAS-SPARC RNAi-2* female guts were stained with Phalloidin, which stains F-actin filaments in the cell (*Figure 3.31*). Because the F-actin filaments are found throughout the tissue, results were quantified using the mean intensity of phalloidin staining between control and overexpression/knockdown midguts. Results showed a significant decrease in phalloidin intensity in SPARC-overexpressing guts (*Figure 3.31A*) and in *5961^{GS} > SPARC-RNAi-1 (Figure 3.31B)*, but no significant change between controls and the other SPARC knockdown line, *SPARC RNAi-2* (*Figure 3.31C*).

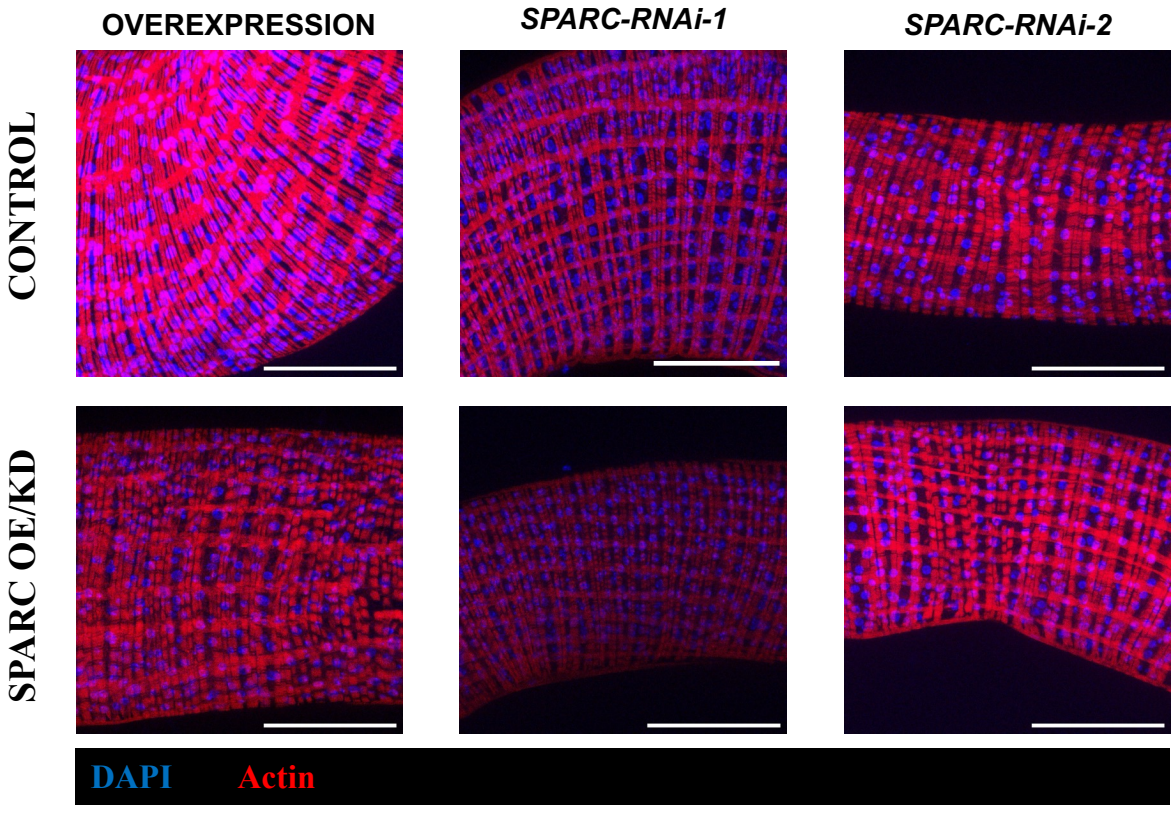

Figure 3.31. The actin filament network in SPARC overexpression and knockdown guts. Overexpression of SPARC and knockdown with RNAi line-1 seem to decrease the strength of phalloidin staining compared to control guts. Moreover, in SPARC overexpression guts, the actin filaments seem to be disrupted. No striking phenotypic changes are observed when SPARC is knocked down with SPARC RNAi line 2. Guts were stained with phalloidin (1:100) and DAPI. Scale bars in the bottom right corner represent 100μm.

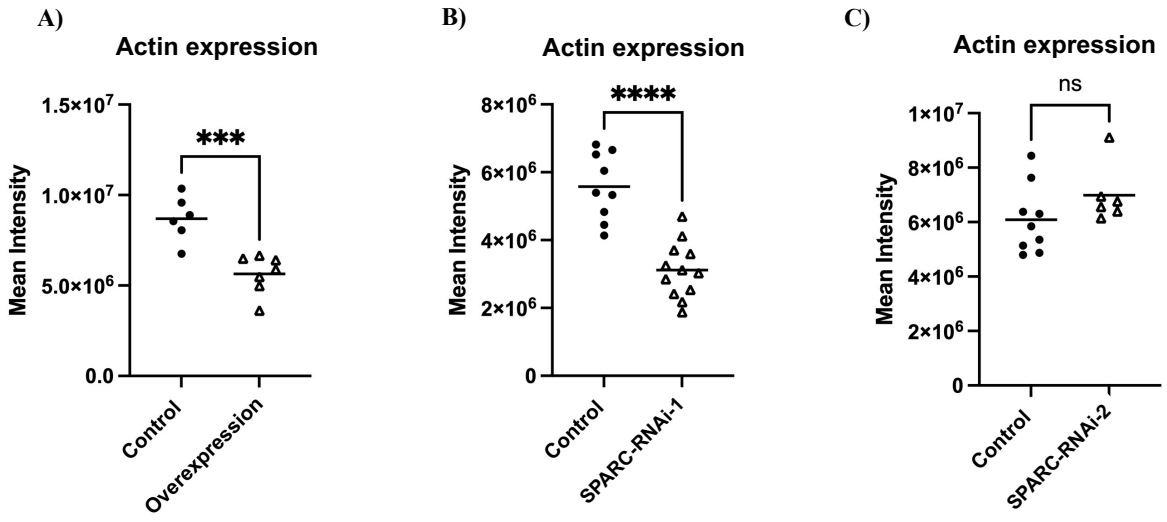

Figure 3.32. Changes to SPARC expressions levels alter the intensity of actin filament staining. Overexpression of SPARC (*5961^{GS} > UAS SPARC*) (control n = 6, OE n = 7) (***A***) and knockdown of SPARC with RNAi line 1 (*5961^{GS} > SPARC-RNAi-1*) (control n = 9, KD n = 12) (**B**) significantly decrease the intensity of actin filament staining ($p = 0.0006$ and $p < 0.0001$, respectively). Knockdown of SPARC with RNAi line 2 (*5961^{GS} > SPARC-RNAi-2*) does not affect actin staining ($p = 0.08$) (control n = 9, KD n = 6) (***C***). Unpaired t-tests were used for the statistical analysis of normally-distributed data (A, B), and Mann- Whitney U-tests for non-normally distributed data (C). Each data point represents a gut.

In order to further characterize the relationship between SPARC and the different ECM components, and how SPARC knockdown affected the basement membrane of the epithelial tissue, *5961^{GS} > SPARC RNAi-2* samples were prepared for transmission electron microscopy (TEM). However, issues beyond my control pertaining to the electron microscopy facility meant these experiments were delayed, and only protocol optimization was carried out. At the time of this submission, these samples are being processes by the team at the electron microscopy facility at Durham University. These will hopefully help to better understand the effects of SPARC on BM integrity.

Taken together, these results show that manipulation of SPARC in the stem and progenitor cells of the *Drosophila* midgut has a significant, impact on both collagen and actin levels in the tissue, although there are inconsistent variabilities between experiments.

3.3.7. The impact of SPARC on *Drosophila* gut signalling

In parallel to looking at the effects of SPARC at the cellular and ECM levels, its impact on gut signaling was also explored. Guts where SPARC overexpression or knockdown was driven by 5961^{GS} were stained with MAPK, SMAD and SAPK/JNK antibodies. Quantification of results is expressed as total number of cells positive for each antibody, per field of view. Overall active MAPK expression was significantly lower in SPARC-overexpressing guts compared to controls (*Figures 3.33 and 3.34*), as well as in *SPARC-RNAi-1* knockdown guts (*Figures 3.35 and 3.36*), and significantly higher in guts where SPARC was knocked down with SPARC-RNAi-2 (*Figures 3.37 and 3.38*). These results suggest that SPARC could be acting upstream of Ras/MAPK signaling to negatively regulate pathway activity.

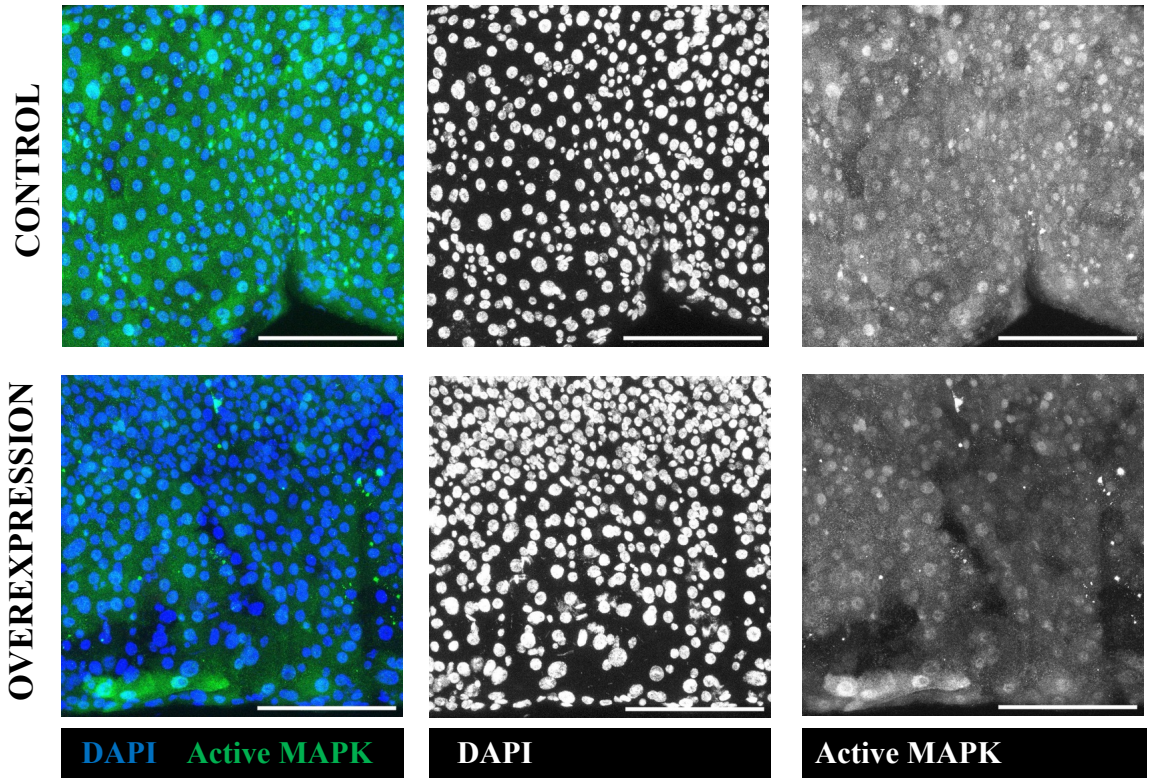

Figure 3.33. The expression of active MAPK in SPARC-overexpressing guts. Overexpression of SPARC (*5961^{GS} > UAS SPARC*) reduces the number of active MAPK-positive cells in the posterior midgut. Guts were stained with α- phospho-p44/42 MAPK (Erk1/2) (1:200) and DAPI. Scale bars in the bottom right corner represent 100μm.

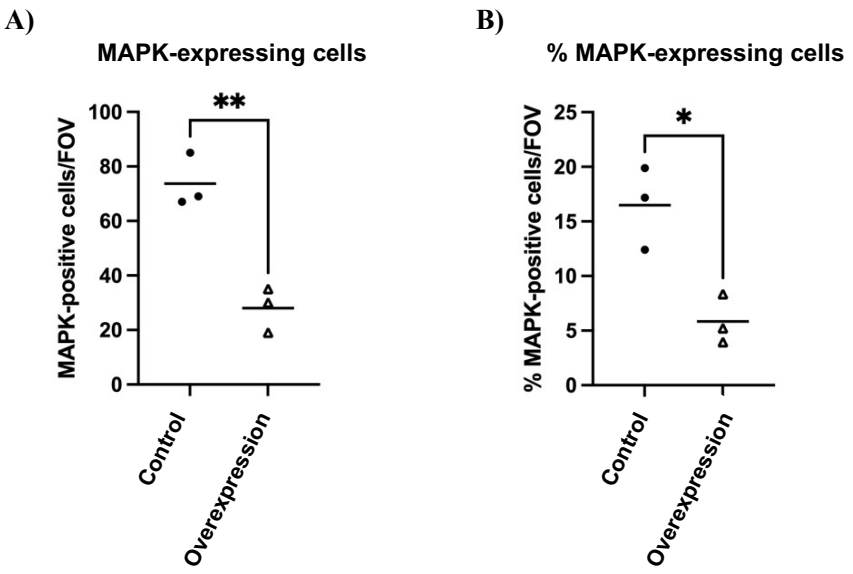

Figure 3.34. Active MAPK expression significantly decreases with SPARC overexpression. Overexpression of SPARC (*5961^{GS} > UAS-SPARC*) significantly decreases the levels of active MAPK expression in SPARC-overexpressing guts compared to controls ($p = 0.003$) ($n = 3$) (***A***). The proportion of active MAPK-positive cells normalized to total cell number is also significantly decreased with SPARC overexpression ($p = 0.01$) ($n = 3$) (***B***). Data was normally distributed so unpaired t-tests were used for the statistical analysis. Each data point represents a gut.

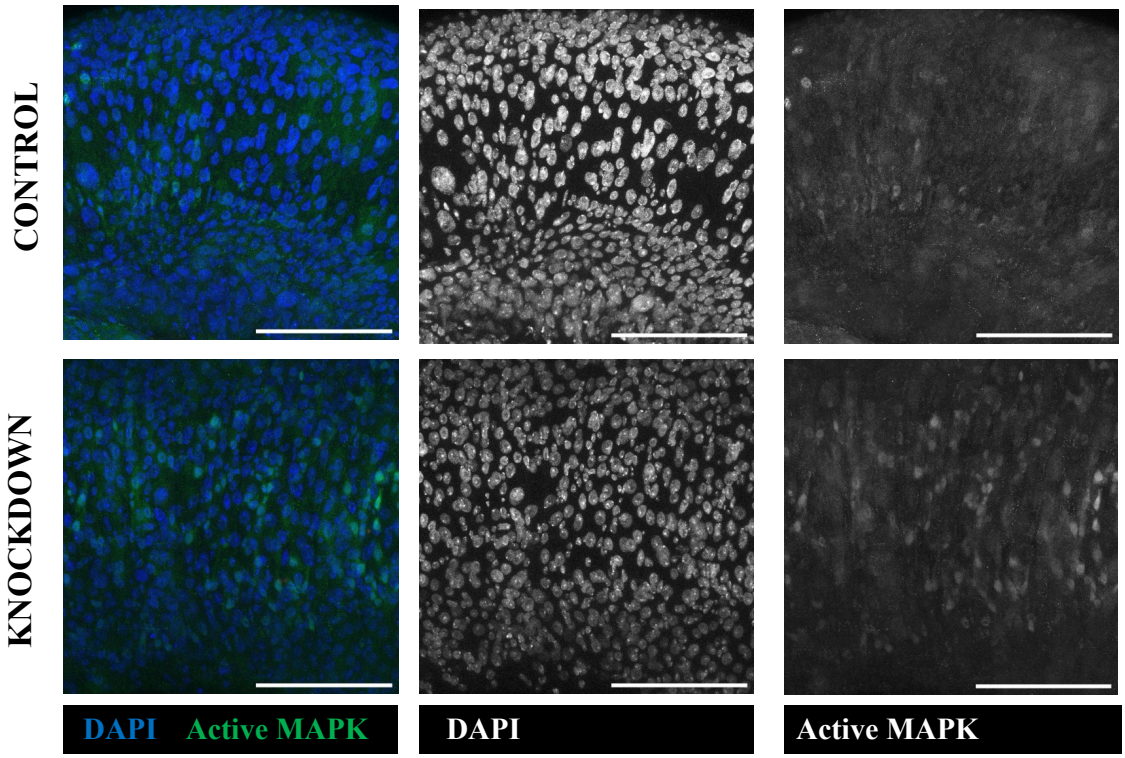

Figure 3.35. The expression of active MAPK in *SPARC-RNAi-1* knockdown guts. Knockdown of SPARC (*5961^{GS} > SPARC-RNAi-1*) increases the number of active MAPK-positive cells in the posterior midgut. Guts were stained with α- phospho-p44/42 MAPK (Erk1/2) (1:200) and DAPI. Scale bars in the bottom right corner represent 100μm.

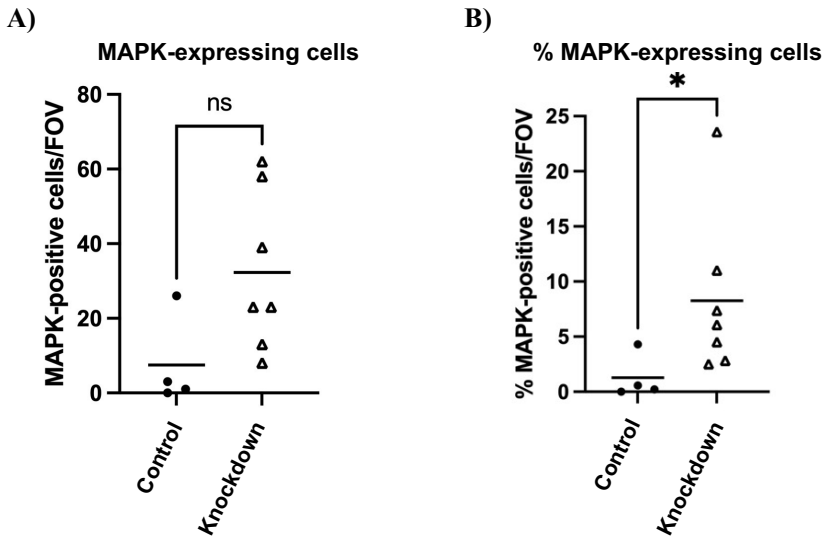

Figure 3.36. Active MAPK expression increases with SPARC knockdown with *SPARC-RNAi-1*. Knockdown of SPARC (*5961^{GS} > SPARC-RNAi-1*) increases the levels of active MAPK expression in SPARC-knockdown guts compared to controls, but this change is not statistically significant (p = 0.06) (control n = 4, OE n = 7) (***A***). However, the proportion of active MAPK-positive cells normalized to total cell number is significantly increased with SPARC overexpression (p = 0.02) (control n = 4, OE n = 7) (***B***). Data was not normally distributed, so non-parametric Mann Whitney-U tests were used for statistical analysis. Each data point represents a gut.

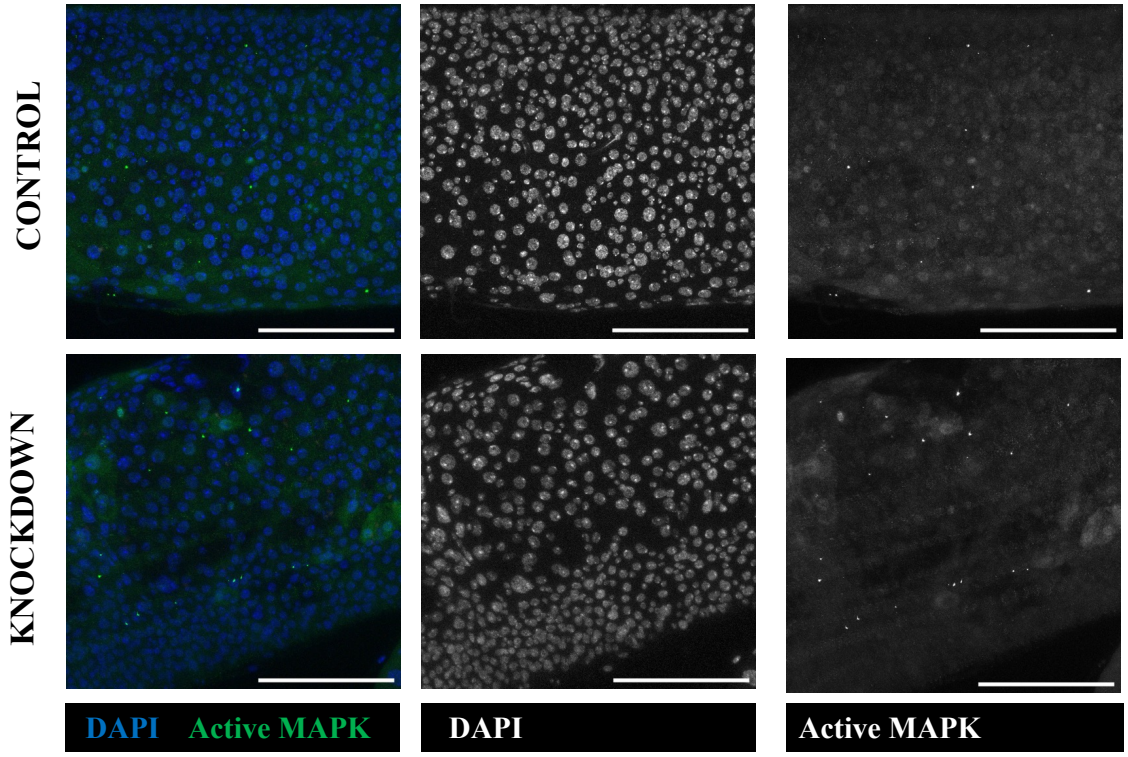

Figure 3.37. The expression of active MAPK in *SPARC-RNAi-2* knockdown guts. Knockdown of SPARC (*5961^{GS} > SPARC-RNAi-2*) does not change the number of active MAPK-positive cells in the posterior midgut. Active MAPK expression is low in both experimental groups. Guts were stained with α- phospho-p44/42 MAPK (Erk1/2) (1:200) and DAPI. Scale bars in the bottom right corner represent 100μm.

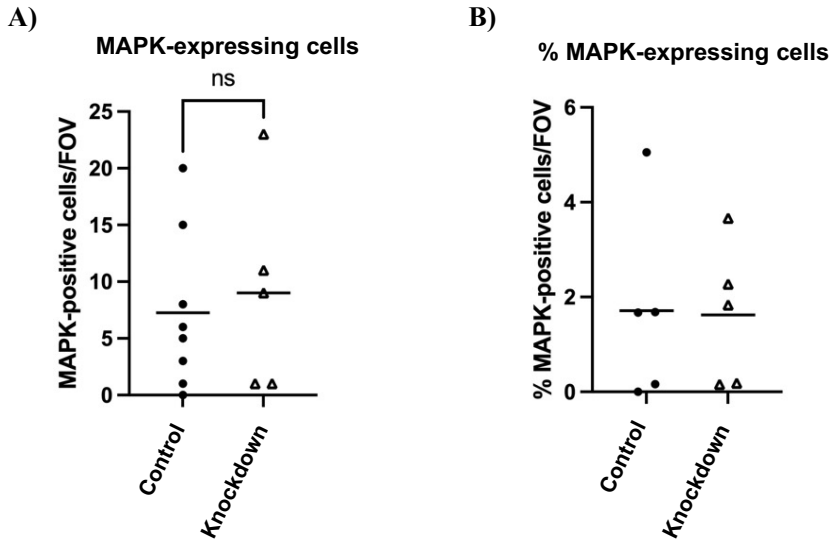

Figure 3.38. Active MAPK expression does not change in *SPARC-RNAi-2* knockdown guts. Knockdown of SPARC (*5961^{GS} > SPARC-RNAi-2*) slightly increases the levels of active MAPK expression in SPARC-knockdown guts compared to controls, but this change is not statistically significant (control n = 8, OE n = 5) (***A***). The proportion of active MAPK-positive cells normalized to total cell number remains unchanged between control and knockdown guts (n = 5) (***B***). Data was normally distributed so unpaired t-tests were used for the statistical analysis. Each data point represents a gut.

SMAD staining showed opposite trends. SMAD levels were higher in the overexpression guts, in both total number and % of SMAD-expressing cells compared to controls (*Figures 3.39 and 3.40*). In guts were SPARC has been knocked down, SMAD expression levels do not differ compared to controls (*Figures 3.40 and 3.41)*.

Staining of SAPK/JNK in *SPARC RNAi-2* knockdown guts (*Figure 3.42*) showed no significant change in active SAPK (*Figure 3.42A*), but interestingly, the percentage of SAPK-positive cells normalized against the total number of cells showed an increase in knockdown guts compared to controls (*Figure 3.42B*), although this trend was not statistically significant.

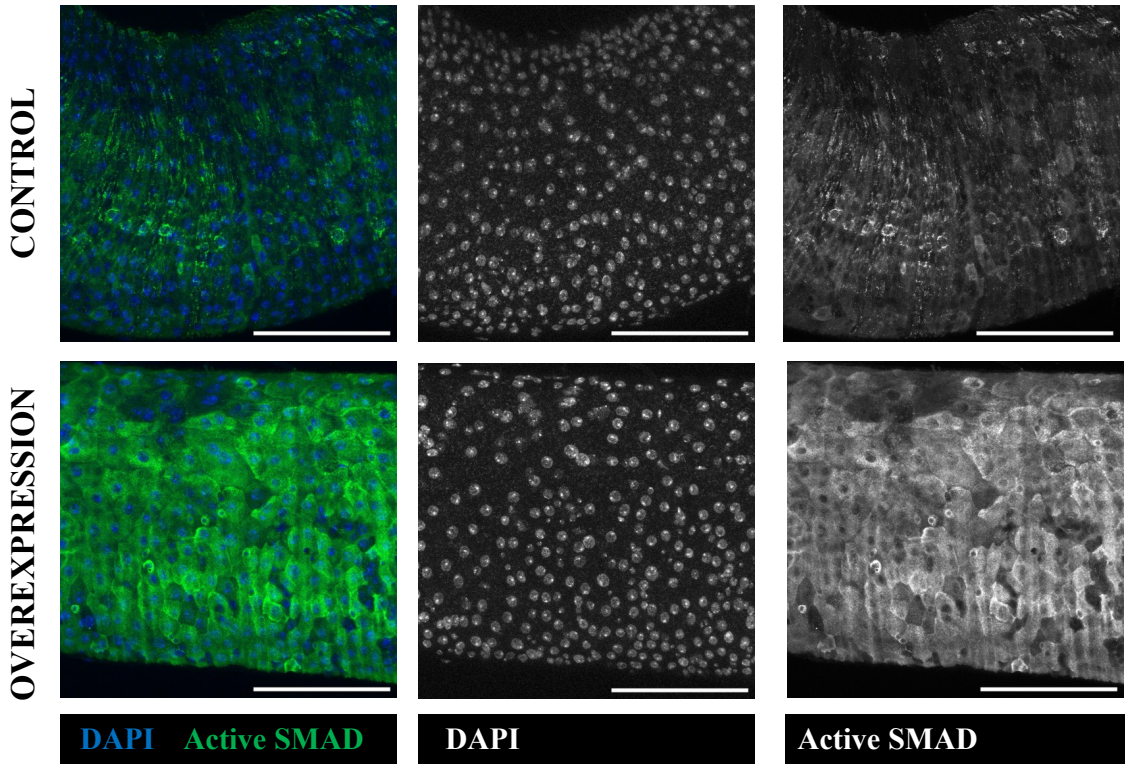

Figure 3.39. The expression of active SMAD in SPARC-overexpressing guts. Overexpression of SPARC (*5961^{GS} > UAS SPARC*) increases active SMAD expression in the posterior midgut. Guts were stained with α- phospho-Smad3 (1:100) and DAPI. Scale bars in the bottom right corner represent 100μm.

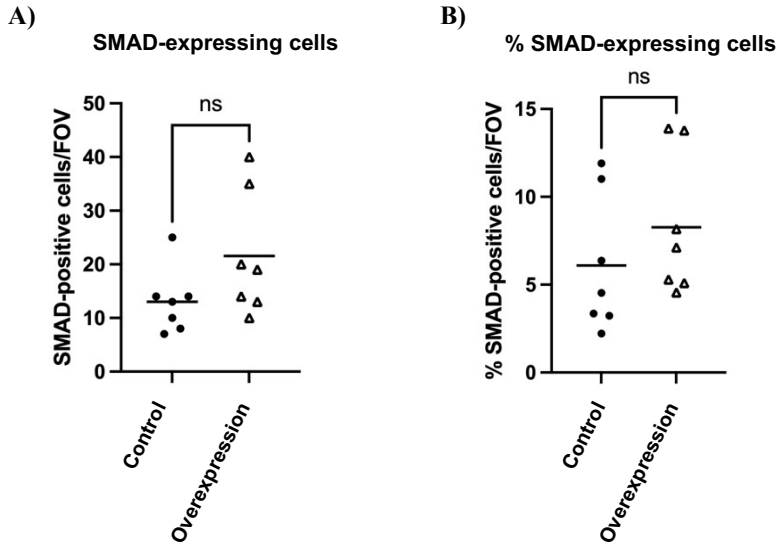

Figure 3.40. Active SMAD expression increases with SPARC overexpression. Overexpression of SPARC (*5961^{GS} > UAS-SPARC*) increases the levels of active SMAD expression in SPARC-overexpressing guts compared to controls, but this trend is not statistically significant (p = 0.1) (n = 7) (***A***). The proportion of active SMAD-positive cells normalized to total cell number is also increased with SPARC overexpression, but statistical analysis did not deem this change significant (p = 0.3) (n = 7) (***B***). Data was normally distributed so unpaired t-tests were used for the statistical analysis. Each data point represents a gut.

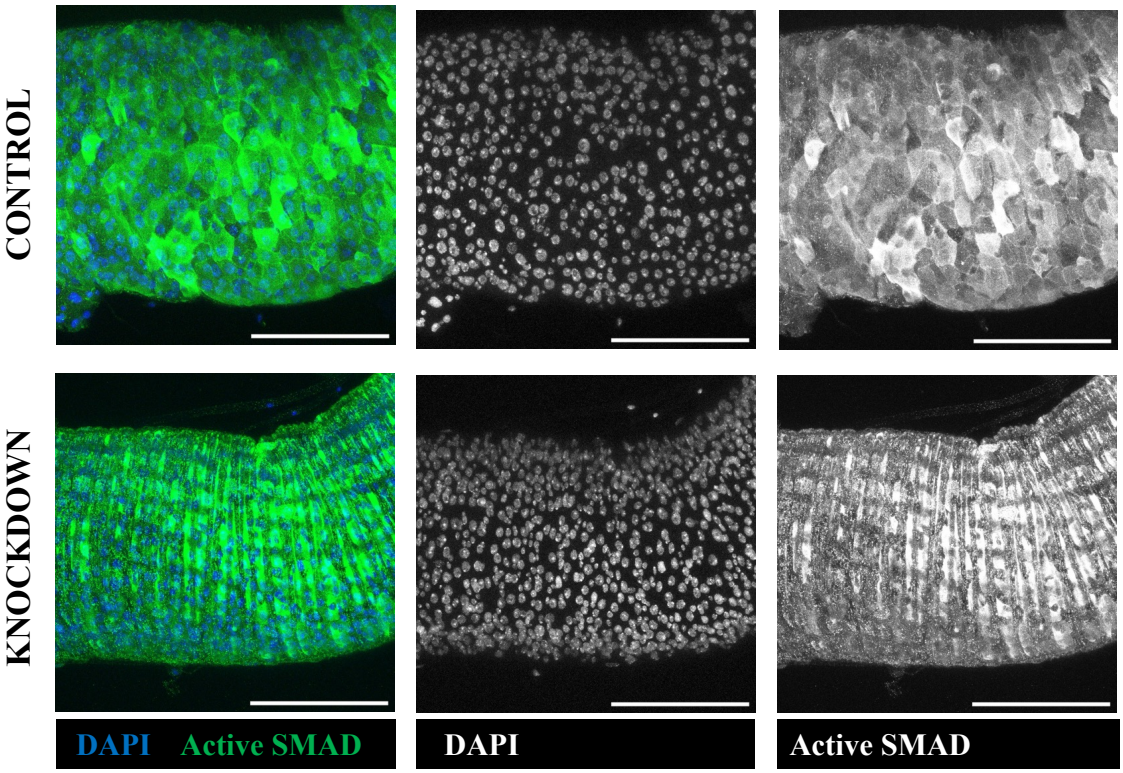

Figure 3.41. The expression of active SMAD in SPARC knockdown guts. Knockdown of SPARC (*5961^{GS} > SPARC-RNAi-1)* does not change active SMAD expression in the posterior midgut. Guts were stained with α- phospho-Smad3 (1:100) and DAPI. Scale bars in the bottom right corner represent 100μm.

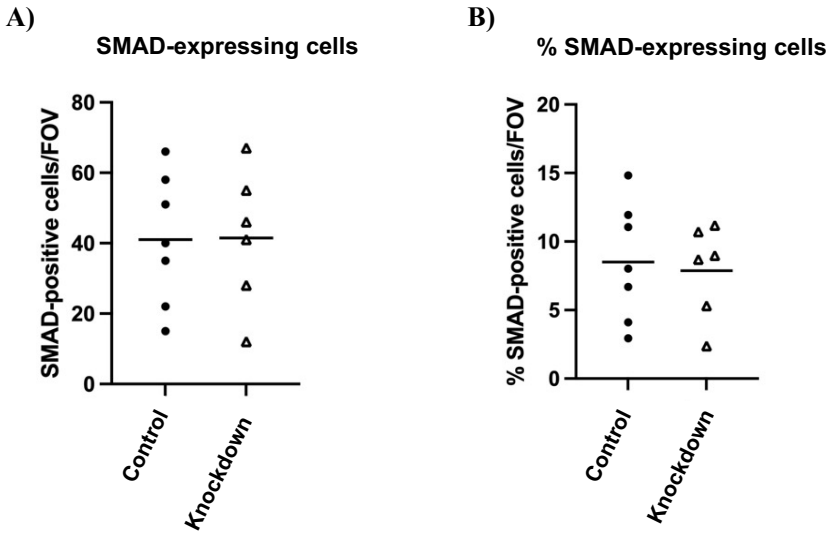

Figure 3.42. Active SMAD expression does not change with SPARC knockdown. Knockdown of SPARC (*5961^{GS} > SPARC-RNAi-1*) does not change the number of SMAD-positive cells observed per field of view (***A***), or the proportion of active SMAD-positive cells normalized to total cell number (***B***). Data was normally distributed so unpaired t-tests were used for the statistical analysis. Each data point represents a gut. (control n = 7, OE n = 6).

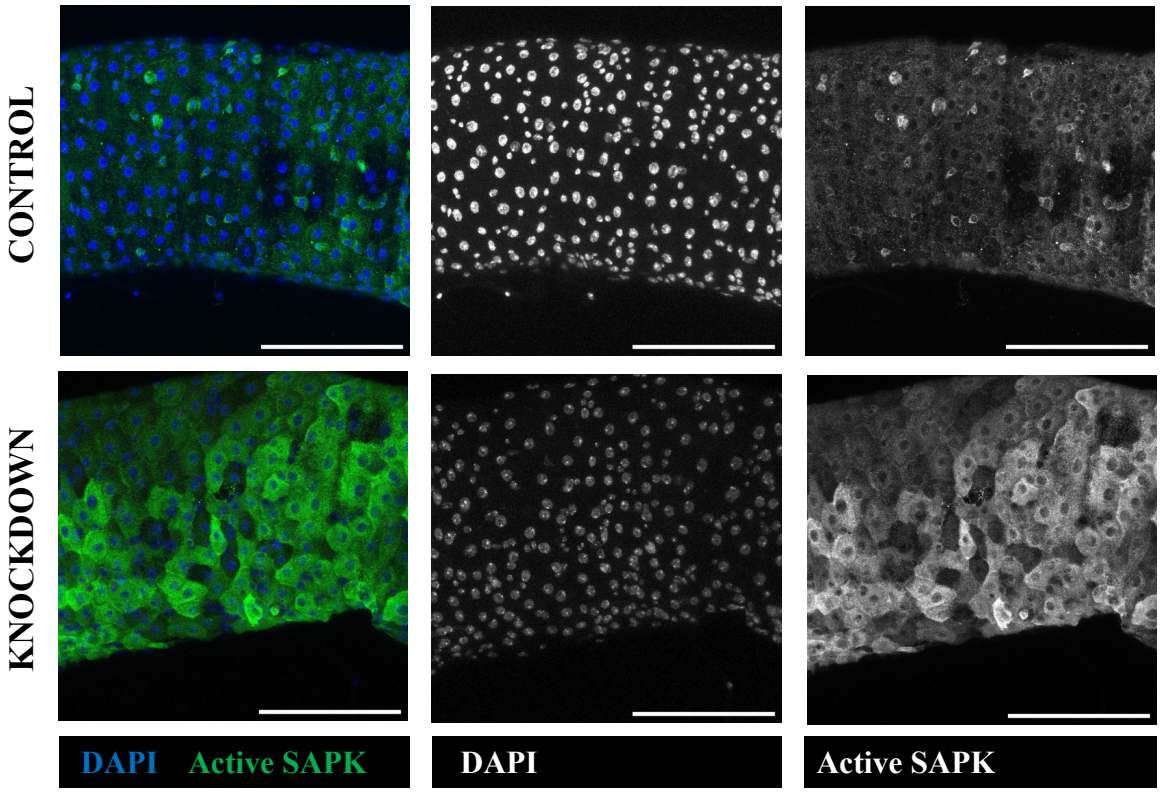

Figure 3.43. The expression of active SAPK/JNK in SPARC knockdown guts. Knockdown of SPARC (*5961^{GS} > SPARC-RNAi-2*) increases the number of active SAPK/JNK-positive cells in the posterior midgut. Guts were stained with α- phospho-SAPK/JNK (1:100) and DAPI. Scale bars in the bottom right corner represent 100μm.

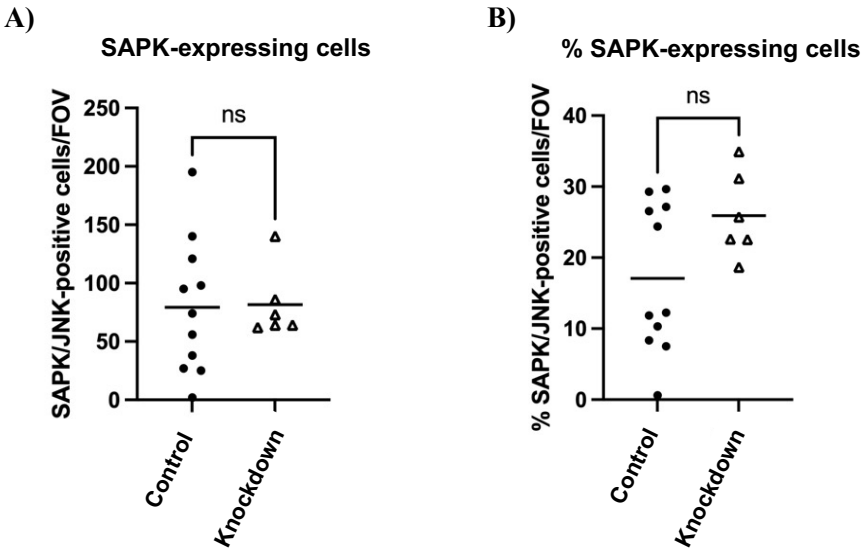

Figure 3.44. The proportion of active SAPK-expressing cells increases with SPARC knockdown. Knockdown of SPARC (*5961^{GS} > SPARC-RNAi-2*) does not change the total number of phospho-SAPK/JNK-positive cells in the posterior midgut (***A***), but the proportion of SAPK-expressing cells normalized to total cell number is increased in knockdown guts compared to controls (***B***). However, statistical analysis did not deem this change significant (p = 0.07) (control n = 11, OE n = 6). Unpaired t-tests were used for normally distributed data (B), and non-parametric Mann Whitney-U tests for non-normally distributed data (A). Each data point represents a gut.

Pathway activity was also assessed by RT-qPCR to determine the expression levels of known pathway targets. Since the Gene Switch driver is specific to stem and progenitor cells, and manipulation of SPARC levels in the immunofluorescence experiments is only occurring in a specific subset of cells of the tissue, *tubGal80^{TS} > UAS SPARC* and *tubGal80^{TS} > UAS SPARC RNAi* samples were analysed using qRT-PCR analysis. This way, the changes in expression levels of the protein are occurring in all cells of the tissue, giving a more accurate indication of which pathways may be acting downstream of SPARC expression in the *Drosophila* gut.

Using qPCR analysis and a combination of primers that have been validated in the literature as being common targets of some of the main signalling pathways in development, we analysed the effects on the JAK/STAT (Soc36e), Notch (m3, m5, m8 and mβ), JNK (puc), MAPK/RTK (pnt) and Dpp (brk and dad) signalling pathways of manipulating SPARC expression with SPARC-RNAi-1 (*Figure 3.45*) and SPARC-RNAi-2 (*Figure 3.46*). Taking together the results for both RNAi knockdown lines, components of the Notch signalling pathway show downregulation trends in SPARC RNAi samples, but these results are not statistically significant. The downregulation of puc suggests that JNK signalling could be one of the main regulators of SPARC expression in the *Drosophila* gut, with Notch also involved.

3.4. Discussion

In summary, the results presented here demonstrate that epithelial derived SPARC may play key roles in maintaining homeostasis of the *Drosophila* midgut, as alterations to the expression levels of the protein result in changes to the cell-composition of the midgut, its proliferative potential, and overall physiology. However, due to variability in results additional work is needed to confirm these findings. Manipulating SPARC levels also affects the collagen IV network of the tissue and thus, could play key roles in the maintenance of basement membrane integrity, and in turn contribute to disease progression. How SPARC is regulated in this context still remains to be elucidated. SPARC is hypothesized to be a regulator of MAPK, Notch and JNK activity in the *Drosophila* gut, but further studies are needed to determine to what extent these pathways are operating and any other potential interacting partners or compensatory mechanisms that could be activated upon manipulation of SPARC.

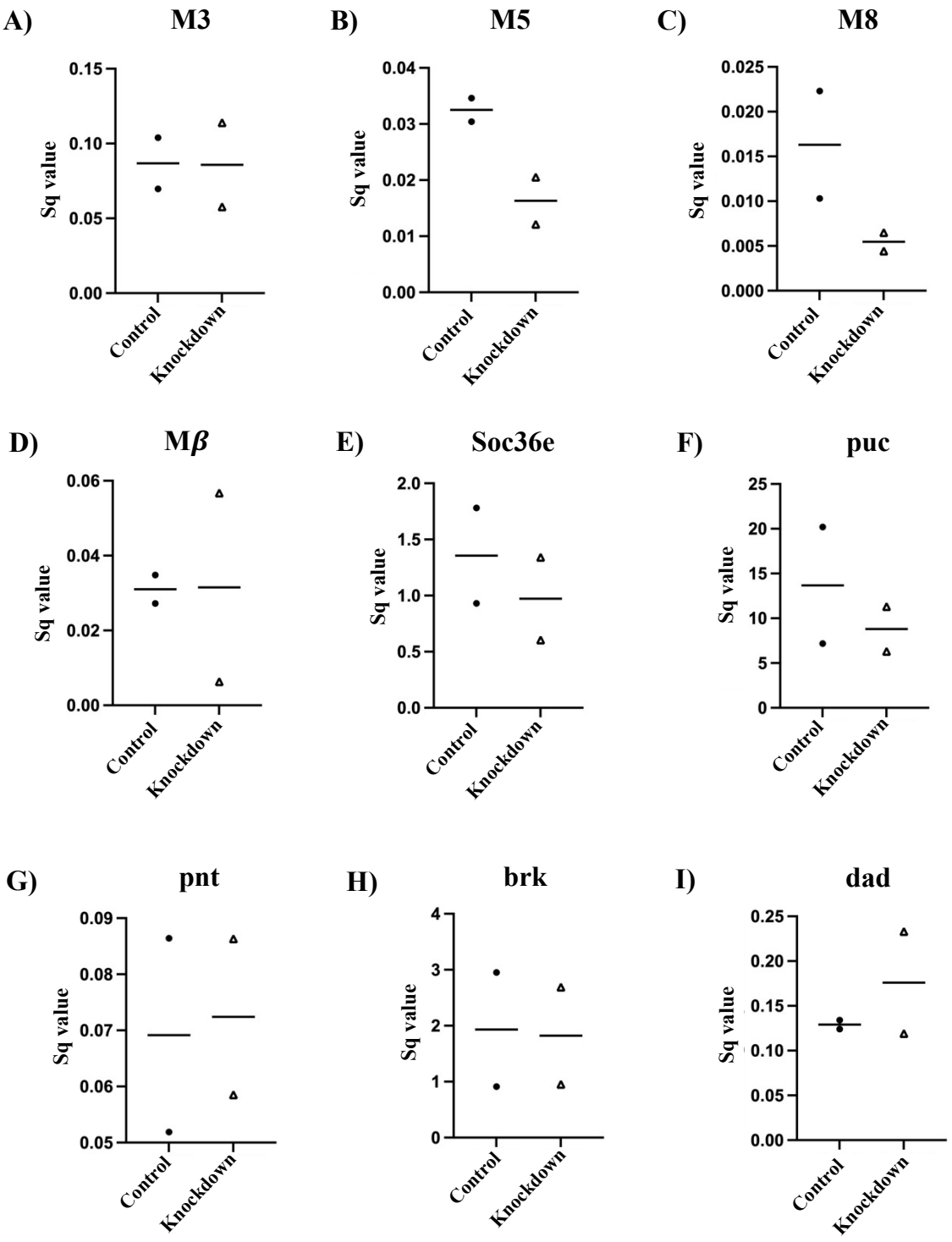

Figure 3.45. Expression changes of known targets of the major regulatory signaling pathways in *SPARC-RNAi-1* knockdown in whole guts. qPCR analysis of the expression levels of known pathway targets of Notch, JAK/STAT, JNK, MAPK/RTK and Dpp signaling showed that knockdown of SPARC (*TubGal80^{TS} > SPARC-RNAi-1*) decreases the expression levels of M5 (***B***), M8 (***C***), Soc36e (***E***), and puc (***F***) .dad levels (***I***) show an increasing trend with SPARC knockdown, and M3 (***A***), Mβ (***D***), pnt (***G***) and brk (***H***) levels remain unchanged. n = 2 for all samples and thus no statistical analysis was carried out. Expression has been normalized to a housekeeping gene (GADPH/α-tubulin). Expression changes have been calculated using Sq values. Each data point represents one sample and each sample contains 10 whole female guts.

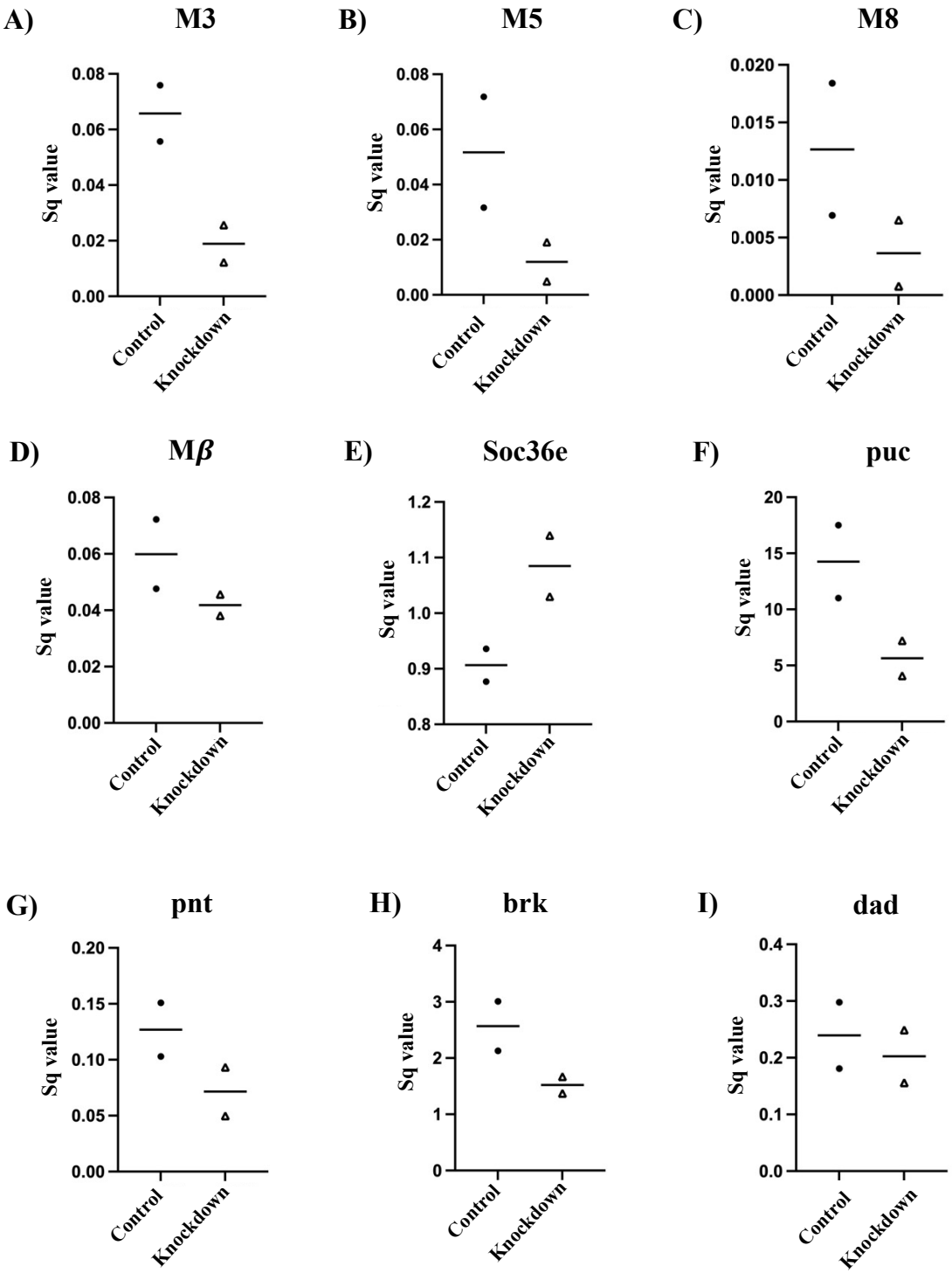

Figure 3.46. Expression changes of known targets of the major regulatory signaling pathways in *SPARC-RNAi-2* knockdown in whole guts. qPCR analysis of the expression levels of known pathway targets of Notch, JAK/STAT, JNK, MAPK/RTK and Dpp signaling showed that knockdown of SPARC (*TubGal80^{TS} > SPARC-RNAi-2*) decreases the expression levels of M3 (***A***), M5 (***B***), M8 (***C***), Mβ (***D***), puc (***F***), pnt (***G***) brk (***H***) and dad levels (***I***). Soc36e (***E***) shows an increasing trend with SPARC knockdown, n = 2 for all samples and thus no statistical analysis was carried out. Expression has been normalized to a housekeeping gene (GADPH/α-tubulin). Expression changes have been calculated using Sq values. Each data point represents one sample and each sample contains 10 whole female guts.

As discussed in the introduction, work from our group demonstrated that SPARC knockdown did not affect the proportion of ISCs and EBs in the *Drosophila* midgut but did impact cell density (Galbraith, unpublished). The aim of this project was to further characterize the expression, function and regulation of this protein in the context of ISC and EB regulation, to understand how epithelial cells contribute to their own niche microenvironment. The results presented in this chapter suggest that epithelial-derived SPARC plays a role in maintaining gut homeostasis, although further experiments are needed to validate these finding and characterize the specific function of this protein. Very few published studies have looked at the role of this protein in the midgut, and even fewer in the context of ISC homeostasis. Many of the studies that focus on characterizing SPARC do so in a tumourigenic context. Reduced levels of SPARC have been shown to increase invasion and migration of breast cancer cells (Ma et al., 2017). Previous reports have demonstrated an direct correlation between increased SPARC levels and enhanced inflammation in intestinal tissues (Fonseca-Camarillo et al., 2021), whereas in ovarian cancer the presence of SPARC reduces inflammation and "normalizes" the tumour microenvironment, slowing down disease progression (John et al., 2019). The proliferation of tumour cells has also been linked to SPARC, where some reports demonstrate that downregulation of SPARC reduces proliferation, invasion and the metastatic potential of the tumour (Liu et al., 2020). This decrease in the proliferative rates of tumour cells as a result of SPARC downregulation is consistent with the data presented here that demonstrates decreased ISC proliferation across the epithelial tissue of the *Drosophila* intestine in SPARC-knockdown guts. To date, no published study has looked at characterizing the role of SPARC expression in midgut ISC/EB homeostasis in the *Drosophila* gut, which makes comparison of the data presented here limited. Further studies are needed to obtain conclusive results about its effect on the tissue, in terms of alterations to its composition, proliferative potential and maintenance of tissue integrity.

Not many studies have assessed how changes to SPARC levels and subsequent imbalances to gut homeostasis affect the lifespan of the fly. Vaughan et al. demonstrated that a reduction in SPARC in cardiac tissue resulted in extended lifespan in *Drosophila*. This change, however, was not seen until after 35 days. Moreover, they did not find any changes to collagen deposition in the basement membrane and hypothesized that the health improvements associated with SPARC reduction in this tissue must be dependent on other mechanisms unrelated to collagen deposition (Vaughan et al., 2018). Despite not finding a significant change in lifespan in SPARC-knockdown guts, our results show a

similar trend of extended lifespan between days 60 and 75, which is a very short time window within the adult life of the fly. One possibility to explain this is that, once SPARC is knocked down at the 10 day timepoint, compensatory mechanisms are activated to offset the effects that this has on the tissue, and that compensation is not visible until later in the experiment. Considering that SPARC has been shown to reduce proliferation of ISCs and it is downregulated in some tumours, it is possible that SPARC extends lifespan by neutralizing, to some extent, some of the deregulations in proliferation associated with age. However, further experiments are needed to characterize this further by establishing if there are any changes to SPARC expression with age that could account for this. One limitation of the lifespan experiments presented here is that SPARC knockdown was not performed at the whole-tissue level, but rather just in a specific subset of gut cells, i.e. ISCs and EBs. Data presented here suggested that SPARC is expressed in a subset of differentiated cells, either ECs or EEs, which could imply that manipulation in the stem and progenitor cells of the tissue will translate into minimal effects on lifespan, as the SPARC levels are not knocked down at the main source. Therefore, in order to obtain conclusive results on the effects of SPARC overexpression and knockdown in the gut tissue on the lifespan of the fly, whole-gut knockdowns using *tub-Gal80^{ts}; tub-Gal4* as the driver would make an optimal sample for this.

The role of SPARC in post-embryonic and adult *Drosophila* tissues still remains to be characterized (Hartley et al., 2016), as most of the published literature has focused on fly larvae or *in vitro* studies. In the larval fat body, loss of SPARC expression results in a lethal phenotype (Shahab et al., 2015), and knockdown in adipocytes results in increased accumulation of collagen IV (Shahab et al. 2015). SPARC also facilitates secretion of collagen IV in hemocytes, and absence of functioning SPARC prevents collagen IV secretion into the basement membrane of *Drosophila* embryos (Bunt et al., 2010). This is not consistent with the data presented in this chapter, as both knockdown and overexpression of SPARC significantly increase vkg expression in the epithelial gut tissue. This could suggest that, in adult tissues, misregulation of SPARC expression of any kind could trigger compensatory mechanisms that inadvertently lead to an increase in collagen deposition in the tissue.

The role of SPARC as a key chaperone of collagen IV in *Drosophila* is well-established. Shahab et al. demonstrated that SPARC controls collagen IV polymerization, maintaining the solubility of the fibers and preventing collagen from rapidly assembling into a dense polymer sheet and from binding to integrins (Duncan et al., 2020). SPARC

and collagen IV form complexes in the endoplasmic reticulum of the cell that in turn allow for correct folding of the collagen chains (Bellenghi et al., 2022). Thus, SPARC is essential to regulate the stability of the basement membrane in epithelial tissues (Hartley et al., 2016). This is consistent with the immunofluorescence data that shows a SPARC-induced changes to vkg expression when the levels of the chaperone are manipulated. Interestingly, Shahab et al. demonstrated that SPARC secretion only acts as a chaperone to extracellular collagen, but manipulation of SPARC did not have significant effect on the levels of intracellular collagen IV. On the contrary, Duncan and colleagues showed accumulation of collagen IV in intracellular vesicles and in fat body cells when SPARC was absent from the tissue. This study goes further in the characterization of the chaperone activity of SPARC and hypothesizes that SPARC could have different affinity for collagen IV depending on the tissue, since the post-translational modifications that these two proteins undergo are context- and tissue-dependant. This context- and tissue-dependent chaperone activity of SPARC could explain why both overexpression and knockdown of SPARC show the same effect on vkg levels in the posterior midgut. Expected results would show contradictory phenotypes upon overexpression/knockdown of SPARC, but both show pronounced increases in collagen expression in the midgut epithelium.

A study in *C. elegans* revealed interesting results about the function of SPARC as a regulator of collagen IV. Morrissey and colleagues found that overexpressing SPARC led to a decrease in collagen IV levels in the BM, where extracellular SPARC inhibits incorporation of the fibrils into the basal lamina and slows down collagen turnover in the BM. This disruption in collagen trafficking weakens the basement membrane and compromises its barrier function, thus facilitating invasion, specially from cells that under homeostatic circumstances would not be able to breach the collagen network in the BM (Morrissey et al., 2016). Preliminary experiments carried out in parallel to this project which investigated the effects of vkg knockdown in the ISC/EBs (*5961^{GS} > vkg RNAi 50895*) and its consequences on the midgut tissue showed no significant changes to epithelium between control and knockdown guts (data not shown). Future work should aim to study the changes to SPARC expression in this genetic background, i.e. if altering collagen levels has a similar effect on SPARC as SPARC does on collagen, in order to characterize the relationship between the two molecules in detail.

This well-characterized relationship between collagen IV and SPARC demonstrates the key role that SPARC plays in the correct assembly of the basal lamina

and the maintenance of its integrity. Haemocytes are responsible for the synthesis of not only SPARC and collagen in *Drosophila* embryos, but also other basement membrane components such as laminin and perlecan (Martinek et al., 2002). The effect of SPARC on the laminin network remains controversial: Martinek et al. showed that mutations in embryonic SPARC results in a fragmented laminin network, whereas Morrissey et al. demonstrated that overexpression of SPARC in *C. elegans* had no significant effect on the laminin network in the BM. Similarly, SPARC has a very close relationship with other ECM and cellular components (Liang et al., 2010). Shahab et al. demonstrated reorganization of the actin filament network in the larval fat body where SPARC expression was lost. Consistent with this, data presented here shows significant changes to the intensity of actin staining in both SPARC overexpression and knockdown guts compared to control, suggesting a possible role of SPARC in the reorganization of the actin network in adult tissues. If these changes are due to the direct interaction between SPARC and actin, or if they are due to a knock-on effect from the effect on SPARC on collagen within the tissue still remains to be elucidated.

The presence of two different SPARC populations in the fly, as proposed by Duncan et al. (2020), would serve as an explanation for the differences in the relationship between SPARC and intracellular/extracellular collagen. Liang et al. has also hypothesized the presence of distinct SPARC populations based on its different biochemical properties, since these vary depending if SPARC comes from an endogenous or exogenous source, i.e. if SPARC is directly coming from the cell or from the ECM. It is important to point out that despite the mentions of distinct SPARC populations, the primary amino acid sequence of the protein has been shown to be conserved among metazoans (Martinek et al., 2002), and no post-translational modification of SPARC that could affect its function have been reported in the literature. The function of SPARC in myeloid cell maturation is also dependent on the source of SPARC secretion, where the combination of the two possible sources in this contexts controls the immunogenic profile of the tumour and thus affects EMT progression (Bellenghi et al., 2022). Similarly, SPARC has been shown to be a protective factor in gastric cancers, where it reduces lymph node metastasis, but only if this SPARC has been secreted by macrophages (Hu et al., 2020). This distinction between two SPARC populations could serve as an explanation for the seemingly contradicting results presented here that show expression of SPARC in both a specific subset of EEs and in ECs using two different experimental approaches. This raises the possibility that different epithelial cells within the midgut could be

contributing to its niche in different ways in regards to the source and maintenance of SPARC.

Moreover, these results could be also explained by the existence of other pathways that compensate and counteract the changes observed by alterations to SPARC levels in the different tissues. These changes are dependent on the status of the cells in the tissue, i.e. healthy or disease state, the stage of the disease and other microenvironmental factors (Ghanemi et al., 2020). Preliminary work attempted to characterize the role and expression pattern of SPARC in damaged guts, by feeding SPARC-overexpressing and -knockdown flies with DSS to induce damage in the intestinal tissue. However, time constrains did not allow for this avenue of work to be explored further.

SPARC not only acts as a regulator of the ECM and the basement membrane in epithelial tissues, it also modulates signalling by acting as a competitive inhibitor of growth factor signaling receptors found on the cell membrane (Liang et al., 2010). Liu et al. reported a direct correlation between SPARC levels and ERK/MMP pathway activity: lower levels of SPARC resulted in downregulation of phosphorylated ERK1/2 and MMP9, thus inhibiting pathway activity. Moreover, upregulation of SPARC increased the levels of these proteins, which facilitates EMT progression of liver cancer cells and the acquisition of stem cell properties in tumour cells (Jiang et al., 2019; Liu et al., 2020) and in limbal epithelial cells (Zhu et al., 2019). Interestingly, both MMP2 and MMP9 have been reported to directly regulate collagen levels in the ECM, degrading the fibrils and contributing to invasion (Liu et al., 2020). Thus, knockdown of SPARC in this tissue leads to decreased levels of MMPs and ERK pathway activity, which in turn slows down invasion and metastasis in liver tissue. This is consistent with the results presented in this chapter that demonstrate that MAPK/ERK signalling pathway components decrease in midguts where SPARC has been downregulated. Moreover, our data shows that SPARC acts upstream of the Ras/MAPK signalling cascade, where it potentially acts as a negative regulator: active MAPK levels significantly increase in SPARC knockdown guts, but decrease in SPARC overexpression guts. Under the control of ERK, SPARC regulates angiogenesis by downregulating vascular-endothelial growth factor (VEGF) and MMP7 expression in gastric tumours (Hu et al., 2020). SPARC prevents the VEGF receptor from recognizing the growth factor, and thus inhibits ERK1/2 signaling and hinders cancer cell proliferation (Ma et al., 2019). SPARC has been shown to activate the MAPK signaling pathway in bone tissue: Wang et al. reported that silencing of SPARC inhibited this signalling cascade by decreasing the levels of phosphorylated p38 MAPK, as well as

ERK, JNK and NFKB. This is consistent with our findings, where qPCR analysis of the E(spl) proteins M3, M5, M8 and Mβ, which are activated by Notch (Fischer and Gessler, 2007) show decreasing trends in SPARC knockdown fly guts.

We have reported decreased levels of c-Jun N-terminal kinase (JNK) signalling in SPARC knockdown *Drosophila* guts. In human tissues, the transcription factor c-Jun, which is part of the JNK signalling pathway, is tightly associated with invasion of ovarian cancer cells: adipocyte-derived SPARC levels negatively correlate with the levels of nuclear cJun found in ovarian tumours, thus inhibiting invasiveness of these cells (John et al., 2019). Previous reports have shown that, SPARC expression occurs independently of JNK in *Drosophila* in the context of cell competition, but that rather SPARC acts downstream of the Dpp signaling pathway (Portela et al., 2010). The results presented here, however, suggest SPARC may be acting upstream of Dpp signalling and therefore controlling its expression, since knockdown of SPARC resulted in a decrease in Dpp signaling pathway components brk and dad. Moreover, we found a highly significant decrease in the JNK phosphatase puckered (puc) in SPARC knockdown guts, indicating that perhaps, in this context of gut tissue homeostasis, SPARC expression regulates JNK signaling.

In its role as an EMT-promoting protein, SPARC has been shown to interact with a wide variety of proteins, such as E-cadherin and vimentin, and promote migration and invasion through the activation of the AKT signalling pathway (Zhong et al., 2019). SPARC has been shown to regulate the expression of the integrin subunit αvβ3 and ZEB1, both components of the AKT signaling pathway, promoting the downregulation of E-cadherin, a key epithelial marker (Jiang et al., 2019), and enhancing the migratory and mesenchymal phenotype of the tumour cells (López-Mancada et al., 2022). Moreover, ioinformatic analysis revealed that both the AKT/mTOR and the MEK/ERK (MAPK) pathways promote stemness in cells and show a correlation to drug resistance of tumours (Ma et al., 2019). Overexpression of SPARC in prostate cancer also regulates E-cadherin levels the EMT programme, where high levels of SPARC promote the loss of E-cadherin and trigger EMT through the TGF-β/SMAD signaling pathway (Carriere et al., 2021). The data shown here does not provide any conclusive results on the effect of SPARC on SMAD, as the increase reported in SPARC overexpressing guts, which could suggest an upstream role of SPARC in the positive regulation of SMAD, was not statistically significant. Interestingly, the regulation of SPARC in the EMT process has been proposed to be both autocrine and paracrine (Carriere et al., 2021), suggesting the

possibility that, in the intestinal epithelium, SPARC could have different contributions to the maintenance of the ISC niche. In summary, our results demonstrate that SPARC in the *Drosophila* gut could be a regulator of MAPK, JNK and Dpp activity, but further studies are needed to complete the characterization of these regulatory mechanisms in the context of ISC and EBs. Our results are consistent with those presented by Zhu et al. who showed that the regulation of limbal epithelial stem cells and their stem cell-associated properties, such as high proliferative potential, are regulated by a combination of MAPK, JNK and AKT signalling (Zhu et al., 2019).

3.5. Conclusions

In summary, the results presented here show that SPARC plays significant roles in the maintenance of gut tissue homeostasis in *Drosophila*. Overexpression of SPARC decreases the proliferative rates of ISCs, as well as the number of differentiated EEs in the posterior midgut. Knockdown of SPARC also significantly alters the proliferation rates in the tissue, but both RNAi lines show contradictory results, with one significantly increases mitoses, and the other one reducing them. Phenotypically, knockdown of SPARC seems to be accompanied by a loss of distribution of cells in the posterior midgut in some cases, but this does not affect the mortality rates of the fly. Preliminary data to characterize the expression pattern of SPARC suggests the protein is expressed in a specific subset of differentiated cells in the tissue, but the use of different reporters and driver lines gives varying results on whether this expression is in EEs or ECs. Increased levels of SPARC significantly enhance the expression of viking, i.e. collagen, in the posterior midgut, and although the data presented here show an increase in collagen associated with SPARC knockdown, statistical analysis did not deem this change significant. The intensity of actin filament staining was also significantly reduced in both SPARC overexpression and knockdown guts. SPARC is suggested to act upstream of the Ras/MAPK signalling cascade, and although qRT-PCR analysis hints to the potential role of SPARC as a potential upstream regulator of Notch signaling, further work is needed to characterize this in detail.

Chapter 4

PLOD as a regulator of intestinal stem cell homeostasis

4.1. Introduction

Procollagen-lysine, 2-oxyglutarate, 5-dioxygenase, commonly referred to as PLOD, is a family of proteins involved in post-translational modifications (PTMs) of collagen. Collagen is the most abundant molecule in the extracellular matrix, where it exists in either fibrillar or non-fibrillar form (Li et al. 2020). Collagen biosynthesis is a complex and tightly regulated process: initially, collagen molecules are synthesized in a pro-collagen form and post-translational modifications are responsible for the correct folding and assembly of the triple helix formation (D'Aniello et al., 2021). In *Drosophila*, the collagen IV trimer contains "imperfections" in its helical structure that increase its flexibility compared to other collagen molecules, like collagen I (Ke et al., 2018). PLODs are enzymes responsible for hydroxylating the lysine residues of collagen IV fibrils, thus stabilizing the structure of the molecule and facilitating its crosslinking (Qi and Xu, 2018; Li et al., 2020). The correct hydroxylation of the procollagen peptide is essential for the stability of the molecule and it is the most important PTM modification that occurs in the

human proteome (D'Aniello et al., 2021). In particular, the hydroxylation of lysine residues by PLOD leads to the formation of the so-called pyridinoline crosslinks, which increases the resistance of collagen fibers to degradation by collagenases (Xu et al., 2021). The hydroxylating function of PLOD has also been shown to extend to any molecule that contains collagen-like domains (Bunt et al., 2011).

In mammals, the PLOD family consists of three genes: PLOD1, PLOD2 and PLOD3 (Zhang et al., 2021), all of which are highly homologous to each other, with a protein sequence identity of 47% (Qi and Xu, 2018; Li et al., 2020; Gong et al, 2022). PLODs are also sometimes referred to as lysyl hydroxylases (Noda et al., 2011), with the three isoforms in mammals denominated LH1-3 (Yang et al., 2020). The fly *Drosophila melanogaster* only has one copy of the PLOD gene, which shares the most homology (45% identity and 66% similarity) with the vertebrate LH3, i.e. PLOD3 (Bunt et al., 2011). The function of *Drosophila* PLOD thus resembles that of PLOD3 in mammals, where the enzyme has both hydroxylase and glycotransferase activity (Bunt et al., 2011). *Drosophila* produces high quantities of collagen IV, the main target of PLOD activity, but lacks fibrillar collagens (Ke et al., 2018). PLOD expression in mammals is regulated at the transcriptional level, and the expression of PLOD1, PLOD2 and PLOD3, although not mutually exclusive, is associated with a degree of functional redundancy (Guo et al., 2021). Because of the functional simplicity compared to other mammalian counterparts, as well as its low genetic redundancy and evolutionary conservation, *Drosophila melanogaster* has emerged as a powerful model to study collagen biology (Ke et al., 2018).

Bunt and colleagues demonstrated that PLOD in the fly has a perinuclear localization and that the expression of the enzyme colocalizes with the collagen IV α2 chain, which in *Drosophila* is known as Viking (vkg) (Ke et al., 2018). Specifically, PLOD has been found to localize inside the rough endoplasmic reticulum (ER) in the fly (Lerner et al., 2012), suggesting that, in this system, collagen IV secretion occurs through a general secretory pathway and does not require a specific mode of transport in vesicles (Ke et al., 2018). Knockdown of PLOD in *Drosophila* leads to retention of collagen IV in the basal compartments of the ER, as well as to the sequestering of other basement membrane components such as laminin and perlecan (*trol* in *Drosophila*) (Lerner et al., 2012). Thus, reduced levels of PLOD in the fruit fly affect basement membrane formation and ECM biosynthesis. Bunt et al. also found PLOD expression in the extracellular space, suggesting that PLOD may also play roles in the post translational modifications of

extracellular collagen. Thus, it is expected that expression of *Drosophila* PLOD is mostly found in tissues and cells that secrete high levels of collagen IV.

Because of its function as a collagen-modifying enzyme, PLOD has an important role in the deposition of collagen fibers into the extracellular matrix (ECM) (Yamada et al., 2019; Zhang et al., 2021). Reduced levels of PLOD lead to deficiencies in collagen cross-linking and therefore facilitate collagen degradation in the ECM (Guo et al., 2021). Esophageal cancer with low expression of PLOD2 presented a loose distribution of collagen in the ECM, whereas the collagen network in high PLOD2-expressing tumours had thicker collagen fibrils that made up a denser network (Gong et al., 2022b). PLOD is also an essential enzyme required in the formation of connective tissues (Gong et al., 2022), and mutations in the LH genes have been associated with a range of connective tissue disorders (Bunt et al., 2011) and fibrosis (reviewed by Qi and Xu, 2018).

Most of the published literature has focused on establishing the role of PLOD using in vitro mammalian samples, where the function of PLOD1-3 has been extensively studied in the context of cancer. In a tumourigenic context, collagen fibers switch from a coiled state to a linear state, which facilitates the rapid migration of cancer cells and their extravasation to the vascular system (Gong et al., 2022b), thus aiding the formation of distant metastatic lesions. Guo et al. demonstrated the mutual exclusivity of PLOD activity in ovarian cancer by showing that PLOD1, PLOD2 and PLOD3 did not have redundant roles and that their functions did not overlap, but rather that all 3 molecules worked in consonance during collagen biosynthesis. This same paper demonstrated that PLOD regulation mainly occurs at the transcriptional level (Qi and Xu, 2018; Guo et al., 2021; Shi et al., 2021). PLOD expression has also been linked to immune cell infiltration in tumours (Zhang et al., 2021), with different PLOD associated with specific immune cells (Yang et al. 2020; Chen et al., 2023). Li et al. showed that all three PLODs were overexpressed in gastric cancer and that this overexpression facilitated the progression of the disease by aiding cancer cell migration. Overexpression of PLOD leads to increased collagen cross-linking and deposition, providing a more stable scaffold for cancer cells to migrate (Shi et al. 2021).

In summary, overexpression of PLOD molecules in mammals promotes tumour development and progression, but the exact function of each PLOD molecule is cell, tissue- and context-dependent. Moreover, in some cases, its expression could also be gender-dependent: Gong et al., demonstrated that PLOD1 in soft tissue sarcoma is more highly expressed in male patients, whereas PLOD2 and PLOD3 did not show any bias.

The conservation of these tumorigenic roles of PLOD in the fly still remains to be elucidated.

Aberrant expression of PLOD has severe consequences, and thus PLOD expression must be tightly controlled by a wide range of cytokines, transcription factors and microRNAs (Qi and Xu, 2018). Noda et al. demonstrated that PLOD expression is induced under hypoxic conditions via activation of the hypoxia-inducible factor-1 (HIF-1) signaling pathway, but the expression of the different PLOD genes in this context is dependent on the cell type. BMP2 signaling regulated PLOD1 expression in adipose tissue mesenchymal stem cells, whereas PLOD2 and PLOD3 were not affected (Knippenberg et al., 2007). Similarly, this same study showed that TGFB-1 signaling decreased PLOD1 and PLOD3 expression, but had no effect on PLOD2 levels. This study, alongside many others, has proposed a differential regulation mechanism for each of the 3 mammalian PLOD enzymes. SHC1, responsible for the link between integrins and the Ras-ERK pathway, has been shown to be a regulatory molecule of PLOD activity in gastric cancer (Li et al., 2020). In these cases, overexpression of PLOD molecules not only modifies the ECM composition to facilitate cancer cell migration, but also leads to increased SHC1 expression, favouring integrin signaling and causing an overactivation of the Ras-ERK signaling pathway that promotes cell cycle progression of tumour cells (Li et al., 2020).

4.2. Aims and objectives

Most of the published PLOD literature study its role using *in vitro* mammalian models, and thus not many papers focus on the role of *Drosophila* PLOD, much less in the gut tissue or in ISC/EB regulation and its contributions to the niche. There is a significant gap in the literature regarding the function of PLOD in intestinal stem cell regulation in the fly gut and its implications in disease development when PLOD is misregulated. Previous work from the Doupé group identified PLOD as a protein specifically secreted by the stem and progenitor cells of the gut, but not by the differentiated EC cells of the tissue (Doupé et al., 2018), and preliminary work suggested that knockdown of this protein could alter the proportion of ISCs and EBs in the posterior midgut (Galbraith, unpublished). This chapter aims to elucidate the function, expression pattern and regulation of PLOD in the *Drosophila* midgut by studying the effects of PLOD knockdown. In particular, the aim is to characterize if this protein is specifically

expressed by ISCs and EBs within the epithelium and whether changes to its expression levels affect epithelial tissue homeostasis and the intestinal stem cell niche.

4.3. Results

4.3.1. The effect of PLOD knockdown in ISCs and EBs in the posterior midgut

Previous work from the Doupé group identified PLOD as an ISC/EB-secreted protein in the *Drosophila* midgut. Preliminary work showed no significant changes to the stem cell population when PLOD was knocked down but an increase in midgut cell density. Thus, the first aim of this project was to characterize the effect of PLOD knockdown on the midgut tissue, in order to elucidate the function of this protein.

For this, Gene Switch flies driving an RNAi construct of PLOD were analyzed using immunofluorescence staining for PH3 and the EE marker prospero. Three different RNAi lines were used for this, to account for any differences in knockdown strength and any potential off-target effects. They will be referred to as PLOD RNAi-1 (*UAS-PLOD RNAi 67935)*, RNAi-2 (*UAS-PLOD RNAi 34911)* and RNAi-3 (*UAS-PLOD RNAi 454848)* from here onwards. *5961GS > UAS-PLOD RNAi-1* (*Figure 4.1*) did not cause a change in the total number of cells observed in the gut, and gut width was also maintained (*Figure 4.2A-B*). However, the total gut area observed per field of view was significantly larger when compared to controls which in turn led to a decrease in cellular density in the tissue (*Figure 4.2C-D*). Since the total number of cells in the gut was maintained after PLOD knockdown, we next looked at potential changes in the cellular composition of the tissue and its mitotic rates. There was a significant increase in the number of EE cells per field of view and in the mitotic rates across the whole gut in PLOD-RNAi-1 knockdown (*Figure 4.3*). *5961GS > UAS-PLOD RNAi-2* did not yield any significant results: all the parameters analyzed were conserved between knockdown guts and controls (*Figures 4.4-4.6*).

The most striking results were observed in guts were PLOD was knocked down by RNAi line 3(*Figure 4.7*). In these guts, PLOD knockdown led to a very highly significant increase of cells in the midgut, but no changes were observed in midgut width or area (*Figure 4.8*). Although results demonstrated an increase in cellular density, as expected, statistical analysis showed this change was not significant (*Figure 4.8D*). From

this, the next step was to determine if the increase in cell number was associated to a particular cell type in the gut. Interestingly, we found that the number of secretory cells observed per field of view was significantly decreased by 5-fold compared to EE cells observed in control midguts: in control guts, about 25% of cells observed per field of view were enteroendocrine cells, whereas this was reduced to about 5% in PLOD knockdown guts (*Figure 4.9A-B*). Knockdown of PLOD by this RNAi construct did not affect the mitotic rates in the tissue (*Figure 4.9C*). The most striking phenotype of this knockdown was the disorganization of cells across the tissue: in guts were PLOD was knocked down, the seemingly neat arrangement of cells observed in control tissues was lost in RNAi guts, with cells forming clusters and what seems to be a higher number of enlarged nuclei, which are characteristic of absorptive EC cells (*Figure 4.7*).

Taken together, we hypothesize that PLOD knockdown leads to an imbalance of differentiation, but RNAi lines 1 and 3 show opposite trends for this. Therefore, to reconcile these findings, the extent of the knockdown induced by each of these lines was analyzed.

No PLOD overexpression lines were readily available at any of the stock centres at the time of these experiments, thus no data is available for comparison.

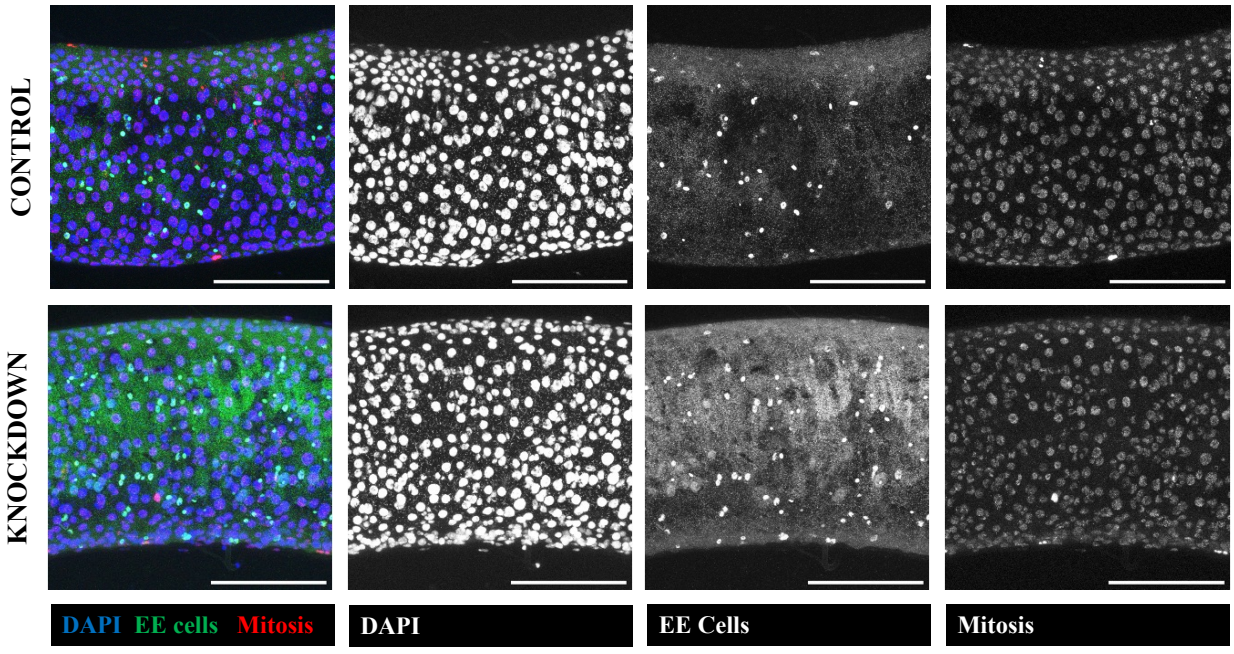

Figure 4.1. The effects of *PLOD-RNAi-1* knockdown in ISCs and EBs of the *Drosophila* midgut. Representative images of PLOD knockdown (5961^{GS} > *PLOD-RNAi-1*) does not induce any striking phenotypical changes in the posterior midgut. Guts were stained with α-prospero (1:100), α-PH3 (1:1000) and DAPI. Scale bars in the bottom right corner represent 100μm.

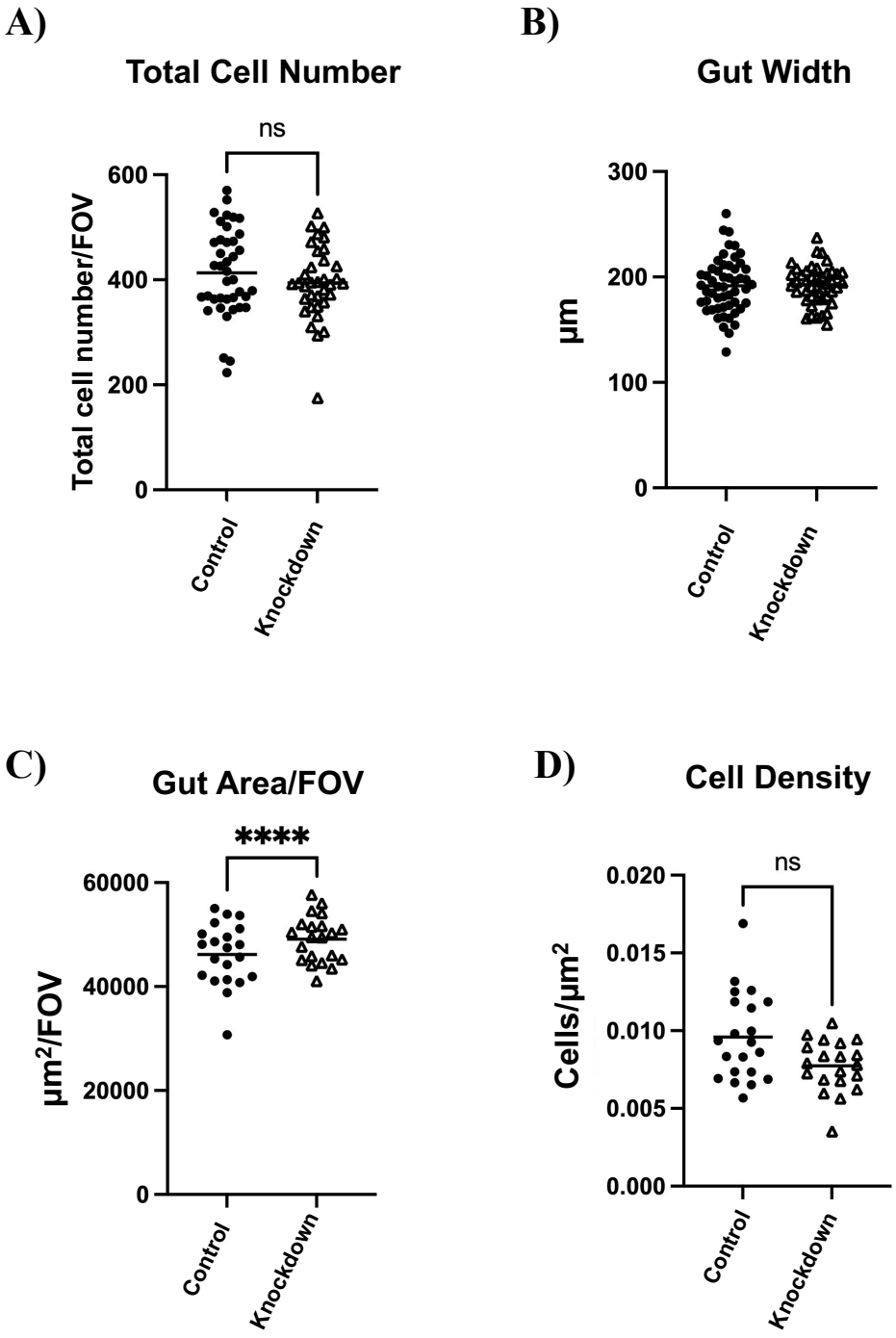

Figure 4.2. PLOD-RNAi-1 knockdown significantly increases the area of the gut. Knockdown of PLOD (*5961^{GS} > PLOD-RNAi-1*) leads to a significant increase in the area of the gut observed/FOV ($p \leq 0.0001$) (n = 21) (***C***), but no changes in total number of cells/FOV (control n = 40, KD n = 35) (***A***) , gut width (control n = 53, KD n = 44) (***B***) or gut density (control n = 21, KD n = 20) (***D***) were observed between knockdown and control guts. All data are normally distributed so unpaired t-tests were used for statistical analysis. Each data point represents a gut.

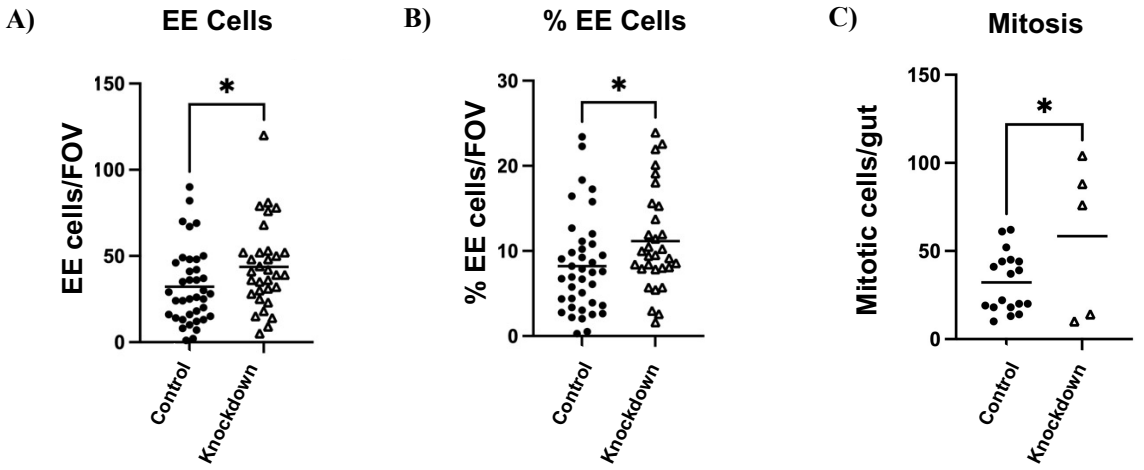

Figure 4.3. *PLOD-RNAi-1* knockdown significantly increases the proliferation rate of ISCs and the number of EE cells in the posterior midgut. Knockdown of PLOD (*5961^{GS} > PLOD-RNAi-1*) in the stem and progenitor cells of the posterior midgut significantly increases the number of EE cells observed per field of view (p = 0.02) (control n = 38, KD n = 32) (***A***), and the ratio of EE cells normalized to total number of cells observed per FOV (p = 0.02) (control n = 39, KD n = 31) (***B***). The number of proliferating ISCs in the whole Drosophila gut (p = 0.05) (control n = 18, KD n = 5) (***C***) is also increased, but statistical analysis showed this trend was not significant. Unpaired t-tests were used for normally distributed data (C), and non-parametric Mann Whitney-U tests for non-normally distributed data (A, B) . Each data point represents a gut.

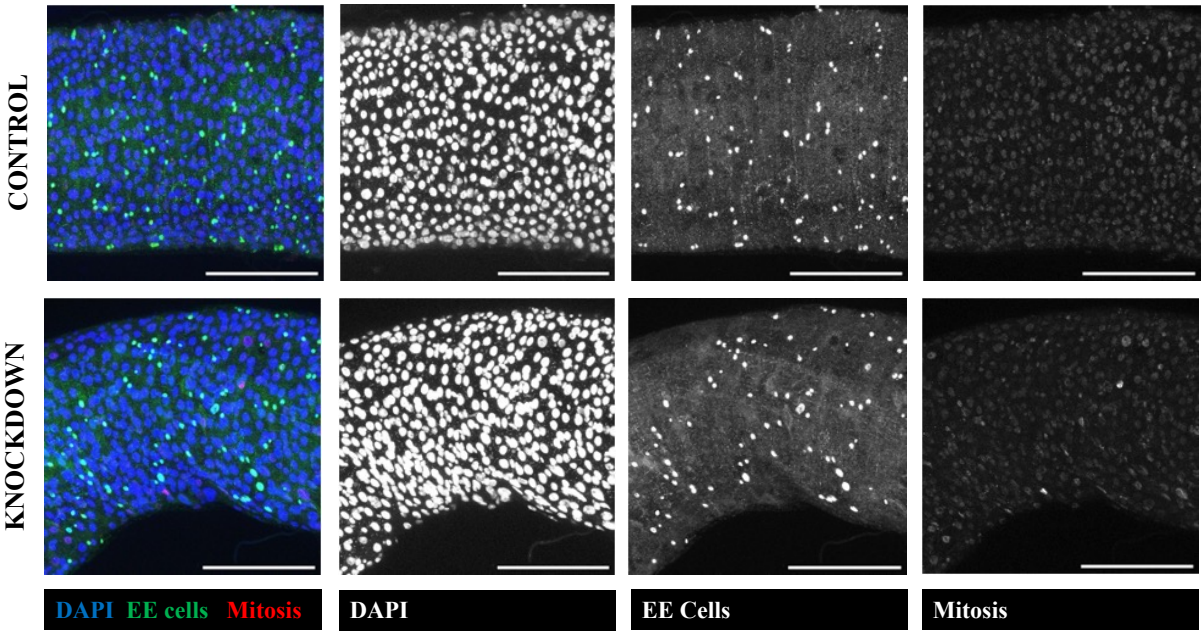

Figure 4.4. The effects of *PLOD-RNAi-2* knockdown in ISCs and EBs of the *Drosophila* midgut. Representative images of PLOD knockdown (*5961^{GS} > PLOD-RNAi-2*) in the posterior midgut. Guts were stained with α-prospero (1:100), α-PH3 (1:1000) and DAPI. Scale bars in the bottom right corner represent 100μm.

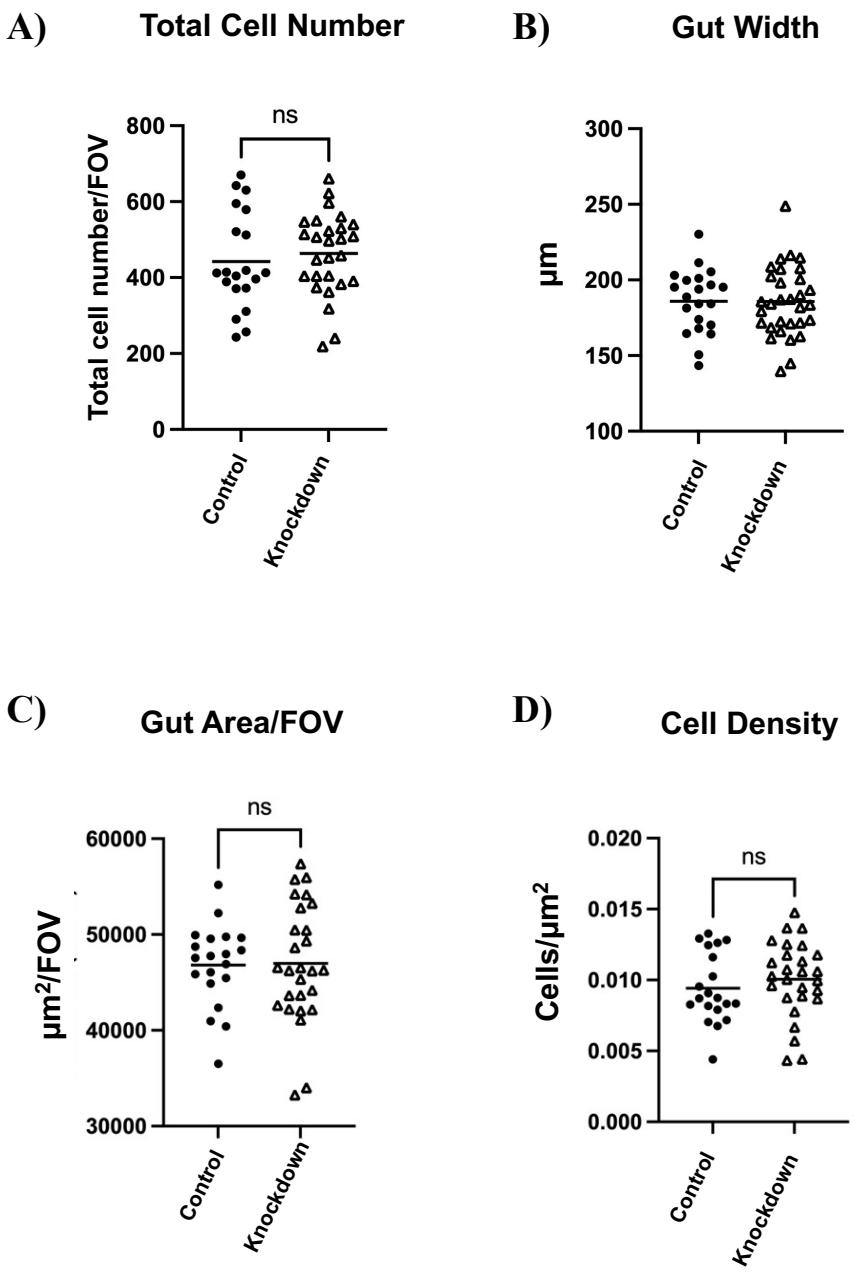

Figure 4.5. *PLOD-RNAi-2* knockdown does not affect midgut homeostasis. Knockdown of PLOD (*5961^{GS} > PLOD-RNAi-2*) does not induce any changes to the total number of cells/FOV (control n = 20, KD n = 27) (***A***), gut width (control n = 21, KD n = 31) (***B***), area of the gut observed/FOV (p = 0.0002) (control n = 20, KD n = 27) (***C***) or gut density (p = 0.01) (control n = 20, KD n = 27) (***D***) compared to control guts. All data was normally distributed, so unpaired t-tests were used for statistical analysis. Each data point represents a gut.

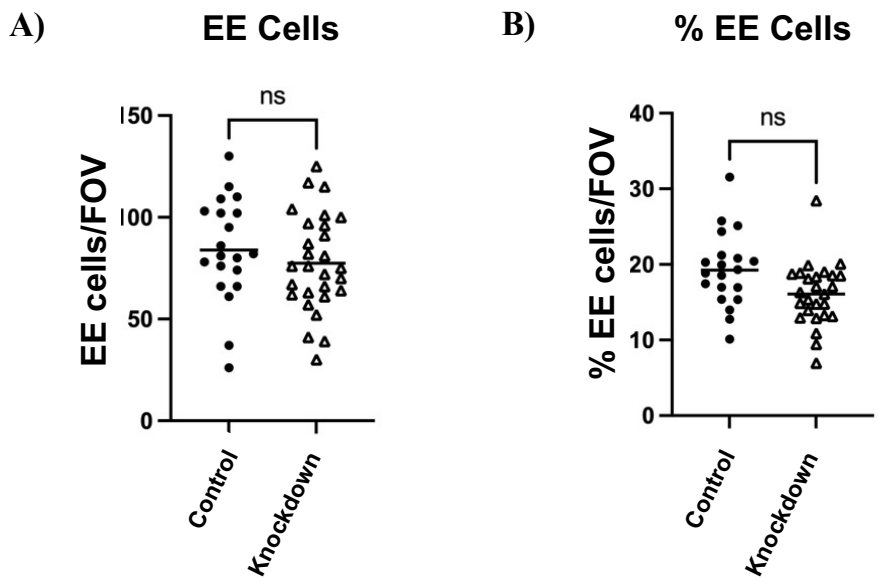

Figure 4.6. *PLOD-RNAi-2* knockdown in the ISCs and EBs has no effect on EE cell number. Knockdown of PLOD (*5961^{GS} > PLOD-RNAi-2*) in the stem and progenitor cells of the posterior midgut does not change the number of EE cells observed per field of view (control n = 20, KD n = 28) (***A***), or the ratio of EE cells normalized to total number of cells observed per FOV (control n = 20, KD n = 26) (***B***). Data was normally distributed, so unpaired t-tests were used for statistical analysis. Each data point represents a gut.

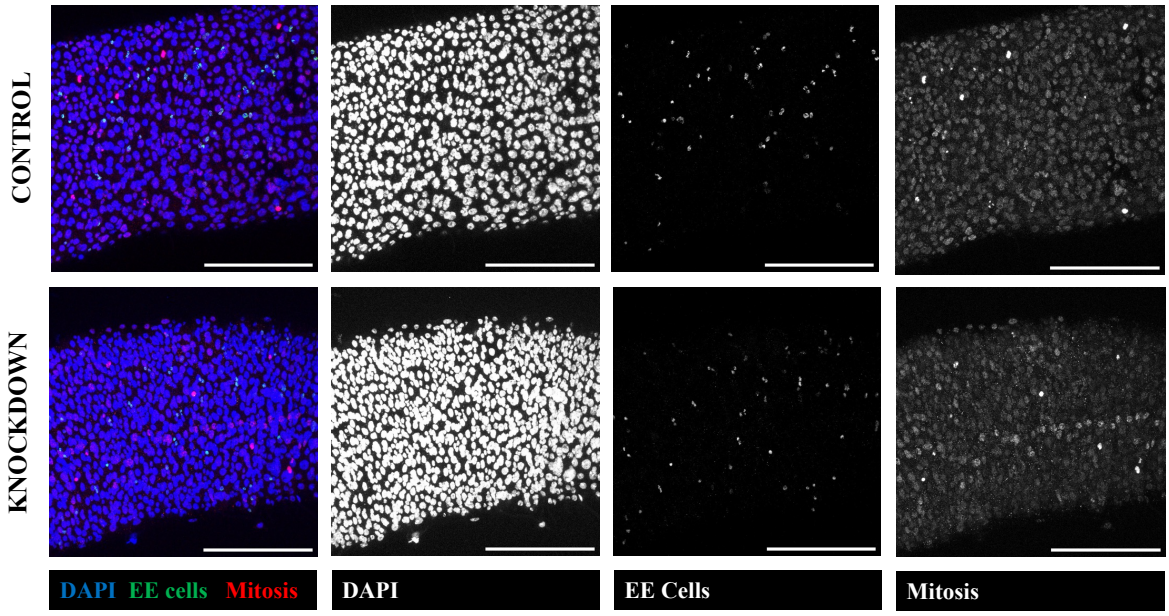

Figure 4.7. The effects of *PLOD-RNAi-3* knockdown in ISCs and EBs of the *Drosophila* midgut. Representative images of PLOD knockdown (*5961^{GS} > PLOD-RNAi-3*) show it leads to the loss of the neat distribution of cells within the tissue, where there is an increase in enlarged guts and nuclei are very closely arranged (bottom left panel). Guts were stained with α-prospero (1:100), α-PH3 (1:1000) and DAPI. Scale bars in the bottom right corner represent 100μm.

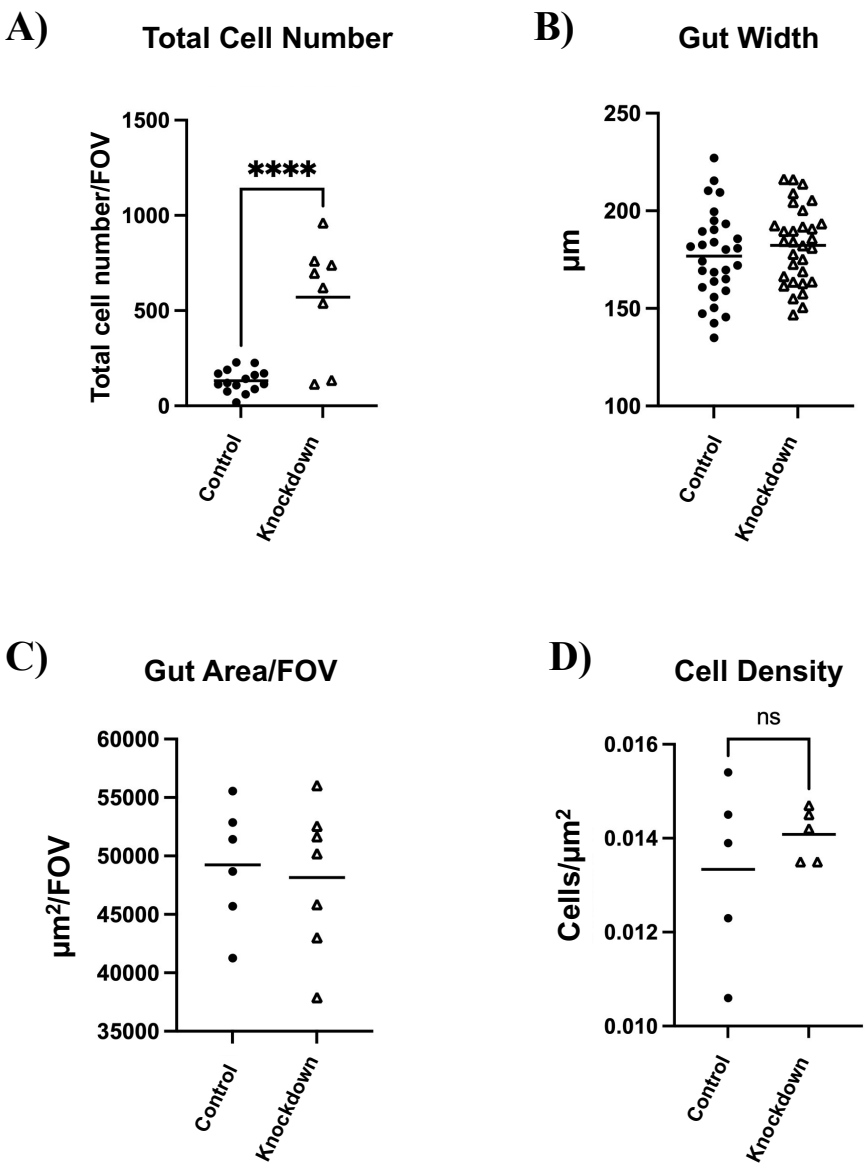

Figure 4.8. *PLOD-RNAi-3* knockdown significantly increases the total number of cells in the posterior midgut. Knockdown of PLOD (*5961^{GS} > PLOD-RNAi-3*) significantly increases the total number of cells/FOV ($p < 0.0001$) (control n = 15, KD n = 8) (***A***) , but gut width (control n = 30, KD n = 31) (***B***), area of the gut observed/FOV (control n = 6, KD n = 7) (***C***) and gut density (control n = 5, KD n = 5) (***D***) remain unchanged compared to control guts. All data was normally distributed, so unpaired t-tests were used for statistical analysis. Each data point represents a gut.

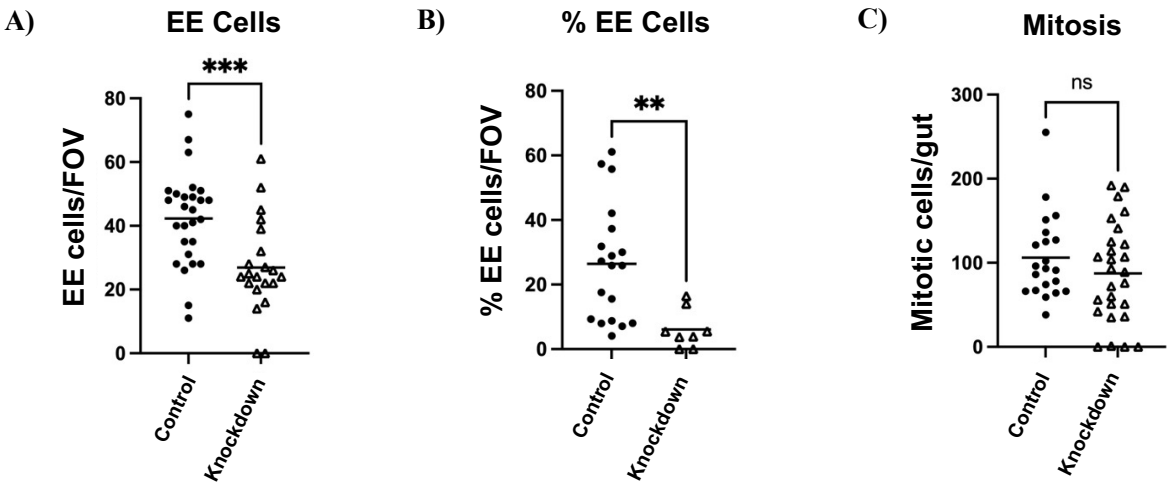

Figure 4.9. *PLOD-RNAi-3* knockdown significantly reduces the number of EE cells in the posterior midgut. Knockdown of PLOD (*5961^{GS} > PLOD-RNAi-3)* in the stem and progenitor cells of the posterior midgut significantly reduces the number of EE cells observed per field of view (p = 0.0008) (control n = 27, KD n = 21) (***A***), as well as the ratio of EE cells normalized to total number of cells observed per FOV (p = 0.004) (control n = 19, KD n = 8) (***B***). The number of proliferating ISCs in the whole Drosophila gut slightly decreases, but statistical analysis demonstrated this change was not significant (p = 0.0008) (control n = 20, KD n = 27) (***C***), but statistical analysis showed this trends were not significant. All data was normally distributed, so unpaired t-tests were used for statistical analysis. Each data point represents a gut.

4.3.2. Validation of the PLOD RNAi lines

Next, qRT-PCR analysis was carried out to determine the extent of the knockdown in each of the lines used in this study, to better interpret the results obtained. For this, *tub-Gal80^{ts}; tub-Gal4/TM6B* was used as the driver line for *UAS RNAi-1* and *-3*, allowing for the knockdown of PLOD in all gut cells. Results were limited by insufficient replicates to enable conclusions to be drawn but both PLOD RNAi-1 and PLOD RNAi-3 showed substantial knockdowns of ~ 70% (*Figure 4.10A and B*). Unfortunately, at the time of these experiments, there were some issues with the PLOD RNAi-2 line and thus no validation data is available for this. This line, as well as the two others, has been widely used in published literature, but we have not been able to validate the reliability of the knockdown as part of this project.

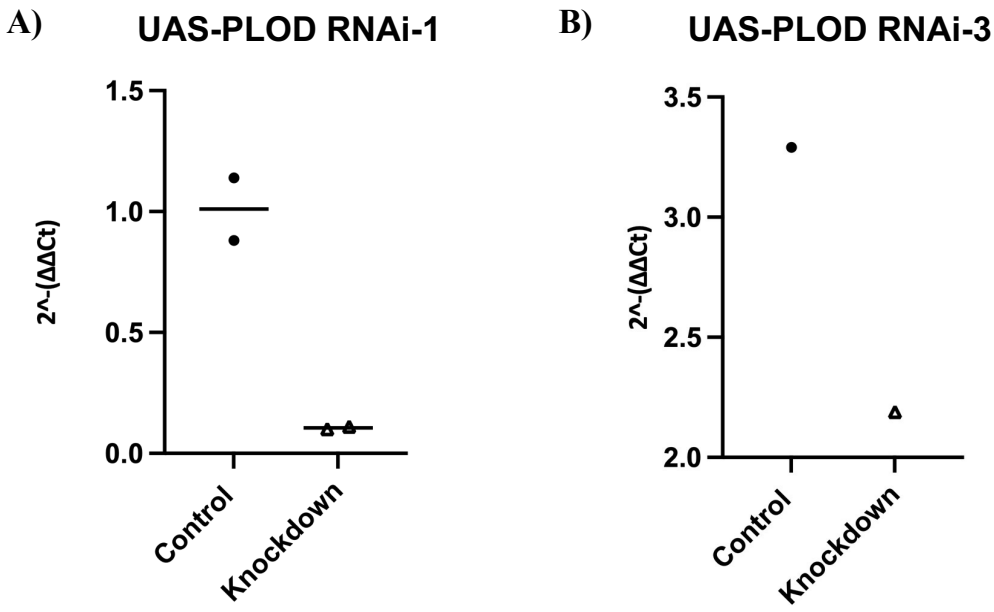

Figure 4.10. *PLOD* and *PLOD RNAi-3* knock down PLOD expression in the *Drosophila* gut. Both *5961^{GS} > PLOD-RNAi-1* (***A***) and *5961^{GS} > PLOD-RNAi-3* (***B***) reduce the levels of PLOD expression in whole-gut *Drosophila* samples. Results were calculated using the ΔΔCt method. n is too low for statistical analysis. Each data point represents a sample, and each sample contains 10 whole guts.

4.3.3. The effect of PLOD on lifespan

Following up from the results observed in normal homeostasis, lifespan experiments were carried out to determine if the changes observed in the midgut were affecting fly survival. *5961Gene Switch*-driven PLOD knockdown was tested using all three RNAi lines. Overall, PLOD knockdown in the stem and progenitor cells of the gut seemed to increase lifespan in the fly, and this result was consistent across all three RNAi lines. However, a second set of lifespans was set up to validate these results and the data obtained was not consistent between them (*Figure 4.11*). The second replicates did not show any significant changes between control and knockdown in regards to overall survival (data not shown). Thus, no conclusive statements can be made from this data sets, because while initial results suggest an effect of PLOD knockdown on the survival rates of the fly, these results have not proven to be reproducible.

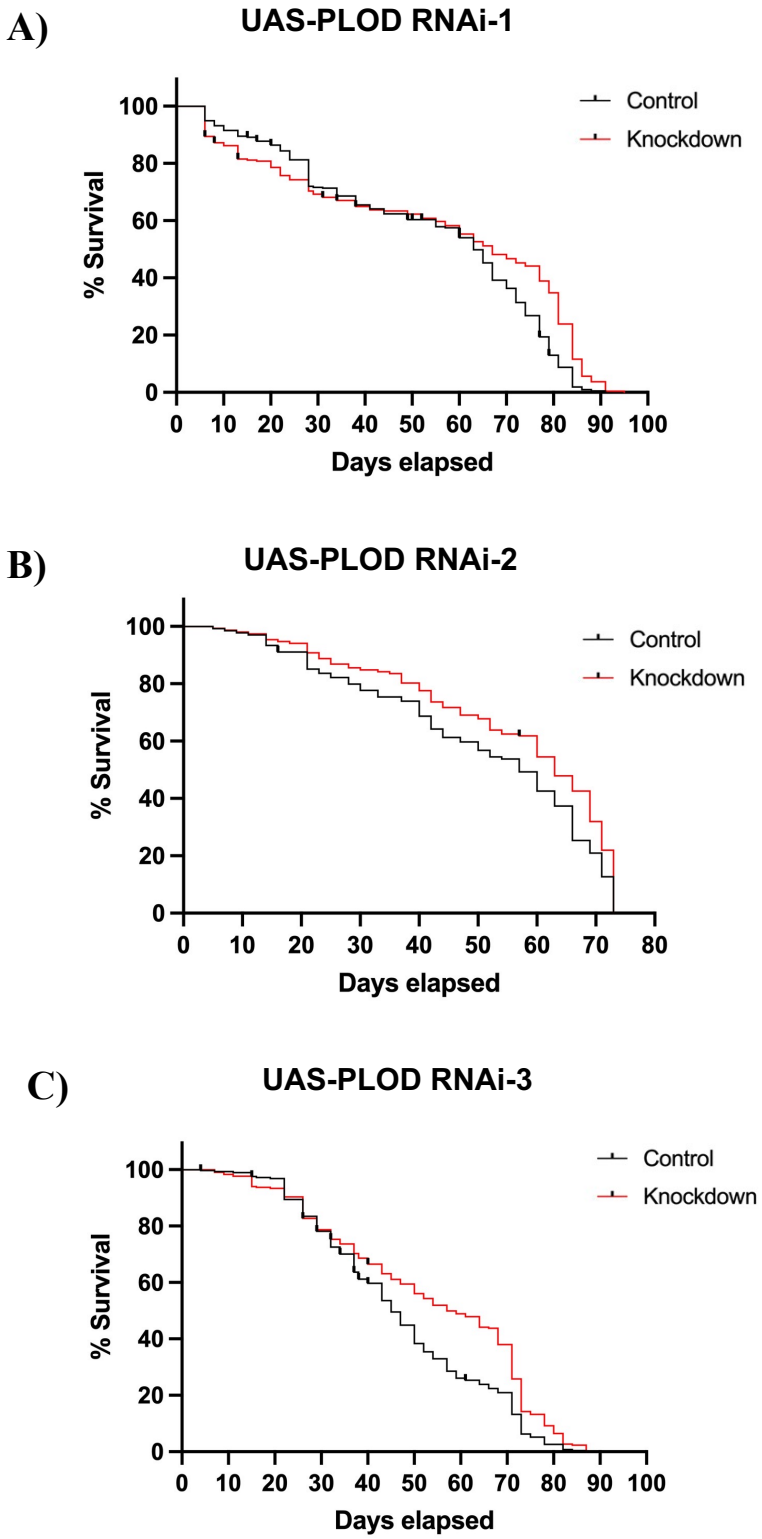

Figure 4.11. Initial results suggested that knockdown of PLOD leads to a slight increase in the lifespan of the fly. Knockdown of PLOD with *PLOD-RNAi-1* (***A***), *PLOD-RNAi-2* (***B***), and *PLOD-RNAi-3* (***C***) all induce an increase in fly lifespan during adulthood ($p < 0.0001$, $p = 0.009$ and $p < 0.0001$, respectively). Knockdown is induced at day 10 of the experiment, when flies are swapped to food containing the mifespristone drug that triggers the knockdown of PLOD ($n = 300$). However, results from second set of replicates did not match these trends.

4.3.4. Knockdown of PLOD using the "Flp-Out" system

To further investigate the effect of PLOD knockdown on the tissue, as well as the quality of the genetic manipulation, the "Flp-Out" system was used to drive *UAS-RNAi-2* and *-3*. As previously explained in Chapter 3, the "Flp-Out" system induces lineage tracing from the ISCs and EBs and all their progeny, where cells are tagged with a fluorescent GFP reporter, and a temperature change induces the expression of PLOD RNAi. Analysis of *esg^{TS}Flip > UAS-PLOD RNAi-1* showed no significant changes in GFP positive cells between control and knockdown guts for any of the parameters quantified (*Figures 4.12 and 4.13*). *esg^{TS}Flip > UAS-PLOD RNAi-3* showed a significant decrease in the percentage of GFP-positive cells and its clones, normalized to the total cell number per field of view, as represented by % GFP positive cells (*Figures 4.14 and 4.15*). No other significant changes were reported. Thus, PLOD knockdown might decrease the number of GFP-positive cells and its clones in the posterior midgut, but there is variability in the results between both RNAi lines used, so no firm conclusions can be drawn from this data set.

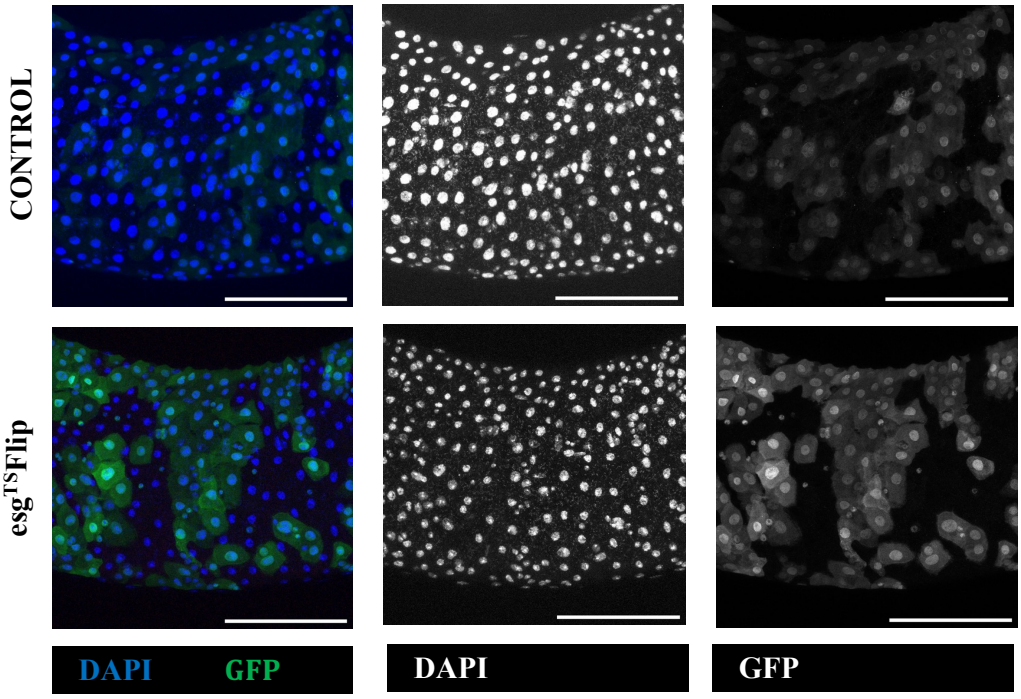

Figure 4.12. Knockdown of *PLOD-RNAi-1* driven by *esg^{TS}Flip* does not show any changes in GFP expression between control and PLOD knockdown guts. PLOD knockdown (*esg^{TS}Flip > UAS-PLOD-RNAi-1)* does not show any differences in GFP levels compared to control guts (*esg^{TS}Flip > Luciferase)*. Guts were stained with α-GFP (1:2000) and DAPI. Scale bars in the bottom right corner represent 100μm.

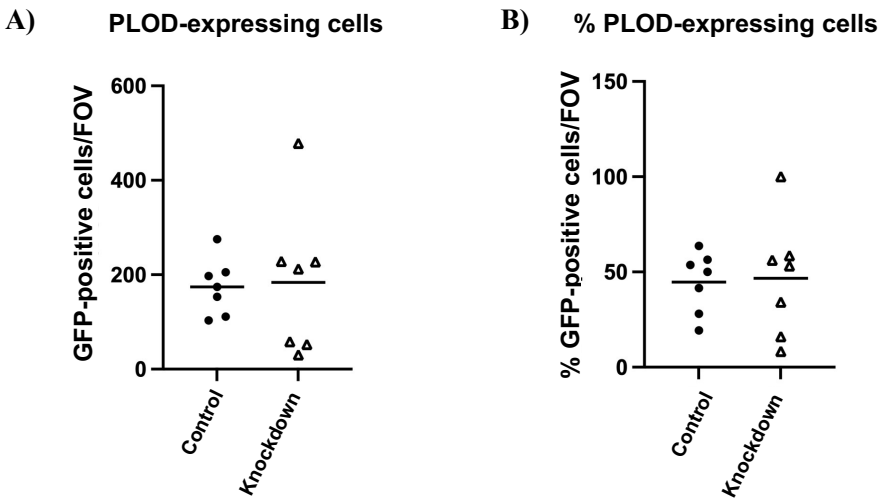

Figure 4.13. Quantification of the knockdown of PLOD using *PLOD-RNAi-1* driven by *esg^{TS}Flip* does not show any changes in GFP expression between control and PLOD-knockdown guts. PLOD knockdown (*esg^{TS}Flip > UAS-PLOD-RNAi-1)* does not show any differences in GFP levels compared to control guts (*esg^{TS}Flip > Luciferase),* both in terms of total number of GFP-positive cells (control n = 18, KD n = 13) (***A***) and % of GFP-positive cells normalized to the total cell number/FOV (Control n = 18, KD n = 13) (***B***) . All data was normally distributed, so unpaired t-tests were used for statistical analysis. Each data point represents a gut.

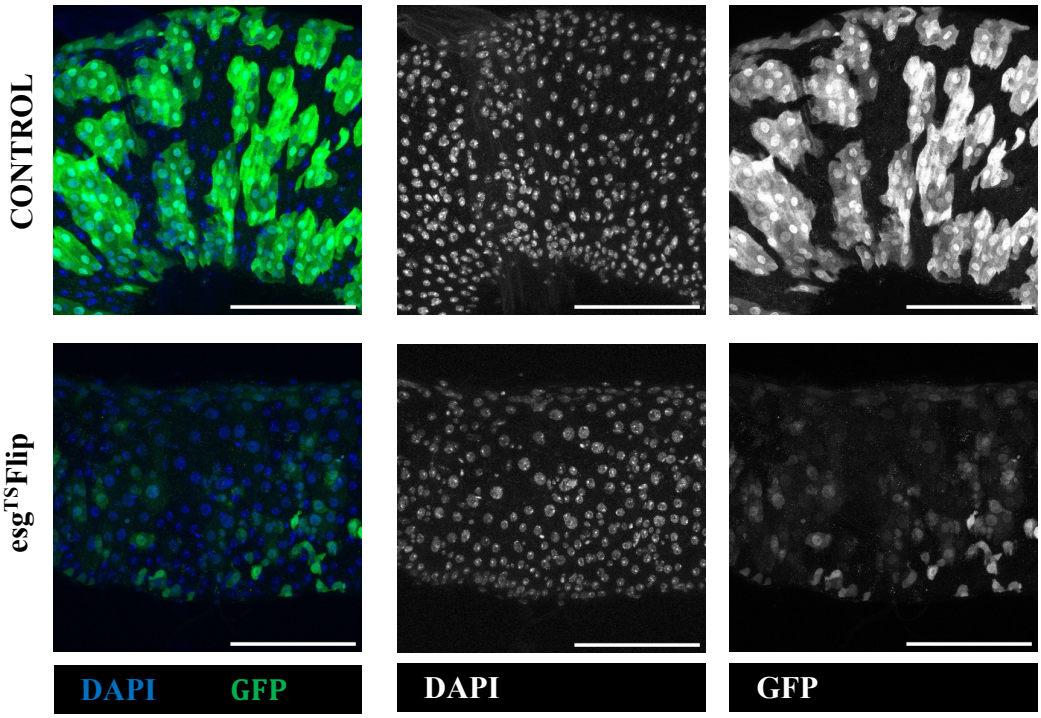

Figure 4.14. Knockdown of *PLOD-RNAi-3* driven by *esg^{TS}Flip* decreases the number of GFP-expressing cells in the posterior midgut. PLOD knockdown (*esg^{TS}Flip > UAS-PLOD-RNAi-4)* shows a reduction in GFP levels compared to control guts (*esg^{TS}Flip > Luciferase).* GFP tags PLOD-expressing cells and its clones. Guts were stained with α-GFP (1:2000) and DAPI. Scale bars in the bottom right corner represent 100μm.

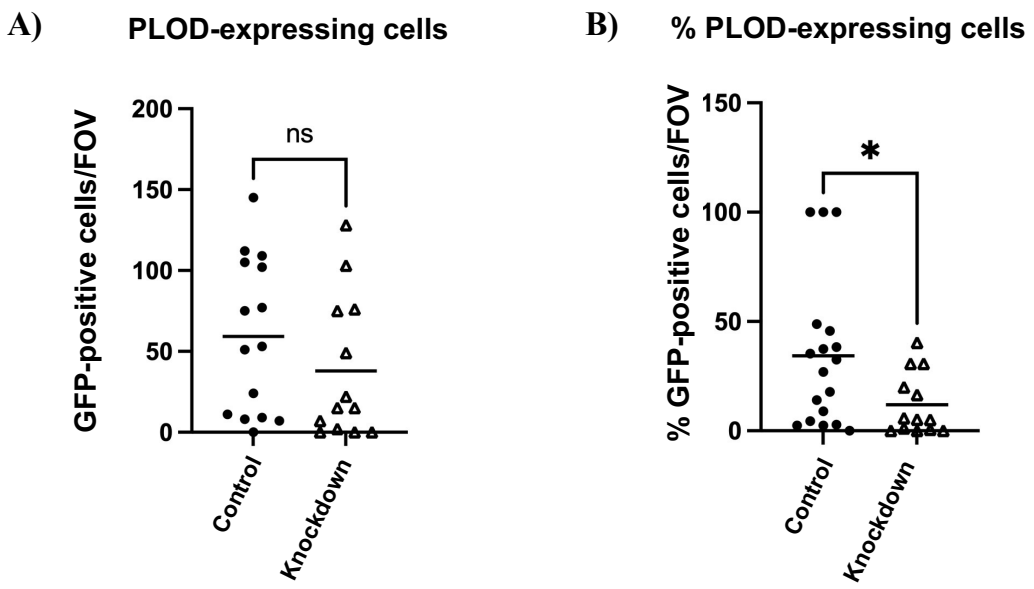

Figure 4.15. Knockdown of PLOD using *PLOD-RNAi-3* driven by *esg^{TS}Flip* significantly reduces the number of GFP-expressing cells. PLOD knockdown (*esg^{TS}Flip > UAS-PLOD-RNAi-3)* reduces the total number of GFP-positive cells/FOV (control n = 15, KD n = 13) (***A***), but this change is not statistically significant (p = 0.1) compared to control guts (*esg^{TS}Flip > Luciferase).* The % of GFP-positive cells normalized to the total cell number/FOV (control n = 18, KD n = 13) is significantly reduced in PLOD knockdown guts (p = 0.03) (***B***) . All data was not normally distributed, so non-parametric Mann-Whitney U-tests were used for statistical analysis. Each data point represents a gut.

4.3.5. PLOD is expressed by the stem and progenitor cells of the midgut

As mentioned, preliminary data from our group identified PLOD as being specifically secreted by stem and progenitor cells, but not expressed by the differentiated cells of the tissue. In order to validate this, an *UAS eGFP* reporter was crossed to a *PLOD-Gal4 gene trap*, which tags PLOD-expressing cells with a GFP marker. The guts were also co-stained with prospero, which tags EE cells (*Figure 4.16*). Results demonstrated that PLOD-positive cells did not colocalize with EE cells. Moreover, PLOD was expressed in cells with smaller nuclei, i.e. PLOD expression was not found in larger enterocyte cells and it is indeed most likely expressed in the stem and progenitor cells. Outside the epithelial tissue, most of the PLOD expression was found in the surrounding visceral muscle, but no follow up experiments were carried out as this was outside the scope of this project.

To further validate these results, *esgLacZ* female fly guts were stained with β-gal, which tags ISCs and EBs, and with PLOD (*Figure 4.17*). This showed some colocalization between PLOD and β-gal, indicating that PLOD is indeed expressed in

some stem and/or progenitor cells, but not in the entire population in the tissue. This suggests that PLOD is perhaps expressed in a small subset of ISCs and EBs, but that its expression is not widespread among the progenitor cells of the tissue.

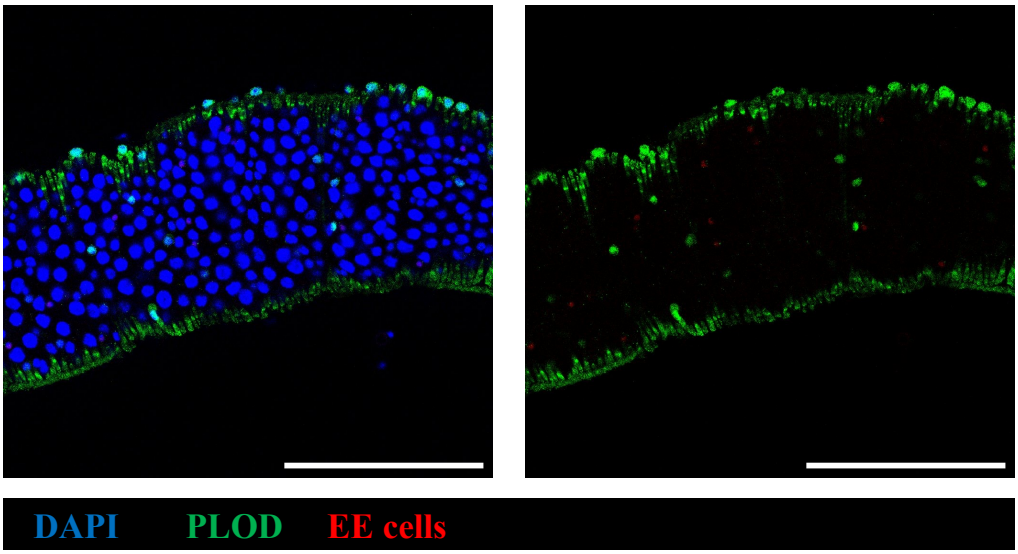

Figure 4.16. PLOD is not expressed in EE cells in the posterior midgut. *PLOD Gal4 Gene Trap > UAS eGFP* showed no colocalization between PLOD-expressing cells and the EE marker prospero. Most of the PLOD expression was found in the surrounding visceral muscle cells. Guts were stained with α-GFP (1:2000), α-prospero (1:100), and DAPI. Scale bars in the bottom right corner represent 100μm.

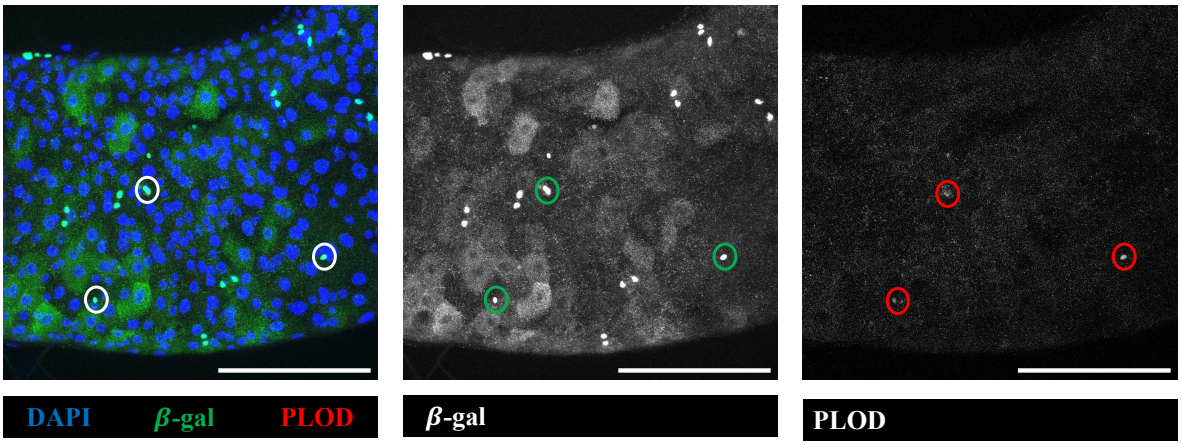

Figure 4.17. PLOD colocalizes with the stem and progenitor cells in the posterior midgut. *esgLacZ* female guts were stained with α-PLOD (1:100), α-β-galactosidase (1:500), and DAPI. β-galactosidase tags stem and progenitor cells and results showed colocalization with PLOD, indicating that PLOD is expressed in ISCs and EBs. Scale bars in the bottom right corner represent 100μm.

As a final step in the elucidation of the PLOD expression pattern in the fly midgut, a *PLOD Gal4 CRIMIC* line, i.e. a gene trap, was used to drive the expression of a nuclear localization sequence containing a fluorescent reporter attached, *nls-GFP* (*Figure 4.18*). A CRIMIC (CRISPR-Integrated Mediation Cassette) forms a loss-of-function allele of the protein of interest, i.e. PLOD in this case, and instead expresses a Gal4 protein with the same spatial and temporal expression pattern as that gene of interest (Kanca et al., 2019). This genetic engineering technique of the *Drosophila* genome was developed by Zhang and colleagues in 2014, and in this case, a GFP-tagged nuclear localization sequence is expressed in those cells where PLOD is found. These results confirmed those observed previously through the use of other driver lines, with PLOD not expressed in enteroendocrine cells. Interestingly, these *PLOD Gal4 Gene Trap > UAS GFP-nls* guts reported PLOD expression in cells with larger nuclei, raising the possibility that PLOD colocalizes to the differentiated enterocyte cells. This line also showed an interesting linear arrangement of the PLOD-expressing cells in the tissue. This suggests that PLOD expression is found in the surrounding muscle, but, as mentioned above, the aim of this project was focused on PLOD expression the intestinal epithelial cells and thus this line of investigation was not carried further. However, it is worth noting that there was some variability among replicates for these experiments, and that the GFP tag was not always expressed, indicating a potential issue with the driver line that could be affecting the results observed.

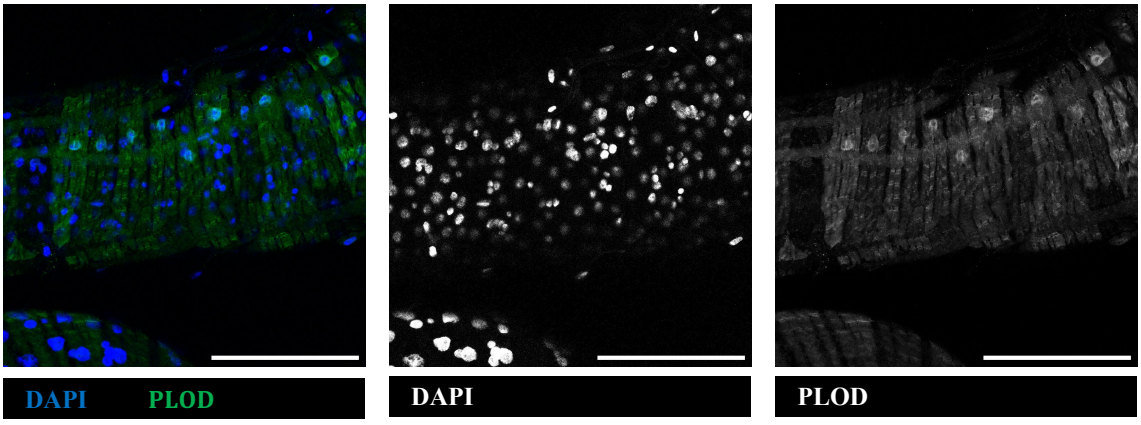

Figure 4.18. A nuclear localization sequence suggest PLOD is expressed in the larger cells of the tissue. *PLOD Gal4 Gene Trap > UAS-GFP nls* guts were stained with α-GFP (1:2000), and DAPI, where GFP tags PLOD-expressing cells, and results suggested that PLOD is expressed in the larger nuclei of the epithelial tissue, i.e. in the ECs. Scale bars in the bottom right corner represent 100μm.

In summary, these results demonstrate that PLOD is expressed in the stem and progenitor cells of the gut, and some results suggest that perhaps this protein could also be found in certain ECs, but further work is needed to determine the reliability of this expression pattern in differentiated cells.

4.3.6. The interactions of PLOD with collagen (vkg) and other ECM molecules

Initial immunofluorescence data revealed that some PLOD RNAi guts presented disorganization of cells within the tissue, but this phenotype did not have full penetrance. Because PLOD is a collagen-modifying enzyme, we hypothesized that this compromise to cell arrangement in the tissue could be due to changes in collagen. *5961 Gene Switch > PLOD RNAi* guts were dissected and stained with Viking (vkg) antibody and prospero. These experiments were carried out for all three RNAi lines used in this study and the results observed were similar across all of them (*Figure 4.19, 4.21 and 4.23*). Knockdown of PLOD increased the amount of vkg-expressing cells in the midgut, but these changes were not deemed statistically significant (*Figure 4..20, 4.22 and 4.24*). Taken together, these results show that although collagen could have a role in the disorganization of cells in midguts in which PLOD levels have been knocked down, it is not the only molecule responsible for these changes.

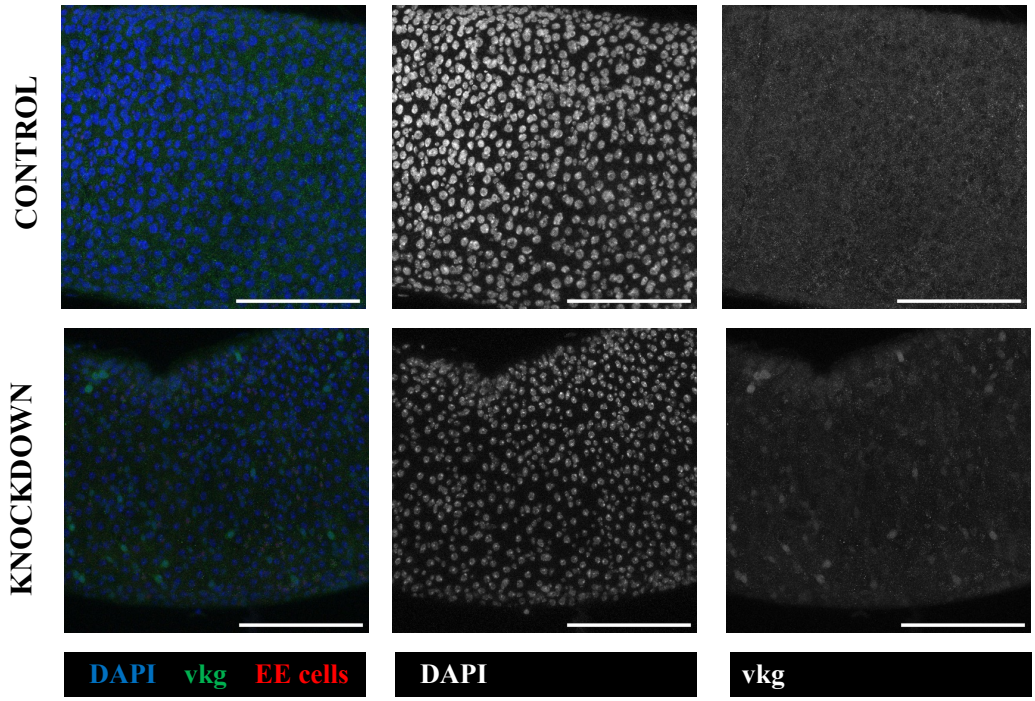

Figure 4.19. Collagen expression in *PLOD-RNAi-1* guts. Knockdown of PLOD (5961^{GS} > *PLOD-RNAi-1*) seems to increase collagen (vkg) staining in the posterior midgut. Guts were stained with α- vkg (1:100) and DAPI. Scale bars in the bottom right corner represent 100μm.

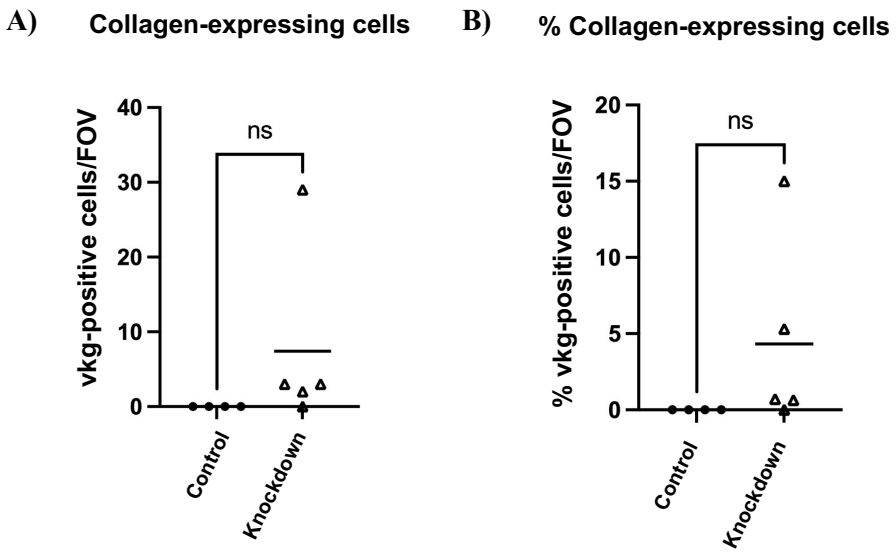

Figure 4.20. *PLOD-RNAi-1* increases the number of vkg-positive cells in the posterior midgut. Knockdown of PLOD (*5961^{GS} > PLOD-RNAi-1*) increases both the total number of vkg-positive cells observed per FOV (p = 0.1) (n = 4) (***A***), as well as the proportion of vkg-positive cells normalized to total cell number/FOV (p = 0.05) (control n = 4, OE n = 5) (***B***), but statistical analysis showed these trends were not significant. All data was not normally distributed, so non-parametric Mann-Whitney U-tests were used for statistical analysis. Each data point represents a gut.

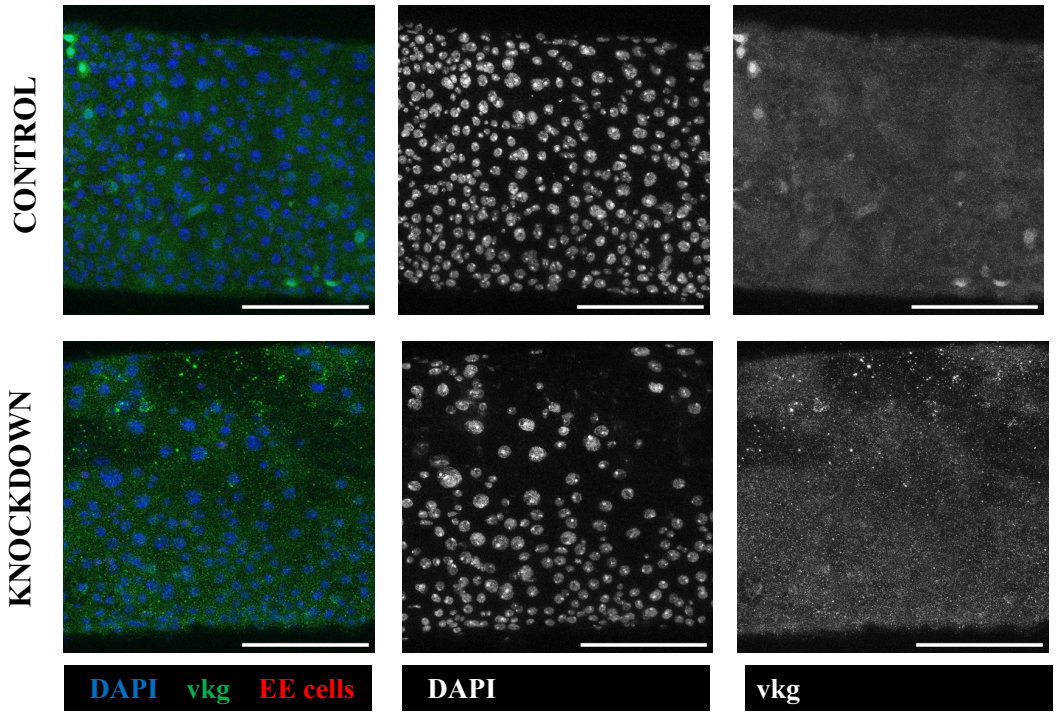

Figure 4.21. Collagen expression in *PLOD-RNAi-2* guts. Representative images showing knockdown of PLOD (*5961^{GS} > PLOD-RNAi-2*) does not induce any changes to collagen (vkg) staining in the posterior midgut. Guts were stained with α- vkg (1:100) and DAPI. Scale bars in the bottom right corner represent 100μm.

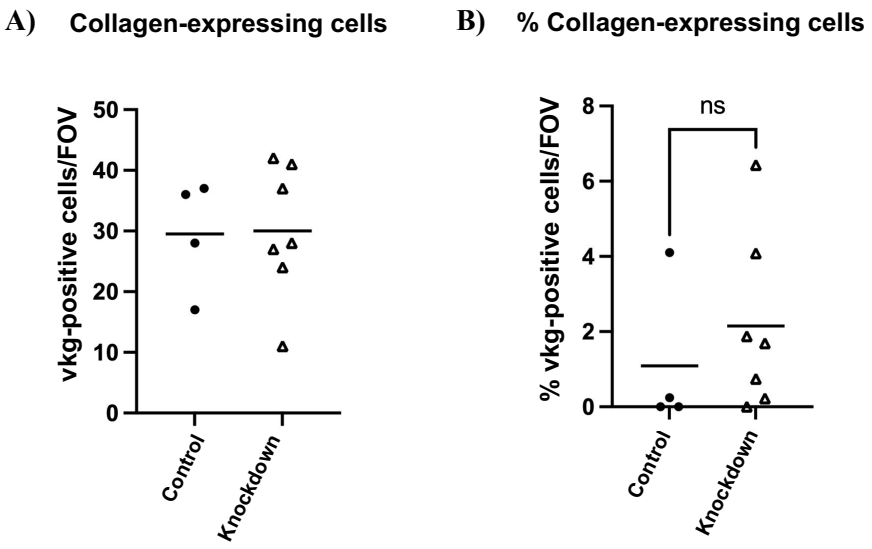

Figure 4.22. *PLOD-RNAi-2* does not affect vkg in the posterior midgut. Knockdown of PLOD (*5961^{GS} > PLOD-RNAi-2*) increases the proportion of vkg-positive cells normalized to total cell number/FOV (p = 0.4) (control n = 4, OE n = 7) (***B***), but statistical analysis showed this trend was not significant. The total number of vkg-positive cells observed per FOV remains unchanged compared to control guts (control n = 3, OE n = 7) (***A***). All data was not normally distributed, so non-parametric Mann-Whitney U-tests were used for statistical analysis. Each data point represents a gut.

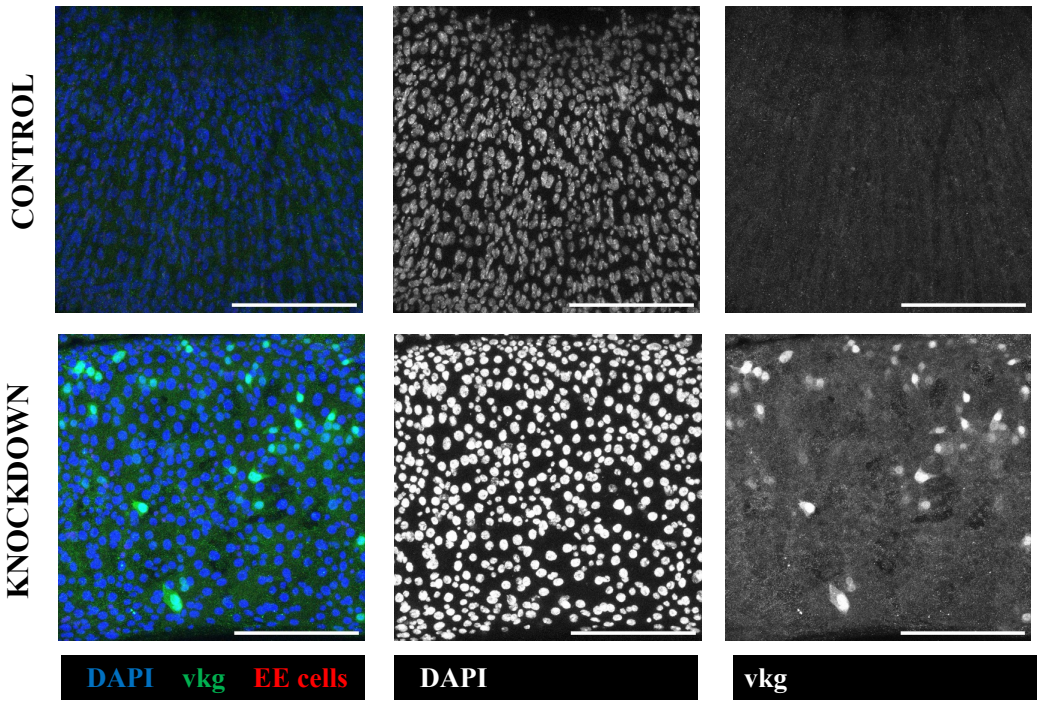

Figure 4.23. *PLOD-RNAi-3* increases vkg expression in the posterior midgut. Knockdown of PLOD (*5961^{GS} > PLOD-RNAi-3*) seems to increase collagen (vkg) staining in the posterior midgut compared to control guts. Guts were stained with α- vkg (1:100) and DAPI. Scale bars in the bottom right corner represent 100μm.

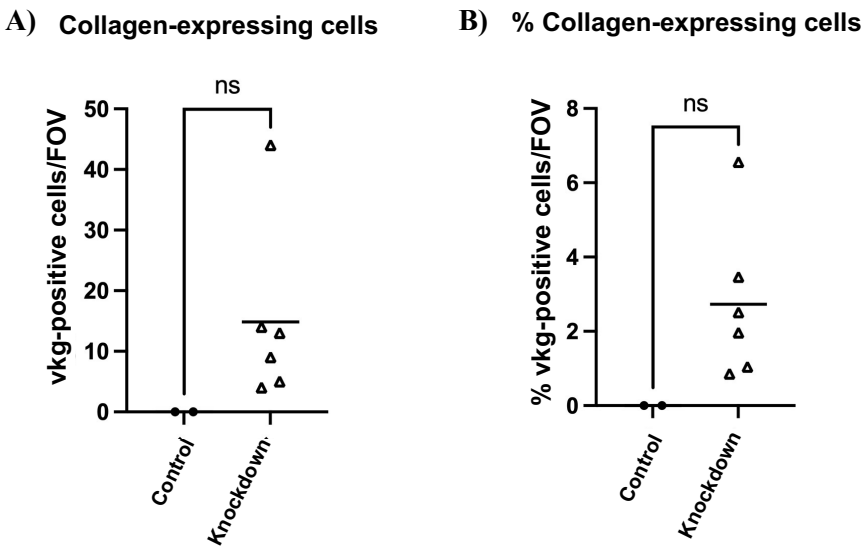

Figure 4.24. *PLOD-RNAi-3* increases the number of vkg-positive cells in the posterior midgut. Knockdown of PLOD (*5961^{GS} > PLOD-RNAi-3*) increases both the total number of vkg-positive cells observed per FOV (p = 0.07) (control n = 2, OE n = 6) (***A***), as well as the proportion of vkg-positive cells normalized to total cell number/FOV (p = 0.07) (control n = 2, OE n = 7) (***B***), but statistical analysis showed these trends were not significant. All data was not normally distributed, so non-parametric Mann-Whitney U-tests were used for statistical analysis. Each data point represents a gut.

In an attempt to further characterize the relationship of PLOD and collagen IV in this context, a *vkg Gal4 CRIMIC* line was crossed to an UAS eGFP reporter midgut (*vkg Gal4 CRIMIC > UAS eGFP*) to determine the expression pattern of collagen in the *Drosophila* midgut (*Figure 4.25*). Guts were co-stained with DAPI and prospero, and results did not show any colocalization between collagen expression and EE cells. This fits in with the PLOD expression pattern suggested above, which showed PLOD expression in the ISCs and EBs, and the published literature that has demonstrated PLOD is essential for collagen secretion in the epithelial tissues. This raises the possibility of an endogenous collagen source in the *Drosophila* gut in the stem and progenitor cells of the tissue.

To look at this further, and as an alternative approach to observe the disorganization of cells in the gut after PLOD knockdown, midguts were stained with phalloidin, which stains F-actin filaments (*Figure 4.26*). The intensity of F-actin staining was quantified in control and knockdown guts (*Figure 4.27*) and results were compared between them: knockdown of PLOD with *UAS-PLOD RNAi-2* and *-3* did not show any changes in actin staining when compared to controls, but interestingly, knockdown of

PLOD with *UAS-PLOD RNAi-1* demonstrated a statistically significant decrease in F-actin levels in the midgut compared to controls. These disparities between RNAi lines could be explained by the different RNAi constructs that knock down PLOD in each of the lines.

Taken together, these results raise the possibility that knockdown of PLOD in the ISC/EBs increases collagen levels but decreases F-actin, thus compromising correct cytoskeletal and ECM assembly. Thus, it can be hypothesized that loss of homeostatic levels of PLOD may lead to a loss of homeostasis in the ECM components, which in turn has a knock-on effect that in some cases presents as cellular disarray.

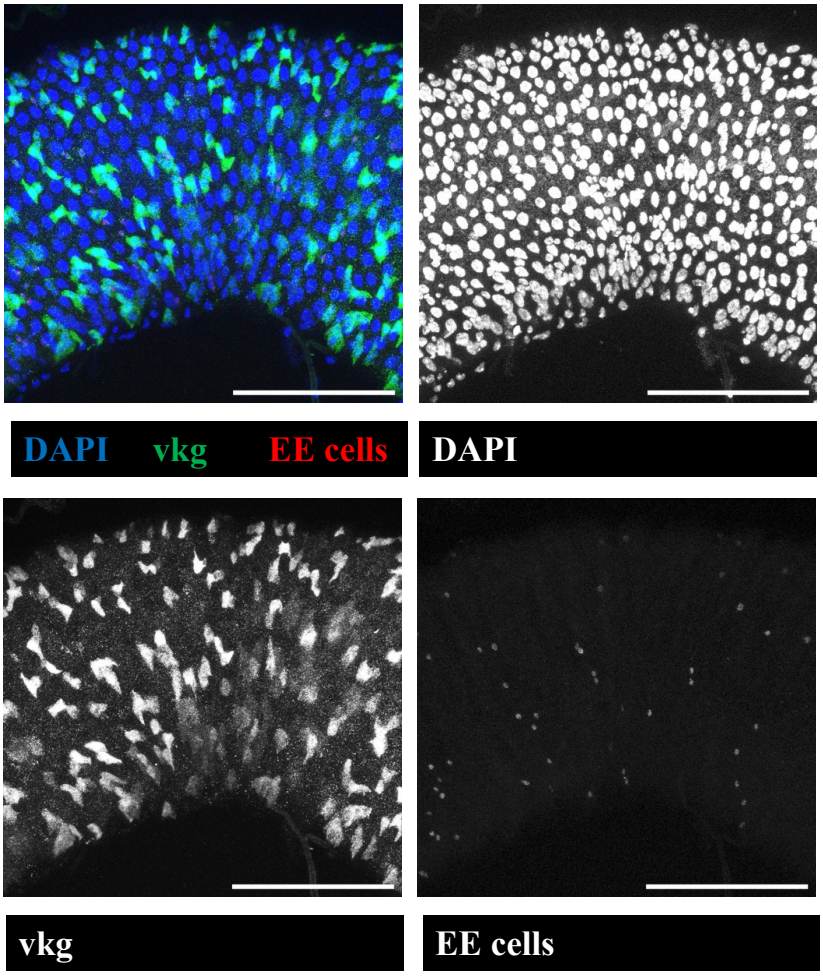

Figure 4.25. Viking expression does not colocalize with EE cells and shows a similar expression pattern to PLOD. Vkg expression (*vkg-Gal4-CRIMIC > UAS eGFP*) showed no colocalization between vkg-positive cells and EEs. Guts were stained with α- vkg (1:100) and DAPI. Scale bars in the bottom right corner represent 100μm.

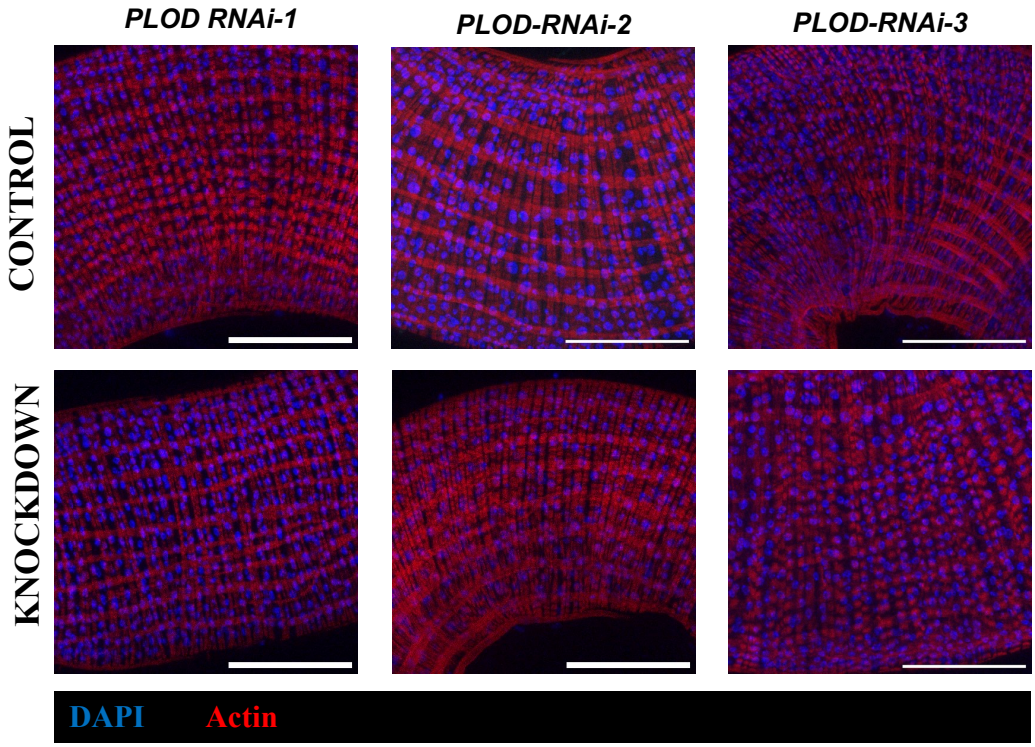

Figure 4.26. The actin filament network in PLOD knockdown guts. Knockdown of *PLOD RNAi line 1-3* does not seem to affect the intensity of phalloidin staining of actin filament network compared to control guts. Guts were stained with phalloidin (1:100) and DAPI. Scale bars in the bottom right corner represent 100μm.

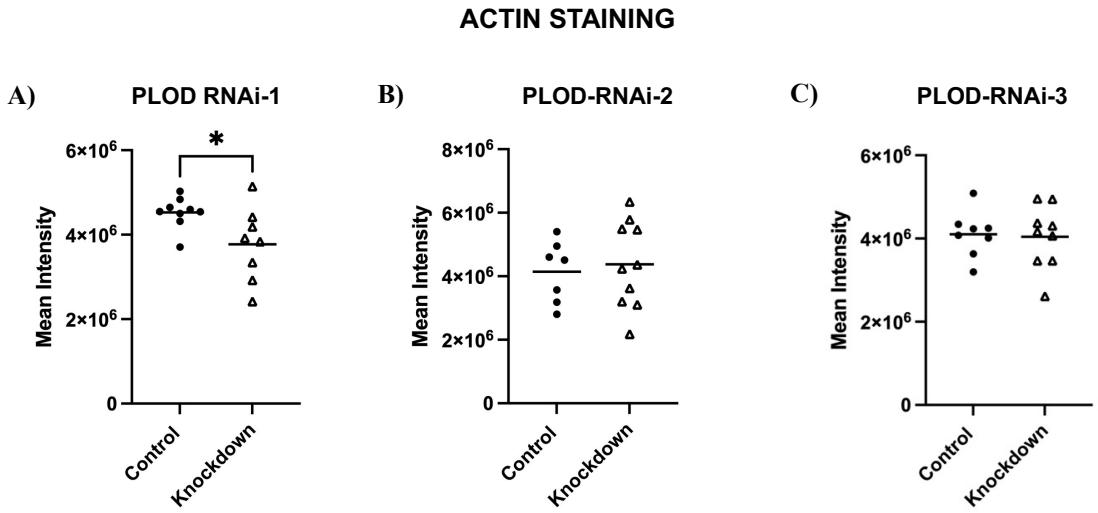

Figure 4.27. PLOD-RNAi-1 knockdown significantly reduces the intensity of actin filament staining. Knockdown of PLOD with *RNAi line-1* significantly decreases the strength of phalloidin staining compared to control guts (p = 0-03) (control n = 9, OE n = 8) (***A***). Knockdown with RNAi line 2 (*5961^{GS} > PLOD-RNAi-2*) (control n = 7, KD n = 10) (***B***) and 3 (*5961^{GS} > PLOD-RNAi-3*) do not affect the intensity of phalloidin staining (control n = 9, KD n = 12) (***C***). All data was normally distributed, so unpaired t-tests were used for statistical analysis. Each data point represents a gut.

4.3.7. Changes to the basement membrane epithelial cells in the *Drosophila* gut as a result of PLOD knockdown

As highlighted in this section, immunofluorescence experiments of PLOD knockdown showed a disorganization of the cells within the midgut tissue. In order to further understand if reduced levels of PLOD affected basement membrane integrity as a result of reduced collagen deposition, *5961 Gene Switch* samples of all 3 PLOD RNAi lines were prepared for transmission electron microscopy (TEM) analysis. However, as mentioned in Chapter 3 of this thesis, issues beyond our control pertaining to the electron microscopy facility in our department meant these experiments were delayed. At the time of the submission of this thesis, these experiments have been restarted and *5961GS > PLOD RNAi-3* females guts are currently undergoing the final stages of sample processing by the electron microscopy team at Durham University.

4.3.8. The impact of PLOD in *Drosophila* gut signalling

After studying the expression pattern and possible effects of PLOD knockdown at the cell and tissue level, the next step was to test whether any of the major homeostatic regulatory pathways were affected by PLOD manipulation. *5961GS > UAS PLOD RNAi* female guts were dissected and stained for anti-MAPK, anti-SMAD and anti-SAPK/JNK antibodies, and results between the three PLOD RNAi lines were variable.

Knockdown of PLOD using *RNAi line-1* showed a significant decrease in MAPK staining in PLOD knockdown guts compared to controls (*Figures 4.28 and 4.29*), but no significant changes were observed in SMAD (*Figures 4.30 and 4.31*) and SAPK/JNK staining (*Figures 4.32 and 4.33*). Active SMAD levels were low in both control and knockdown guts, and quantification of SMAD staining revealed a slight decrease in staining in PLOD-knockdown guts compared to controls but this change was not statistically significant (*Figure 4.31*). It is worth nothing that the percentage of SAPK/JNK-positive cells in the midgut showed a bimodal distribution of the data: some guts had a very high proportion of SAPK/JNK-positive cells, between 70-90%, whereas a separate population had significantly lower levels of staining, between 0 and 20%.

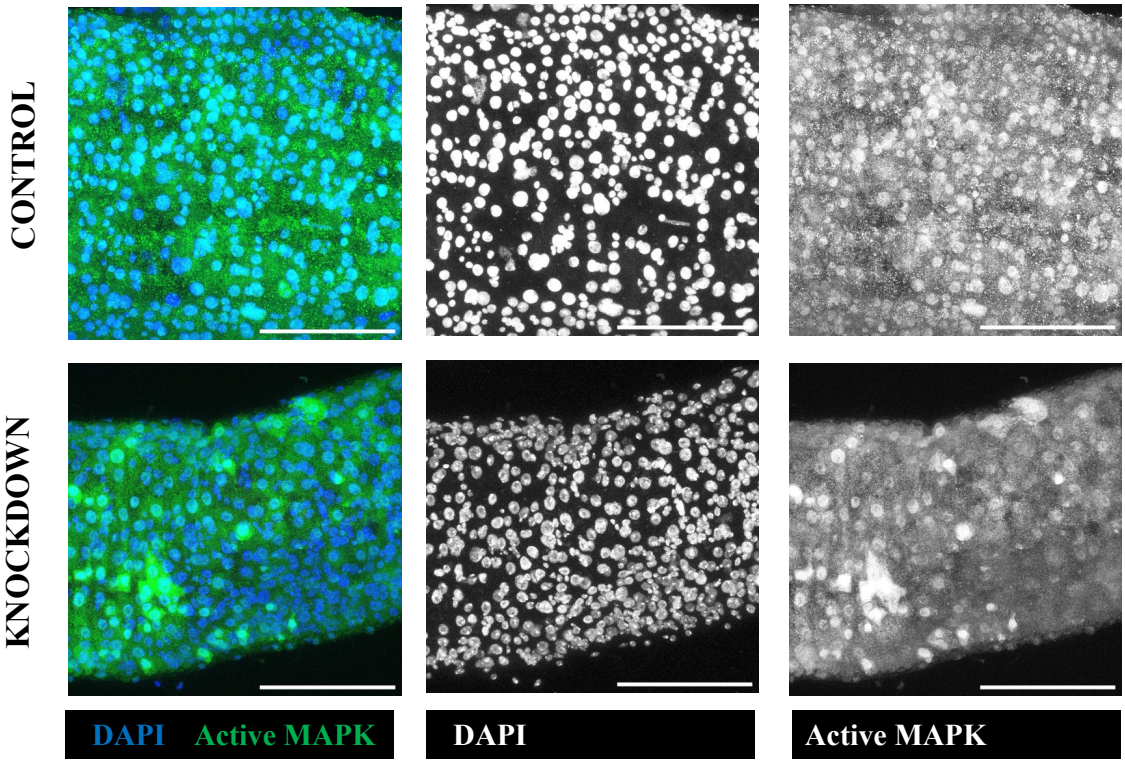

Figure 4.28. The expression of active MAPK in PLOD-RNAi-1 knockdown guts. Knockdown of PLOD (*5961^{GS} > PLOD-RNAi-1*) decreases the number of active MAPK-positive cells in the posterior midgut. Guts were stained with α- phospho-p44/42 MAPK (Erk1/2) (1:200) and DAPI. Scale bars in the bottom right corner represent 100μm.

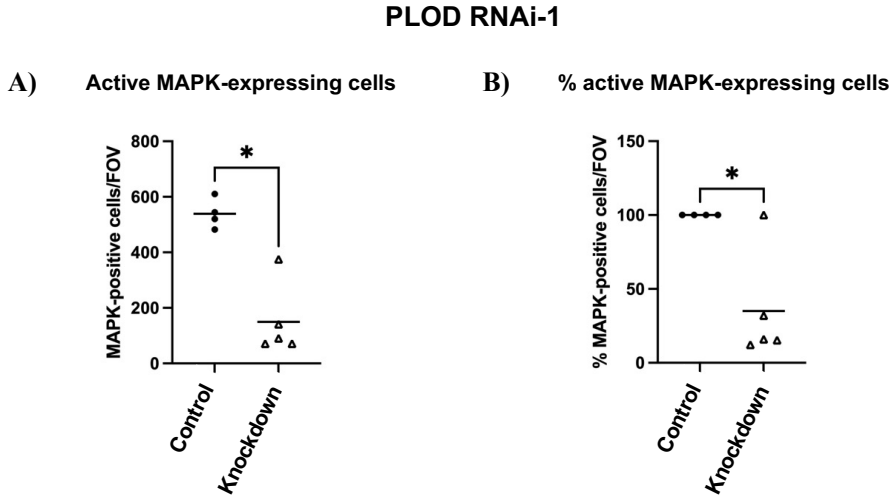

Figure 4.29. Active MAPK expression decreases with *PLOD-RNAi-1* knockdown. Knockdown of PLOD (*5961^{GS} > PLOD-RNAi-1*) significantly decreases the levels of active MAPK expression in PLOD-knockdown guts compared to controls (p = 0.01) (control n = 4, OE n = 5) (***A***), as well as the proportion of active MAPK-positive cells normalized to total cell number (p = 0.04) (control n = 4, OE n = 5) (***B***). Data was not normally distributed, so non-parametric Mann Whitney-U tests were used for statistical analysis. Each data point represents a gut.

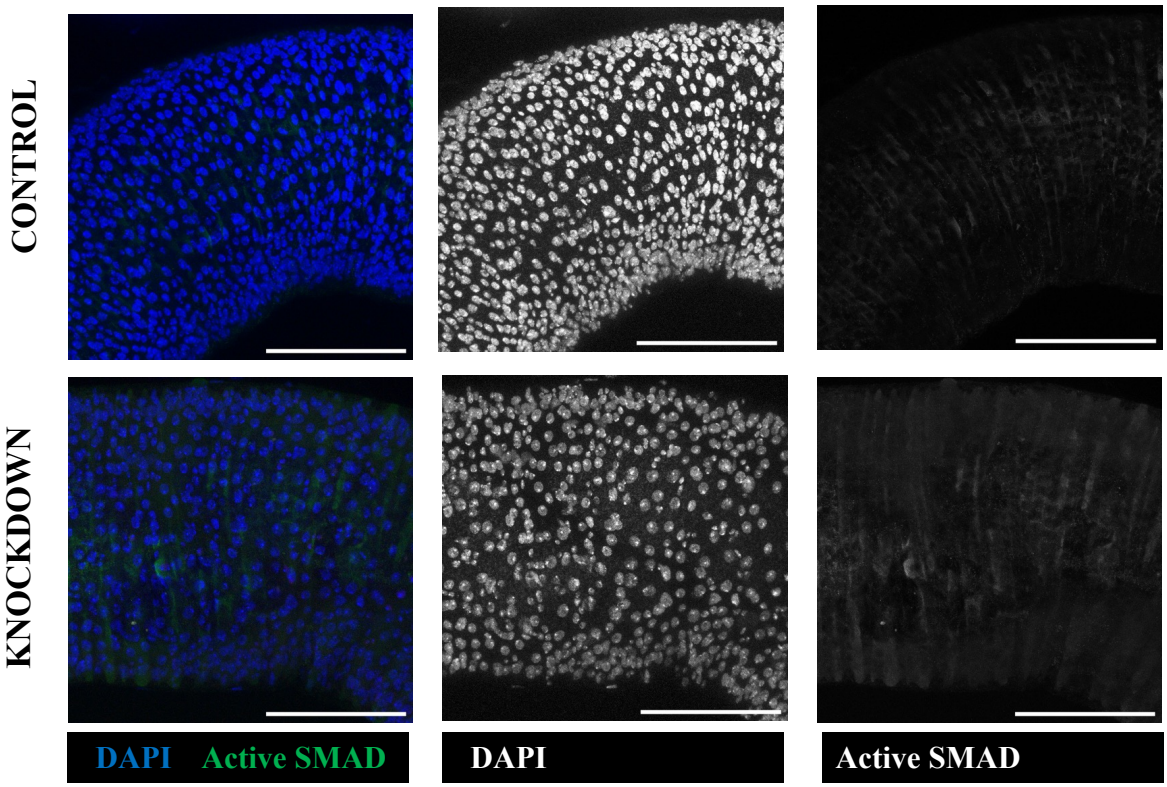

Figure 4.30. The expression of active SMAD in *PLOD-RNAi-1* knockdown guts. Knockdown of PLOD (*5961^{GS} > PLOD-RNAi-1*) does not change active SMAD expression in the posterior midgut. Guts were stained with α- phospho-Smad3 (1:100) and DAPI. Scale bars in the bottom right corner represent 100μm.

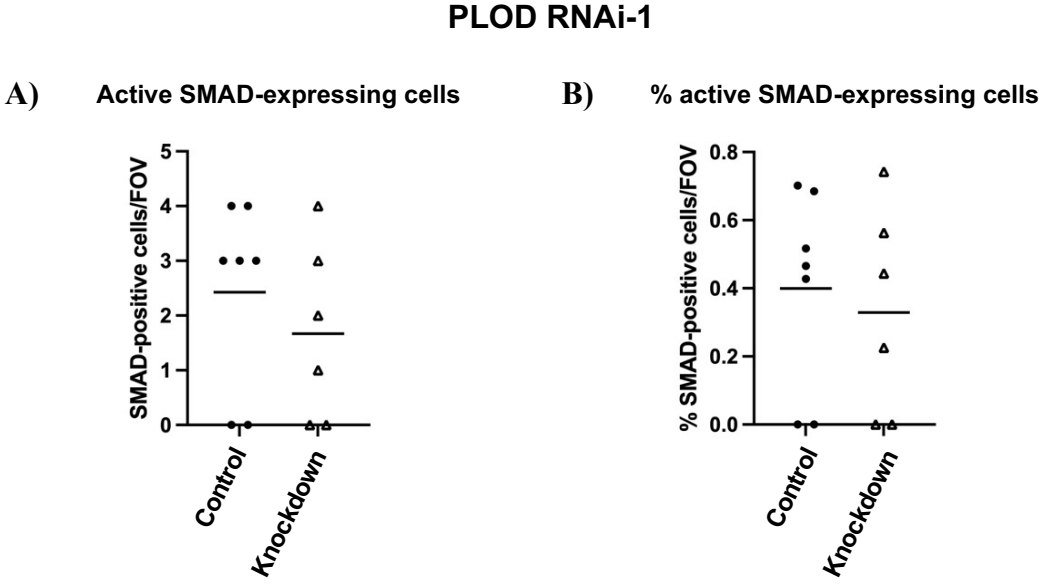

Figure 4.31. Active SMAD expression does not change with *PLOD-RNAi-1* knockdown. Knockdown of PLOD (*5961^{GS} > PLOD-RNAi-1*) decreases the number of SMAD-positive cells observed per field of view (***A***), and the proportion of active SMAD-positive cells normalized to total cell number (***B***) but these changes are not statistically significant (control n = 7, KD n = 6). Unpaired t-tests were used for normally distributed data (B), and non-parametric Mann Whitney-U tests for non-normally distributed data (A) . Each data point represents a gut.

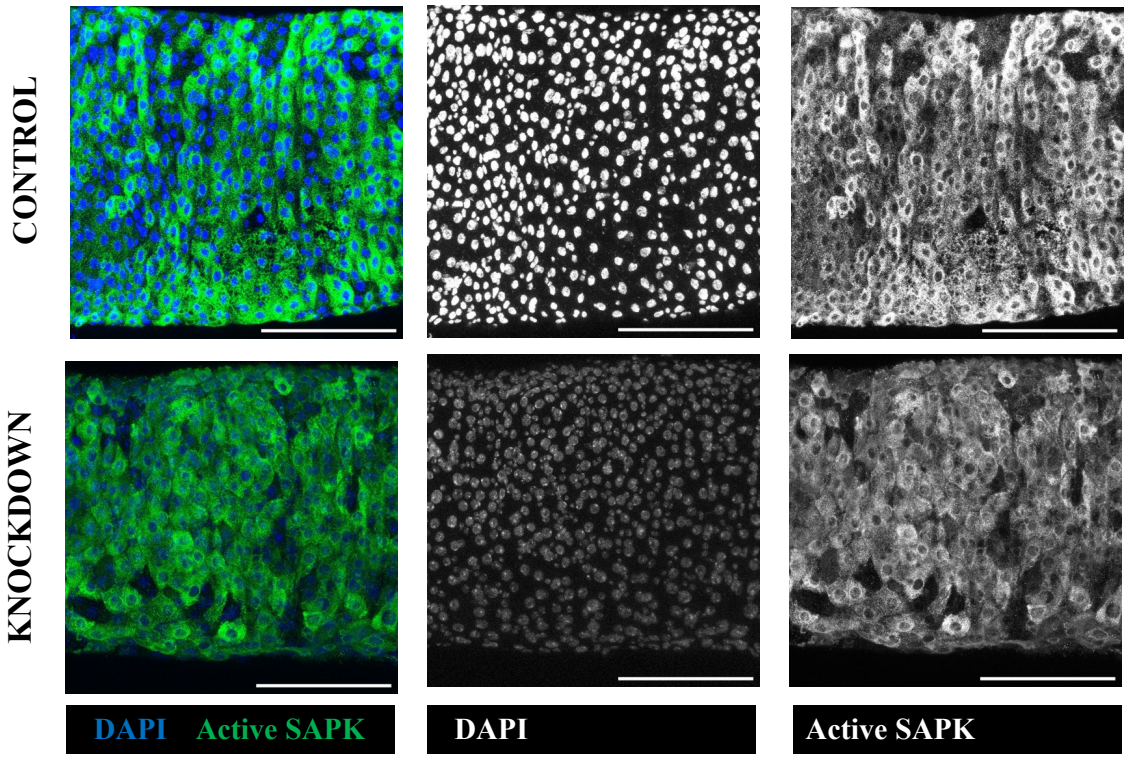

Figure 4.32. The expression of active SAPK in *PLOD-RNAi-1* knockdown guts. Knockdown of PLOD (*5961^{GS} > PLOD-RNAi-1*) does not reduce the active SAPK expression observed in control midguts. Guts were stained with α- phospho-SAPK/JNK (1:100) and DAPI. Scale bars in the bottom right corner represent 100μm.

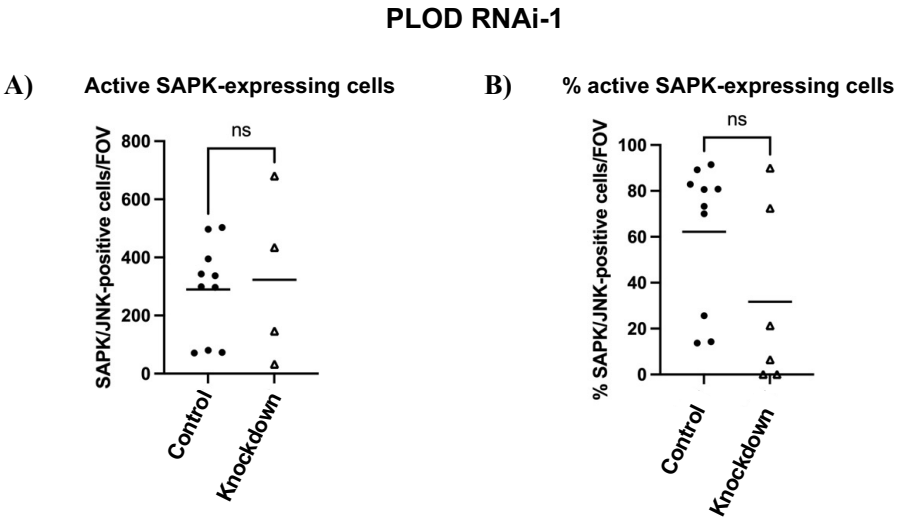

Figure 4.33. Active SAPK expression does not change with *PLOD-RNAi-1* knockdown. Knockdown of PLOD (*5961^{GS} > PLOD-RNAi-1*) slightly increases the number of SAPK-positive cells observed per field of view (control n = 10, KD n = 4) (***A***), but decreases the proportion of active SAPK-positive cells normalized to total cell number (control n = 10, KD n = 6) (***B***). Both of these changes are not statistically significant (p = 0.7, and p = 0.1, respectively). Unpaired t-tests were used for normally distributed data (A), and non-parametric Mann Whitney-U tests for non-normally distributed data (B) . Each data point represents a gut.

Knockdown of PLOD with *UAS-PLOD-RNAi-2* yielded different results, which showed in a highly significant increase of MAPK staining in the midgut (*Figures 4.34 and 4.35*), which points to an inverse correlation between PLOD levels and RAS/MAPK pathway activity, and to the localization of PLOD upstream of this signaling cascade. On the contrary, knockdown of PLOD using this same line led to a significant decrease in SMAD-positive cells (*Figures 4.36 and 4.37*), as well as in SAPK/JNK-expressing cells (*Figures 4.38 and 4.39*). From this line, we concluded that PLOD plays a role in the regulation of Ras/MAPK, TGF-β (a SMAD-dependent signaling pathway), and JNK signalling. In particular, levels of SMAD and TGF-β signaling positively correlate with PLOD levels, whereas the Ras/MAPK pathway seems to be a negative regulator of PLOD in the ISC/EBs.

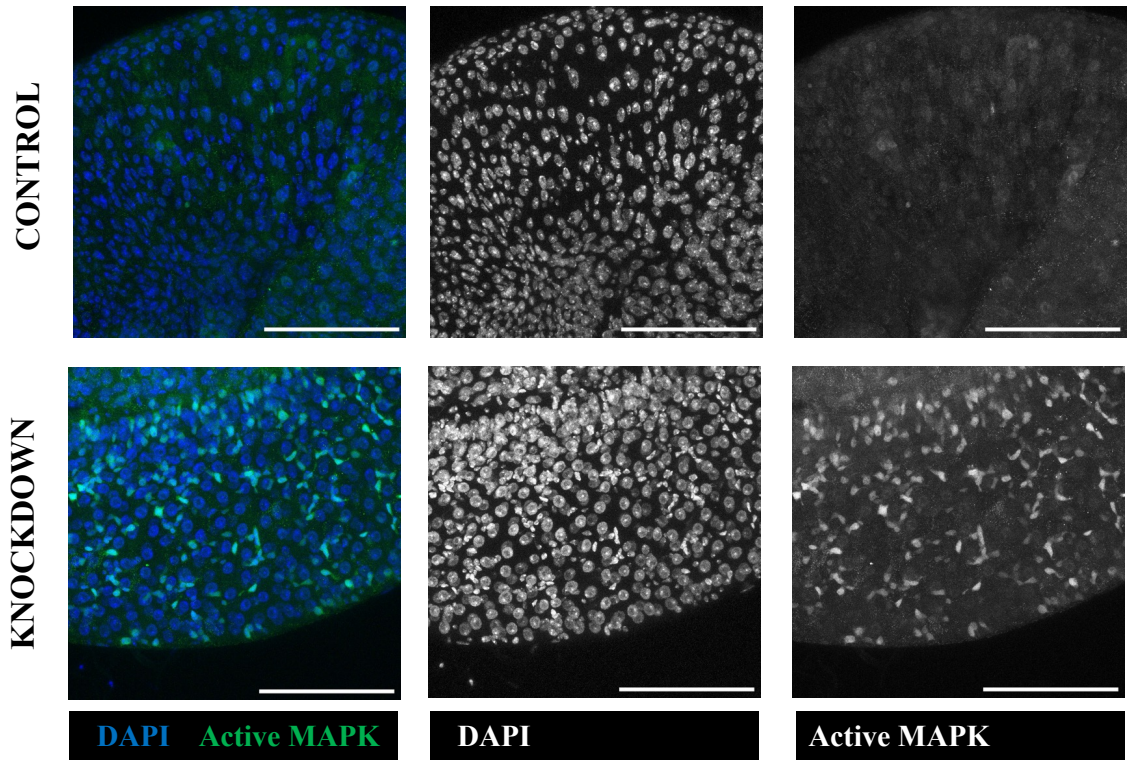

Figure 4.34. The expression of active MAPK in *PLOD-RNAi-2* knockdown guts. Knockdown of PLOD (*5961^{GS} > PLOD-RNAi-2*) increases the number of active MAPK-positive cells in the posterior midgut. Guts were stained with α- phospho-p44/42 MAPK (Erk1/2) (1:200) and DAPI. Scale bars in the bottom right corner represent 100μm.

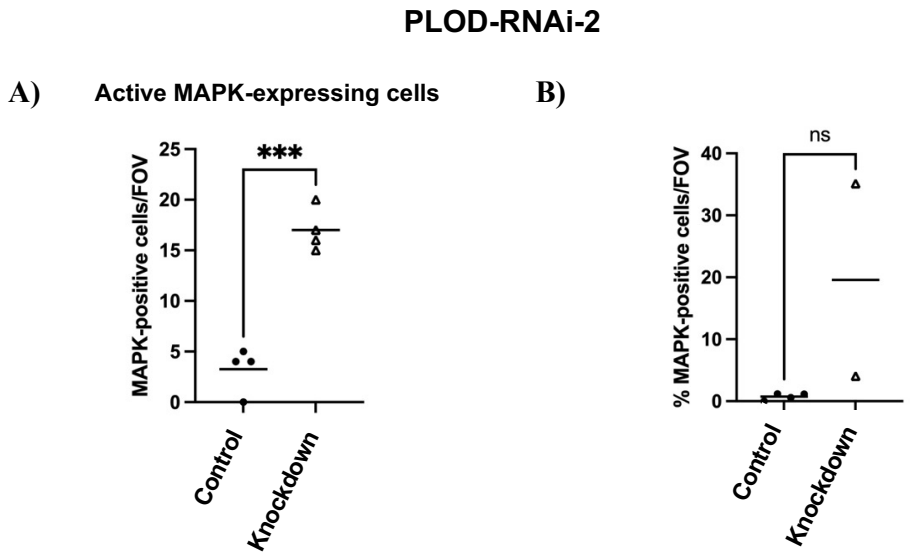

Figure 4.35. Active MAPK expression increases with *PLOD-RNAi-2* knockdown. Knockdown of PLOD (*5961^{GS} > PLOD-RNAi-2*) significantly increases the levels of active MAPK expression in PLOD-knockdown guts compared to controls (p = 0.0001) (n = 4) (***A***), but the increasing trend in the proportion of active MAPK-positive cells normalized to total cell number is not statistically significant (p = 0.1) (control n = 4, OE n = 2) (***B***). All data was normally distributed, so unpaired t-tests were used for statistical analysis. Each data point represents a gut.

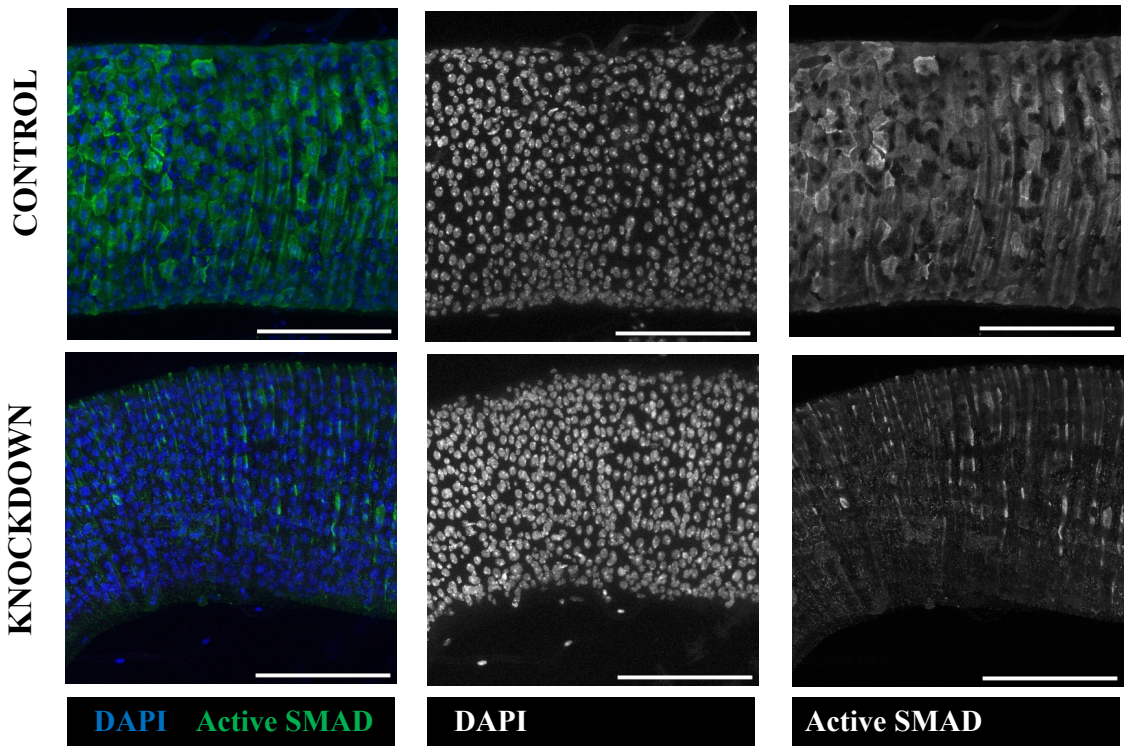

Figure 4.36. The expression of active SMAD in *PLOD-RNAi-2* knockdown guts. Knockdown of PLOD (*5961^{GS} > PLOD-RNAi-2*) increases the number of active SMAD-expressing cells in the posterior midgut. Guts were stained with α- phospho-Smad3 (1:100) and DAPI. Scale bars in the bottom right corner represent 100μm.

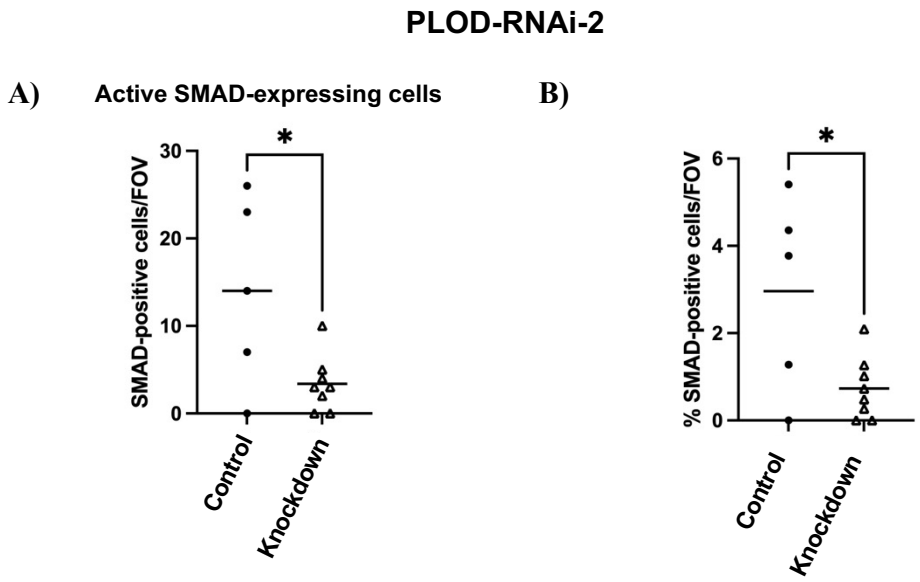

Figure 4.37. Active SMAD expression significantly decreases with *PLOD-RNAi-2* knockdown. Knockdown of PLOD (*5961^{GS} > PLOD-RNAi-2*) significantly decreases both the number of SMAD-positive cells observed per field of view (p = 0.02) (***A***), and the proportion of active SMAD-positive cells normalized to total cell number (p = 0.02) (***B***) (control n = 5, KD n = 8). All data was normally distributed, so unpaired t-tests were used for statistical analysis. Each data point represents a gut.

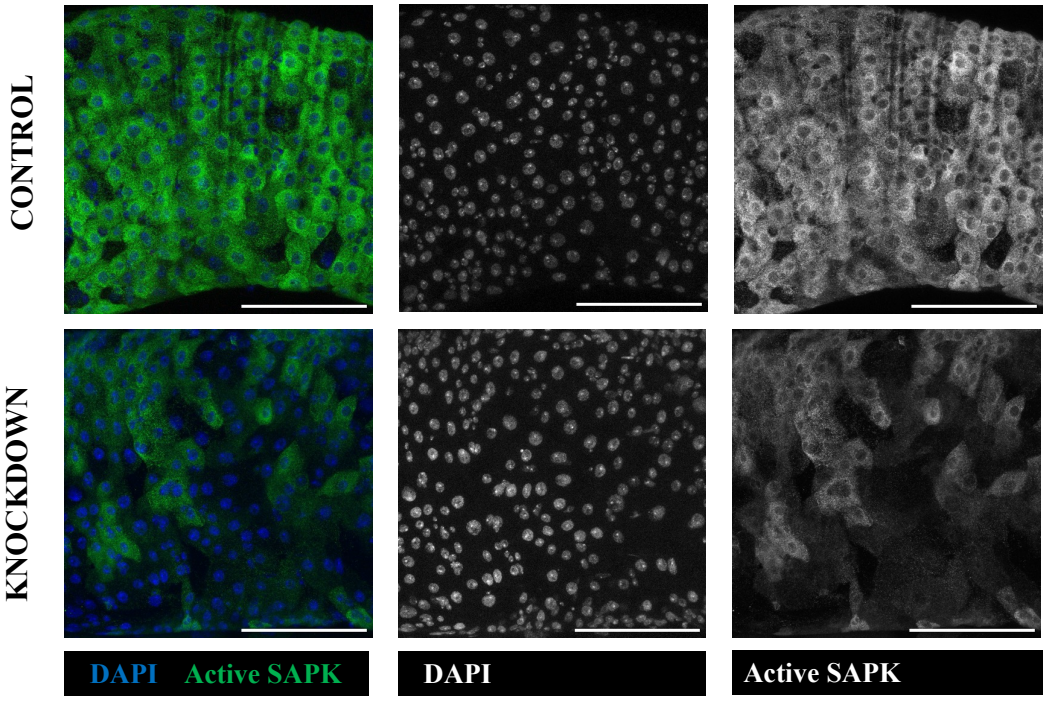

Figure 4.38. The expression of active SAPK in *PLOD-RNAi-2* knockdown guts. Knockdown of PLOD (*5961^{GS} > PLOD-RNAi-2*) reduces active SAPK expression in control midguts. Guts were stained with α- phospho-SAPK/JNK (1:100) and DAPI. Scale bars in the bottom right corner represent 100μm.

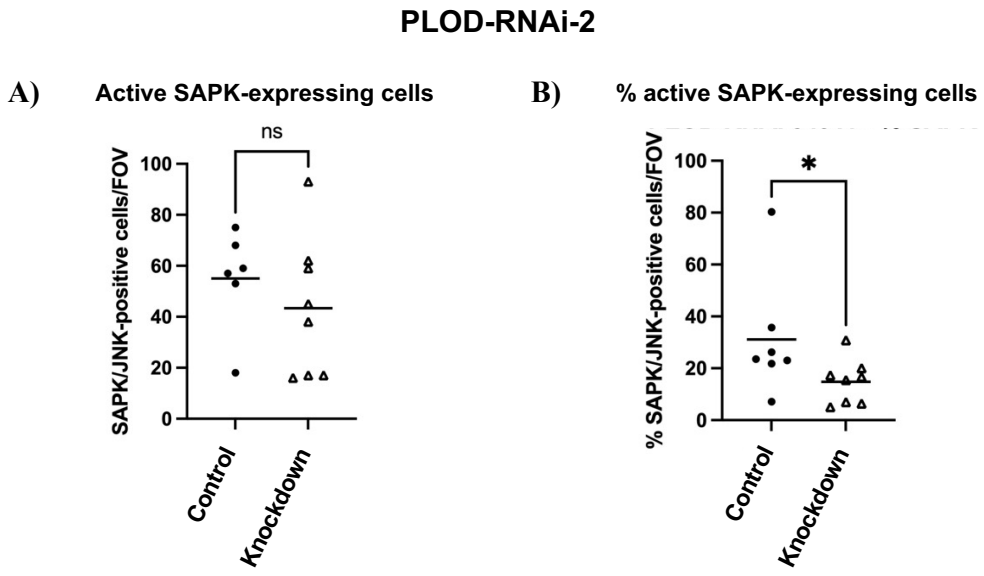

Figure 4.39. Active SAPK expression is reduced with *PLOD-RNAi-2* knockdown. Knockdown of PLOD (*5961^{GS} > PLOD-RNAi-2*) decreases the number of SAPK-positive cells observed per field of view but this change is not statistically significant (p = 0.3) (control n = 6, KD n = 8) (***A***). However, the proportion of active SAPK-positive cells normalized to total cell number is significantly decreased compared to control guts (p = 0.02) (control n = 7, KD n = 8) (***B***). Unpaired t-tests were used for normally distributed data (A), and non-parametric Mann Whitney-U tests for non-normally distributed data (B) . Each data point represents a gut.

Lastly, immunofluorescence analysis of *PLOD RNAi-3* female guts showed no significant changes in MAPK (*Figures 4.40 and 4.41*), SMAD (*Figures 4.42 and 4.43*) or SAPK/JNK staining (*Figures 4.44 and 4.45*) compared to controls. Both MAPK and SAPK presented the bimodal distribution explained above, where the data are clearly arranged in 2 groups of varying antibody expression. Thus, the lack of significance of these immunofluorescence results could be due to this particular distribution of the data.

Taken together, the immunofluorescence data shown here suggests that PLOD might be upstream of Ras/MAPK, SMAD/ TGF-β, and JNK signaling, and that it perhaps acts as a positive regulator of SMAD/ TGF-β, and a potential negative regulator of Ras/MAPK, at least in ISCs and EBs in the tissue. However, the variability between the controls and the high levels of active MAPK expression observed in the control midguts could be affecting the phenotypes observed in PLOD knockdown samples.

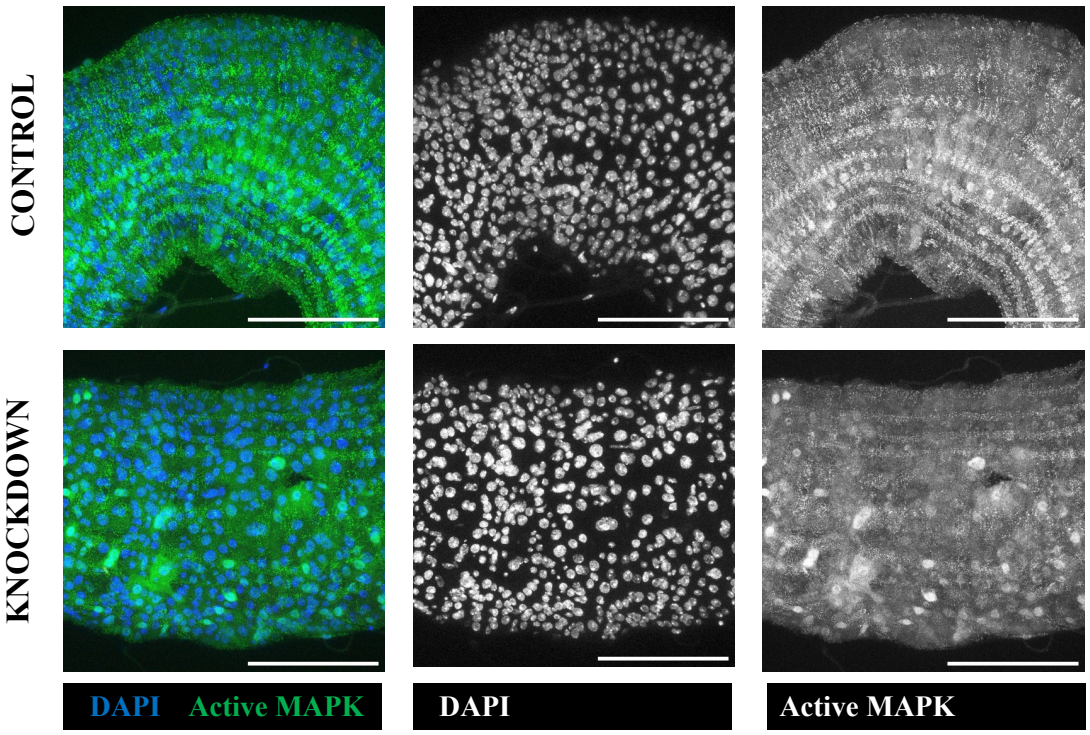

Figure 4.40. The expression of active MAPK in *PLOD-RNAi-3* knockdown guts. Knockdown of PLOD (*5961^{GS} > PLOD-RNAi-3*) does not affect the number of active MAPK-positive cells in the posterior midgut. Guts were stained with α- phospho-p44/42 MAPK (Erk1/2) (1:200) and DAPI. Scale bars in the bottom right corner represent 100μm.

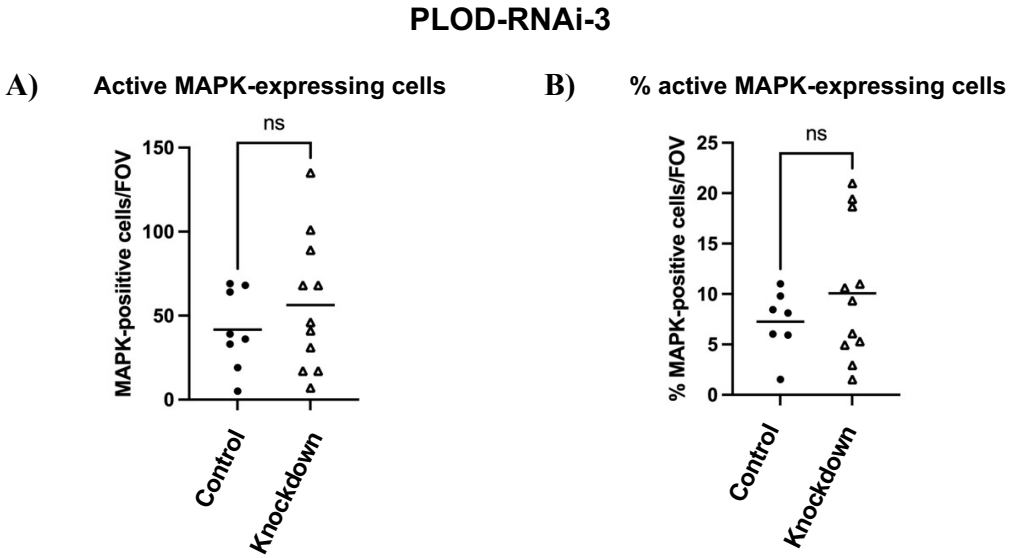

Figure 4.41. Active MAPK expression increases with *PLOD-RNAi-3* knockdown. Knockdown of PLOD (*5961^{GS} > PLOD-RNAi-3*) increases the levels of active MAPK expression in PLOD-knockdown guts compared to controls (p = 0.3) (control n = 8, OE n = 11) (*A*), as well as the proportion of active MAPK-positive cells normalized to total cell number (p = 0.3) (control n = 7, OE n = 11) (*B*), but both these trends are not statistically significant. All data was normally distributed, so unpaired t-tests were used for statistical analysis. Each data point represents a gut.

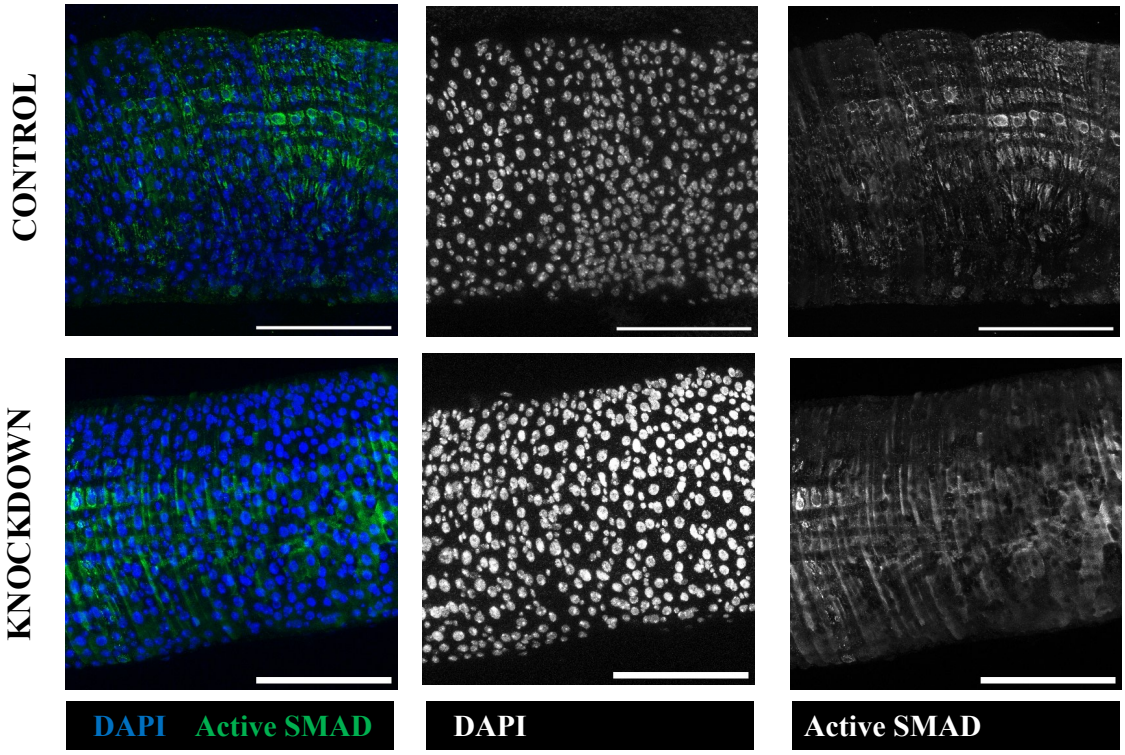

Figure 4.42. The expression of active SMAD in *PLOD-RNAi-3* knockdown guts. Knockdown of PLOD (*5961^{GS} > PLOD-RNAi-3*) does not change active SMAD expression in the posterior midgut. Guts were stained with α- phospho-Smad3 (1:100) and DAPI. Scale bars in the bottom right corner represent 100μm.

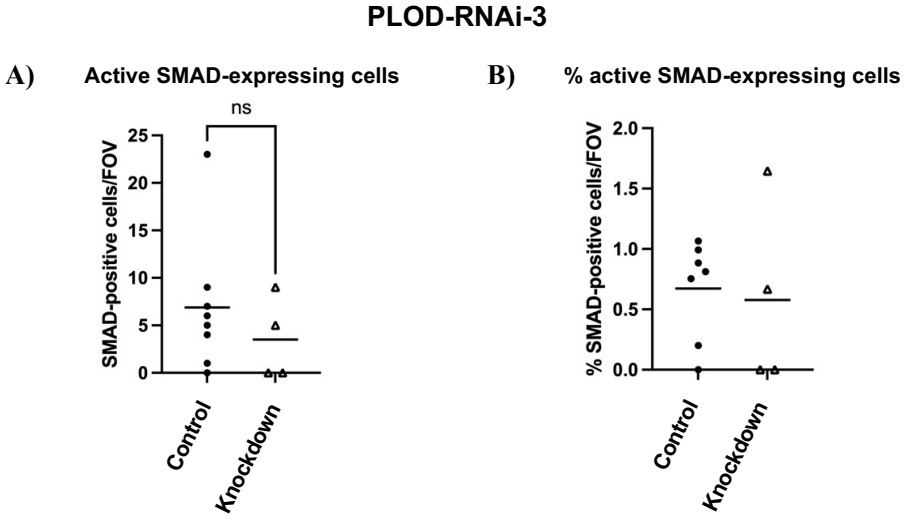

Figure 4.43. Active SMAD expression does not change with *PLOD-RNAi-3* knockdown. Knockdown of PLOD (*5961^{GS} > PLOD-RNAi-3*) decreases the number of SMAD-positive cells observed per field of view (***A***), and the proportion of active SMAD-positive cells normalized to total cell number (***B***) but these changes are not statistically significant (control n =7, KD n = 4). All data was normally distributed, so unpaired t-tests were used for statistical analysis. Each data point represents a gut.

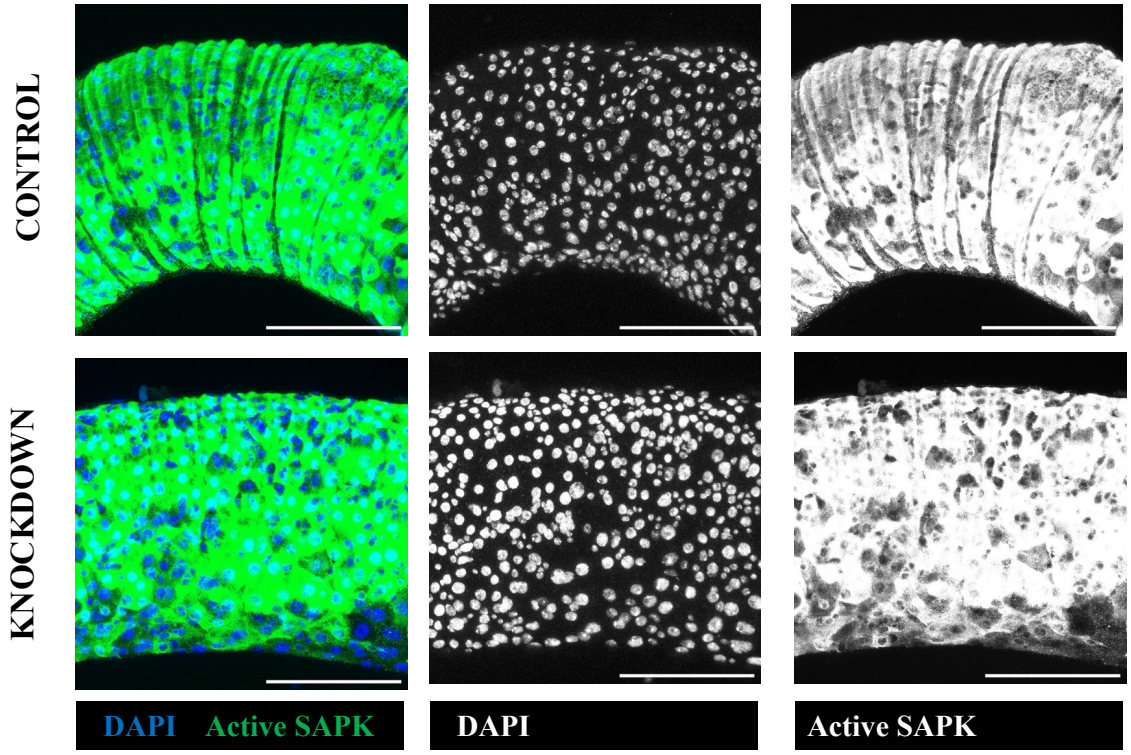

Figure 4.44. The expression of active SAPK in *PLOD-RNAi-3* knockdown guts. Knockdown of PLOD (*5961^{GS} > PLOD-RNAi-3)* increases active SAPK expression in control midguts. Guts were stained with α- phospho-SAPK/JNK (1:100) and DAPI. Scale bars in the bottom right corner represent 100μm.

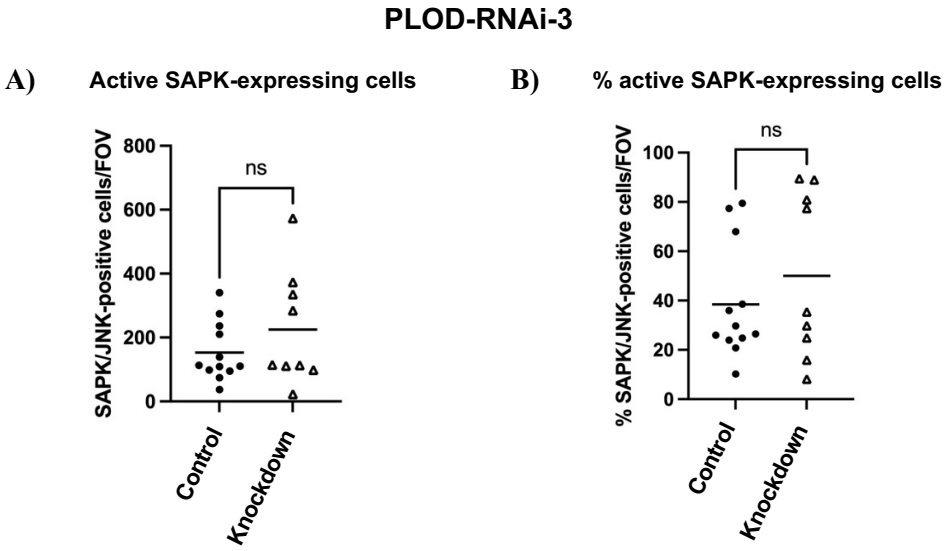

Figure 4.45. Active SAPK expression is increased with *PLOD-RNAi-3* knockdown. Knockdown of PLOD (*5961^{GS} > PLOD-RNAi-3*) increases the number of SAPK-positive cells observed per field of view (control n = 12, KD n = 9) (***A***) as well as the proportion of active SAPK-positive cells normalized to total cell number (control n = 12, KD n = 9) (***B***), but neither of these changes is statistically significant (p = 0.2, and p = 0.4, respectively). Unpaired t-tests were used for normally distributed data (A), and non-parametric Mann Whitney-U tests for non-normally distributed data (B) . Each data point represents a gut.

Since the Gene Switch driver only knocks down PLOD in stem and progenitor cells, and the immunofluorescence data presented here showed varying results between the different RNAi lines, full gut PLOD knockdown samples of PLOD RNAi lines 1 and 3 using the temperature-sensitive *tub-Gal80^{ts}; tub-Gal4* driver were analysed using RT-qPCR. The primers tested against these PLOD knockdown samples were widely-studied and well-characterized targets of some of the key pathways in development, and included: Soc36e, a negative regulator of JAK/STAT signaling; m3, m5, m8 and Mβ, E(spl) proteins regulated by Notch signaling; puc, a target gene of JNK; pnt, a transcription factor target of receptor-tyrosine kinase (RTK) Ras/MAPK signalling; and brk and dad, which are targets and negative regulators of Dpp signaling in *Drosophila*. All these genes have been widely referenced in the literature as known regulators of their respective signaling pathways, but it should be noted that there may be crosstalk in their regulation and variability between tissues. It is worth noting that due to sample and time constraints, there are only two replicates available for these RT-qPCR experiments and thus statistical analysis is not available to draw reliable conclusions.

tub-Gal80^{ts}; tub-Gal4 > UAS PLOD RNAi-1 showed a decrease in all 4 of the Notch targets m3, m5, m8 and mβ. In particular, the decrease in m3 as results of PLOD knockdown was stricking compared to control samples. Soc36e, pnt and dad also showed a decrease, whereas puc and brk levels were upregulated upon PLOD knockdown (*Figure 4.46*).

tub-Gal80^{ts}; tub-Gal4 > UAS-PLOD RNAi-3 showed opposite results. M3 was upregulated but the other 3 Notch receptors, m5, m8 and mβ were downregulated upon PLOD knockdown. This downregulation is consistent with the results showed in *PLOD-RNAi-1*. Soc36e, puc, pnt, brk and dad were also all upregulated in knockdown guts but the clear disparity between the two samples analyzed here makes it difficult to draw conclusions from this data (*Figure 4.47*).

In summary, these results suggest that PLOD could be an upstream regulator of Notch activity, but further studies are needed to determine if it is a positive or negative regulator of Notch. Results from the knockdown of RNAi line 3 suggest that PLOD could be a negative regulator of JAK/STAT, JNK and Ras/MAPK signalling but the disparities between RNAi lines 2 and 3 and the low number of replicates prevent any definitive conclusions from being drawn from this data set.

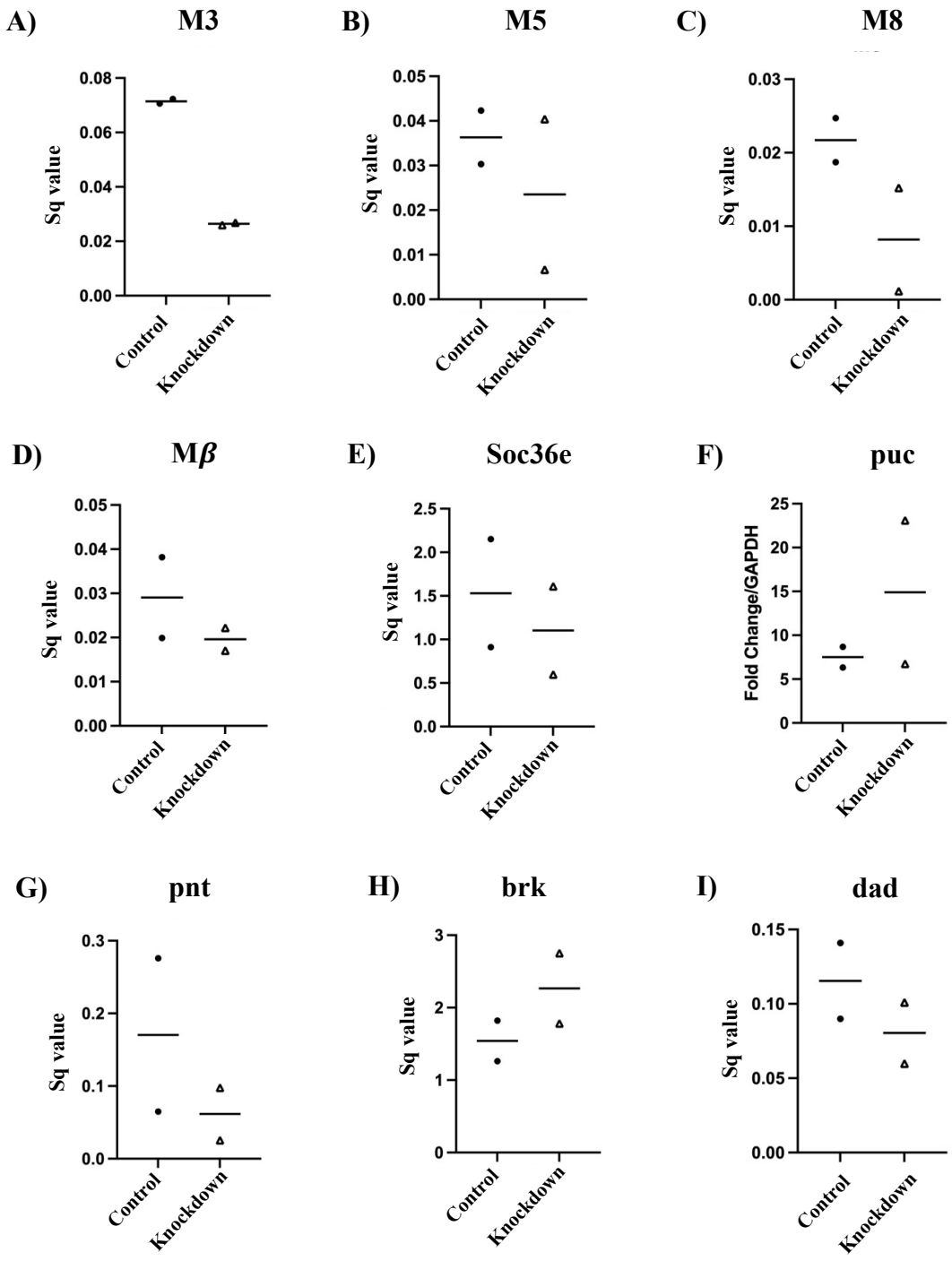

Figure 4.46. Expression changes of known targets of the major regulatory signaling pathways in *PLOD-RNAi-1* knockdown in whole guts. qPCR analysis of the expression levels of known pathway targets of Notch, JAK/STAT, JNK, MAPK/RTK and Dpp signaling showed that knockdown of PLOD (*TubGal80^{TS} > PLOD-RNAi-1*) decreases the expression levels of M3 (***A***), M5 (***B***), M8 (***C***), Mβ (***D***), Soc36e (***E***), pnt (***G***), and dad levels (***I***). Puc (***F***), and brk (***H***) levels show an increasing trend in knockdown guts compared to controls. n = 2 for all samples and thus no statistical analysis was carried out. Expression has been normalized to a housekeeping gene (GADPH/α-tubulin). Expression changes have been calculated using Sq values. Each data point represents one sample and each sample contains 10 whole female guts.

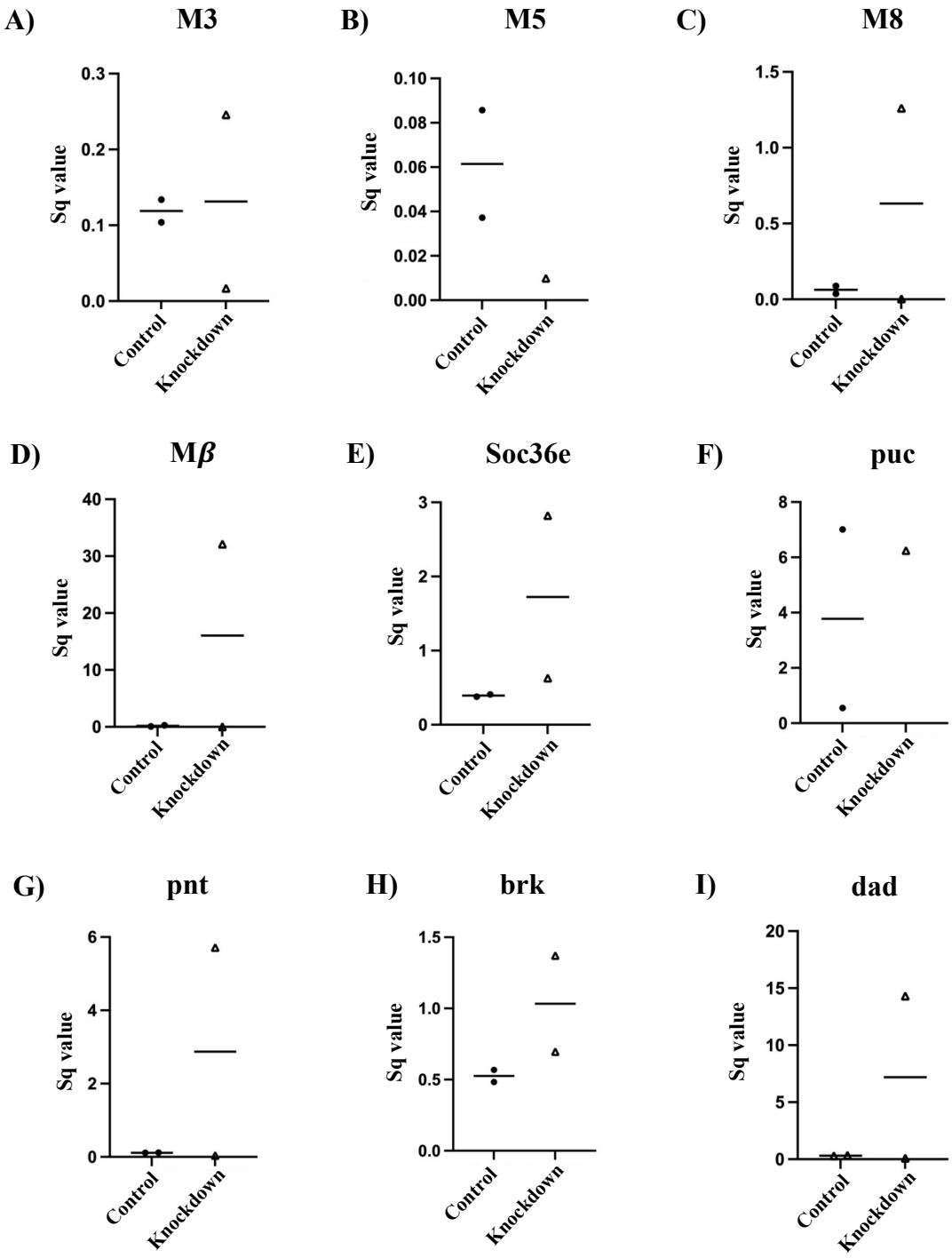

Figure 4.47. Expression changes of known targets of the major regulatory signaling pathways in *PLOD-RNAi-3* knockdown in whole guts. qPCR analysis of the expression levels of known pathway targets of Notch, JAK/STAT, JNK, MAPK/RTK and Dpp signaling showed that knockdown of PLOD (*TubGal80^{TS} > PLOD-RNAi-3*) increases the expression levels of M8 (***C***), Mβ (***D***), Soc36e (***E***), puc (***F***), pnt (***G***), brk (***H***) and dad levels (***I***). M5 (***B***) levels show an decreasing trend in knockdown guts compared to controls, and M3 (***A***) remains unchanged. n = 2 for all samples and thus no statistical analysis was carried out. Expression has been normalized to a housekeeping gene (GADPH/α-tubulin). Expression changes have been calculated using Sq values. Each data point represents one sample and each sample contains 10 whole female guts.

4.4. Discussion

In this chapter, the data presented show that PLOD plays a significant role in the regulation of intestinal stem cell homeostasis in the *Drosophila* midgut. Knockdown of PLOD leads to a significant increase in the number of cells in the gut and a decrease in EE cells, suggesting that PLOD could act to control EE differentiation in the posterior midgut, and in cases were there is a deficiency in PLOD, EC differentiation is favoured over EEs. However, this hypothesis is not consistent between RNAi lines, and thus the only firm conclusion that can be drawn about the effects of PLOD knockdown on tissue homeostasis is that it controls imbalances of differentiation in the midgut epithelium. PLOD does not have an effect on the proliferation of ISCs, but rather works to maintain a balance in ISC differentiation. Moreover, loss of PLOD leads to a loss of distribution of cells in the posterior midgut, which potentially leads to a decrease in lifespan, but further work is needed to characterize both of these phenotypes in detail. Consistently with preliminary work from our group, PLOD has been shown to be expressed in a subset of ISC and EB cells, although some data suggests that perhaps a small population of ECs could also express the protein. This expression pattern fits in with that described for collagen, as observed using a vkg Gal4 CRIMIC line, where both vkg and PLOD are expressed in the stem and progenitor cells of the tissue. This explains the changes in collagen expression observed after the manipulation in PLOD, although statistical analysis did not deem these significant. PLOD is proposed to be upstream of the Ras/MAPK, SMAD/ TGF-β, and JNK signaling cascades, but further work is needed to determine the exact role it plays in the regulation of each of these pathways. Preliminary data from qRT-PCR analysis also suggests PLOD might be found upstream of Notch, Dpp and JAK/STAT signaling.

4.4.1. The effects of PLOD misregulation in different tissues and its regulatory mechanisms

As mentioned in the introduction of this chapter, there is a significant gap in the literature regarding the role of PLOD in the *Drosophila* intestine, and most of the published literature focuses on the roles of mammalian PLOD molecules in cancer development. Therefore, the comparison between the data presented here and that found in published literature is limited. Moreover, the increased complexity of the mammalian

systems and the presence of the three orthologs makes this comparison even harder. The data presented here suggests that misregulation of PLOD affects the homeostasis of the *Drosophila* gut by altering ISC differentiation.

Despite the lack of evidence for the role of PLOD in ISC regulation in the fly intestine, there is a consensus that mammalian PLODs regulate the acquisition of stem cell phenotypes in epithelial cancer development and maintenance of cancer stem cells in tumours. The extrapolation of these conclusions and comparison to the fly model, and the results presented in this chapter could lead to the hypothesis that, in the *Drosophila* midgut, PLOD is expressed in the stem and progenitor cells of the tissue and acts to maintain their stem cell properties. The function of PLOD as a regulator of stem cell properties could explain the changes observed in our data that show pronounced shifts in differentiated cells of the tissue when PLOD levels are reduced. Therefore, downregulation of PLOD levels could lead to stem cell misregulation in the fly intestinal tissue, loss of homeostasis and changes in proliferation. We reported the importance of Ras/MAPK, SMAD and TGF-β signaling in the regulation of PLOD expression, which is consistent with published literature (Gjaltema et al., 2015; Yang et al., 2020). However, these papers suggest that the mammalian ortholog PLOD2 is downstream of TGF-β1 signaling, whereas the data presented here suggest PLOD is found upstream, as manipulation of PLOD results in changes to SMAD expression. Moreover, the results presented here were highly variable between RNAi lines and experimental approaches, i.e. immunofluorescence versus qRT-PCR, and thus further in-depth analyses are needed to elucidate the specific roles of these signaling cascades in the regulation of PLOD expression in the fly midgut.

To my knowledge, no published data has explored the effect of PLOD knockdown or overexpression on the lifespan of *Drosophila melanogaster*. The extensive evidence in the literature that demonstrates PLOD overexpression promotes tumour development and correlates with the invasive capabilities of tumour cells, prompts the hypothesis that overexpression of PLOD in the *Drosophila* gut would have a negative impact on lifespan, whereas knockdown of this potentially oncogenic molecule would increase lifespan with age by preventing or slowing down cancer progression. Evidence in the literature has already shown that the reduction of all three mammalian PLODs (PLOD1-3) is able to reduce tumour progression in bladder, colorectal and renal cancer, respectively (Yamada et al., 2021; Song et al., 2022; Chen et al., 2023). The results obtained from the initial replicates of the lifespan experiments presented in this chapter would fit with this

hypothesis, where, later in life, reduced levels of PLOD in the tissue lead to a significant increase in fly survival. Although these results were consistent among all RNAi lines, they were not replicated in the second set of lifespan experiments, which found no change between control and knockdown guts. Thus, further replicates of this are needed to draw conclusive answers to the effect of PLOD changes in survival. Since these experiments exclusively knocked down PLOD in stem and progenitor cells in the gut, future work should focus on elucidating what changes are induced when PLOD is knocked down specifically in the differentiated cells of the tissue, through the use of specific driver lines, e.g. prosGal4TS to induce PLOD knockdown in EE cells. The comparison between these, and full gut knockdown of PLOD would provide a clear picture of which cells are the main source of PLOD expression in the *Drosophila* gut. Initial attempts to characterize changes to PLOD expression with age were carried out as part of this project, where 10-day-old (young) and 30-day-old (old) female fly guts were dissected and stained with α-PLOD antibody, as well as with the EE-marker prospero, to quantify changes in PLOD expression with age. However, these experiments did not yield any meaningful data, as the PLOD antibody staining was very weak. Future work should focus on optimizing this experimental approach to better understand any age-related changes to PLOD expression that could be affecting the mortality rates of the fly.

4.4.2. The effect of PLOD on collagen deposition in the basement membrane

The relationship between PLOD and collagen is so interlinked that mutations or changes to the expression of either protein have pleiotropic phenotypes (Bunt et al., 2011), i.e. that mutations or misregulation of either PLOD or collagen have overlapping effects.

Correct deposition of collagen IV in the ECM is necessary for the recruitment of other ECM molecules such as laminins, nidogen and perlecan (Wilmes et al., 2018). In vitro analysis of PLOD revealed that this protein is regulated by tumour-necrosis factor-alpha (TNF-α): this cytokine induces the expression of MMP3, which in turn enhances PLOD expression (Ah-Kim et al., 1999). Moreover, TNF-α expression increases collagenase activity in a variety of cell types and inhibits bone formation (reviewed by Larrick and Kunkel, 1988) by reducing the rates of collagen biosynthesis (Bertolini et al., 1986). This is consistent with the trends observed here between PLOD knockdown in ISC/EB cells in the *Drosophila* gut and vkg expression: results presented in this chapter showed that a reduction in PLOD levels resulted in increased collagen staining in the

posterior midgut. In other words, PLOD could be a regulator of collagenase activity in the fly gut, where reduced levels of PLOD leads to decreased rates of collagen breakdown, thus explaining why PLOD knockdown leads to increased collagen levels in the *Drosophila* intestinal tissue.

Electron microscopy analysis of the basement membrane in *Drosophila* epithelial tissue reported that BM thickness is around 100nm (Isabella and Horne-Badovinac, 2015), although a recent review records varying BM thickness depending on the tissue (Ramos-Lewis and Page-McCaw, 2019). These thin sheets are made up of collagen IV fibers, laminins, nidogen and the HSPG perlecan (Pozzi et al., 2017) that form an extensive network with associated accessory proteins that have the ability to alter the biochemical and structural properties of the BM (reviewed by Isabella and Horne-Badivinac, 2015). The expression of all four key BM components is independent of one another, and their contribution to the regulation of the mechanical properties of the BM differs between them (Töpfer et al. 2022)

The simplicity of the *Drosophila* BM proteins compared to their mammalian counterparts, as well as the reduction in protein diversity and redundancy in the fly, makes *Drosophila* a wonderful model to study basement membrane formation and the function of its individual components. As part of the troubleshooting process of the preparation of transmission electron microscopy (TEM) samples to analyse the effects of PLOD knockdown on basement membrane integrity, wild-type CantonS female guts were dissected and analysed. From the data obtained (not shown), quantification of BM thickness under the different cell types (ISCs vs ECs) revealed no significant difference in the thickness of the basement membrane underlying these two different cell types. The BM of ISCs had a mean thickness of 305nm, whereas EC BM was slightly thinner at an average of 285nm. Out of the four main components of BMs in *Drosophila* epithelial tissues, collagen IV is the main contributor to basement membrane stiffness and the regulation of its mechanical properties (Töpfer et al., 2022), and thus alterations in its structure as a result of changes to PLOD expression should have a prominent effect on BM thickness. Ongoing analysis is in the process of determine changes to BM thickness in PLOD (and SPARC) knockdown guts compared to WT samples to determine the effect of PLOD in the maintenance of BM integrity. This will contribute to characterize the relationship between PLOD and collagen IV in the BM of the gut epithelium, and the potential contribution of actin to this process. The actin cytoskeleton is also responsible

for collagen production in vitro (Qin et al., 2017), suggesting that PLOD and actin work in tandem to ensure the correct deposition of collagen in the BM of the *Drosophila* gut.

4.4.3. The implication of PLOD in signalling and consequences of its misregulation

As previously stated, most of the literature published on PLOD focuses on its roles during mammalian tumour development and the regulator pathways that control PLOD expression in the context of cancer, complicating the comparison of published results with the data sets presented here. Moreover, the increased complexity of the mammalian model systems and the presence of multiple orthologs compared to the fly model organism make this understanding of our results within the framework of published literature even harder.

Overall, all three mammalian PLOD molecules carry out slightly different functions and therefore play different roles in tumour progression. PLOD1 is upregulated in bladder cancer, where high levels of the enzyme are associated with poor prognosis compared to bladder cancer samples with low PLOD1 expression (Yamada et al., 2021). Moreover, silencing PLOD1 expression in these samples significantly reduced the proliferative and invasive abilities of the cancer cells, and the use of a PLOD1 inhibitor significantly increased the number of apoptotic cells in the tumour and led to cell-cycle arrest of malignant cells (Yamada et al., 2021). Expression of PLOD2 is triggered under hypoxic conditions, specifically regulated by hypoxia-inducible factor 1α (HIF-1α) (Qi and Xu, 2018). Gong et al. hypothesized that this relationship between hypoxia and PLOD2 might regulate the epithelial to mesenchymal transition (EMT) and perhaps the maintenance of cancer-stem cells (CSCs). TGF-β1 induces expression of PLOD2 in cervical cancer, where PLOD2 expression triggers migration and invasion of cancer cells (Qi and Xu, 2018). The relationship between PLOD2 and TGF-β1 signaling seems to be mediated by the transcription factors SMAD3 and SP1 (Gjaltema et al., 2015; Yang et al., 2020). This relationship between TGF-β and PLOD expression through SMAD is consistent with the immunofluorescence data presented in this chapter, where changes to expression levels of PLOD affect active SMAD in the cells of the posterior midgut. PLOD2 expression was significantly upregulated in cancer-associated fibroblast (CAFs) and silencing its expression significantly reduced the tumour phenotype (Qi and Xu, 2018). Knockdown of PLOD2 reduced proliferation, migration and the invasive potential of colorectal cancer cells through integrin B1-activation of IL-6/STAT3 signaling (Song

et al., 2022). These results suggests that PLOD acts as a tumour suppressor in this context, as its downregulation reduces the invasive capabilities of the tumour. This is consistent with the preliminary lifespan data shown here, where knockdown of PLOD seems to increase the lifespan of the fly. However, the lack of reproducibility and consistency between the first and second replicates of these lifespans prevents any firm conclusions from being drawn from this data set.

PLOD2 overexpression has been proposed to increase the expression of stem cell makers in the surface of laryngeal cancer cells, thus promoting the acquisition of stem cell phenotypes (Song et al. 2022). Baek et al. demonstrated that PLOD3 is able to interact with STAT3 to suppress immune signals in lung cancer, which causes a dysregulation of the Ras/MAPK signaling cascade and promotes metastasis in this tumour type (Baek et al., 2018). Notch signaling has also been shown to regulate PLOD3 expression (Shi et al., 2021). The results presented here that suggest a potential role of *Drosophila* PLOD in the regulation of Ras/MAPK and Notch signaling in the context of the *Drosophila* gut are consistent with these data. Interestingly, PLOD3 is found bound to the cellular membrane and exists in homodimeric form (Chen et al., 2023). This extracellular localization of PLOD3 has led to hypothesis that propose that PLOD3 could modify proteins in the ECM, besides collagen, and therefore control ECM remodelling (Knippenberg et al. 2007). This fits in with the hypothesis suggested here that PLOD and actin could be working together to control collagen IV deposition and distribution in the BM of the gut epithelium in the fly, as PLOD knockdown seems to decrease the intensity of stained F-actin in the posterior midgut.

4.5. Conclusions

As mentioned, there is a lack of evidence in the literature regarding the specific role of *Drosophila* PLOD in the regulation of intestinal stem cells and its effect on gut tissue homeostasis. Most of the studies employ in vitro mammalian models and exclusively focus on the function of PLOD in disease development, mostly during the different stages of tumour development. The existence of 3 orthologs in mammals compared to the single gene in *Drosophila* complicates the comparison between the data even further. In this chapter, we have demonstrated that knocking down PLOD in the ISC and EBs in the *Drosophila* gut leads to a loss of homeostasis in the tissue, that manifests in changes to the cellular composition of the posterior midgut, the distribution of cells

within this area of the gut tissue and the levels of collagen expressed. Moreover, data presented here corroborate the preliminary work that this project is based on that identified PLOD as being specifically secreted by the stem and progenitor cells in the tissue. Using a variety of experimental approaches, the data presented here demonstrate that PLOD is expressed in the ISCs and EBs in the posterior midgut, although further work is necessary to firmly conclude this. Future experiments should focus on further characterizing the expression pattern of the protein and determining if its expression is exclusive to stem and progenitor cells or if, at some point during ageing, the distribution of PLOD changes to be expressed in the differentiated cells of the tissue. Furthermore, the concrete relationship between changes to PLOD expression and collagen levels in the midgut should be explored, through the generation of genetic engineering tools that allow for the simultaneous manipulation of both genes within the same background in combination with molecular biology approaches. The results presented here suggest a potential epithelial source of collagen which is dependent on PLOD and which is independent on the collagen produced by the visceral muscle. Lastly, PLOD is proposed to regulate a range of signaling pathways in the fly gut, including Ras/MAPK, TGF-β (through the SMAD proteins), and Notch, which is consistent with the data reported in the literature in other tissues and organisms. Taken together, all these results strongly suggest that PLOD plays a role in the maintenance of gut homeostasis in the *Drosophila* gut and contributes to the maintenance of the stem cell niche in this tissue.

Chapter 5

TIMP as a regulator of intestinal stem cell homeostasis

5.1. Introduction

Matrix metalloproteinases (MMPs) are proteins that play fundamental roles in the degradation of the ECM, which is essential at different states of development, morphogenesis and tissue remodelling (reviewed by Nagase and Woessner, 1999). Their activity and the controlled degradation of the ECM is regulated, among other cytokines and inhibitors, by tissue inhibitors of metalloproteinases (TIMPs), which act as the key local regulators of MMP activity in the tissue (Brew et al., 2000; Visse and Nagase, 2003). MMPs can degrade key ECM components such as collagen fibers and laminins, and contribute to the tissue-specific special features of the ECM, as well as to cell migration and growth factor release (Hughes et al., 2020).

Drosophila melanogaster has two MMP genes (Mmp1 and Mmp2) and a singular TIMP gene (Wen et al., 2020), compared to the four TIMP family members (TIMP1-4) and the 28 different MMPs that have been identified in mammals (Laronha and Caldeira, 2020). The functions, structure and biochemical properties of mammalian MMPs vary between family members, with the percentage similarity of their protein sequence ranging from just 33% to 86% (Laronha and Caldeira, 2020), but there is an overlap in TIMP

function between isoforms (Murphy, 2011). Mammalian TIMP-2, -3 and -4 have the highest sequence similarity between then, about 45-50%, whereas TIMP-1 only shares around 40% of residues with the other family members (Brew, 2019). In terms of protein evolution, TIMP-1 and -3 have an earlier evolutionary origin than TIMP-2 and TIMP-4, and evidence suggests TIMP-1 is the most evolutionary conserved out of the 4 mammalian proteins (reviewed in Murphy, 2011).

Inhibition of MMP activity by TIMPs occurs through their N-terminal domain, which folds indepently and forms its own separate unit within the structure of the protein (Visse and Nagasse, 2003). Mammalian MMP-1, -8 and -13 are also known as collagenases, which digest fibrillar collagens, and MMP2, a gelatinase, degrades, among other ECM molecules, collagen IV fibers (Shiomi et al., 2010).

Drosophila TIMP was the first invertebrate homolog identified, and clonal analysis revealed it only presents a 35% identity to human TIMPs (Pohar et al., 1999). Moreover, the structure of *Drosophila* TIMP and its organization within its genetic locus is conserved between flies and humans (Pohar et al., 1999). Phylogenetic tree analysis has revealed a close relationship between *Drosophila* TIMP and the mammalian ortholog TIMP2 (Wen et al., 2020). The N-terminal domain of *Drosophila* TIMP resembles the mammalian TIMP3 N terminal domain (Wei et al., 2003), in both sequence conservation and functional properties (Murphy, 2011). *Drosophila* TIMP has the ability to inhibit both fly MMP molecules (Wen et al., 2020) which carry out complementary roles (Hughes et al., 2020) and resemble mammalian membrane-tethered MMPs (Llano et al., 2002). *Drosophila* MMP1 and MMP2 have distinct, but overlapping and complementary, roles in tissue remodelling (Wen et al., 2020). Moreover, both of these proteins have been shown to exist in membrane-tethered and soluble forms, but the substrates of each of these *Drosophila* MMP forms vary among them (LaFever et al., 2017). In-depth studies of TIMP functions have revealed that they carry out a wider set of functions than previously considered. Initially, the role of TIMPs was restricted to the protease inhibitor function over MMPs, but further characterization of the enzyme has shown that it has additional roles pertaining to the regulation of cell growth, cell migration and apoptosis, by controlling the activity of certain cell surface receptors (reviewed by Stetler-Stevenson, 2008). *Drosophila* TIMP has been shown to be involved in cell signaling pathways and in cellular adhesion (Godenschwege et al.., 2000). Moreover, TIMPs can interact with a range of matrisome components (reviewed by Peeney et al., 2023), i.e. ECM and ECM-related components (Naba et al., 2016). Reductions in MMPs in

Drosophila leads to the formation of protein aggregates in the ECM, modulating the biochemical properties of the matrix (Hughes et al., 2020).

Proteomics analysis has revealed the fundamental role of TIMP in the regulation of collagen IV levels in the ECM of the *Drosophila* ovary (Pearson et al., 2016). TIMP is selectively distributed in the *Drosophila* embryo, and it has been shown to have similar phenotypes to integrin mutants, suggesting a potential interaction between these two molecules (Godenschwege et al., 2000). This is consistent with other studies that have attributed cell signaling roles to TIMP. Among it many functions, TIMP is essential to maintain the germline stem cell niche in female flies (Pearson et al., 2016). MMPs have been described as a negative regulator of follicle stem cells in the *Drosophila* ovary, which antagonizes Wnt signaling in this tissue (Wang and Page-McCaw, 2014).

Disruption of the balance between MMP expression and TIMP activity can have detrimental effects on the tissue, with uncontrolled tissue turnover and degradation of the ECM leading to tumour development, fibrosis, cardiovascular and neurodegenerative diseases, and arthritis, among other conditions (Brew et al., 2000; Godenschwege et al., 2000). However, the exact role of TIMPs in disease development seems to be context- and tissue-dependent and still remains to be elucidated, as the different mammalian TIMPs have been shown to have antagonistic roles regarding the regulation of apoptosis: TIMP-3 is pro-apoptotic, whereas TIMP-1 and -2 inhibit cell death (reviewed in Visse and Nagase, 2003).

Besides MMPs, TIMPs have also been shown to inhibit another family of proteinases found in the extracellular matrix, a desintegrin and metalloproteinases (ADAM), which are heavily involved in cancer development and progression (Murphy, 2011). TIMP activity on ADAMs occurs thorugh their N-terminal domain, which is highly homologous to MMP N-terminal structure (reviewed by Shiomi et al., 2010).

5.2. Aims and objectives

Previous work from the Doupé group identified TIMP as a protein specifically expressed by the stem and progenitor cells of the tissue (Doupé et al., 2018). Initial characterization of the expression of this protein and the effects of its misregulation in the *Drosophila* midgut suggested a role in the maintenance of tissue homeostasis (Sutherland, unpublished). The aim of this project is to further characterize the roles of TIMP in the

Drosophila midgut, and to establish an expression pattern and a regulatory mechanism for TIMP in this tissue. Moreover, this project aimed to establish if these findings were conserved in mammalian systems (see Chapter 8).

5.3. Results

5.3.1. The effects of TIMP overexpression on the posterior midgut of the fly

As mentioned above, work from the group attempted to elucidate the function of TIMP in stem and progenitor cell homeostasis in the *Drosophila* midgut, and evidence from this demonstrated that this protein plays a role in maintaining tissue homeostasis in the fruit fly intestinal tissue (Sutherland, unpublished). In order to study this further, initial immunofluorescence experiments carried out as part of this PhD project focused on the effect of the overexpression and knockdown of this protein in ISCs and EBs using the Gene Switch driver. Two TIMP overexpression lines (*5961^{GS} > UAS-TIMP 58707* and *5961^{GS} > UAS-TIMP 58708*) were compared and yielded similar results. These lines will be referred to as UAS-TIMP line 1 and line 2, respectively, from here onwards.

Overexpression of TIMP with *UAS-TIMP-1* (*Figure 5.1*) did not show any significant changes in the total number of cells observed per field of view, gut width, area or density (*Figure 5.2*). Overexpression of TIMP using *UAS-TIMP-2* (*Figure 5.4*) led to a significant increase in the total number of cells in the gut (*Figure 5.5A*) but gut size, measured in terms of gut width and area observed per field of view (FOV) remained unchanged between control and TIMP-overexpression guts (*Figure 5.5B and C*). As expected, these two results together translated to an increase in cellular density in the midgut, as shown by quantification analysis, calculated by dividing the number of cells observed by the area per FOV (*Figure 5.5D*). This increase was deemed statistically significant. Next, we wanted to determine if this increase in cell number was due to an increase in the mitotic rates of the tissue, for which the number of PH3-positive cells in the whole gut was quantified. As previously mentioned, PH3 is a mitotic marker and labels cells that are undergoing division at the time of dissection. There was no significant increase in the number of mitoses per gut between control and *UAS-TIMP-1* overexpression guts (*Figure 5.3C*) (no data available for *UAS-TIMP-2*). In order to determine if overexpression of TIMP was affecting the differentiation of cells in the

midgut, cells were labelled with an EE-specific marker, prospero, and quantified. Overexpression of TIMP in both UAS-TIMP lines significantly increases the number of secretory enteroendocrine cells in the posterior midgut, both in terms of raw number observed per field of view and in the proportion of secretory cells normalized to the total cell number per FOV. This result was consistent across both overexpression lines used (*Figures 5.3 and 5.6*).

Taken together, these results suggest that increased levels of TIMP in the tissue do not affect the mitotic rates of the cells. This leads to an increase of cells in the tissue and therefore a higher cellular density. Moreover, overexpression of TIMP changes the cellular composition of the tissue, as demonstrated by the increase in the differentiated secretory enteroendocrine cells.

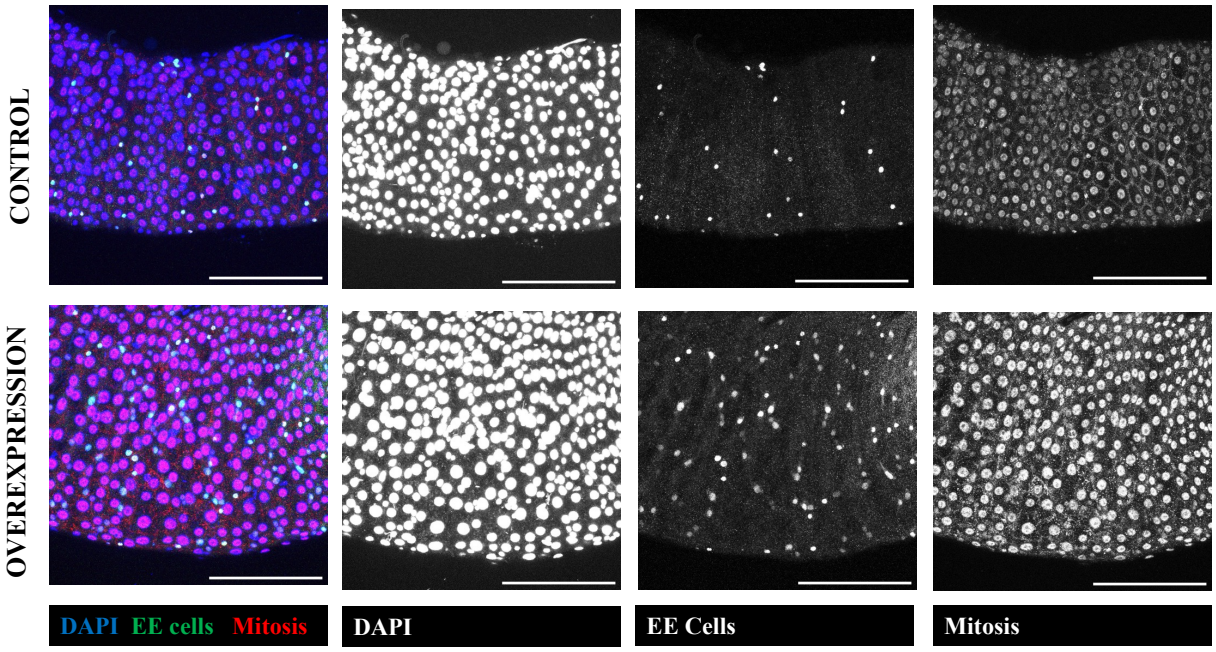

Figure 5.1. The effects of TIMP overexpression with *UAS-TIMP-1* in ISCs and EBs of the posterior midgut. Overexpression of TIMP (*5961^{GS}> UAS-TIMP-1*) seems to increase the width and area of the gut, as well as the number of EE cells observed per field of view in overexpression guts compared to controls. Guts were stained with α-prospero (1:100), α-PH3 (1:1000) and DAPI. Scale bars in the bottom right corner represent 100μm.

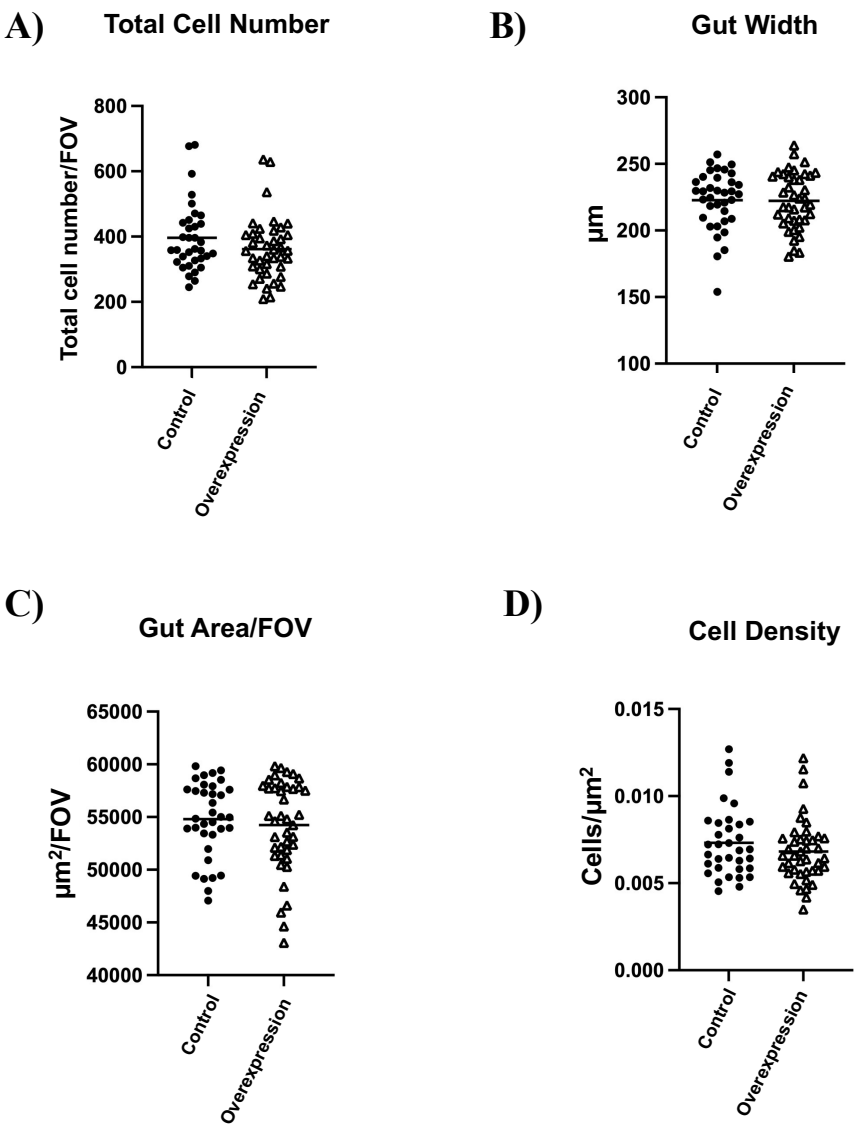

Figure 5.2. TIMP overexpression with *UAS-TIMP-1* does not significantly affect the posterior midgut. Overexpression of TIMP (*5961^{GS}> UAS-TIMP-1*) does not cause any significant changes to the total number of cells observed per FOV (control n = 34, OE n = 40) (***A***), gut width (control n = 36, OE n = 40) (***B***), gut/FOV) (control n = 35, OE n = 41) (***C***), or cell density (control n = 34, OE n = 41) (***D***). All data was not normally distributed, so non-parametric Mann Whitney-U tests were carried out for statistical analysis. Each data point represents a gut.

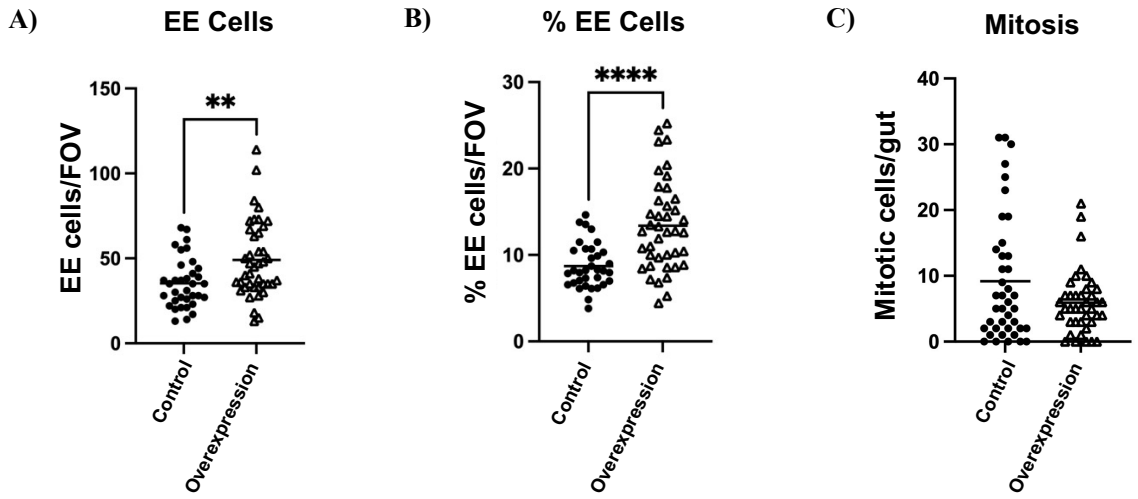

Figure 5.3. TIMP overexpression with *UAS-TIMP-1* significantly increases EE cells in the posterior midgut. Overexpression of TIMP (*5961^{GS} > UAS-TIMP-1*) significantly increases to the number of EE cells observed per FOV (p =0.003) (control n = 35, OE n = 41) (***A***), as well as the proportion of EE cells normalized to the total number of cells (p < 0.0001) (control n = 34, OE n = 41) (***B***). The number of mitoses observed across the whole gut are maintained between control and overexpression guts (control n = 40, OE n = 40) (***C***). Unpaired t-tests were used for normally distributed data (B), and non-parametric Mann Whitney-U tests for non-normally distributed data (A, C). Each data point represents a gut.

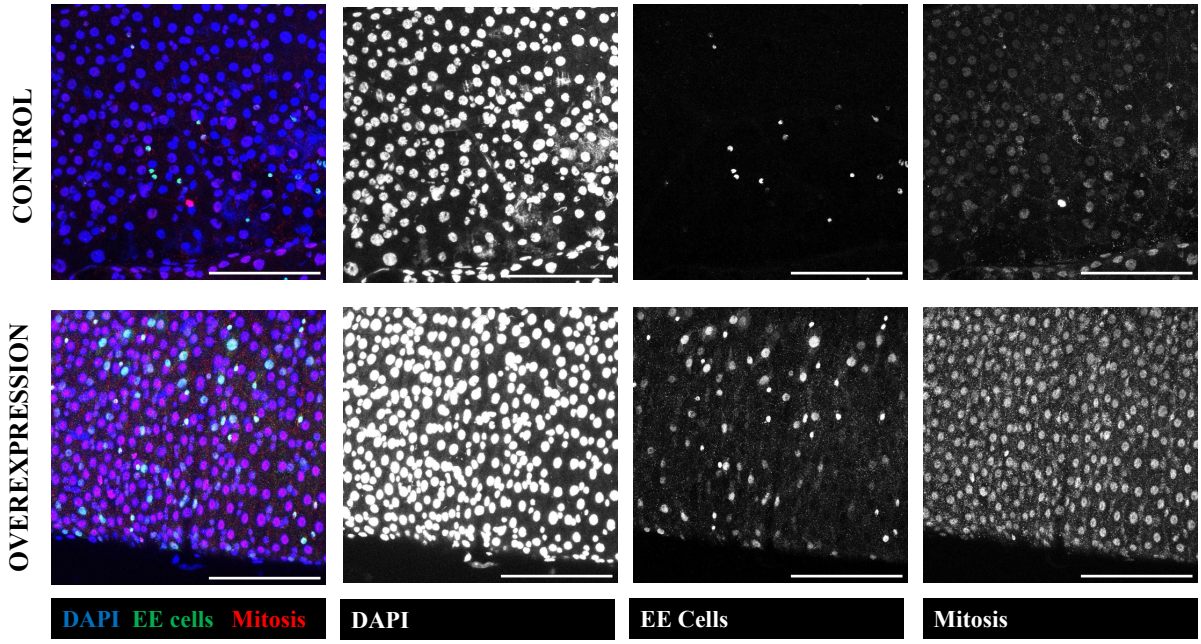

Figure 5.4. The effects of TIMP overexpression with *UAS-TIMP-2* in ISCs and EBs of the posterior midgut. Overexpression of TIMP (*5961^{GS} > UAS-TIMP-2*) seems to increase the number of EE cells in the posterior midgut compared to controls. Guts were stained with α-prospero (1:100), α-PH3 (1:1000) and DAPI. Scale bars in the bottom right corner represent 100μm.

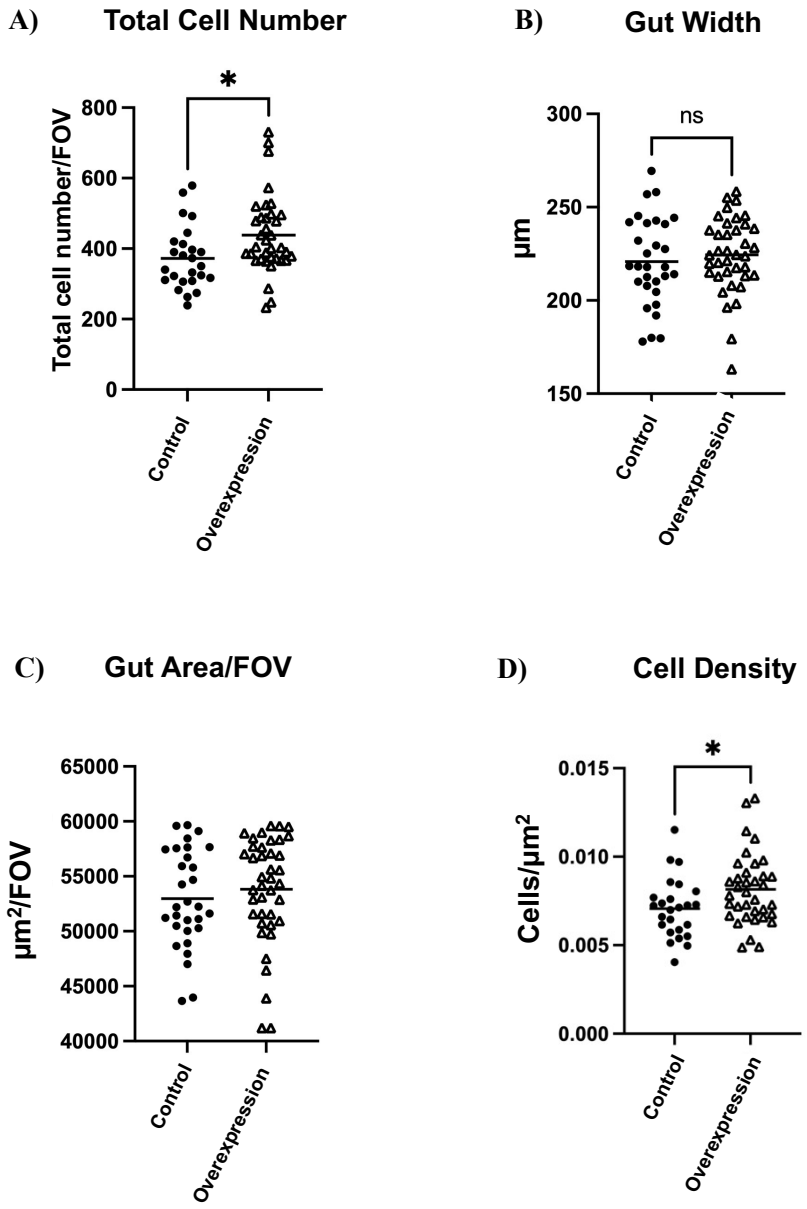

Figure 5.5. TIMP overexpression with *UAS-TIMP-2* significantly increases the total number of cells and cell density in the posterior midgut. Overexpression of TIMP (*5961^{GS}> UAS-TIMP-2*) significantly increases the total number of cells observed per FOV (p = 0.01) (control n = 25, OE n = 36) (***A***), and cell density (p = 0.02) (control n = 25, OE n = 36) (***D***). Gut width (control n = 30, OE n = 38) (***B***), and gut area/FOV (control n = 30, OE n = 40) (***C***) remain unchanged between control and overexpression guts Unpaired t-tests were used for normally distributed data (B, D), and non-parametric Mann Whitney-U tests for non-normally distributed data (A, C). Each data point represents a gut.

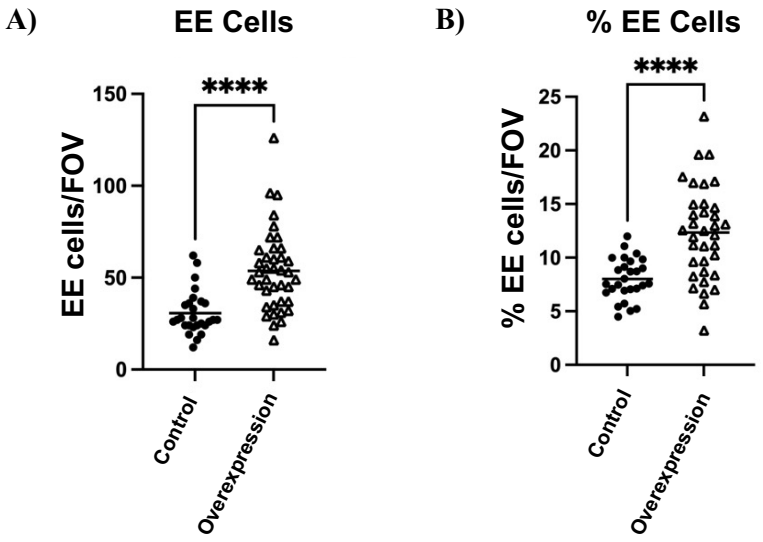

Figure 5.6. TIMP overexpression with *UAS-TIMP-2* significantly increases EE cells in the posterior midgut. Overexpression of TIMP (*5961^{GS}> UAS-TIMP-2*) significantly increases to the number of EE cells observed per FOV ($p < 0.0001$) (control n = 27, OE n = 39) (***A***), as well as the proportion of EE cells normalized to the total number of cells ($p < 0.0001$) (control n = 27, OE n = 35) (***B***). Unpaired t-tests were used for normally distributed data (B), and non-parametric Mann Whitney-U tests for non-normally distributed data (A). Each data point represents a gut.

5.3.2. The effects of TIMP knockdown in ISCs and EBs of the *Drosophila* midgut

The opposite experiment was also carried out, where TIMP was knocked down in the stem and progenitor cells of the gut, to see if this had antagonistic results to the overexpression data obtained. This was also studied using two different RNAi constructs to account for potential off-target effects different efficiencies of the knockdown. Both knockdown lines, *5961^{GS} > UAS-Timp RNAi 61294* (referred to as *TIMP-RNAi-1*) and *5961^{GS} > UAS-Timp RNAi 15372*, (referred to as *TIMP-RNAi-2*), yielded similar results with very little change (*Figures 5.7 and 5.10*). Knockdown of TIMP in ISCs/EBs did not cause any changes to the total number of cells observed per field of view, and although measurements of gut width and area/FOV were slightly increase in the knockdowns compared to controls, these changes were not statistically significant (*Figures 5.8 and 5.11*). Thus, cell density also remains unchanged. The number of enteroendocrine cells was maintained between knockdown and control guts (*Figures 5.9 and 5.12*), but interestingly, *TIMP-RNAi-2* showed a highly significant increase in the number of PH3-

positive cells in knockdown guts (*Figure 5.12C*), indicating that reduced levels of this protein may trigger an increase in ISC division across the entire *Drosophila* gut. Since this increase in proliferation does not correlate with a higher number of cells in the tissue, this raises the possibility that this increase in proliferation is matched by an increase in the cell death rate, thus maintaining a homeostatic balance of cells in the tissue.

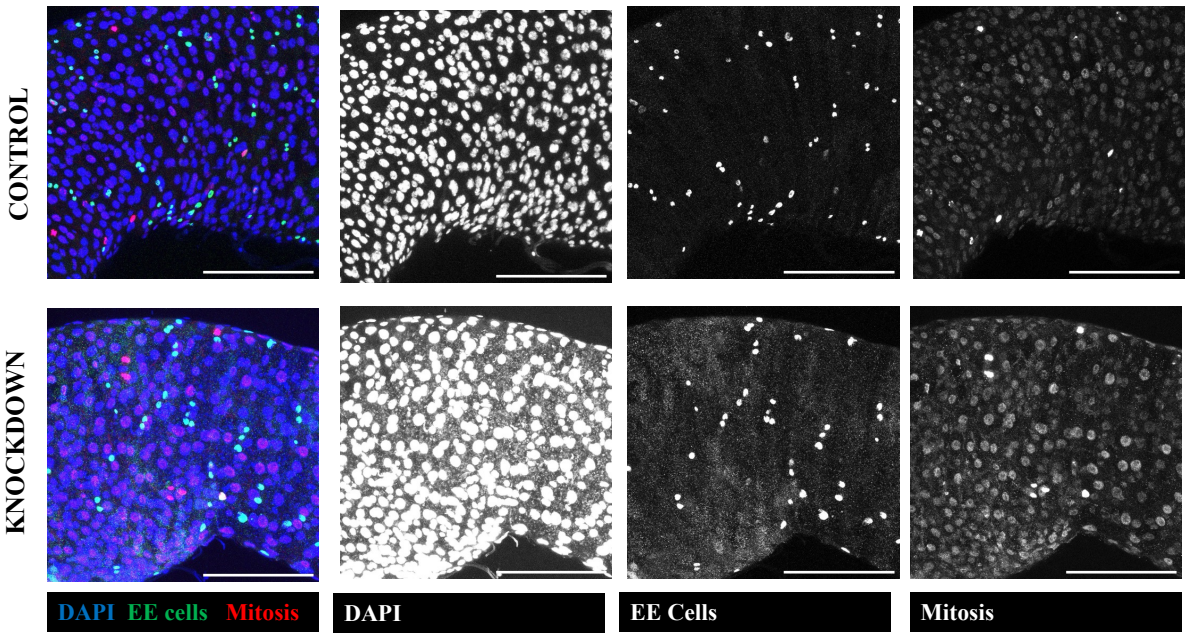

Figure 5.7. The effects of TIMP knockdown with *TIMP-RNAi-1* in ISCs and EBs of the posterior midgut. Knockdown of TIMP (*5961^{GS}> TIMP-RNAi-1*) does not seem to induce any phenotypical changes in the posterior midgut compared to controls. Guts were stained with α-prospero (1:100), α-PH3 (1:1000) and DAPI. Scale bars in the bottom right corner represent 100μm.

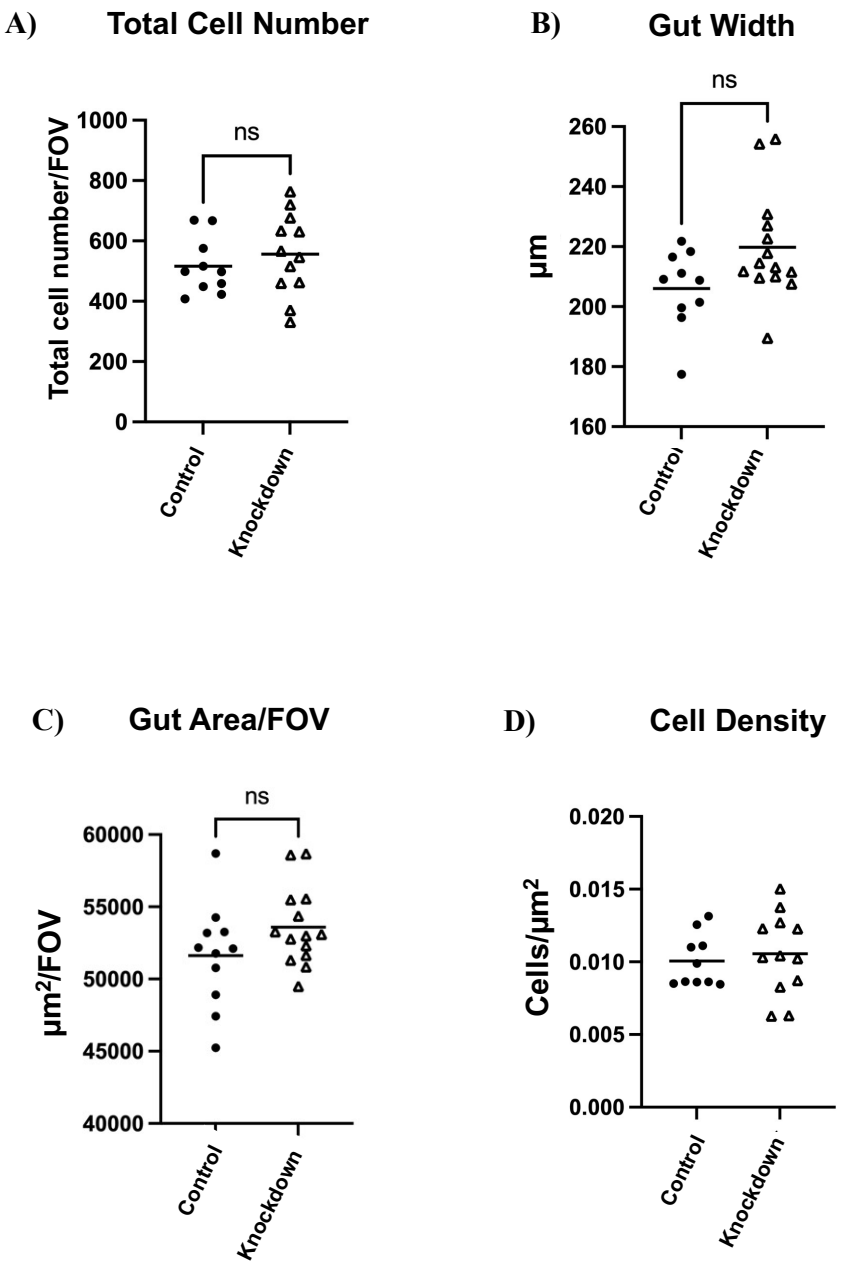

Figure 5.8. TIMP knockdown with *TIMP-RNAi-1* does not induce any significant changes in the posterior midgut. Knockdown of TIMP (*5961^{GS} > TIMP-RNAi-1*) does not affect the total number of cells observed per FOV (control n = 10, KD n = 12) (***A***), gut width (p = 0.05) (control n = 10, KD n = 14) (***B***), gut area/FOV (control n = 11, KD n = 14) (***C***), or cell density (control n = 10, KD n = 12) (***D***). Unpaired t-tests were used for normally distributed data (A, B, C), and non-parametric Mann Whitney-U tests for non-normally distributed data (D). Each data point represents a gut.

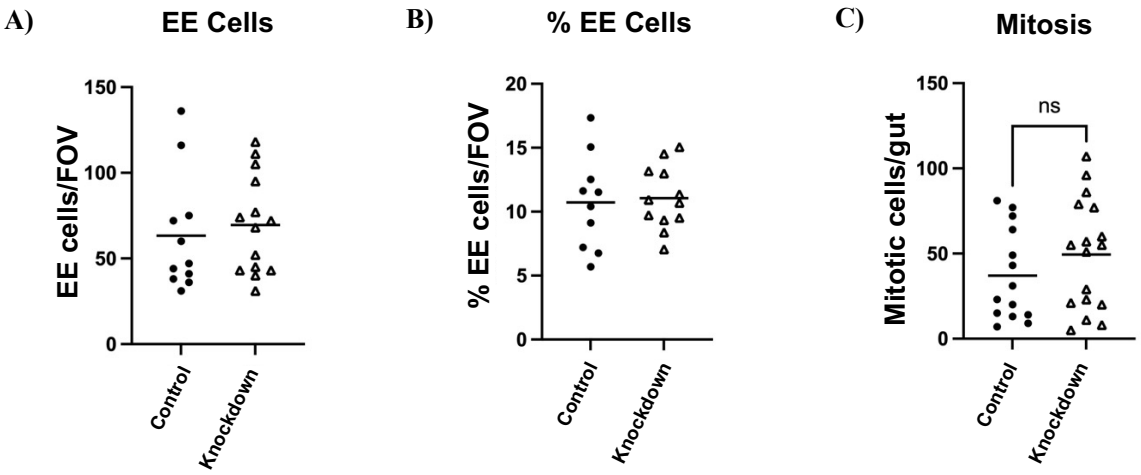

Figure 5.9. TIMP knockdown with *TIMP-RNAi-1* does not affect the number of EE cells in the posterior midgut or the proliferation rates of the gut. Knockdown of TIMP (*5961^{GS} > TIMP-RNAi-1*) does not change the number of EE cells observed per FOV (control n = 11, KD n = 14) (***A***), or the proportion of EE cells normalized to the total number of cells (control n = 10, KD n = 12) (***B***). The proliferation rates across the whole gut tissue seem to increase, but this trend if not statistically significant (p = 0.2) (control n = 14, KD n = 17) (***C***). Unpaired t-tests were used for normally distributed data (B, C), and non-parametric Mann Whitney-U tests for non-normally distributed data (A). Each data point represents a gut.

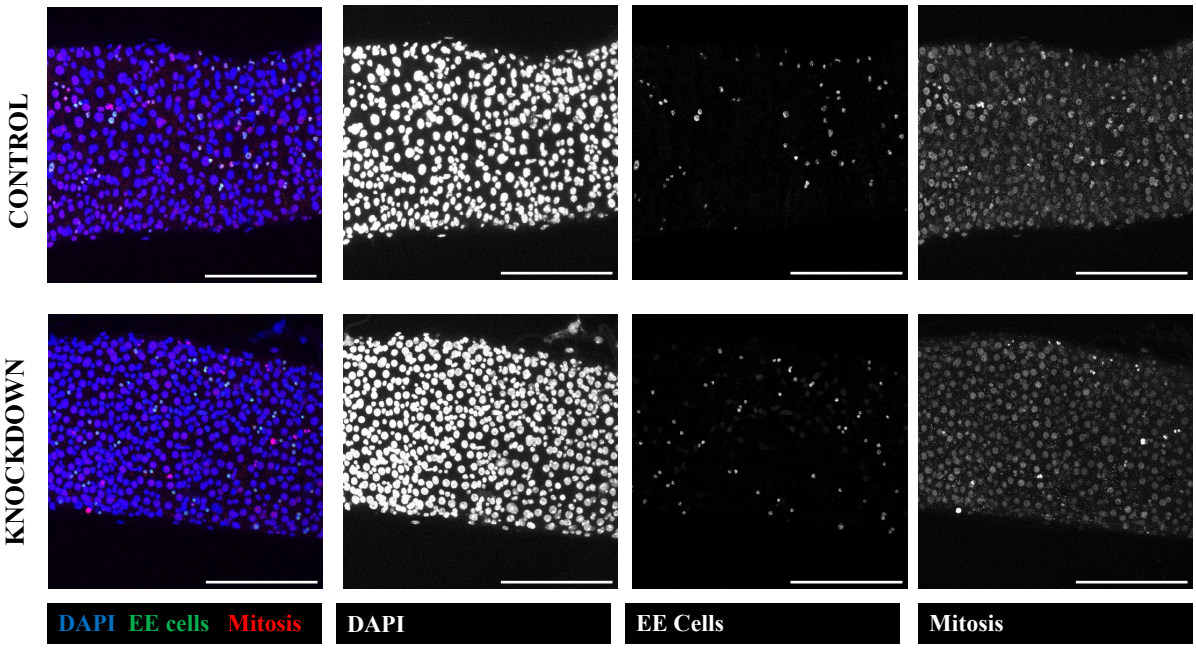

Figure 5.10. The effects of TIMP knockdown with *TIMP-RNAi-2* in ISCs and EBs of the posterior midgut. Knockdown of TIMP (*5961^{GS}> TIMP-RNAi-2*) does not seem to induce any phenotypical changes in the posterior midgut compared to controls. Guts were stained with α-prospero (1:100), α-PH3 (1:1000) and DAPI. Scale bars in the bottom right corner represent 100μm.

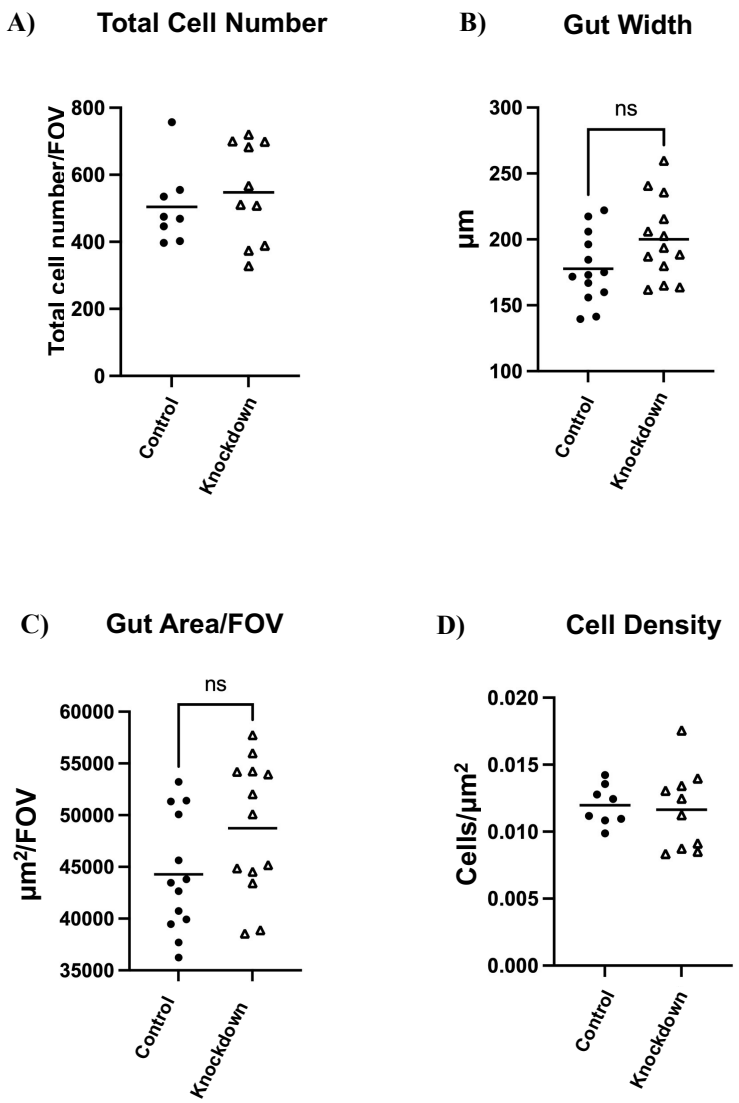

Figure 5.11. TIMP knockdown with *TIMP-RNAi-2* does not induce any significant changes in the posterior midgut. Knockdown of TIMP (*5961^{GS} > TIMP-RNAi-2*) does not affect the total number of cells observed per FOV (control n = 8, KD n = 10) (***A***), gut width (p = 0.05) (control n = 13, KD n = 13) (***B***), gut area/FOV (p = 0.07) (control n = 13, KD n = 13) (***C***), or cell density (control n = 8, KD n = 10) (*D*). All data was normally distributed, so unpaired t-tests were used for statistical analysis. Each data point represents a gut.

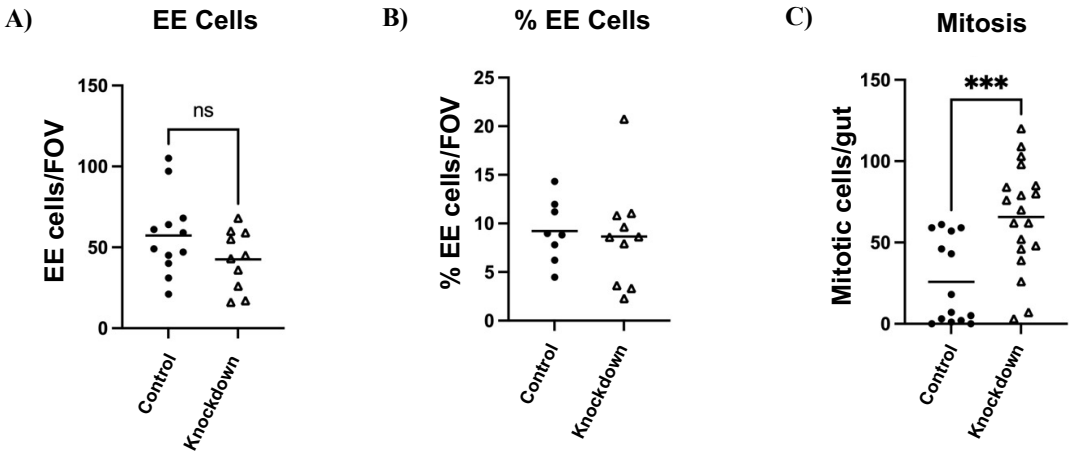

Figure 5.12. TIMP knockdown with *TIMP-RNAi-2* significantly increases the proliferation rates of the gut. Knockdown of TIMP (*5961^{GS} > TIMP-RNAi-2*) does not change the number of EE cells observed per FOV (control n = 12, KD n = 10) (***A***), or the proportion of EE cells normalized to the total number of cells (control n = 8, KD n = 10) (***B***). Knockdown of TIMP significantly increases the proliferation rates across the whole gut tissue, (p = 0.0005) (control n = 14, KD n = 19) (***C***). Unpaired t-tests were used for normally distributed data (B), and non-parametric Mann Whitney-U tests for non-normally distributed data (A,C). Each data point represents a gut.

5.3.3. Validation of *TIMP RNAi line-1*

Validation of the *TIMP RNAi-1* was carried out in order to test the reliability of the RNAi line and the extent of the knockdown in the tissue. For this, whole-gut TIMP knockdown samples (*tub-Gal80^{ts}; tub-Gal4 > UAS-TIMP RNAi-1)* were analyzed using qRT-PCR and TIMP levels quantified using the ΔΔCt method (*Figure 5.13*). Results from this did not demonstrate a reduction in TIMP levels in the *Drosophila* gut. On the contrary, it showed an increase in TIMP levels, although results were not statistically significant. It is worth nothing that these validation experiments were done at very early stages of the project, when samples were not prepared using RNA extraction kits and the levels of RNA were not measured using a nanodrop prior to cDNA synthesis. Thus, there is a high chance of error during sample preparation that could have led to these results, as this RNAi line has been extensively used in published literature. No validation data is available for the other TIMP RNAi line used as part of this project, as the line was not available at the time of these experiments.

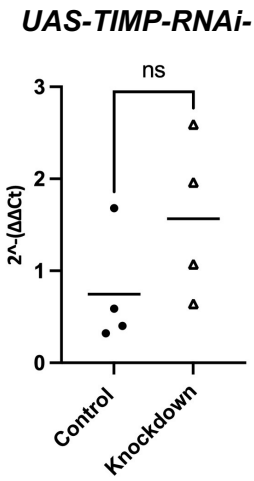

Figure 5.13. Validation of TIMP-RNAi-1 knockdown line. qRT-PCR analysis of whole gut TIMP knockdown samples with RNAi lines 1 (*tub-Gal80^{TS}; tub-Gal4 > TIMP-RNAi-1*) shows an increase in TIMP expression in knockdown samples compared to controls. Expression changes were calculated using the ΔΔCt method. All data was normally distributed, so unpaired t-tests were used for statistical analysis. Each data point represents a sample, and each sample contains 10 whole guts.

5.3.4. Knockdown of TIMP might lead to a decreased lifespan in the fly

Because of the function of TIMP as an inhibitor of metalloproteinases and its widely-studied implication in cancer progression, and as a result of the immunofluorescence data obtained as part of this project, a lifespan analysis was carried out in order to determine if knockdown of TIMP in the gut tissue affected the survival of the fly (*Figure 5.14*). Knockdown of TIMP in *5961^{GS} > TIMP-RNAi-1* female flies was induced 10 days into the experimental procedure and within 5 days a significant drop in survival was observed. This increased death rate in TIMP-knockdown flies became more prominent as adulthood progressed, and it was not until the final week of the experiment, from day 73 onwards, where the survival of both control and TIMP-knockdown flies levelled out. Thus, knockdown of TIMP in the ISC and EBs of the *Drosophila* gut significantly decreases the probability of survival of the organism. This could be due to the increase in proliferation across the gut associated with reduced levels of TIMP in ISCs and EBs. This could lead to tissue hyperplasia could disrupt homeostasis and normal gut function that has detrimental effects for organism survival.

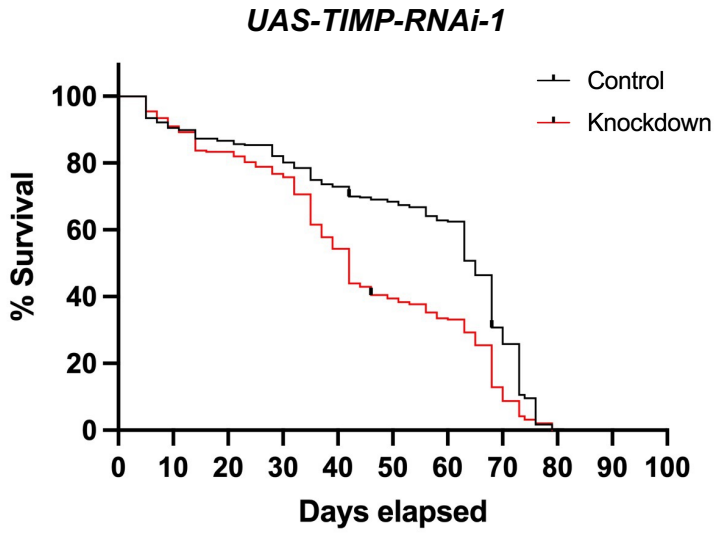

Figure 5.14. Knockdown of TIMP significantly reduces the lifespan of the fly. Knockdown of TIMP (*5961^{GS} > TIMP-RNAi-1*) significantly reduces the lifespan of the fly ($p < 0.0001$) (n = 300). TIMP knockdown is induced on day 10, when the flies are flipped into food containing the mifepristone (RU) drug.

5.3.5. The role of TIMP in major proliferative signaling pathways in the midgut

After determining that changes to TIMP expression levels can affect on posterior midgut homeostasis and *Drosophila* lifespan, the next step was to elucidate possible mechanisms of TIMP function and which signalling pathways its misexpression might impact. For this, *5961^{GS} > UAS-TIMP-2* overexpression guts were dissected and stained with α-phospho-MAPK to quantify the expression levels of active MAPK (*Figure 5.15*). Results showed no significant difference in active MAPK levels between control and overexpression guts (*Figure 5.16*). This demonstrates that overexpression of TIMP in ISC/EBs does not trigger an increase in Ras/MAPK signalling, suggesting that TIMP is not found upstream of the Ras/MAPK signalling cascade. Similar approaches were undertaken to establish if TGF-β and JNK signalling were downstream of TIMP, through α-phospho-SMAD and α-phospho-SAPK/JNK staining, respectively, but issues relating to the microscopy facilities did not allow for sample observation and hence no data is available.

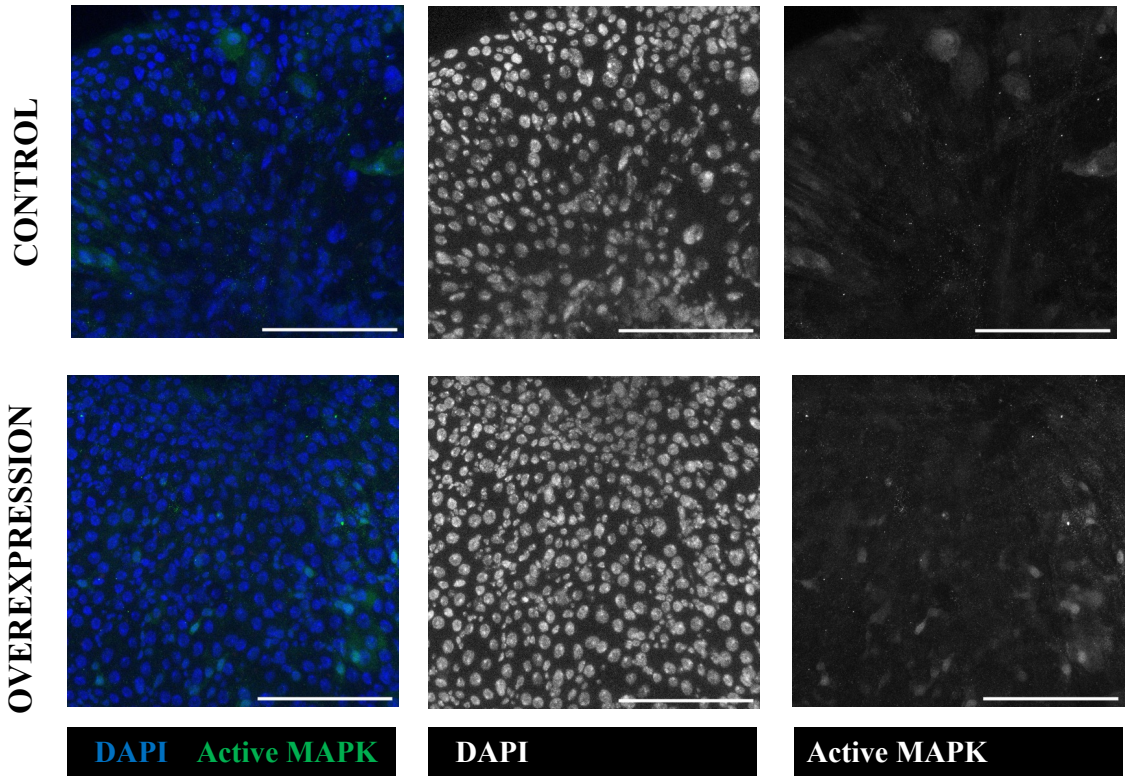

Figure 5.15. Changes in active MAPK expression in TIMP overexpression guts. Overexpression of TIMP (*5961^{GS} > UAS-TIMP-2*) increases the levels of active MAPK in dlp overexpression guts compared to controls. Guts were stained with α- phospho-p44/42 MAPK (Erk1/2) (1:200) and DAPI. Scale bars in the bottom right corner represent 100μm.

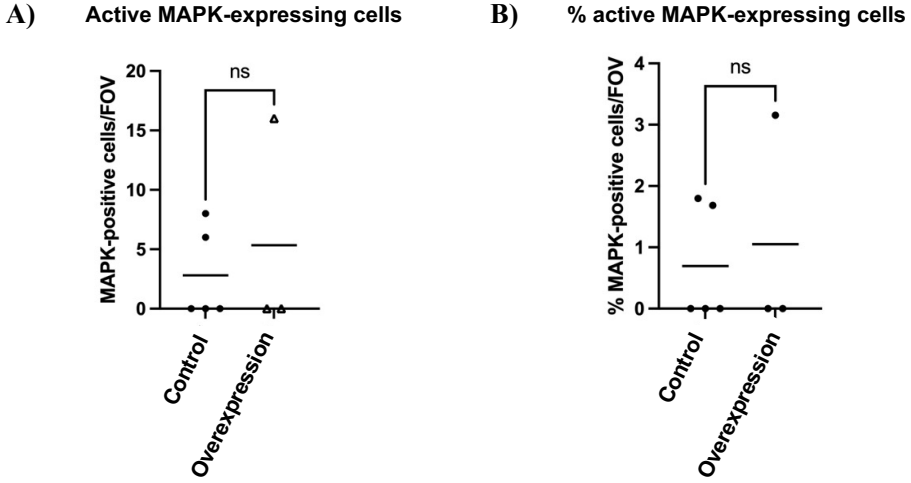

Figure 5.16. Active MAPK expression does not increase with TIMP overexpression. Overexpression of TIMP (*5961^{GS}> UAS-TIMP-2*) shows increasing trends in the levels of active MAPK expression in dlp overexpression guts compared to controls (control n = 5, OE n =3) (***A***). The proportion of active MAPK-positive cells normalized to total cell number is also not significantly increased with TIMP overexpression (control n = 5, OE n = 3) (***B***). All data was not normally distributed, so non-parametric Mann Whitney-U tests were used for statistical analysis (B). Each data point represents a gut.

Possible upstream regulation of TIMP in the fly gut was also explored using qRT-PCR analysis in lines activating specific stem cell regulatory pathways. These results are presented in depth in Chapter 7 of this thesis, but in summary, preliminary results suggest that the Hippo and JAK/STAT signalling pathways could be positive regulators of TIMP expression in the gut, since their overactivation leads to increased levels of the protein. On the contrary, Ras/MAPK signalling was highlighted as a potential negative regulator of TIMP. However, no statistically significant effects were observed due to a small sample size, so the characterization of these trends requires further work.

5.4. Discussion

The results presented here demonstrate that changes to TIMP levels in the stem and progenitor cells in the fly gut affect tissue homeostasis by inducing changes to the tissue regarding proliferation rates and the size of the EE population in the posterior midgut. The data presented in this chapter is consistent with previous work from our group (Sutherland, unpublished)

In particular, results suggest that elevated TIMP levels favour EE differentiation over ECs, raising the possibility that TIMP overexpression leads to biased differentiation. However, evidence in the literature has demonstrated that TIMP overexpression in the fly induces a significant increase in ISC proliferation in the midgut (Lee et al., 2012), which is not consistent with the data presented here. Furthermore, our results suggest that in the fly midgut, it is not overexpression, but rather the knockdown of TIMP that induces an increase in proliferation. To my knowledge, no studies have attempted to elucidate the role of TIMP in the regulation of ISC differentiation, and thus no data is available to compare against the model proposed here that TIMP is key to maintain a homeostastic balance of IS differentiation. The results presented here are consistent with previous work from the Doupé group that showed a differentiation-promoting role of TIMP on ISCs in the posterior midgut (Sutherland, unpublished). Considering that differentiation in the homeostatic tissue is strongly biased toward enterocyte cells (90% of differentiated cells are ECs, compared to 10% of EEs) (Amcheslavskly et al., 2009), the increase in EE cells could have detrimental effects on the tissue, both structurally and physiologically.

Drosophila MMP1 expression has been shown to increase with age, and its reduction leads to hyperplasia in the gut tissue (Lee et al., 2012). This increase in MMP1 could translate to changes in TIMP levels in two ways: on the one hand, the increase in MMP1 levels with age could be due to a decrease in TIMP expression with age, limiting the ability of MMP inhibition in the tissue. On the other hand, the increase in MMP1 levels with age could trigger an increase in TIMP activity in an attempt to re-establish a homeostatic balance in MMP1 levels. The first hypothesis would help to explain the significant decrease in survival in TIMP knockdown guts shown in this chapter. Immunofluorescence experiments with the UAS-TIMP-2 line showed a significant increase in cell density in TIMP overexpression guts compared to control guts, suggesting that TIMP overexpression in ISCs and EBs of the *Drosophila* gut leads to a hyperplastic phenotype in the posterior midgut. Knockdown experiments did not show any changes to cell density in the midgut, but it triggered a highly statistically significant increase in proliferation in the gut. Sutherland (unpublished) recorded similar findings relating to density changes as a result of TIMP overexpression and knockdown: consistently with the results presented here, they found a significant increase in cell density in TIMP-overexpressing guts and a highly significant reduction in cell density in TIMP-knockdown guts. Further experiments are needed to characterize this further, starting with the appropriate validation of the TIMP knockdown and overexpression lines to establish the reliability of the genetic tools. This project attempted to characterize if the expression levels of TIMP in wild-type adult guts changed with age, and which cells within the gut tissue expressed the inhibitor. However, these experiments did not yield any results, as staining with α-TIMP (Dear et al., 2016) did not show any antibody expression. The reduced availability of reagents for the study of TIMP expression in *Drosophila* limited the scope of experimental approaches of this project. Future studies should look to characterize TIMP expression changes with age and establish if it is the overexpression or knockdown of TIMP that is responsible for the increase in hyperplastic phenotypes in the tissue. Preliminary work from the Doupé group suggest that TIMP expression significantly decreases with age in the posterior midgut of the fly (Sutherland, unpublished).

Despite the varying results, our data and that found in the literature suggest that ageing could have an effect on TIMP expression (Lee et al., 2012). The preliminary lifespan analysis presented here suggests that knockdown of TIMP in the stem and progenitor cells of the *Drosophila* gut significantly reduces the lifespan of the fly. This

would fit in with the hypothesis outlined above that the overexpression of MMP1 increases with age, which could be a result of an age-associated decrease in TIMP levels that is not able to control MMP1 activity in the tissue, thus contributing to the induction of a hyperplastic phenotype. All of this will translate into detrimental effects in the gut tissue, which could lead to tumour development.

TIMP has been shown to play an important role in the maintenance of the structure and morphology of the germarium of the *Drosophila* ovary in aged flies (Pearson et al., 2016), suggesting a potential role in the stem cell niche. Moreover, TIMP mutant ovaries present reduced levels of viking expression (Pearson et al., 2016), i.e. one of the two collagen chains in *Drosophila*. Hughes et al. suggested viking as a proteolytic target of *Drosophila* MMP2 (Hughes et al., 2020). This establishes a link between TIMP and collagen expression in the context of stem cell niche maintenance. Overexpression of TIMP inhibits proteinase activity and leads to ectopic deposition of ECM proteins (Hughes et al., 2020) Furthermore, overexpression of TIMP in larval cardiac tissue induced fibrotic phenotypes in the tissue and resulted in ectopic expression and accumulation of collagen IV molecules in the pericardium and lumen of the heart (Hughes et al., 2020). Thus, changes to TIMP expression could be affecting tissue homeostasis by triggering changes to the collagen levels. Overexpression of TIMP, and the associated integrin-mediated reduction in MMP activity led to accumulation of basement membrane in tissues of *Drosophila* larvae (Hughes et al., 2020). In the context of the *Drosophila* gut tissue, this could mean that TIMP plays a role in maintaining collagen IV levels for appropriate assembly of the basement membrane of the epithelial tissue. Immunofluorescence experiments were set up to observe this in the *Drosophila* midgut, where $5961^{GS} > UAS\ TIMP\text{-}2$ adult female guts were stained with α-vkg (1:400), but issues with the fluorescence microscope hindered data collection. Short term future work will involve imaging and analysis of these samples.

Activation of the epidermal growth factor (EGF) receptor is necessary to induce early expression of mammalian TIMP1 and TIMP3 in vitro (Li and Curry, 2009). Moreover, this EGF activation leads to the accumulation of TIMP1 mRNAs in vitro by triggering MAPK/ERK signalling (Qiu et al., 2004), suggesting that TIMP could be acting downstream of the MAPK signaling cascade. These results fit in with the immunofluorescence data presented here that suggests TIMP acts downstream of MAPK, since the overexpression of TIMP in ISCs and EBs of the *Drosophila* gut do not increase the levels of active MAPK signaling. In the fly, MMP1 expression plays a role in the

regulation of the intestinal stem cell niche and the maintenance of gut tissue homeostasis through the EGFR pathway (Lee et al., 2012).

The regulatory mechanism of TIMP activity has been shown to be a complex one, relying on the interplay of many signalling cascades. Leivonen et al. proposed a model of TIMP3 regulation in vitro by which ERK1/2, p38 MAPK and Smad3 act together to control the effect of TGF-B signaling on TIMP3 expression in fibroblasts in vitro (Leivonen et al., 2013). Analysis of the active SMAD expression in TIMP-overexpressing guts would shed some light into the potential conservation of this proposed model in the posterior midgut of the fly. However, there are some inconsistencies among the published literature on the exact mechanism of regulation that these pathways have on TIMP expression. MMP1, MMP2 and TIMP were significantly upregulated in gut RasV12-overexpression models in vivo in the fly (Wang et al., 2013), whereas upregulation of the phosphorylated, i.e. active, forms of ERK1/2, p38 and JNK reduced the expression of TIMP1 and collagen I in in vivo rat models (Peng et al., 2013). Moreover, upon infection, MAPK, JNK and NF-KB have been shown to regulate TIMP and MMP expression in vitro (Cai et al., 2022). The results presented in this chapter do not provide any conclusive results on the relationship between MAPK and TIMP in the midgut, and further experiments are necessary to provide a clear picture of the involvement of TIMP in the major homeostatic pathways in this tissue.

In summary, the published data show a variation in the interactions between MAPK and TIMP expression. However, what could at first be seen as inconsistencies could actually be due to underlying differences in the TIMP molecules, since different TIMPs have slight variation in their protein sequence and in their function, and most studies focus on different cells/tissues and use different models. Thus, taken together, these results suggest that the regulation of TIMP expression is dependent on the physical and biochemical properties of the TIMP molecule in a tissue- and context-dependent manner.

The consequences of TIMP misregulation have been extensively documented in the literature. In a *Drosophila* larval model, MMP1 acts upstream of TGF-B signalling in the fat body to disrupt protein localization in the basement membrane and in the ECM in tumours (Lodge et al., 2021). MMPs have been shown to be fundamental for the ability of tumours to metastasize in the fly (Beaucher et al., 2006), suggesting that aberrant expression of TIMP could promote the formation of metastatic sites in the organism. TIMP expression in the wing imaginal disc suppresses the invasive capacity of tumour

cells through the cooperation of JNK and Ras signaling (Uhlirova and Bohmnann, 2006), suggesting that TIMP might act as a tumour suppressor in this tissue. Ras^{V12} overactivation triggers JNK signaling in the eye disc of the fly, activating TIMP and preventing ECM breakdown, thus reducing the metastatic potential of the tumour cells (reviewed by Patel and Edgar, 2014). This phenotype was consistent in *Drosophila* ovarian tumours, raising the possibility of a conserved role in fly epithelial tissues.

5.5. Conclusions

In summary, TIMP may play an important role in the maintenance of intestinal stem cell homeostasis in the *Drosophila* gut, as demonstrated by the immunofluorescence data presented in this chapter, and supported by previous work from our group. Overexpression of TIMP in ISCs and EBs increases the number of EE cells in the posterior midgut, suggesting a role for TIMP in ISC differentiation. Knockdown of TIMP increases proliferation in the gut epithelium and significantly reduces the lifespan of the fly, but the mechanisms that trigger this, or that regulate TIMP expression in the context of the ISC niche remain to be elucidated. Further characterization of the function, expression pattern and regulation of TIMP has proven difficult because the lack of reliable tools available for its study, but results from this project and published data suggest a role for MAPK signalling in the regulation of TIMP in the *Drosophila* gut, but the location of the inhibitor within the signalling cascade is yet to be determined. The validation of the available tools, and perhaps the development of new genetic manipulation tools, and reagents that appropriately target this protein are necessary in order to carry on with this work and be able to provide a conclusive picture of the role of TIMP in ISC/EBs of the *Drosophila* midgut and in overall gut tissue homeostasis.

Chapter 6

Dally-like protein (dlp) as a regulator of stem cell homeostasis

6.1. Introduction

6.1.1. The function and structure of HSPGs and glypicans

Heparan sulfate proteoglycans (HSPGs) can be found in different forms within the tissue: as cell surface macromolecules, in the extracellular matrix, or in soluble forms (Stewart and Sanderson, 2014). They have the ability to interact with a wide range of molecules, including growth factors, proteases, inhibitors and other ECM molecules, but, most importantly, HSPGs act as co-receptors for secreted proteins of the Hh, Wnt/Wg, TGF-B and FGF signaling pathways (Baeg and Perrimon, 2000). They regulate a group of signalling molecules known as morphogens, which mediate tissue patterning during development through the formation of concentration gradients (Han et al., 2005). Moreover, HSPGs play important roles in disease progression, inflammation and cancer development (Stewart and Sanderson, 2014).

A family of HSPG proteins, the glypicans, are found tethered to the cell membrane through a glycosylphosphatidynositol (GPI) anchor (Filmus, 2001; Fico et al., 2011), and

normally accumulate in cholesterol-rich regions of the membrane and on the apical surface of polarized cells (De Cat and David, 2001). Six glypican genes have been identified in mammals (GPC1-6), which can be further subdivided into two groups (glypicans 1/2/4/6 and glypicans 3/5) with only 25% conservation in their amino-acid sequence (Filmus et al., 2008). The *Drosophila* genome encodes two glypicans, Division abnormally delayed (dally) and Dally-like protein (Dlp), both of which play important roles in the regulation of Wnt signaling (Desbordes and Sanson, 2003). Dally is considered the ortholog of glypicans 3/5 and dlp is closely related to glypicans 1/2/4/6 (Filmus et al., 2008). Thus, D. melanogaster provides an excellent simple model to study the function and regulation of glypicans in vivo.

All glypicans have a similar size, ranging between 60-70kDa (Filmus, 2001), and their core protein is highly conserved, with a conserved sequence of 14 cysteine residues that is responsible for maintaining the three-dimensional structure of glypican molecules (Fico et al., 2007). Despite their well-characterized roles in adult tissues, glypicans expression is highest during development, where the molecules play essential roles in morphogenesis (Filmus, 2001). Their expression levels are tightly controlled in a tissue- and stage-specific manner (Filmus, 2001).

Their characteristic GPI anchor makes glypicans a target for post-translational modifications (PTMs), including the cleavage of the molecule from the cell surface and its release into the extracellular environment (reviewed in Fico et al., 2011). This discovery challenged the initial characterization of glypican function as a membrane-tethered protein. Membrane-associated glypicans act as platforms to regulate a broad range of signaling pathways, including Wg, Hh, BMP and FGF (Filmus et al., 2008), whereas these free, secreted glypican molecules can be transported through the organism and have broader roles in the tissues. Studies on the imaginal disc of the fruit fly revealed that the cleavage of HSPGs from the cell membrane occurs through the lipase Notum, which is a target of Wg signalling that allows this pathway to control its own gradient (Giráldez et al., 2002).

6.1.2. Dally-like protein (dlp), one of the two glypicans in *Drosophila*

In line with the characteristic structure of glypicans described above, the *Drosophila* glypican Dlp localizes to the cell membrane and is anchored through a GPI

link (Desbordes and Sanson, 2003). Dlp activity is regulated by the Hippo signaling pathway, in particular by the transcriptional coactivator Yorkie (Baena-López et al., 2008). Baena-López and colleagues proposed Hippo signalling as an important regulator of dlp activity, implying that misregulation of any component of this signaling pathway could have a knock-on effect on the wide range of cascades that are regulated by dlp.

Dlp has been best-studied in the context of its role in the regulation of Hh and Wg signaling, but results still remain controversial. Some studies have shown that both Dlp and Dally are essential for the regulation of Wg morphogens in the wing imaginal disc (Han et al., 2005), whereas others have suggested that dlp expression is not necessary for Wg signaling in *Drosophila* embryos (Desbordes and Sanson, 2003) or in cells cultured in vitro (Lum et al., 2003). Notum has been proposed to modulate the activity of the *Drosophila* glypicans to negatively regulate Wg signaling (Han et al., 2005), by cleaving Dlp from the cell membrane and transforming it from its membrane-tethered form to a secreted protein (Kreuger et al., 2004). Out of the two *Drosophila* glypicans, dlp has been proposed as the main substrate for the lipase Notum (Kirkpatrick et al., 2004). In particular, dlp and Notum have been shown to interact in the extracellular matrix to collectively restrict the levels of Wg signaling in the development of the imaginal disc (Kirkpatrick et al., 2004). This relationship between Notum and dlp highlights the importance of post-translational modifications of the glypican in determining its role within the tissue. Moreover, the roles of dlp been shown to differ depending on the levels of Wg present in the tissue: dlp acts to increase Wg levels in low-expressing tissues, and reduces Wg activity in contexts were there are high levels of the morphogen (Kreuger et al., 2004).

In the Hedgehog (Hh) signaling pathway, Dlp is essential downstream of Hh for signal transduction and acts either upstream or at the level of the Patched (ptc) receptor (Desbordes and Sanson, 2003; Lum et al., 2003). Desbordes and Sanson suggested that Dlp binds to Hh and enables its interaction with the ptc receptor. The interaction of Dlp with Hh occurs through the core protein of the glypican (Williams et al., 2010; Yan et al., 2010), where it acts to differentially regulate Hh signaling strength during development based on the tissue environment (Yan et al., 2010). Both Dally and dlp act as substrates of another *Drosophila* HSPG molecule, tout-velu (Ttv), to move the Hh protein along the cell membrane, and have fundamental roles in cellular patterning (Han et al., 2004). Gallet and colleagues demonstrated the importance of the GPI-anchorage of Dlp to the apical cell membrane in the wing imaginal disc. This study showed how Dlp is internalized and

translocated to the basolateral compartment of epithelial cells, and that this internalization is coupled with that of the Hh receptor Patched (Gallet et al., 2008), which acts downstream of dlp in the signalling cascade. The role of Dlp in the regulation of Hh morphogens is conserved between the *Drosophila* glypican and its mammalian orthologs in vitro and in vivo in embryonic tissues (Williams et al., 2010).

In the context of stem cell maintenance, high levels of dlp are expressed in male germline stem cells and it is essential for the regulation of the stem cell niche in this tissue (Hayashi et al., 2009). This same study suggested a possible mechanism of action for dlp activity in this tissue through interactions with the JAK/STAT ligand unpaired.

The functions of dlp within the *Drosophila* intestine are not well-studied. In the adult midgut, HSPGs are required to activate the Dpp signaling pathway and maintain tissue homeostasis (Ma et al., 2019). No published data has looked at the role of dlp within the ISCs, but some studies have reported roles of HSPGs in the regulation of embryonic stem cell fate in vitro (Nurcombe et al., 2008) The heparan sulfate endosulfatase Sulf1 is required for ISC maintenance in the *Drosophila* midgut, and loss of Sulf1 prevents adequate termination of ISC division during intestinal regeneration by overactivation of JAK/STAT, EGFR and Hh signaling (Takemura and Nakato, 2017).

6.2. Aims and Objectives

My previous work during my undergraduate MBiol project focused on the function of dally-like protein (dlp) in the regulation of ISC homeostasis in the posterior midgut. Because of the short duration of this project and circumstances relating to the outbreak of the Covid-19 pandemic, many questions relating to the function and regulation of this protein remained unanswered. The aim of this chapter was to validate the preliminary results I had obtained during my MBiol and to further investigate the function, expression pattern and regulation of this protein in the context of the intestinal stem cell regulation in the posterior midgut. Moreover, this project aimed to elucidate if the results observed in the fly were conserved in human samples.

6.3. Results

6.3.1. Overexpression and knockdown of dlp in the stem and progenitor cells of the posterior midgut goes not affect homeostasis

Initial experiments looked to replicate those observed during my undergraduate project, using immunofluorescence approaches to elucidate if manipulation of dlp levels affected posterior midgut homeostasis. Both the overexpression and knockdown of dlp were studied in this context.

Overexpression of dlp driven by Gene Switch (*5961^{GS} > UAS-dlp 9160*) (*Figure 6.1*) showed no changes to the posterior midgut of adult female flies in terms of number of cells observed per field of view, and gut width and cell density were also maintained when compared to controls (*Figure 6.2*). The total area of the gut observed per field of view was, however, significantly decreased in dlp-overexpressing guts (*Figure 6.2C*). Next, changes to the specific cell types in the gut were studied. The number of enteroendocrine cells observed per field of view were quantified, using the EE-specific marker prospero, as well as the proportion of EE cells in relation to the total number of cells observed per FOV. These results showed that dlp overexpression correlated with a small increase in both the number and the percentage of EE cells observed per field of view, but these changes were not statistically significant (*Figure 6.3A-B*). Moreover, dlp overexpression seemed to increase the number of proliferating cells in the gut (*Figure 6.3C*), although upon statistical analysis this trend was not deemed significant. In summary, dlp overexpression does not seem to cause any striking changes to the homeostasis in the posterior midgut of the fly, raising the possibility that either dlp does not play any significant roles in this context, or that there are perhaps compensatory mechanisms in place to account for changes in dlp expression.

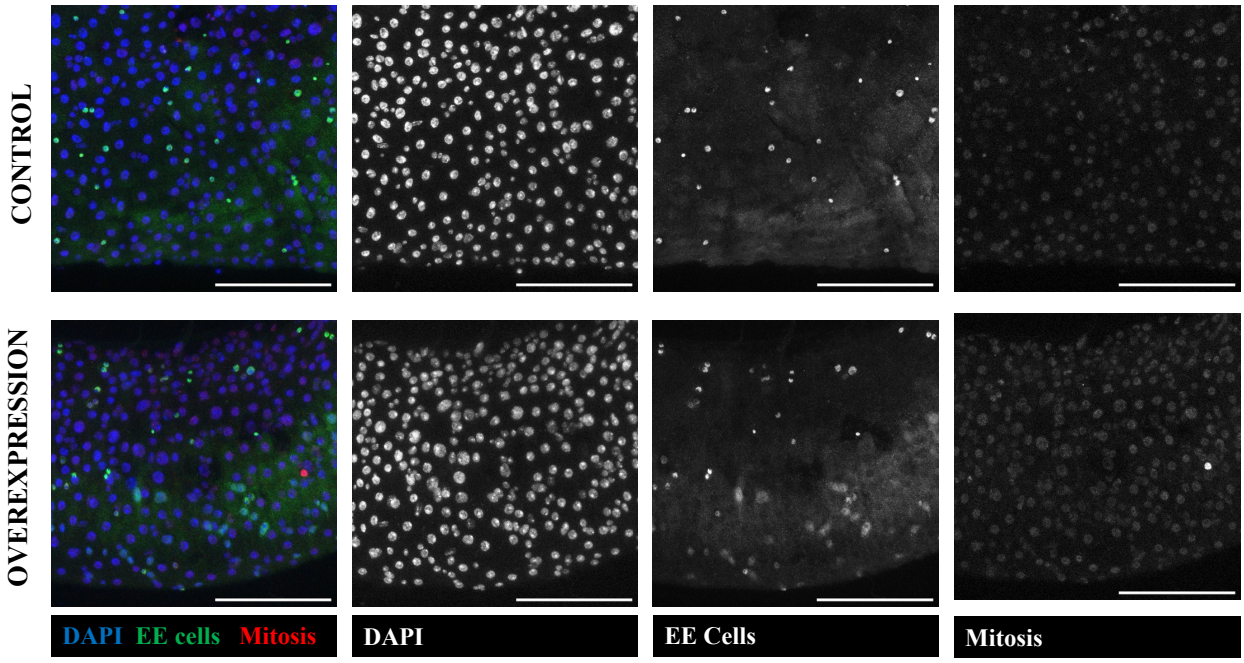

Figure 6.1. The effects of dlp overexpression in ISCs and EBs of the posterior midgut. Overexpression of dlp (*5961^{GS}> UAS-dlp*) reduces the area of the gut observed per field of view but those not induce any striking phenotypical changes compared to control guts. Guts were stained with α-prospero (1:100), α-PH3 (1:1000) and DAPI. Scale bars in the bottom right corner represent 100μm.

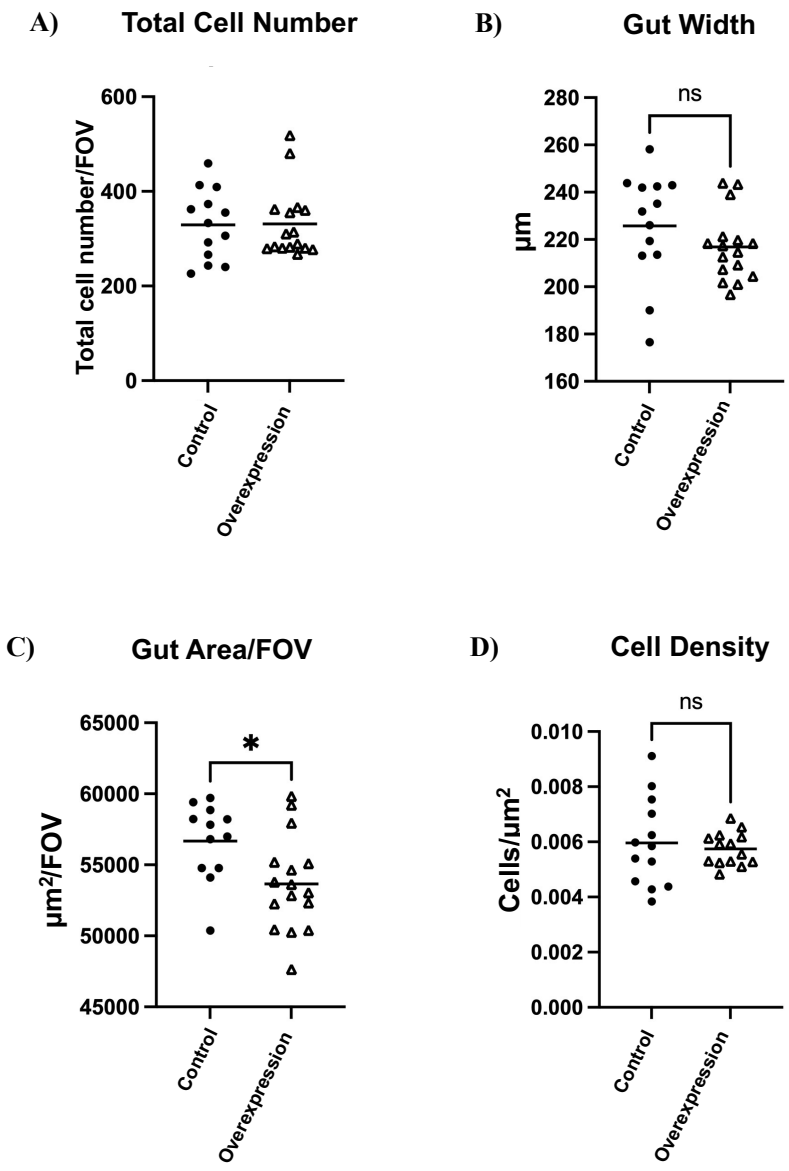

Figure 6.2. Dlp overexpression significantly reduces the area of the gut observed per field of view. Overexpression of dlp (*5961^{GS}> UAS-dlp*) does not cause any significant changes to the total number of cells observed per FOV (control n = 13, OE n = 16) (***A***), gut width (control n = 13, OE n = 16) (***B***), or cell density (control n = 13, OE n = 14) (***D***), but significantly reduces the area of the gut observed per FOV (p = 0.01) (control n = 12, OE n = 16) (***C***). Unpaired t-tests were used for normally distributed data (B,C,D), and non-parametric Mann Whitney-U tests for non-normally distributed data (A). Each data point represents a gut.

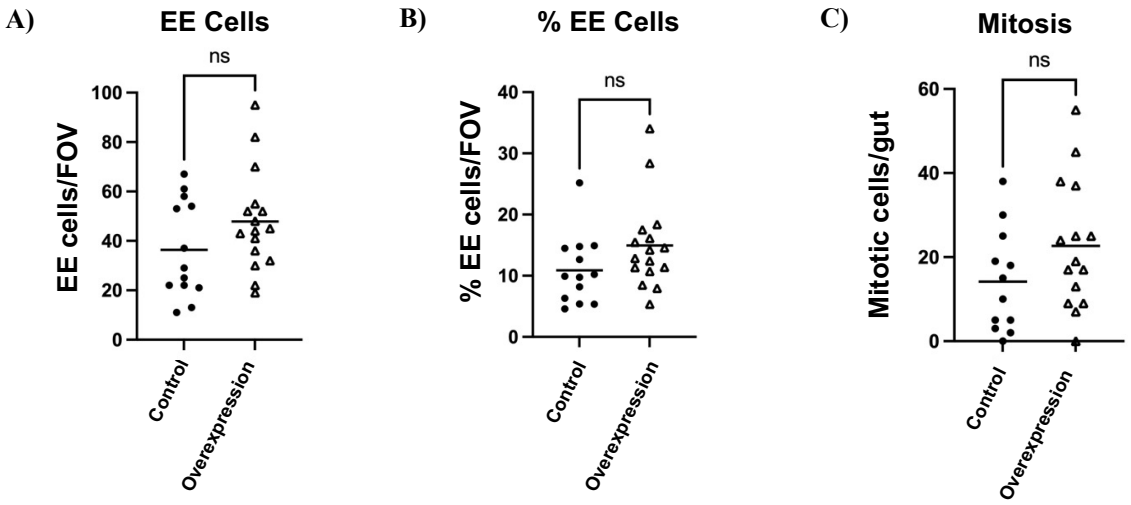

Figure 6.3. Dlp overexpression does not affect the EE cells in the posterior midgut or the proliferation rates of the whole gut tissue. Overexpression of dlp (*5961^{GS} > UAS-dlp*) does not cause any significant changes to the number of EE cells observed per FOV (control n = 13, OE n = 16) (***A***), or to the % of EE cells normalized to total cell number (control n = 13, OE n = 16) (***B***). The proliferation rates of the whole gut tissue show an increasing trend with in dlp overexpression guts (***C***) but this change is not statistically significant (p = 0.1) (control n = 12, OE n = 15) . Unpaired t-tests were used for normally distributed data (C), and non-parametric Mann Whitney-U tests for non-normally distributed data (A, B). Each data point represents a gut.

Next, the opposite genetic manipulation was carried out, where dlp was knocked down in stem and progenitor cells using the same Gene Switch driver, to elucidate if the reduction in glypican levels induced any changes in the fly midgut. For this, four different RNAi lines were used in order to account for any off-target effects that may occur and different knockdown efficiencies (*5961^{GS} > UAS-dlp RNAi 34089*, *5961^{GS} > UAS-dlp RNAi 34091*, *5961^{GS} > UAS-dlp RNAi 50540*, and *5961^{GS} > UAS-dlp RNAi 10299*). These lines will be referred to as *UAS-dlp RNAi lines 1-4* respectively, to simplify the understanding of the results. The results observed were consistent between all four RNA lines, with the exception of a few observations (*Figures 6.4, 6.7, 6.10 and 6.13*). Knockdown of dlp does not have an effect on the total number of cells in the posterior midgut between knockdown and control guts . Gut width, tissue area observed per field of view and cellular density were also maintained in dlp-knockdown guts when compared to controls (*Figures 6.5, 6.8, 8.11 and 6.14*). An investigation into potential changes to tissue composition in terms of cell types yielded interesting results. While *UAS-dlp-RNAi*

lines 1-3, which are interestingly all obtained from the same stock centre (BDSC), showed no changes to the number of EE cells observed per field of view (*Figures 6.6, 6.9 and 6.12*), the *UAS-dlp-RNAi-4*, obtained from the Vienna *Drosophila* Research Centre, showed a statistically significant increase in both the total number of EE cells observed per field of view as well as in the percentage of secretory enteroendocrine cells normalized against total cell number per FOV (*Figure 6.14*). This results raises the possibility that dlp knockdown might favour ISC differentiation rather than ISC renewal, and more specifically, that this differentiation is skewed towards the secretory cell type. However, the variability between the RNAi lines from the different stock centres hinders the ability to draw reliable conclusions from these results, and the lack of any effect on RNAi lines 1-3 suggests that this is perhaps an off-target effect. Dlp knockdown seems to induce a slight increase in the proliferative rates across the entire gut (*Figures 6.6, 6.9 and 6.14*) but statistical analysis showed this trend was not significant.

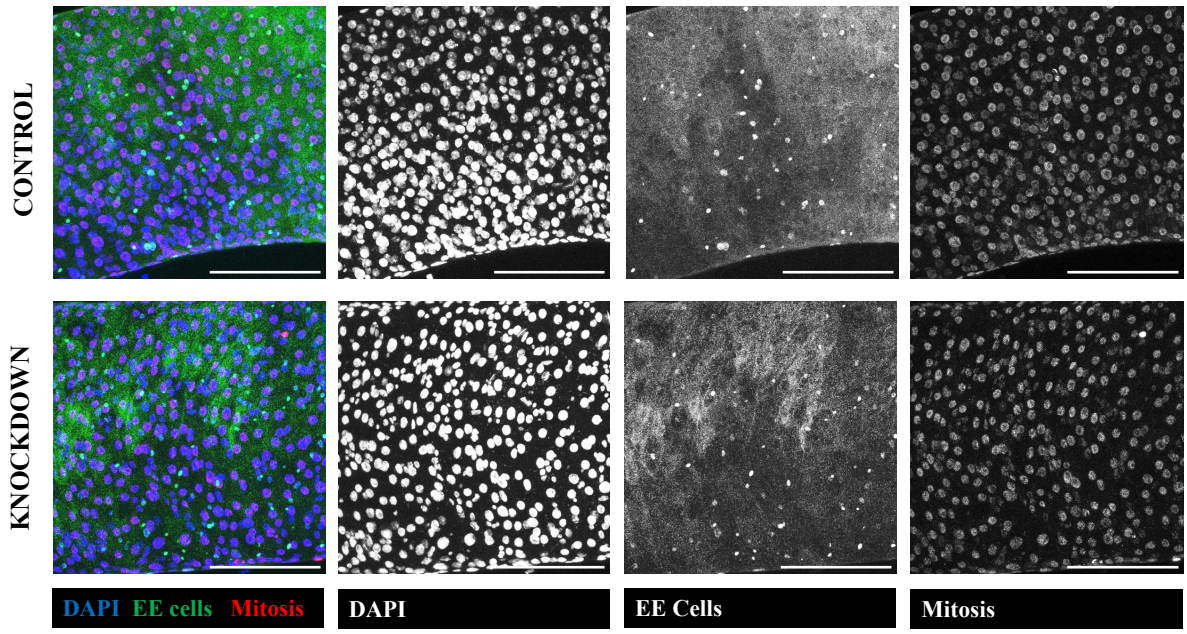

Figure 6.4. Knockdown of dlp using *dlp-RNAi-1* does not cause any changes to the posterior midgut. Knockdown of dlp (5961^{GS} > *dlp-RNAi-1*) does not induce any phenotypical changes compared to control guts. Guts were stained with α-prospero (1:100), α-PH3 (1:1000) and DAPI. Scale bars in the bottom right corner represent 100μm.

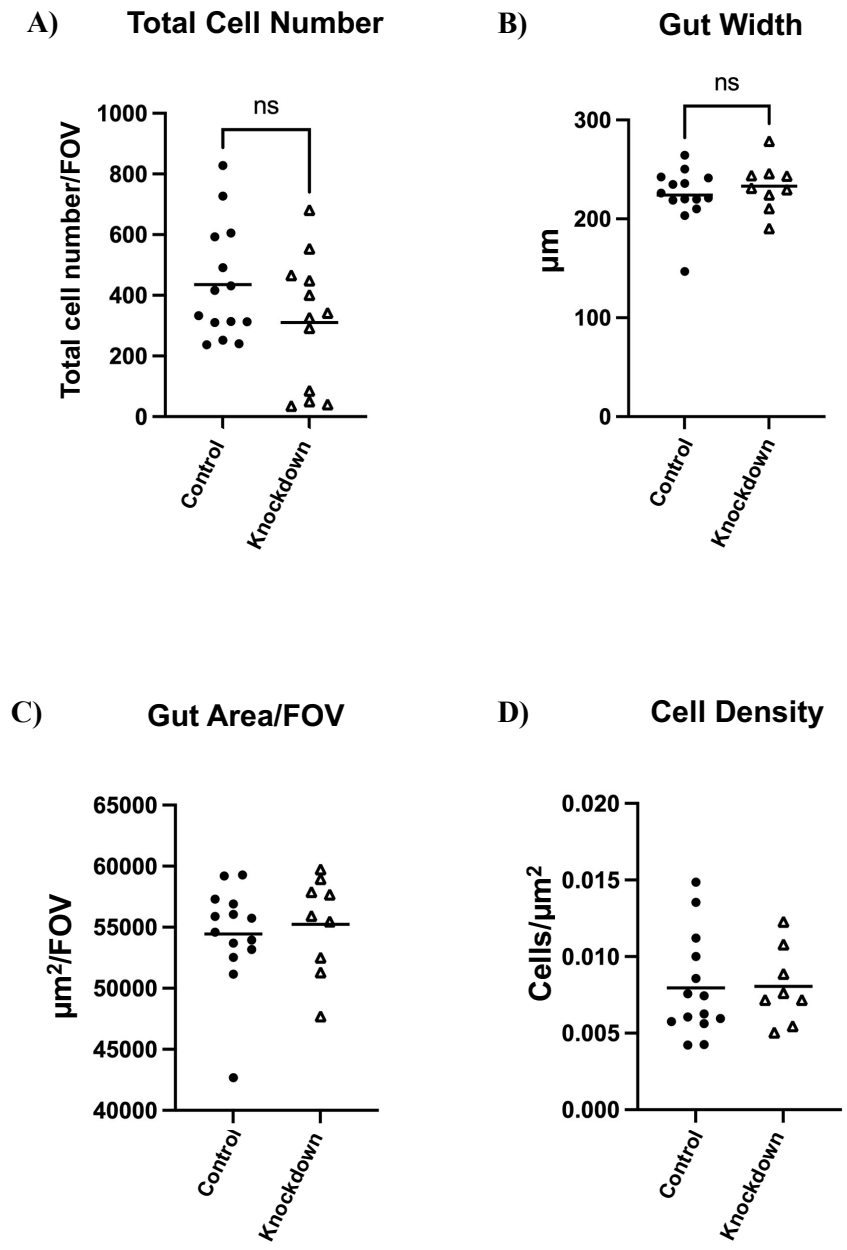

Figure 6.5. Quantification of dlp knockdown with *dlp-RNAi-1* shows no changes between knockdown and control midguts. Knockdown of dlp (*5961^{GS} > dlp-RNAi-1*) does not cause any significant changes to the total number of cells observed per FOV (control n = 14, KD n = 12) (***A***), gut width (control n = 14, KD n = 9) (***B***), area/FOV (control n = 14, KD n = 9) (***C***), or cell density (control n = 14, KD n = 8) (*D*). Unpaired t-tests were used for normally distributed data (B,C), and non-parametric Mann Whitney-U tests for non-normally distributed data (A, D). Each data point represents a gut.

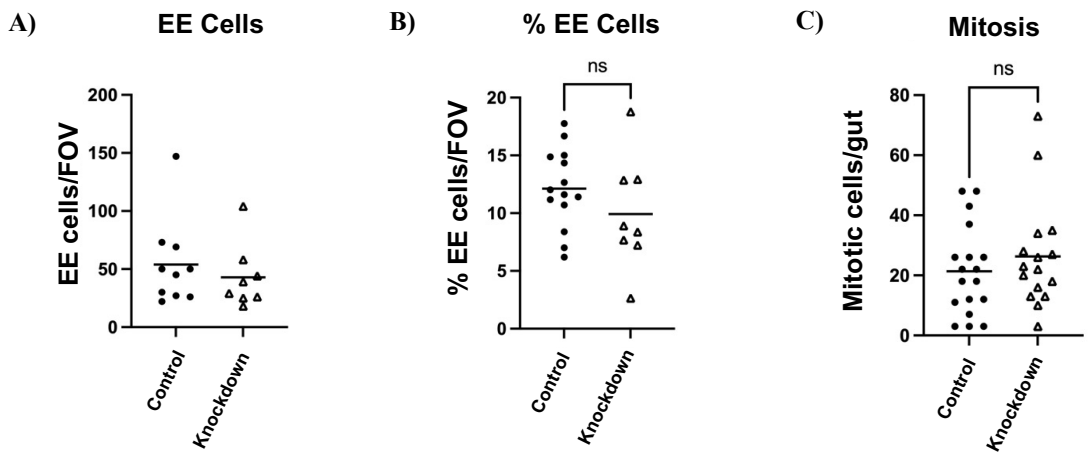

Figure 6.6. Quantification of dlp knockdown with *dlp-RNAi-1* shows no changes in EE cells or proliferation between knockdown and control guts. Knockdown of dlp (*5961^{GS} > dlp-RNAi-1*) does not cause any significant changes to the number of EE cells observed per FOV (control n = 10, KD n = 8) (***A***), or the % of EE cells observed per FOV normalized to total cell number (control n = 14, KD n = 8) (***B***). The number of mitoses observed across the whole gut is slightly increased (control n = 18, KD n = 16) (***C***), but it is not statistically significant. All data was normally distributed, so unpaired t-tests were used for statistical analysis. Each data point represents a gut.

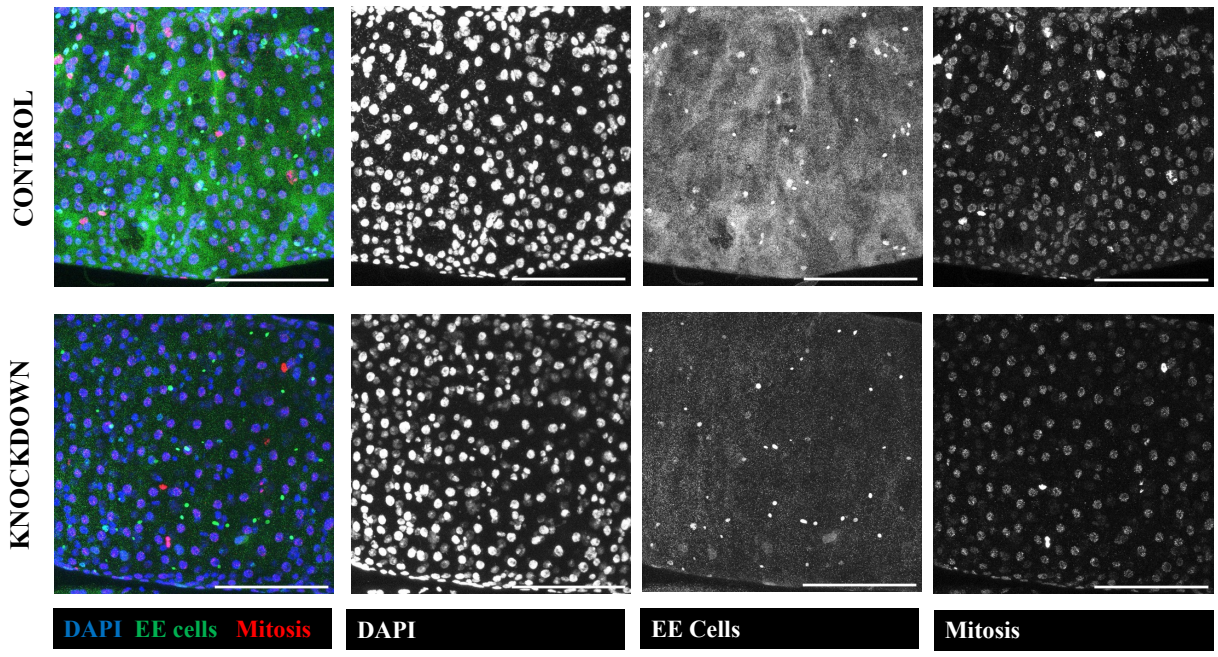

Figure 6.7. Knockdown of dlp using *dlp-RNAi-2* does not cause any changes to the posterior midgut. Knockdown of dlp (*5961^{GS} > dlp-RNAi-2*) does not induce any phenotypical changes compared to control guts. Guts were stained with α-prospero (1:100), α-PH3 (1:1000) and DAPI. Scale bars in the bottom right corner represent 100μm.

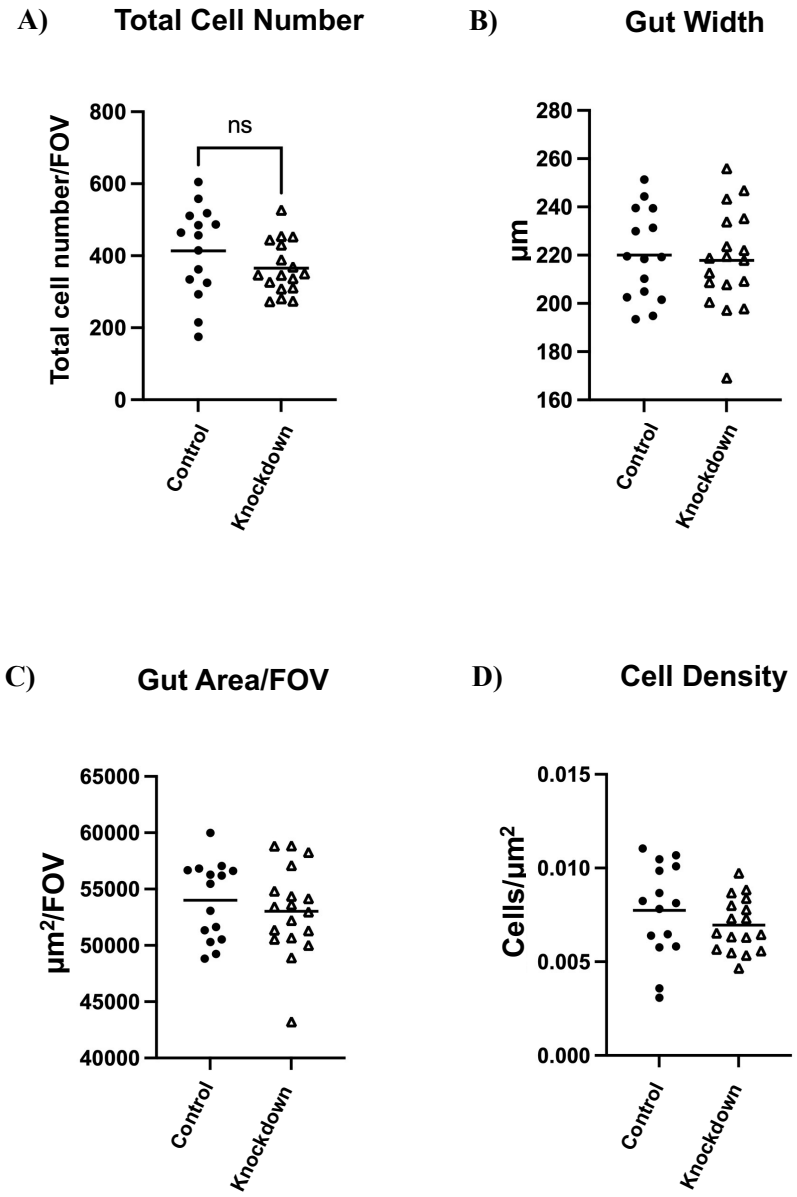

Figure 6.8. Quantification of dlp knockdown with *dlp-RNAi-2* shows no changes between knockdown and control midguts. Knockdown of dlp (*5961^{GS} > dlp-RNAi-2*) does not cause any significant changes to the total number of cells observed per FOV (control n = 15, KD n = 17) (***A***), gut width (control n = 15, KD n = 18) (***B***), area/FOV (control n = 15, KD n = 18) (***C***), or cell density (control n = 15, KD n = 17) (*D*). All data was normally distributed, so unpaired t-tests were used for statistical analysis. Each data point represents a gut.

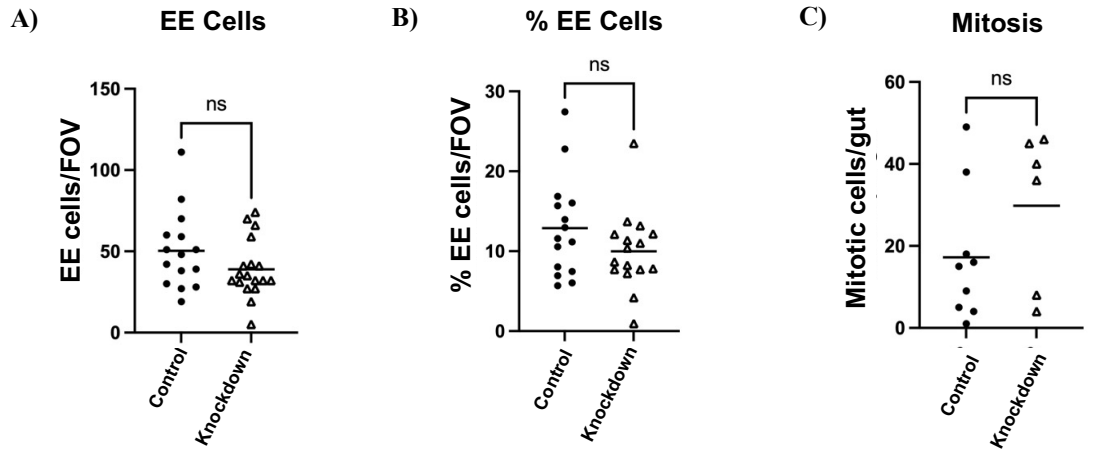

Figure 6.9. Quantification of dlp knockdown with *dlp-RNAi-2* shows no changes in EE cells or proliferation between knockdown and control guts. Knockdown of dlp (*5961^{GS} > dlp-RNAi-2*) does not cause any significant changes to the number of EE cells observed per FOV (control n = 15, KD n = 18) (***A***), or the % of EE cells observed per FOV normalized to total cell number (control n = 15, KD n = 16) (***B***). The number of mitoses observed across the whole gut is increased (control n = 9, KD n = 6) (***C***), but the change is not statistically significant. All data was normally distributed, so unpaired t-tests were used for statistical analysis. Each data point represents a gut.

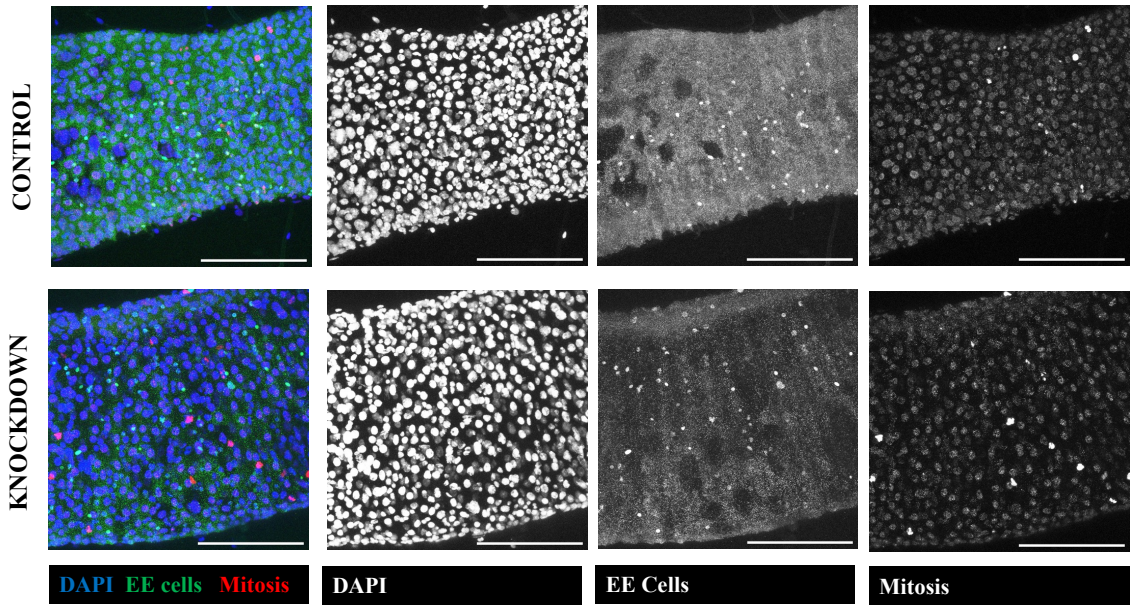

Figure 6.10. Knockdown of dlp using *dlp-RNAi-3* does not cause any changes to the posterior midgut. Knockdown of dlp (*5961^{GS} > dlp-RNAi-3*) does not induce any phenotypical changes compared to control guts. Guts were stained with α-prospero (1:100), α-PH3 (1:1000) and DAPI. Scale bars in the bottom right corner represent 100μm.

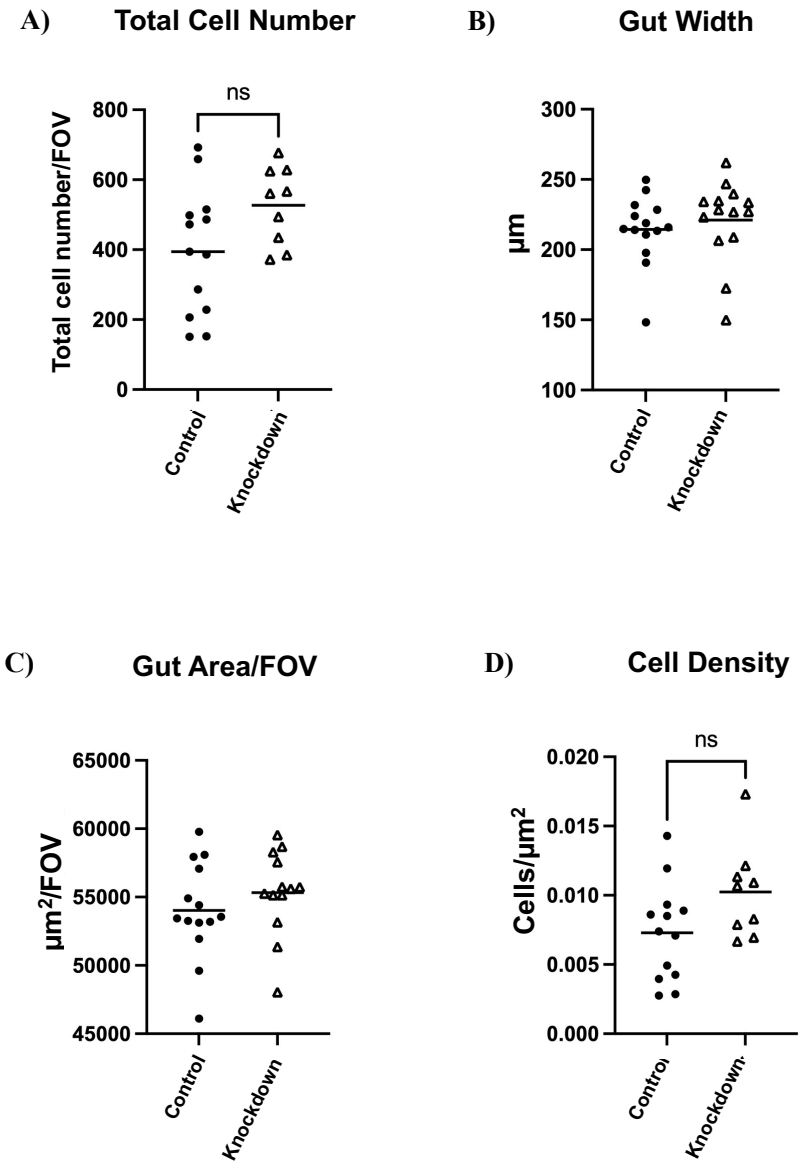

Figure 6.11. Quantification of dlp knockdown with *dlp-RNAi-3* shows no changes between knockdown and control midguts. Knockdown of dlp (*5961^{GS} > dlp-RNAi-3*) does not cause any significant changes to the total number of cells observed per FOV (control n = 13, KD n = 9) (***A***), gut width (control n = 14, KD n = 14) (***B***), area/FOV (control n = 14, KD n = 13) (***C***), or cell density (control n = 13, KD n = 9) (***D***). Both total cell number and cell density show increased trends in knockdown guts compared to controls, but this change was not statistically significant (p = 0.06 in both cases). Unpaired t-tests were used for normally distributed data (A, D), and non-parametric Mann Whitney-U tests for non-normally distributed data (B, C). Each data point represents a gut.

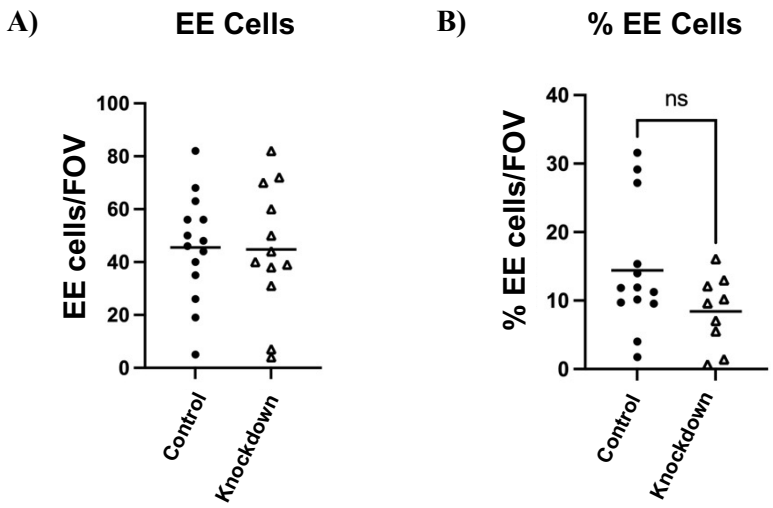

Figure 6.12. Quantification of dlp knockdown with *dlp-RNAi-3* shows no changes in EE cells between knockdown and control guts. Knockdown of dlp (*5961^{GS} > dlp-RNAi-3*) does not cause any significant changes to the number of EE cells observed per FOV (control n = 14, KD n = 12) (***A***), whereas the % of EE cells observed per FOV normalized to total cell number shows a decreasing trend (***B***), but this is not statistically significant (p = 0.09) (control n = 13, KD n = 9). All data was normally distributed, so unpaired t-tests were used for statistical analysis. Each data point represents a gut.

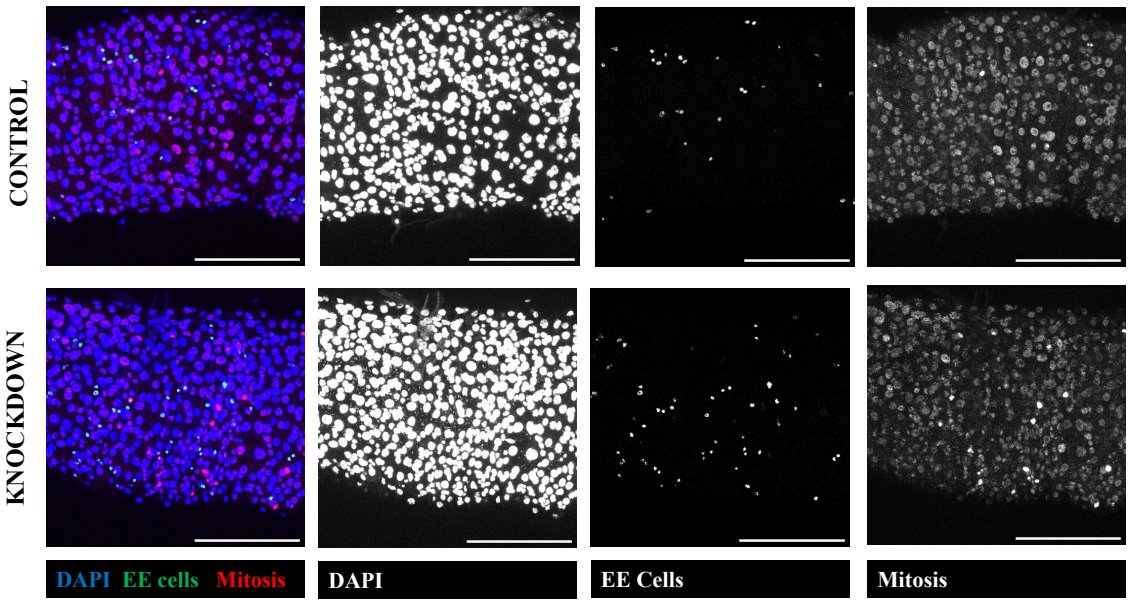

Figure 6.13. Knockdown of dlp using *dlp-RNAi-4* increases the number of EE cells in posterior midgut. Knockdown of dlp (*5961^{GS} > dlp-RNAi-4*) increases the number of EE cells in the posterior midgut compared to controls, but does not induce any other phenotypical changes. Guts were stained with α-prospero (1:100), α-PH3 (1:1000) and DAPI. Scale bars in the bottom right corner represent 100μm.

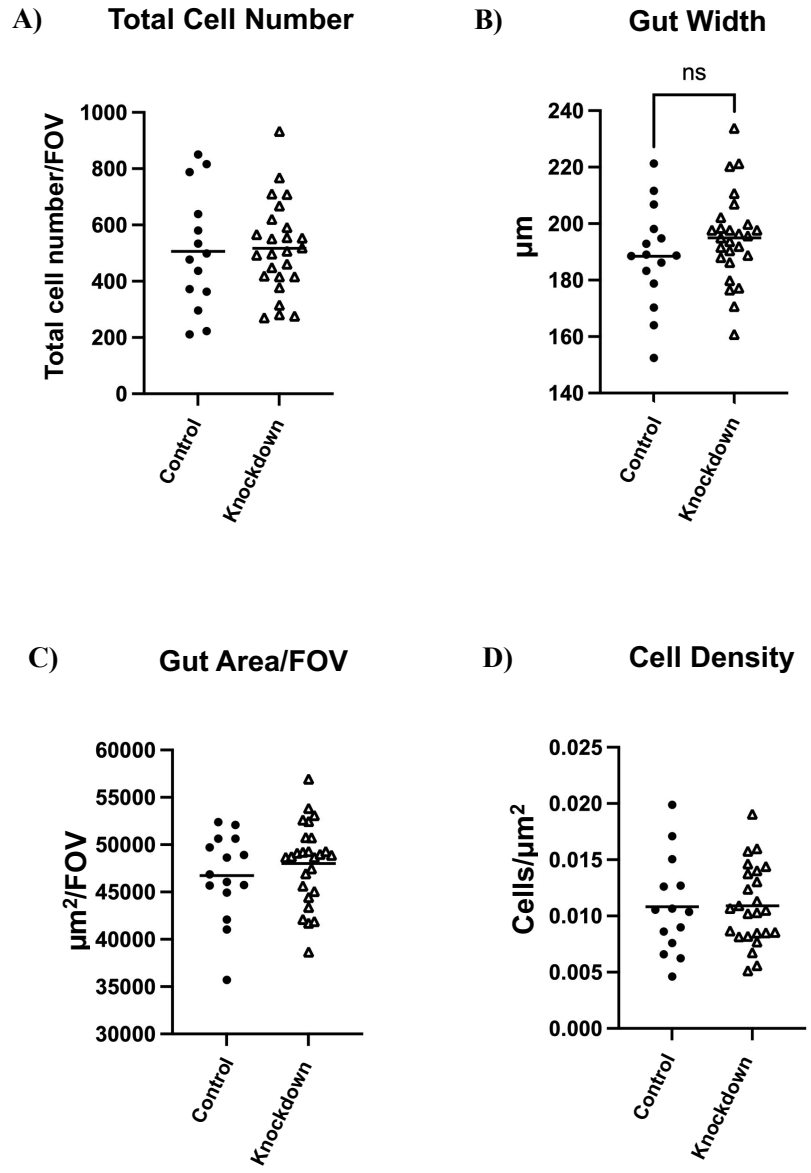

Figure 6.14. Quantification of dlp knockdown with *dlp-RNAi-4* shows no changes between knockdown and control midguts. Knockdown of dlp (*5961^{GS} > dlp-RNAi-4*) does not cause any significant changes to the total number of cells observed per FOV (control n = 14, KD n = 25) (***A***), gut width (control n = 15, KD n = 26) (***B***), area/FOV (control n = 15, KD n = 26) (***C***), or cell density (control n = 14, KD n = 25) (***D***). All data was normally distributed, so unpaired t-tests were used for statistical analysis. Each data point represents a gut.

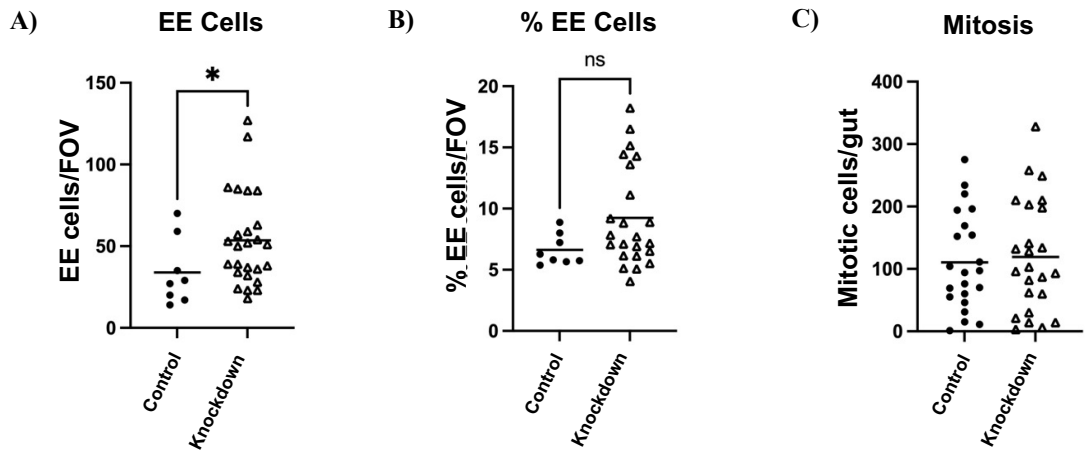

Figure 6.15. Dlp knockdown with *dlp-RNAi-4* significantly increases the number of EE cells in knockdown midguts compared to controls. Knockdown of dlp (*5961^{GS} > dlp-RNAi-4*) significantly increases the number of EE cells observed per FOV (p = 0.04) (control n = 8, KD n = 26) (***A***), whereas the % of EE cells observed per FOV normalized to total cell number, despite showing an increasing trend, does not significantly change between knockdown and control guts (***B***) (p = 0.1) (control n = 8, KD n = 23). The proliferation rates across the whole gut are not affected by dlp knockdown (***C***) (control n = 22, KD n = 24). Unpaired t-tests were used for normally distributed data (C), and non-parametric Mann Whitney-U tests for non-normally distributed data (A, B). Each data point represents a gut.

6.3.2. Validation of the dlp RNAi lines

The previous use of RNAi lines 1-3 during my MBiol project resulted in a high variability of the results obtained as part of that project, and subsequent validation of the knockdown lines did not demonstrate appropriate dlp knockdown across all RNAi constructs (Ferraces-Riegas, unpublished). Therefore, an optimized version of these validation experiments was initially carried out as part of this PhD project, in order to elucidate which of the RNAi lines were effectively knocking down the gene of interest and to understand the lack of effects shown in the immunofluorescence data described above. For this, whole-gut knockdown of dlp was induced using the temperature sensitive *tub-Gal80^{ts}; tub-Gal4* driver (*tub-Gal80^{ts}; tub-Gal4 > UAS-dlp RNAi 1, tub-Gal80^{ts}; tub-Gal4 > UAS-dlp RNAi 2 and tub-Gal80^{ts}; tub-Gal4 > UAS-dlp RNAi 3)*. At the time of these experiments, the UAS-dlp RNAi 4 was not available for testing. qRT-PCR analyisis of these samples and quantification of dlp levels using the ΔΔCt method showed that dlp-RNAi lines 1 and 2 caused an average of 50% reduction in dlp expression, whereas dlp RNAi-3 showed ~75% reduction in dlp expression compared to control guts (*Figure 6.16*).

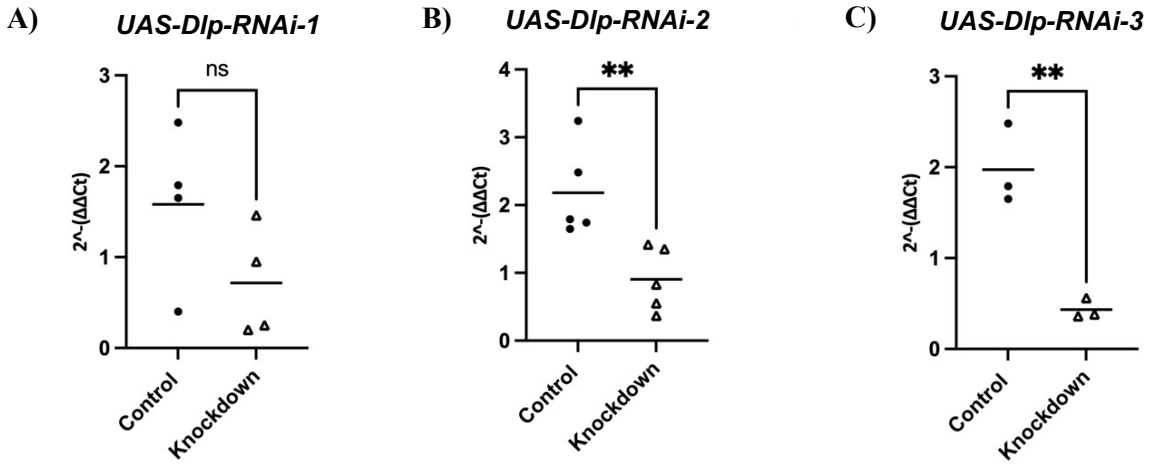

Figure 6.16. Validation of dlp RNAi knockdown lines. qRT-PCR analysis of whole gut dlp knockdown samples with RNAi lines 1-3 (*tub-Gal80^{TS}; tub-Gal4 > dlp-RNAi*) shows a reduction in dlp expression in knockdown guts compared to controls in all three cases. The reduction in dlp expression with *dlp-RNAi-1* (***A***) is not statistically significant (p = 0.1), whereas both *dlp-RNAi-2* (***B***) and *dlp-RNAi-3* (***C***) both induce statistically significant reductions in dlp expression compared to controls (p = 0.008, and p = 0.004, respectively). All data was normally distributed, so unpaired t-tests were used for statistical analysis. Each data point represents a sample, and each sample contains 10 whole guts.

6.3.3. The involvement of dlp in the major regulatory pathways in the midgut

In order to understand if dlp is involved in any of the fundamental signaling pathways in the midgut, guts overexpressing dlp in the stem and progenitor cells of the tissue (*5961^{GS} > UAS-dlp 9160*) were stained with α-phospho-42/44 MAPK (1:200) (*Figure 6.17*) and MAPK-positive cells quantified. Results showed a significant increase in active MAPK expression in the posterior midgut when dlp is overexpressed (*Figure 6.18*). This significance was maintained in both total number of MAPK-positive cells observed per field of view and in the proportion of MAPK-positive cells in relation to the total number of cells. Thus, these results suggest that dlp overexpression triggers an increase in MAPK activity, and that dlp could be acting upstream of Ras/MAPK signalling. Interestingly, the localization of active MAPK also differs between the control and dlp-overexpressing guts: control guts present cytoplasmic staining of active MAPK, whereas in the overexpression guts, this staining is exclusively nuclear (*Figure 6.18*).

Similar approaches to study the role of TGF-β through anti-phospho-SMAD staining (1:100) and anti-phopsho-SAPK/JNK (1:100) were prepared but issues with the Leica SP5 FLIM microscope used for imaging of all immunofluorescence experiments meant no data is available for analysis. Similarly, an investigation into the role of the ECM components collagen IV and actin were initiated in order to determine if, in its role as an ECM component after cleavage from the cell membrane, dlp has the ability to interact or affect the expression levels or the distribution of ECM molecules, but data collection did not take place.

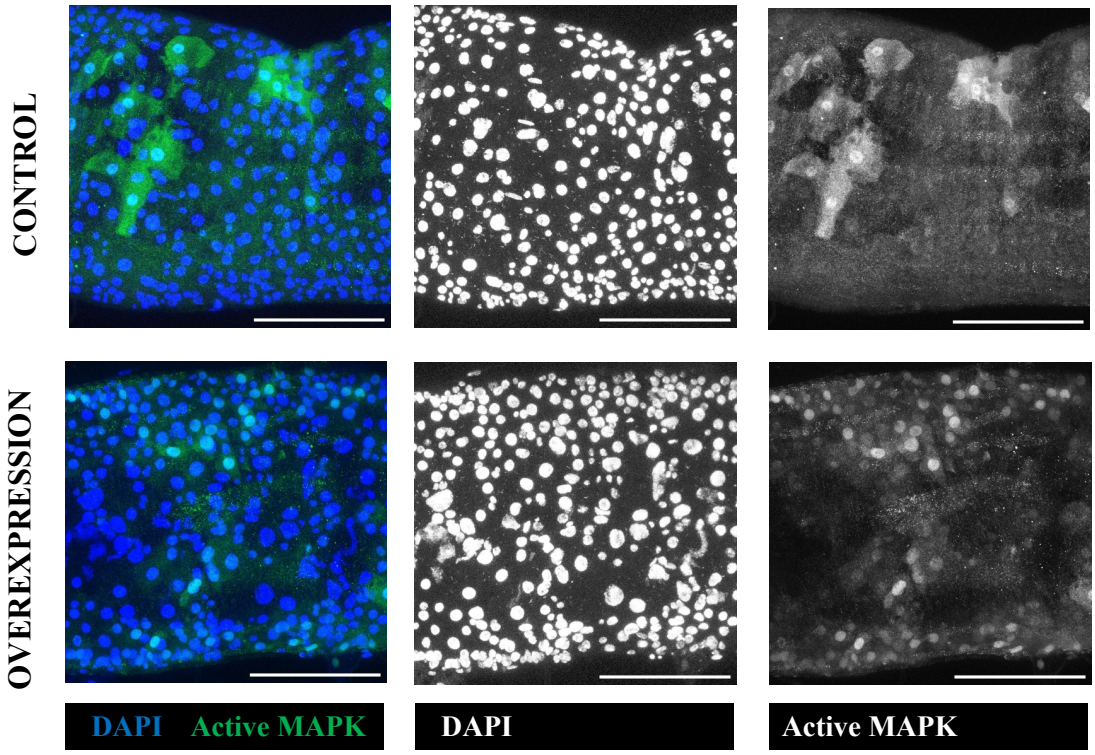

Figure 6.17. Changes in active MAPK expression in dlp overexpression guts. Overexpression of dlp (*5961^{GS} > UAS-dlp*) increases the levels of active MAPK in dlp overexpression guts compared to controls. Guts were stained with α- phospho-p44/42 MAPK (Erk1/2) (1:200) and DAPI. Scale bars in the bottom right corner represent 100μm.

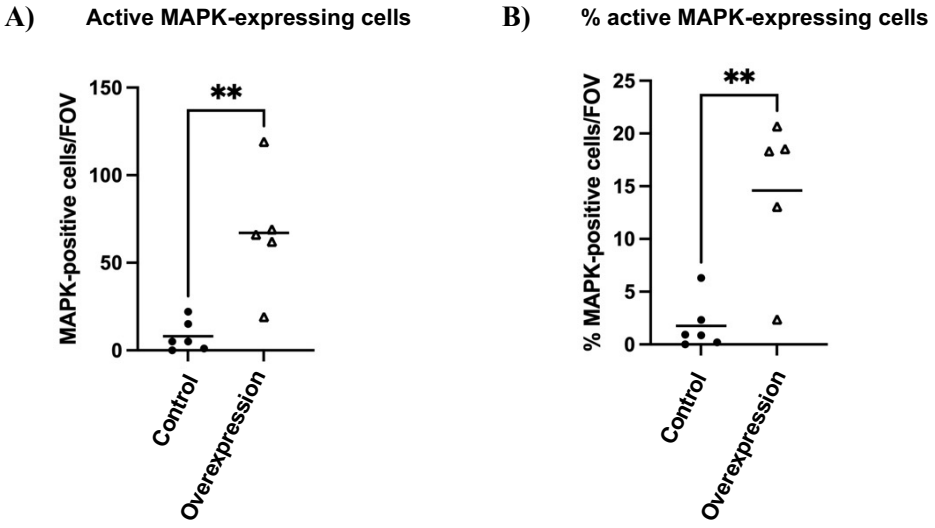

Figure 6.18. Active MAPK expression significantly increases with dlp overexpression. Overexpression of dlp (*5961^{GS} > UAS-dlp*) significantly increases the levels of active MAPK expression in dlp overexpression guts compared to controls (p = 0.003) (control n = 6, OE n = 5) (***A***). The proportion of active MAPK-positive cells normalized to total cell number is also significantly enhanced with dlp overexpression (p = 0.008) (control n = 6, OE n = 5) (***B***). Unpaired t-tests were used for normally distributed data (A), and non-parametric Mann Whitney-U tests for non-normally distributed data (B). Each data point represents a gut.

6.4. Discussion

The results presented here show that dlp has a minimal effect, if any, on the maintenance of tissue homeostasis. Only one of the 4 RNAi lines demonstrated that dlp knockdown in the stem and progenitor cells leads to a significant decrease in the number of EE cells in the posterior midgut. Therefore, the conclusions that can be drawn from the immunofluorescence data are limited, and point to a lack of involvement of dlp in ISC turnover. Published literature have demonstrated that HSPGs are essential in *Drosophila*, at different stages of embryonic and adult development (Lin and Perrimon, 2000; Nybakken and Perrimon, 2002; You, 2013; Trisnadi and Stathopoulos, 2015) and in the maintenance of *Drosophila* gut homeostasis (Wei et al., 2020). However, among the different HSPG molecules found in the fly, Dlp expression has actually been found to be low in the midgut epithelium, with most of its expression in the visceral muscle surrounding the gut tissue (Wei et al., 2020). Thus, it is not surprising that overexpression and knockdown of Dlp in the ISCs and EBs showed minimal effects on the midgut. Broadie and colleagues reported Dlp expression in the visceral mesoderm in *Drosophila*

(Broadie et al., 2011), which raises the possibility that perhaps Dlp expression is more prevalent in the foregut and the hindgut regions of the fly gut, as they both stem from the mesoderm from development, whereas the midgut has endodermal origin. Moreover, the data presented here suggest an EE-specific expression of dlp in the posterior midgut, which further supports the conclusion that dlp has no effect on ISC maintenance. Future experiments should focus on elucidating the role of Dlp in the stem and progenitor cells of these gut regions, as the different subregions of the gut have been shown to be controlled by independent ISC population with their own characteristic functions (Buchon et al., 2013).

The low expression of Dlp in the midgut reported by Wei and colleagues is consistent with preliminary experiments that reported low levels of the glypican in the midgut (data not shown). Thus, in order to elucidate the exact roles of this protein in the maintenance of the ISC niche, it is important to take both age and gut compartment into consideration. Moreover, if Dlp expression is low in the midgut, it is not surprising that Dlp knockdown experiments showed any significant changes in the immunofluorescence experiments shown here. If the levels are inherently low in control guts, further knockdown could have minimal effects on gut homeostasis. It is worth noting that work from my MBiol project reported the opposite results, where dlp expression was significantly increased with age (Ferraces-Riegas, unpublished). Therefore, future work should prioritise conclusively establishing the expression changes of this glypican with age, using a different α-dlp antibody and exploring other genetic tools available for the characterization of dlp expression, such as gene or protein traps. The significant increase in gut width with age was consistent between the results presented as part of this PhD project and my MBiol work.

One surprising result was the apparent colocalization of Dlp staining with EE cells in the posterior midgut. This is not consistent with the initial genome-wide expression study that has served as the basis of this project, which reported Dlp as a protein specifically secreted by the stem and progenitor cells of the gut (Doupé et al., 2018). Moreover, to my knowledge and at the time of this submission, no other papers have reported Dlp expression in the enteroendocrine cells specifically. Thus, this also contributes to explain the minimal effects observed in the Dlp overexpression and knockdown experiments: manipulation of Dlp expression was specifically carried out using an ISC and EB specific Gene Switch driver, so if Dlp is expressed in the EE cells, this manipulation is not occurring in the normal cells of dlp expression and will not be

causing any phenotypic changes. Future work should look at the effects of Dlp expression changes using an EE-specific driver, such as *prosGal4^{TS}*, or a whole-gut driver like *tub-Gal80^{ts}; tub-Gal4*. The combination of this with the switch in focus to other regions of the gut of mesodermal origin might provide a clearer picture of the roles of Dlp within the ISC niche in *Drosophila* and the maintenance of gut homeostasis, if any. There is evidence in the literature that supports a role of Dlp in the regulation of the stem cell niche: Dlp is required in the maintenance of the male germline stem cells, whereas Dally regulates female GSCs (Hayashi et al., 2009), suggesting differing roles for each glypican in the maintenance of the stem cell niche. HSPGs are key in the regulation of embryonic stem cell fate in vitro (reviewed by Kraushaar et al., 2013), but the specific role of Dlp is not described here.

In the context of dlp regulation, there is a significant gap in the literature regarding the regulation of this glypican in the gut and its involvement in signaling cascades in the adult tissue, as most of the published data focus on tis roles during development. The results shown here suggest dlp acts upstream of the Ras/MAPK signaling cascade, but no other evidence of its involvement in other pathways is available. Published data has demonstrated that activation of Hippo signaling in the wing imaginal disc causes a downregulation of Dlp expression (Baena-López et al., 2008). In this same tissue, co-expression of dlp and dally yields similar phenotypes to overexpression of Yorkie (Yki) (Baena-López et al., 2008), and since Yki is required in the midgut to drive ISC proliferation in response to damage, infection or stress (Shaw et al., 2011), it is possible that Hippo-driven Dlp activity is triggered upon stress induction, in disease states or in tissue regeneration. Future work should look to elucidate this further, by inducing damage in the gut tissue and observing the role of dlp in this context, while simultaneously looking at changes in the different signaling cascades that are known to regulate or be regulated by dlp or HSPG activity. An initial attempt was made to study this as part of this project, where guts were damaged using DSS and the proteins of interest were investigated in this context. However, time constrains meant this avenue was not pursued further.

It is not known if the role of Hippo in ISC proliferation is solely due to Yki activity, or if Hippo triggers any other signaling pathways downstream. Downregulation of Hippo signaling leads to increased stem cell proliferation and triggers the expression of JAK/STAT ligands in an ISC context (Shaw et al., 2011). Loss of Dlp directly correlates with the loss of Unpaired ligand distribution and a reduction in JAK/STAT signalling (Zhang et al., 2013), suggesting a potential link between Dlp, Hippo and JAK/STAT.

Therefore, the cooperation of multiple signaling cascades to regulate the ISC niche and maintain homeostasis cannot be ruled out.

Other signalling pathways have been reported to control HSPG activity in the fly at different stages of development. Abnormal synthesis of some HSPG family members has been shown to affect Wg, Hh and Dpp signalling in vitro (Bornemann et al., 2004), but this study does not look into the specific role of Dlp in this context. It is worth noting that in the regulation of JAK/STAT, Hh and Wg signaling, Dlp has been shown to have redundant roles with the other *Drosophila* glypican, Dally (Su et al., 2018), and thus the possibility that changes to Dlp expression can be compensated by Dally should not be excluded, and could account for some of the results presented in this chapter.

The elucidation of the role and regulatory mechanism that control Dlp expression in the *Drosophila* gut is of great importance, as misregulation of glypicans in *Drosophila* and in other organisms are implicated in disease and cancer progression (reviewed by Filmus, 2001; Nagarajan et al., 2018). Downregulation of GPC4, one of the mammalian orthologs of Dlp, facilitates proliferation, migration and invasion of tumour cells in breast cancer in vivo (Munir et al., 2020), suggesting that GPC4, and by direct correlation dlp, could perhaps have tumour suppressor roles in certain tissues. This role of GPC4 in cancer progression could be mediated by Wnt/Wg signalling (Sakane et al., 2011). On the contrary, GPC4 has oncogenic properties in pancreatic cancer, where it is involved in the maintenance of stemness of the tumour cells and their resistance to chemotherapy through the activation of the Wnt/β-catenin pathway (Cao et al., 2018). Taken together, these results, alongside our findings presented in Chapter 8 of this thesis, raise the possibility that the role of GPC4 is context- and tissue-dependent, and thus does not exclude Dlp from behaving similarly in *Drosophila*.

Finally, future work should attempt to characterize the expression pattern of Dlp within the intestinal tissue, in order to determine in which subregions of the gut dlp is expressed. Dlp is a GPI-tethered receptor on the cell membrane, but can also be found in a soluble form in the ECM after cleavage by Notum (Kreuger et al, 2004). Moreover, some studies have reported the presence of HSPGs in the nucleus of fibroblasts (Richardson et al., 2001), which are the main producers of ECM proteins in all organs (reviewed by DeLeon-Pennell et al., 2020). The translocation of HSPGs to the nucleus has been well-documented in recent years, proposing important roles of these proteins in the regulation of cell cycle progression, proliferation and transcription (reviewed by Stewart and Sanderson, 2014). This translocation to the nucleus is dependent on the

presence of a nuclear localisation sequence (NLS) within the core protein sequence (Liang et al., 2014; Stewart and Sanderson, 2014). Although none of these reports use *Drosophila* as the model organism, or focus specifically in the potential roles of Dlp in the nucleus, it raises the possibility of a third localization of Dlp within the tissues that could play important roles in the regulation of tissue homeostasis.

6.5. Conclusions

In summary, the combination of a small pool of genetic manipulation tools and reagents available for the study of Dlp, as well as the results obtained here, did not provide sufficient evidence to continue the study of dlp in the context of ISC regulation in the *Drosophila* gut. Multiple independent knockdown and overexpression lines suggest dlp does not have a significant role in the ISCs and EBs of the posterior midgut in normal homeostasis, but the expression pattern in EEs warrants further characterization. Future experiments should primarily focus on determining the expression pattern of dlp in the gut tissue, i.e. which cells express the protein, and the levels of dlp present in intestinal tissue, particularly in the midgut region. Initial characterization experiments should follow up on the EE-specific expression of dlp reported here, which contradicts the initial sequencing study that identified dlp as a protein specifically secreted by stem and progenitor cells in the *Drosophila* gut. Manipulation of dlp expression through the use of an EE-specific driver such as the *prosGal4^{TS}* line used in other parts of this project would provide a good indication of the expression pattern. Despite the lack of cellular phenotype, the data presented here suggests that dlp acts upstream of the Ras/MAPK signaling cascade, and evidence in the literature highlights its potential links with Hippo and JAK/STAT signaling, through interactions with the transcriptional activator Yorkie and the Unpaired ligands, respectively. Evidence in the literature suggests a role for Dlp in the maintenance of the stem cell niche in certain tissues, as well as its function in the regulation of ISC proliferation and differentiation. However, no published papers have looked into the role of dlp within the ISC niche of different gut subregions, which could be important to understand the involvement of dlp in disease, particularly in cancer progression, and could perhaps provide a new therapeutic target for drug and therapy development.

Chapter 7

The study of SPARC, PLOD, TIMP and dlp in the context of overproliferative models of the *Drosophila* gut

7.1. Introduction

As mentioned in Chapter 1, the maintenance of gut and ISC homeostasis is regulated by a wide range of signaling pathways, including Notch, JAK/STAT, Hippo, EGFR/Ras/MAPK, Wnt, JNK, the insulin pathway, and BMP/Dpp (reviewed by Miguel-Aliaga, 2018). The dynamic interplay between all these signalling pathways and any additional factors and feedback mechanisms is essential to maintain tissue homeostasis and misregulation of any of these components could give rise to tissue overproliferation or the depletion of the stem cell population (Yamashita et al., 2005; Doupé et al., 2018; Ma et al., 2019).

One of the main aims of this project was to characterize the regulatory mechanisms that control the expression of the 4 genes of interest studied here: SPARC. PLOD, TIMP and dlp. Data pertaining to this has been presented in the corresponding chapters, 3-6, where immunofluorescence approaches looked at the levels of active MAPK, SMAD and SAPK/JNK in the context of overexpression and knockdown of the proteins of interest in ISCs and EBs. Moreover, qRT-PCR of full-gut knockdowns of

SPARC and PLOD was used to complement this data, by analysing the effect of gene knockdown on known targets of several signaling pathways: Notch, JAK/STAT, JNK, MAPK/RTK, and Dpp.

In summary, SPARC was proposed to act upstream of Ras/MAPK signaling as a negative regulator of pathway activity, whereas SMAD/TGF-B activity was reduced in SPARC-overexpressing guts. PLOD levels positively correlated with SMAD, whereas Ras/MAPK could be negatively regulated by PLOD in the midgut, but results among the different RNAi lines were variable. Moreover, data suggested PLOD could be upstream of Notch, but additional replicates are necessary to establish the statistical significance of the changes observed. TIMP data suggests it is not found upstream of the Ras/MAPK signaling cascade, whereas dlp is, as the levels of active MAPK staining were significantly upregulated in dlp-overexpressing guts.

7.2. The regulation of stem cell secreted proteins

In the early stages of this project, initial attempts to elucidate which major signaling pathways regulated the expression of SPARC, PLOD, dlp and TIMP relied on the use of three overproliferation models of the *Drosophila* gut, to test whether overactivation of three key regulatory signaling pathways affected the expression levels of the proteins of interest. The three overproliferative models were obtained by: overactivation of a mutant form of the Ras protein, Ras^{V12}, a key component of the Ras/MAPK signalling pathway, which can in turn function as a fundamental effector of the EGFR pathway, which is the major driver of gut turnover; overxpression of Yorkie (Yki), a transcriptional activator whose function is repressed by Hippo signaling, which is essential for the maintenance of midgut homeostasis in the fly (Poernbacher et al., 2012); and overexpression of Unpaired-3 (Upd3), the major ligand of the JAK/STAT signaling pathway which, when activated, acts to control ISC division (Xu et al., 2011). These three genes were specifically overexpressed in stem and progenitor cells in the gut, using the 5961^{GS} driver. Immunofluorescence staining was used to validate each model was working as expected, and confirmed the hypothesis that their overexpression would drive proliferation in the gut.

7.3. Results

7.3.1 Overexpression of Ras^{V12}, Yorkie and Unpaired-3 drive overproliferation in the *Drosophila* gut

Immunofluorescence analysis demonstrated the hypothesis that overexpression of Ras^{V12} (*5961^{GS} > UAS-Ras85D.V12)*, Yorkie (*5961^{GS} > UAS-yki.S168A)*, and Upd-3 (*5961^{GS} > UAS-Upd3*) significantly increase proliferation in the *Drosophila* gut (*Figure 7.1*), as shown by the changes in the mitotic marker phospho-histone-3 (PH3). This increase was consistent across all three overproliferative models.

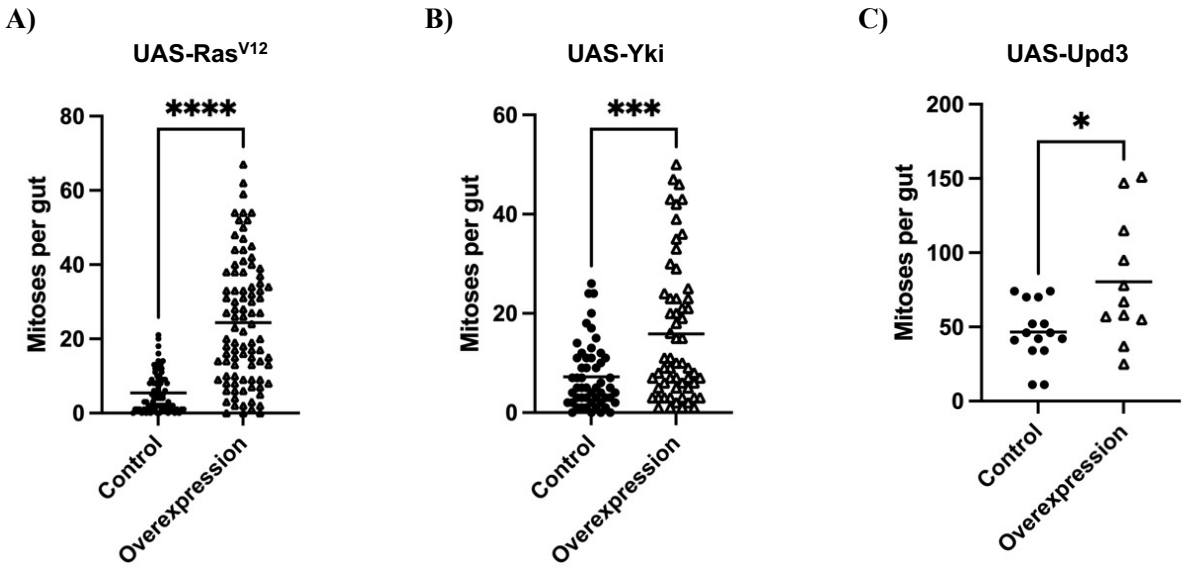

Figure 7.1 . Overproliferative models of the *Drosophila* gut. Overexpression of Ras^{V12} (*5961^{GS} > UAS-Ras^{V12}*) increases proliferation in the gut tissue ($p < 0.0001$) (control n = 77, OE = 91) (***A***). Overexpression of Yorkie (Yki) *(5961^{GS} > UAS-Yki*) increases the number of mitotic cells in the gut ($p = 0.0005$) (control n = 53, OE = 59) (***B***). Overexpression of the JAK/STAT ligand Upd3 (*5961^{GS} > UAS-Upd3*) increases the number of proliferative cells in the *Drosophila* gut ($p = 0.001$) (control n = 15, OE = 11) (C). All data was normally distributed, so unpaired t-tests were used for statistical analysis. Each data point represents one whole gut.

7.3.2. Changes in expression levels of SPARC, PLOD, TIMP and dlp in oveproliferative models of the *Drosophila* gut

qPCR analysis of whole gut samples was carried out to analyse any changes to the expression levels of the genes of interest when each signalling pathway was overactivated in stem and progenitor cells. The hypothesis was that if the overactivated signalling pathway regulates any of the proteins of interest, its levels should be significantly affected: an increase would be expected if the pathway positively regulates gene expression, or a proportional decrease in RNA levels should be observed if the pathway negatively regulates gene expression.

Overactivation of the Ras^{V12} protein did not yield any significant results regarding expression of SPARC, PLOD, TIMP or dlp (*Figure 7.2*). PLOD levels are increased, indicating that perhaps Ras/MAPK controls its expression in stem and progenitor cells, but this change is not statistically significant. On the contrary, Timp levels are decreased when Ras/MAPK is overactivated, hence raising the possibility that Ras/MAPK is a negative regulator of TIMP expression but these changes were not statistically significant. In summary, we can conclude that Ras/MAPK signaling is not the main regulator of the expression of these 4 genes in stem and progenitor cells in the *Drosophila* gut. The extent of its role in PLOD and TIMP expression remains to be uncovered, and further experiments are needed to get a clear picture of the role of Ras/MAPK in controlling their expression.

Similarly, overactivation of Yorkie showed no significant change in SPARC and PLOD expression (*Figure 7.3A-B*). There was a highly increasing trend in the expression of Timp when Hippo was overactivated but this change was not statistically significant ($p = 0.05$) (*Figure 7.3C*). This result indicates that Timp expression in ISCs/EBs could be directly regulated by Hippo signalling, but further experiments are needed to clarify the significance of these results. The extent of this regulation and how key Hippo is for appropriate Timp expression in the gut still remains unanswered. Dlp levels remained unchanged between Yki-overexpressing guts and controls (*Figure 7.3D*).

Overactivation of JAK/STAT signaling led to a significant increase in SPARC expression ($p = 0.001$) (*Figure 7.4A*), indicating that this signaling pathway may positively regulate with SPARC expression. PLOD and TIMP expression also showed an increase in Upd3-overexpressing guts, but these changes were not statistically significant

(*Figure 7.4B-C*). No data is available for dlp, as the primer pairs showed formation of primer dimers upon validation.

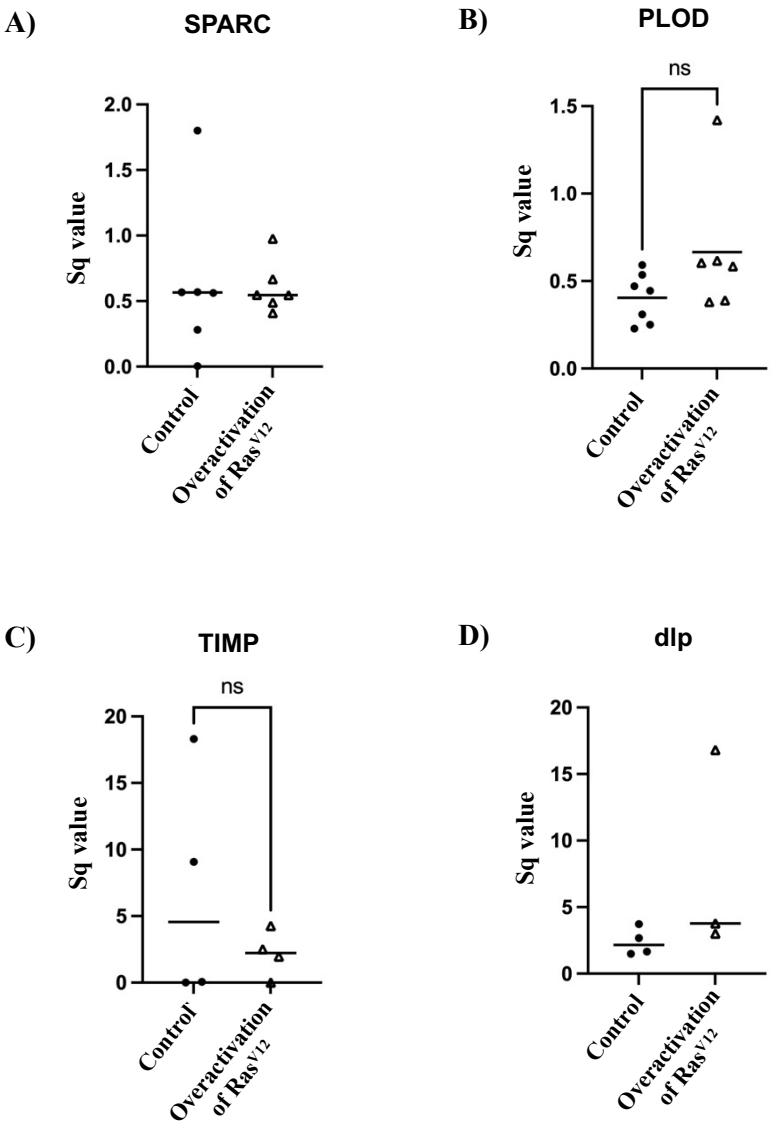

Figure 7.2. Expression changes of SPARC, PLOD, TIMP and dlp in the guts overexpressing Ras^{V12}. Overactivation of the Ras/MAPK signaling pathway (*5961^{GS} > UAS-Ra^{V12}*) does not significantly affect the levels of SPARC (control n = 5, OE n = 6) (***A***), PLOD (p = 0.1) (n = 7) (***B***), TIMP (p = 0.3) (n = 4) (***C***) or dlp (control n = 4, OE n = 3) (***D***). Unpaired t-test were used for statistical analysis of normally-distributed data (A, C, D), and non-parametric Mann Whitney-U tests were used for non-normally distributed data sets (B) Each data point represents one sample and each sample contains 10 whole female guts. OE stands for overexpression/overactivation.

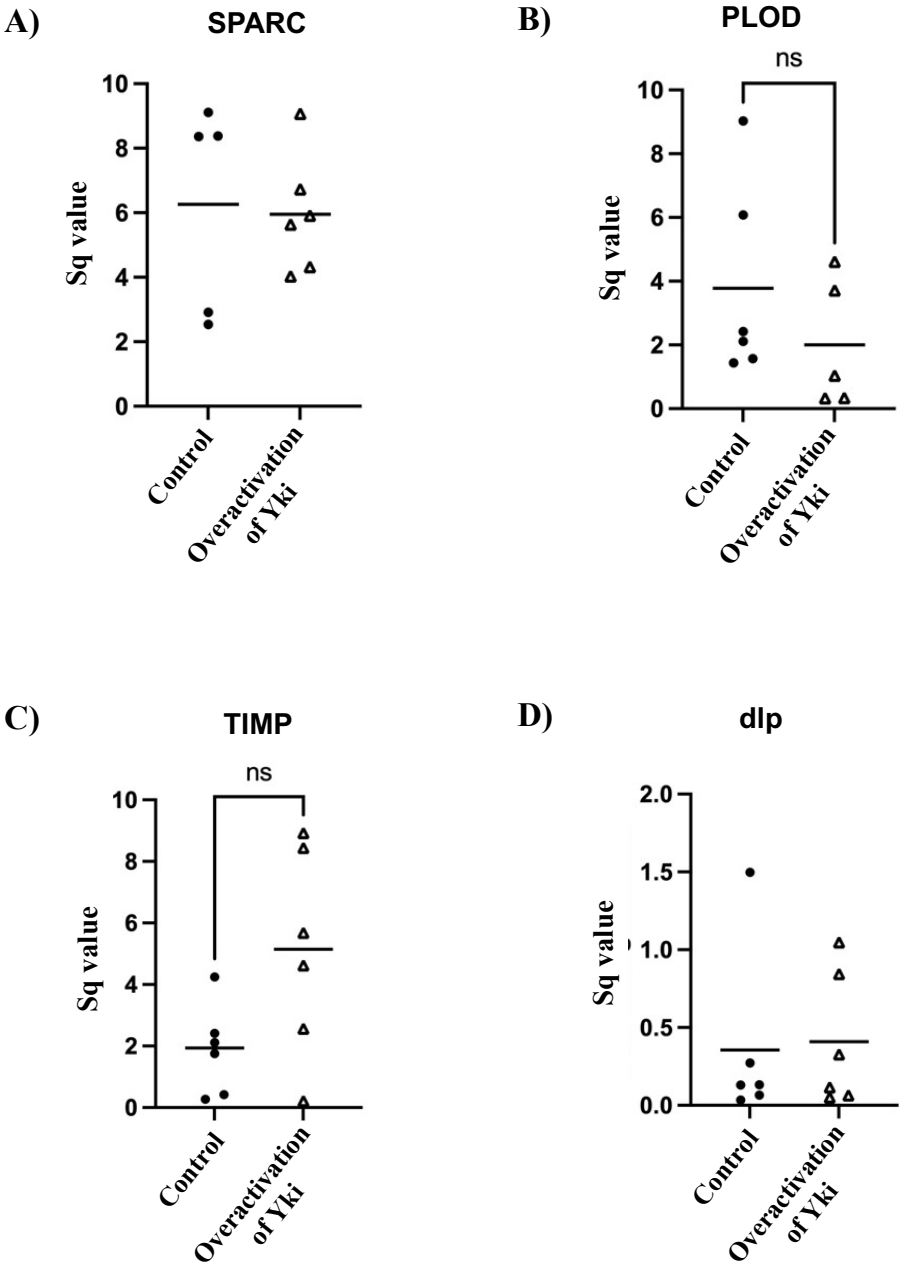

Figure 7.3. Expression changes of SPARC, PLOD, TIMP and dlp in the guts overexpressing Yorkie. Overactivation of the Hippo signaling pathway (*5961^{GS} > UAS-Yki*) does not significantly affect the levels of SPARC (control n = 5, OE n = 6) (***A***), PLOD (p = 0.3) (control n = 6, OE n = 5) (***B***), TIMP (p = 0.05) (n = 6) (***C***) or dlp (n =6) (***D***). Unpaired t-test were used for statistical analysis of normally-distributed data (B, C, D), and non-parametric Mann Whitney-U tests were used for non-normally distributed data sets (A) Each data point represents one sample and each sample contains 10 whole female guts. OE stands for overexpression/overactivation.

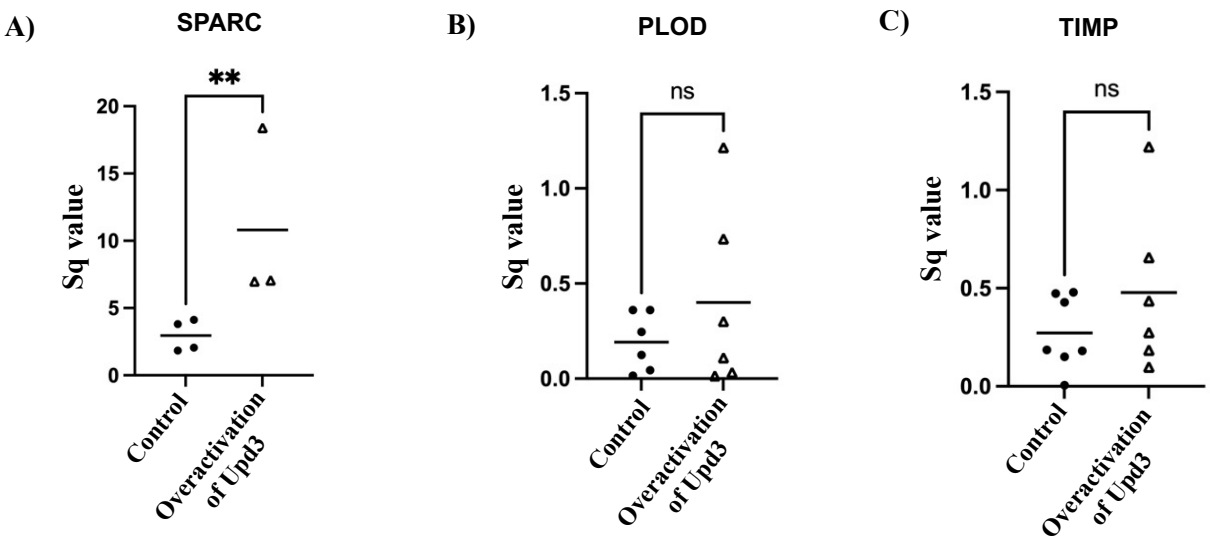

Figure 7.4. Expression changes of SPARC, PLOD, and TIMP guts with overactive JAK/STAT signaling. Overactivation of the JAK/STAT signaling pathway (*5961^{GS} > UAS-Upd3*) significantly increases SPARC expression levels (p = 0.001) (control n = 4, OE n = 3) (***A***)**.** PLOD levels show a small increase with Upd3 overactivation but changes are not statistically significant (p = 0.3) (n = 6) (***B***). TIMP expression slightly increases with overactivation of JAK/STAT signaling, but changes are not statistically significant (p = 0.2). (control n = 7, OE n = 6) (***C***). Unpaired t-test were used for statistical analysis of normally-distributed data (B, C), and non-parametric Mann Whitney-U tests were used for non-normally distributed data sets (A) Each data point represents one sample and each sample contains 10 whole female guts. OE stands for overexpression/overactivation.

7.3.3. Expression changes of other stem cell-specific secreted proteins

SPARC, PLOD, Timp and dlp were just 4 of the hits identified by Doupé and colleagues as stem and progenitor cell-specific secreted proteins. In the early stages of this project, I wanted to determine if there were any other hits from this original study that could complement the characterization of SPARC, PLOD, Timp and/or dlp, i.e. if among the other hits that have known mammalian orthologs, there were any proteins working alongside them. Since the main aim of the project is to elucidate how stem cell-derived signals could be involved in the misregulation and proliferation of ISCs, and how these stem cell-derived proteins could be contributing to the maintenance of the niche, parallel work attempted to test whether the broader set of genes may be regulated by some of the fundamental proliferative pathways and may warrant further study in the future. In order to do this, some of these other hits were also studied in the context of the three

overproliferative models presented in this chapter. The hypothesis was that, if the stem cell-specific genes are regulated in a similar manner and prior evidence in the literature has established akin functions between them, perhaps the proteins are working in consonance or can be found upstream/downstream of each other in the signalling cascades. qRT-PCR samples of all three overproliferative models were analysed using primers targeting the following genes: laminin A, B1 and B2 (*LanA*, *LanB1* and *LanB2*); midkine pleiotrophin 1 and 2 (*miple1* and *miple2*); Niemann-pick type C 2a (*Npc2a*); Thioester-containing protein 4 (*Tep4*); the germline stem cell regulator *magu*; transferrin 2 (tsf2); brainiac (*brn*); and perlecan (*tro1*). All primers were validated using a wild-type standard sample. No data is available for trol, as the primers presented the formation of primer dimers when tested in wild-type flies.

Overexpression of Ras/MAPK signaling significantly increases the expression of miple2 ($p = 0.01$), brn ($p = 0.01$), magu ($p = 0.02$) and all three of the laminins, LanA ($p = 0.04$), LanB1 ($p = 0.005$), and LanB2 ($p = 0.03$) (*Figure 7.5A-C, D, H, J*). Tep4 and Npc2a levels are also increased, but these change are not statistically significant (*Figure 7.5F-G*). The expression levels of miple1 and tsf2 were maintained in Ras^{V12}-overexpressing guts compared to controls (*Figure 7.5D and I*). Taken together, these results show that Ras/MAPK regulates laminin, miple2, magu and brn expression in the *Drosophila* gut.

Overactivation of Yorkie leads to increased levels of the laminins LanA and LanB1, miple1 and 2, Npc2a and brn (*Figure 7.6A-B, C-D, F, H*). On the contrary, levels of Tep4 are decreased (*Figure 7.6G*), and there is no effect on LanB2 expression (*Figure 765C)*. Overeactivation of Yki had no significant effect on any of these proteins, but the trends observed hint to a potential regulatory role of Yki on these stem cell-specific proteins. No data is available for magu and tsf2 in this overproliferative model.

And lastly, overactivation of JAK/STAT signalling significantly increases the levels of laminin A ($p= 0.01$) (*Figure 7.7A*), and although increases in the levels of LanB1, LanB2, miple1, Tep4, Npc2a and magu were also observed (*Figure 7.7B-D, F-H*), these were not statistically significant. Interestingly, miple2 levels have a decreasing trend in overactive JAK/STAT (*Figure 7.7E*). The levels of brainiac (brn) were maintained in the overproliferative model compared to control guts (*Figure 7.7I*). No data is available for tsf2 expression changes in this model.

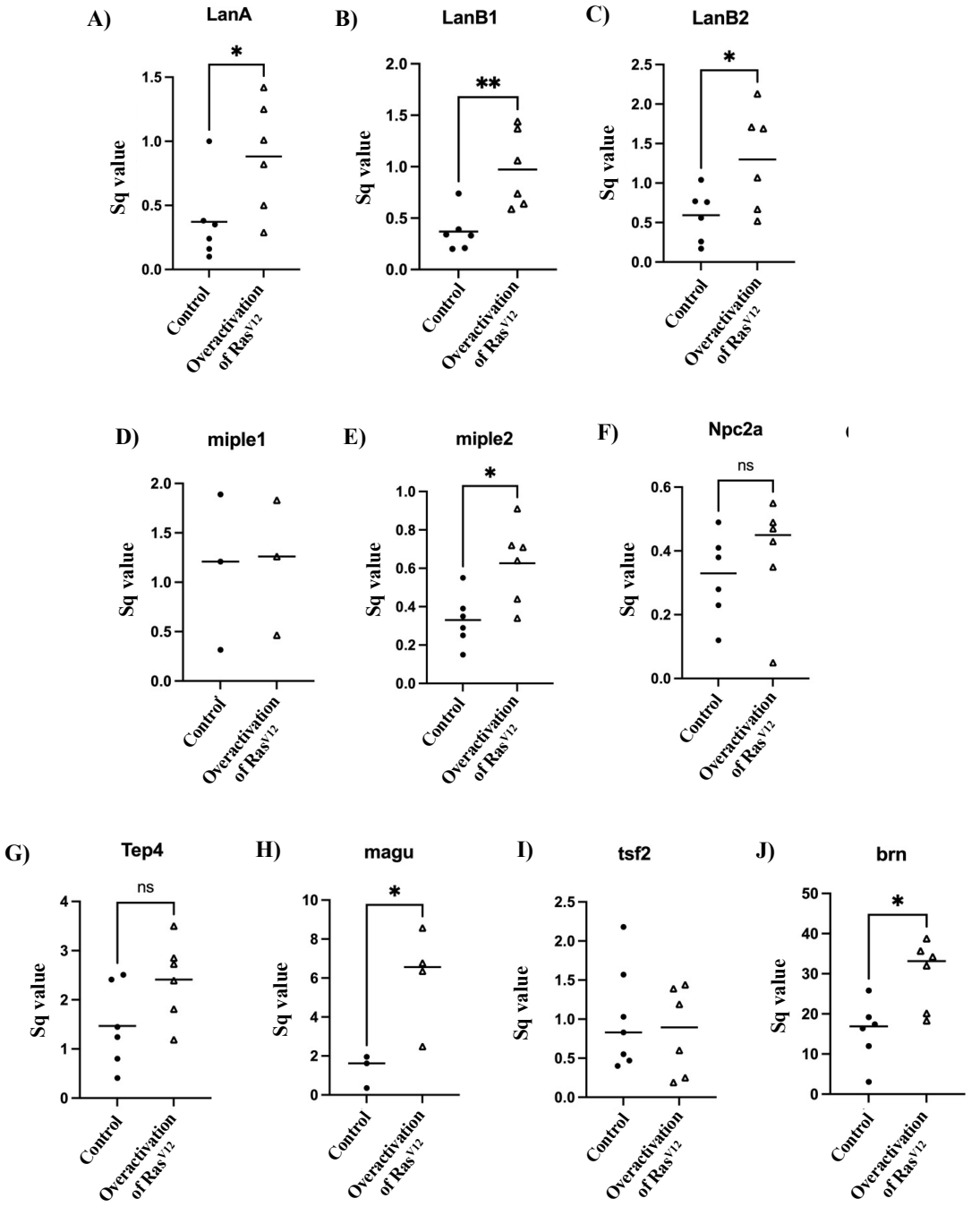

Figure 7.5. Expression changes of ISC/EB-specific secreted proteins in RasV^{12} overactivated guts. qPCR analysis of the expression levels of stem cell-specific proteins in guts with overactive Ras^{V12} signaling pathway (*5961^{GS} > UAS-Ras^{V12}*). Overaction of the Ras/MAPK pathway significantly increases the levels of LanA (p = 0.04) (***A***), LanB1 (p = 0.005) (***B***), LanB2 (p = 0.03) (***C***), miple-2 (p = 0.01) (***E***), magu (p = 0.02) (***H***), and brn (p = 0.01) (***J***). Npc2a levels (F) and Tep4 levels (***G***) show increasing trends but these changes are not statistically significant (p = 0.4 and p = 0.07, respectively). The levels of miple 1 (***D***) and tsf2 (***I***) remain unchanged. n = 6 for all samples. Unpaired t-test were used for statistical analysis of normally-distributed data (A-C, E-J), and non-parametric Mann Whitney-U tests were used for non-normally distributed data sets (D) Each data point represents one sample and each sample contains 10 whole female guts.

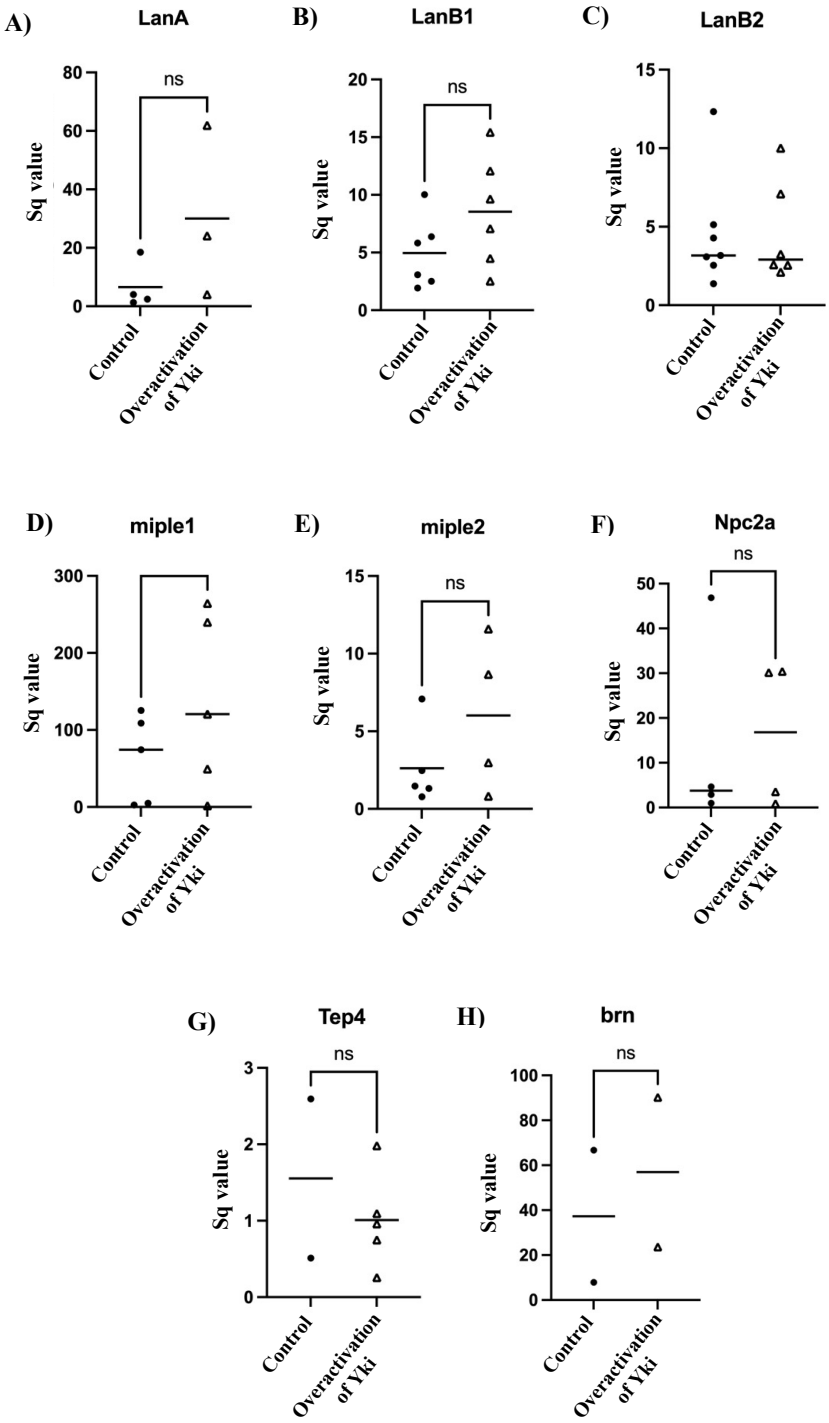

Figure 7.6. Expression changes of ISC/EB-specific secreted proteins in Yki overactivated guts. qPCR analysis of the expression levels of stem cell-specific proteins in guts with increased Hippo pathway activity (*5961^{GS} > UAS-Yki*). Overactivation of Yki increases the levels of LanA (p = 0.1) (control n = 4, OE n = 3) (***A***), LanB1 (p = 0.1) (n = 6) (***B***), miple-1 (p = 0.2) (n = 5) (***D***) miple-2 (p = 0.2) (control n = 5, OE n = 4) (***E***), Npc2a (p > 0.9) (n = 4) (***F***) and brn (p = 0.7) (***H***). Tep4 levels (***G***) show a decreasing trend but this change is not statistically significant (p = 0.4) (control n = 2, OE n = 5). The levels of LanB2 (***C***) remain unchanged (control n = 7, OE n =63) . Unpaired t-test were used for statistical analysis of normally-distributed data (B, D), and non-parametric Mann Whitney-U tests were used for non-normally distributed data sets (A, C, E, F, J) Each data point represents one sample and each sample contains 10 whole female guts. OE stands for overexpression/overactivation.

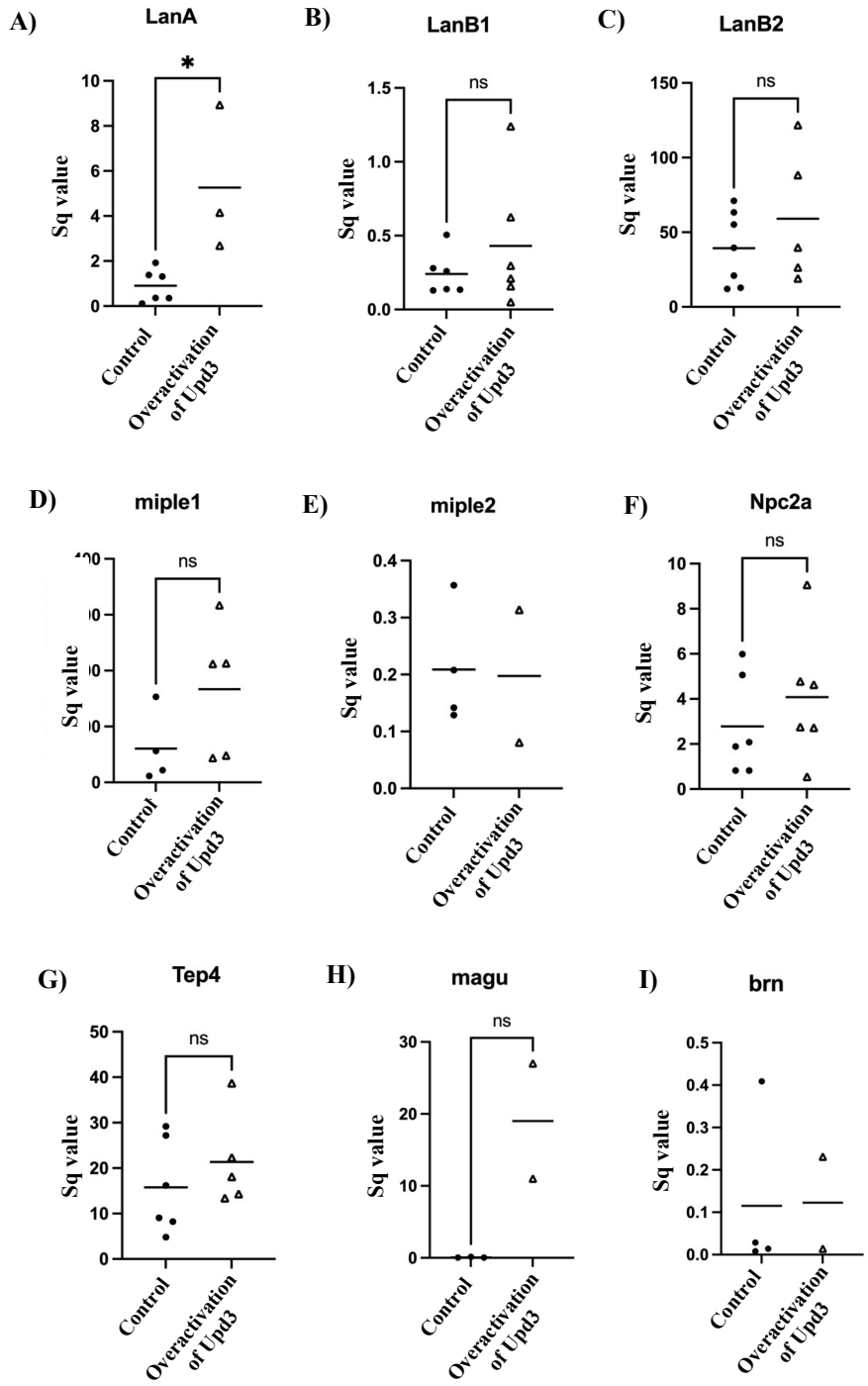

Figure 7.7. Expression changes of ISC/EB-specific secreted proteins in Upd3 overactivated guts. qPCR analysis of the expression levels of stem cell-specific proteins in guts with increased JAK/STAT pathway activity (*5961^{GS} > UAS-Upd3*). Overactivation of Upd-3 leads to a significant increase of LanA expression (p = 0.01) (control n = 6, OE n = 3) (***A***). The levels of LanB1 (p = 0.3) (n = 6) (***B***), Lan B2 (p = 0.3) (control n = 7, OE n = 5) (***C***), miple-1 (p = 0.1) (control n = 4, OE n = 5) (***D***), Npc2a (p = 0.4) (n = 6) (***F***), Tep 4 (p = 0.3) (control n = 6, OE n = 5) (***G***) and magu (p = 0.05) (control n = 3, OE n = 2) (***H***) all show increasing trends, but the changes are not statistically significant. Expression of miple-2 (***E***) and brn (***I***) remain unchanged (control n = 4, OE n = 2). Unpaired t-test were used for statistical analysis of normally-distributed data (A, B, C, D, F, G, H,I), and non-parametric Mann Whitney-U tests were used for non-normally distributed data sets (E) Each data point represents one sample and each sample contains 10 whole female guts. OE stands for overexpression/overactivation.

7.4. Discussion and conclusions

In conclusion, these experiments show that JAK/STAT signaling is important in the regulation of SPARC expression and that this pathway, alongside Hippo and Ras/MAPK signaling, play varying roles on the regulation of the other proteins studied in this project. SPARC has been shown to interact with STAT3 by regulating the phosphorylation of the transcription factor in vitro (Bhoopathi et al., 2011), where it acts to control the expression of neuronal markers and induce cell cycle arrest in tumour cells (Chetty et al., 2011). In the context of the *Drosophila* gut, JAK/STAT signalling in ISCs is activated to control stem cell division (Xu et al., 2011), but data suggests that in this tissue, JAK/STAT is part of a wider signaling cascade, which encompasses Notch, Wg Hh and EGFR, in order to maintain tissue homeostasis (Lin et al., 2009; Lin et al., 2010; Xu et al., 2011). Hippo, Ras/MAPK and JAK/STAT have all been shown to interact in the *Drosophila* midgut, where p38-MAPK activation regulates the expression of the unpaired ligands through Hippo, TGF-β and Dpp signaling (Houtz et al., 2017).

One limitation of these experiments were the reduced number of independent replicates available, compared to the rest of the data presented in this thesis. In some cases, this limited the statistical analysis of the data and prevented the establishment of reliable conclusions. Moreover, the sample preparation differs from later work, as the RNA extraction and cDNA synthesis were not done using readily-available kits, which increases the changes of variability in the data. Future experiments should look to expand on this and compare these results with the effects of overexpressing Ras^{V12}, Yki and Upd3 in all gut cells and not just in ISC/EB cells, since some of the results presented in this thesis show the potential expression of the genes of interest in differentiated cells and not in ISCs and EBs.

The most striking results obtained from this data were the changes in laminin expression in all three of the overproliferative models. Laminins highly conserved molecules that play key roles in the regulation of basement membrane assembly and morphogenesis (Urbano et al., 2009). Disruption of the laminin network has been described as a consequence of SPARC mutations in embryos (Martinek et al., 2008), although no SPARC has not been shown to directly affect laminin deposition in the BM (Morrissey et al., 2016). Laminins have been shown to bind to collagen IV and perlecan (trol in *Drosophila*), one of the other stem cell specific hits studied here, suggesting potential interactions between some of these ISC secreted proteins. Moreover, some

studies have looked at the relationship between PLOD, collagen and the laminin network in the fly (Ke et al., 2018). There is also a potential link between TIMP and dlp with laminins (Broadie et al., 2011; Sun et al., 2021), as both TIMP and dlp play critical roles in the maintenance of the ECM in the fly, suggesting that laminins in the *Drosophila* gut might be part of a network that acts to ensure tissue homeostasis and that SPARC, PLOD, dlp and TIMP could be found within this network. However, ongoing work in the group is already focusing on the in-depth study of these proteins in the *Drosophila* gut, and thus no further work was carried out as part of this project. No other conclusive results were obtained and thus further experiments are needed to elucidate the concrete regulatory mechanism for SPARC, PLOD, TIMP and dlp in the stem and progenitor cells of the *Drosophila* gut. The regulatory network that control homeostasis of the *Drosophila* gut is extensive, with many components and pathways working in consonance for tissue maintenance. Thus, the elucidation of a clear control mechanism for SPARC, PLOD, TIMP and dlp is a challenging feat, since the pool of other proteins and pathways with the ability to compensate for the misregulation of one another is large. Since no further conclusions have been drawn from these initial attempts to characterize the signaling pathways the genes of interest are involved in, the relevant discussion on the significance of these results in the framework of published data and the rest of the data sets presented in this thesis can be found in the relevant chapters for each gene.

Chapter 8

Conservation of SPARC, PLOD, TIMP and dlp expression in mammalian tissues

8.1. Introduction

As mentioned in Chapters 3-6, there is extensive evidence in the literature that demonstrates that misregulation of the mammalian orthologs of SPARC, PLOD, Timp and dally-like protein (dlp) plays important roles in the formation and development of epithelial tumours (Uhlirova and Bohmnann, 2006; Patel and Edgar, 2014; Liu et al., 2020; Munir et al., 2020; Gao et al. 2021; Gong et al., 2022). However, no studies have shown a direct comparison between results obtained from the study of these genes in the *Drosophila* gut and their conservation in mammalian models in vitro. In order to determine the translational application of the results obtained from the study of these genes in the *Drosophila* midgut, the final aim of this project was to determine if their expression pattern was conserved in mammalian tissues, using three-dimensional spheroid models and tissue samples from human patients. This would imply a potential conservation in function, and would provide additional suitable models to study the function of SPARC, PLOD, dlp and TIMP. There is only one SPARC protein in mammals, but the most closely related mammalian orthologs for *Drosophila* PLOD, Timp and dlp were PLOD3, TIMP1 and glypican-4 (GPC4), respectively, based on DIOPT scores and the range reagents available for their study.

8.2. Results

8.2.1. Analysis of SPARC, PLOD, TIMP and dlp expression using definitive endodermal spheroids

Three-dimensional definitive endodermal (DE) spheroids from iPSCs were generated and treated to induce endodermal differentiation, since the epithelial lining of the gut tissue arises from the endoderm during development. In particular, the midgut section of the *Drosophila* gut is the only one with endodermal origin, whereas the foregut and the hindgut arise from the ectoderm (as reviewed by Miccheli, 2012). Spheroids were imaged and measured at days 0, 1, 3 and 5 of treatment to monitor their growth (*Figure 8.1A*). Spheroid growth was quantified as length and area at each timepoint (*Figures 8.1B and 8.1C*). At day 5, samples were embedded in parafinn blocks which were then sectioned and analysed using immunohistochemical (IHC) and immunofluorescent (IF) approaches. Moreover, 10 spheroids were processed for RNA extraction and cDNA synthesis for qPCR analysis.

The immunohistochemical and immunofluorescence analysis of the 3D spheroid models did not yield any results. Time constraints meant no more than one replicate was possible for each experiment presented in this chapter and thus, the data available is limited. Moreover, due to their small size, the handling and sectioning of these samples requires extensive training and expertise, which hindered the sample preparation and the acquisition of data even further.

Reverse-transcriptase quantitative PCR (RT-qPCR) analysis of 3D spheroid samples was performed to determine if there were any changes in SPARC, PLOD3, TIMP1 and GPC4 RNA levels when endodermal differentiation was induced compared to controls. An androgen-sensitive human prostate adenocarcinoma cell line, LNCaP, which has a high level of expression of all genes of interest, was used to test the different primer pairs. All results presented here are normalized against the ribosomal protein RPL13a. When tested in LNCaP cells, all SPARC primers presented non-specific amplification and PLOD3 primers resulted in the formation of primer-dimers. Thus no spheroid data is available for these two genes. GPC4 levels were increased upon endodermal differentiation of the 3D iPSC spheroid (*Figure 8.2A*), whereas TIMP1 levels were maintained compared to controls (*Figure 8.2B*). However, results showed positive

expression of TIMP1, which correlates with results from the *Drosophila* model that demonstrate expression of the protein in the epithelium.

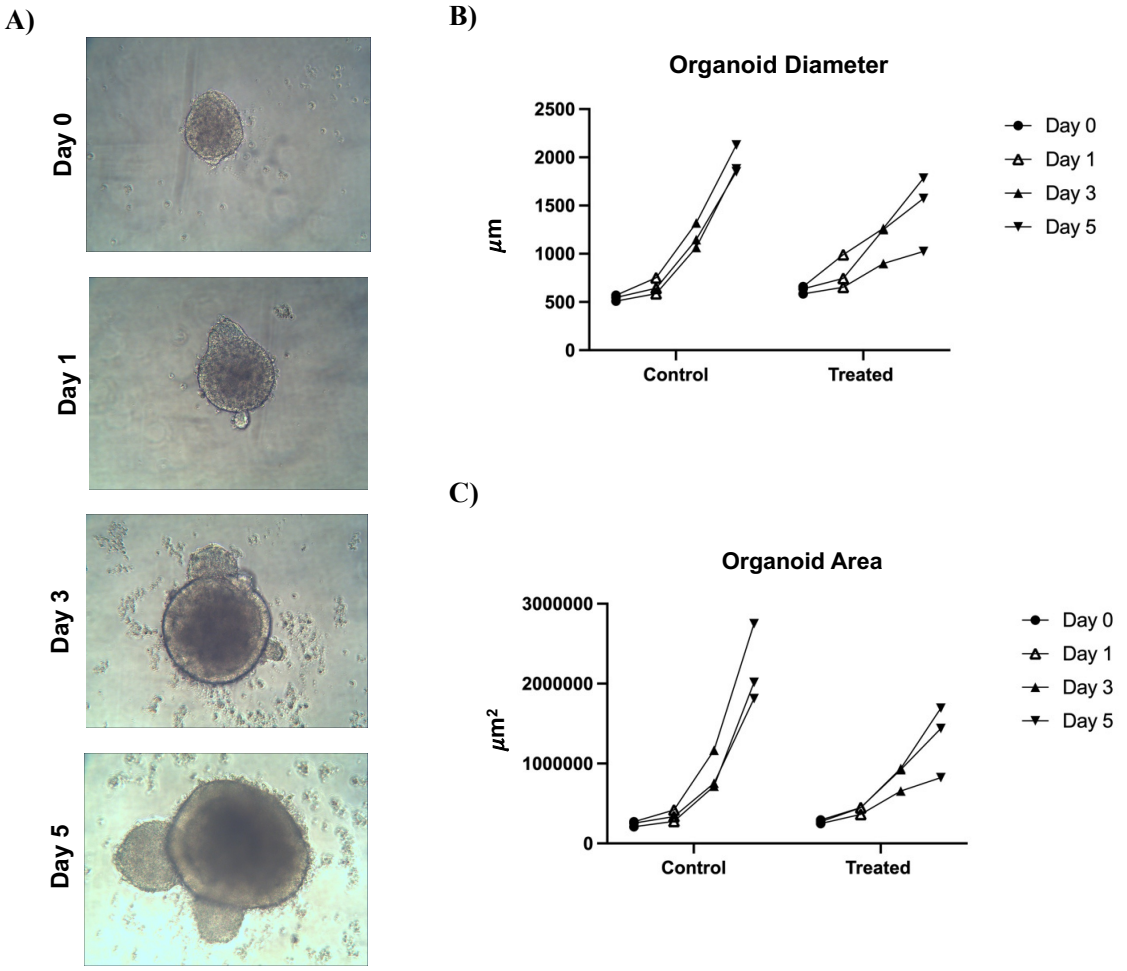

Figure 8.1. Generation of 3D endodermal spheroids. Organoid growth from days 0-5 of treatment for endodermal differentiation induction (***A***). Increase in organoid diameter from day 0 to day 5 in control ($p < 0.0001$) and treated spheroids ($p = 0.0003$) (***B***). Increase in organoid area from day 0 to day 5 in control ($p < 0.0001$) and treated spheroids ($p = 0.0008$) (***C***). Each data point represents one spheroid.

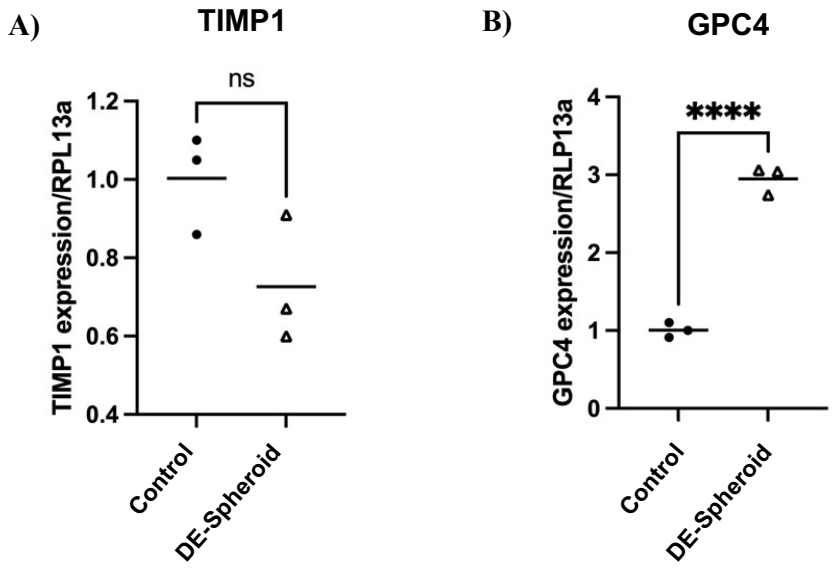

Figure 8.2. Expression changes of TIMP1 and GPC4 in spheroid samples. TIMP expression does not change upon the induction of endodermal differentiation when compared to control spheroid expression ($p = 0.08$) (***A***). GPC-4 significantly increases in endodermal spheroids compared to controls ($p < 0.0001$) (***B***). Each data point represents one replicate.

8.2.2. Analysis of SPARC, PLOD, TIMP and dlp expression using human prostate tissue samples

IHC was carried out on formalin-fixed paraffin embedded (FFPE) tissue slides of human samples to observe the expression pattern of the four proteins of interest in human tissue. One benign prostatic hyperplasia (BPH) control tissue sample (#11972) was compared to two localized prostate cancer patient samples (#12872 and #12910).

In BPH controls, SPARC is found in the cytoplasm of the epithelial gland cells and in basal cells, and there is some SPARC expression in the stroma of the tissue (*Figure 8.3*). Interestingly, in some cells, SPARC expression localizes to the nucleus. In the localized prostate tissue samples, SPARC expression in the nucleus seems to have increased (*Figure 8.4*), and although still expressed in epithelial cells in sample #12910, tissue organization in sample #12782 has been lost, making the differentiation of the cell types complicated (*Figure 8.3*).

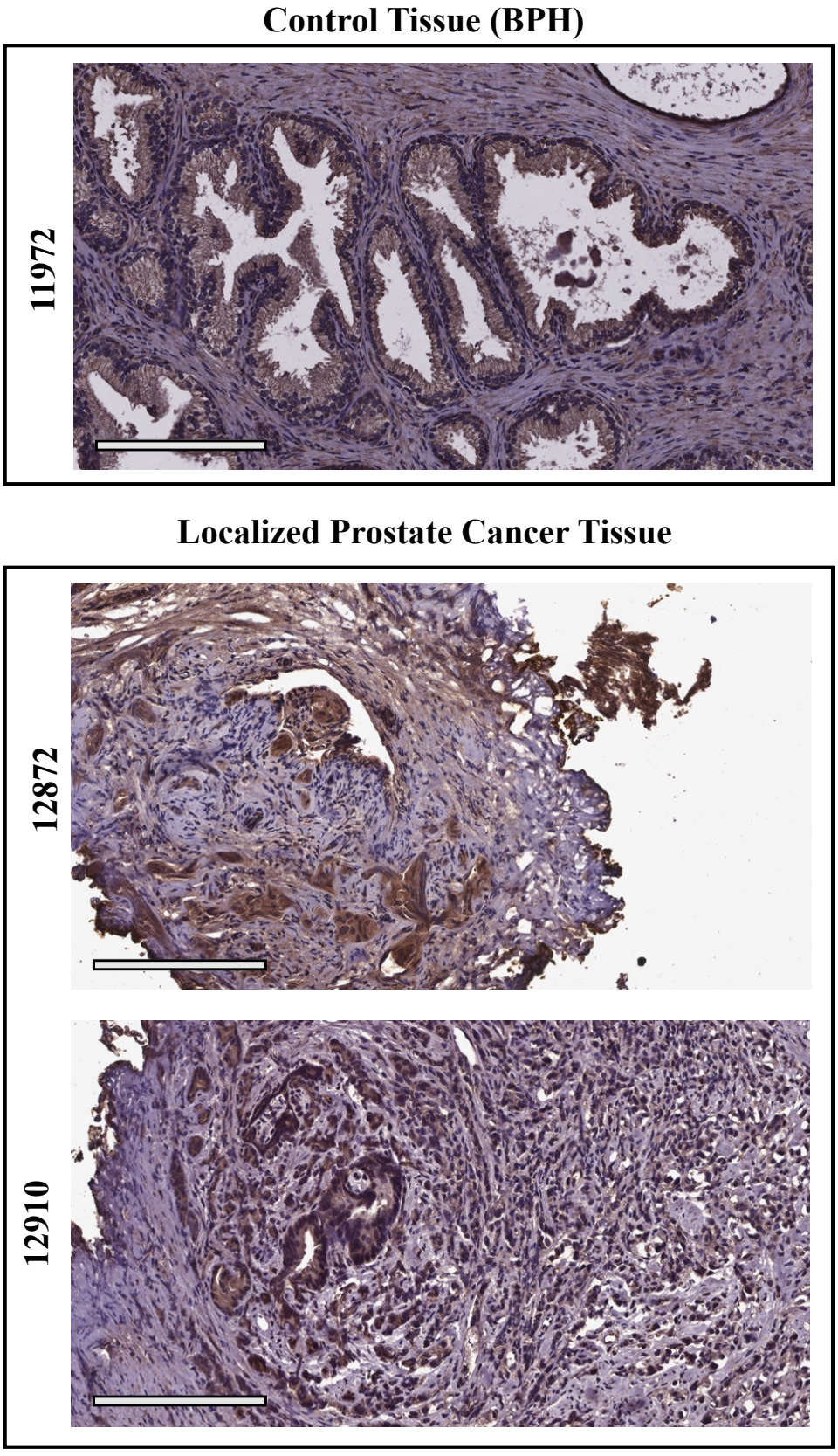

Figure 8.3. IHC analysis of SPARC expression in control and localized prostate cancer patients samples. Samples were stained with α-SPARC (1:50). Scale bars in the bottom left corner represent 200μm.

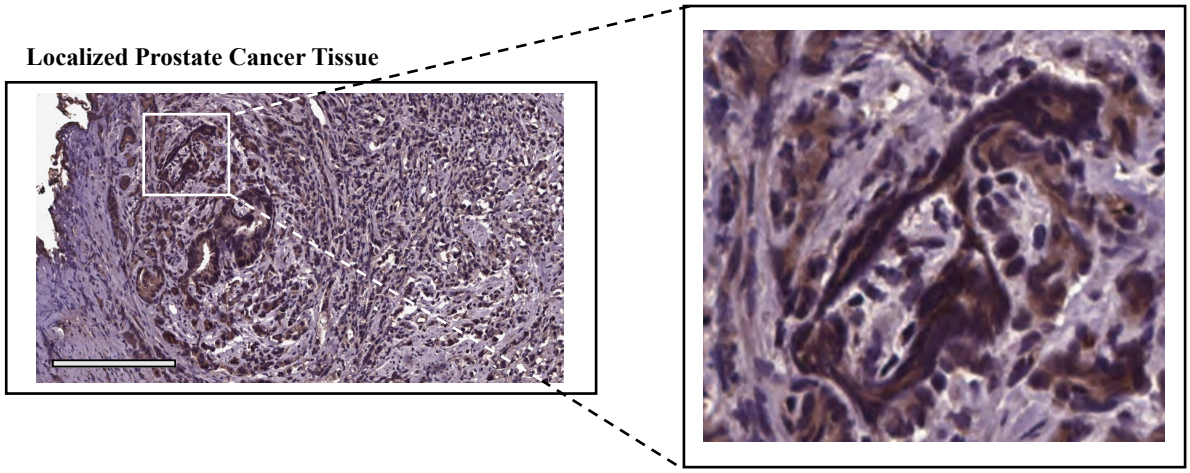

Figure 8.4. Nuclear SPARC expression in localized prostate samples. Enhanced images of SPARC staining in localized prostate cancer samples show high levels of SPARC expression in the nucleus of epithelial cells. Lower levels of nuclear expression were also observed in BPH controls. Scale bars in the bottom left corner represent 200μm.

PLOD3 is highly expressed in the basal cells in control prostate tissue, as well as in the cytoplasm of the epithelial cells and in the stroma surrounding the tissue (*Figure 8.5*). In prostate cancer samples, cytoplasmic expression seems to be conserved compared to controls, with PLOD3 accumulation in basal cells (*Figure 8.5*). This increase in PLOD3 staining intensity could also represent an increase in PLOD3 in the basement membrane of the epithelial cells. Interestingly, PLOD3 seems to localize to the nucleus in prostate cancer samples, whereas its expression in the control tissue samples is exclusively cytoplasmic in the epithelial and basal cells of the prostate glands (*Figure 8.6*).

TIMP1 expression is not as pronounced as the other proteins of interest, with most of the expression localizing to the cytoplasm of epithelial and basal cells, and some expression in the stroma (*Figure 8.7*). Some nuclei in the BPH control express low levels of TIMP1, and this seems to be increased in localized prostate (*Figure 8.8*). Overall, the levels of TIMP1 expression do not present any striking changes in localized prostate cancer compared to the hyperplastic prostate control.

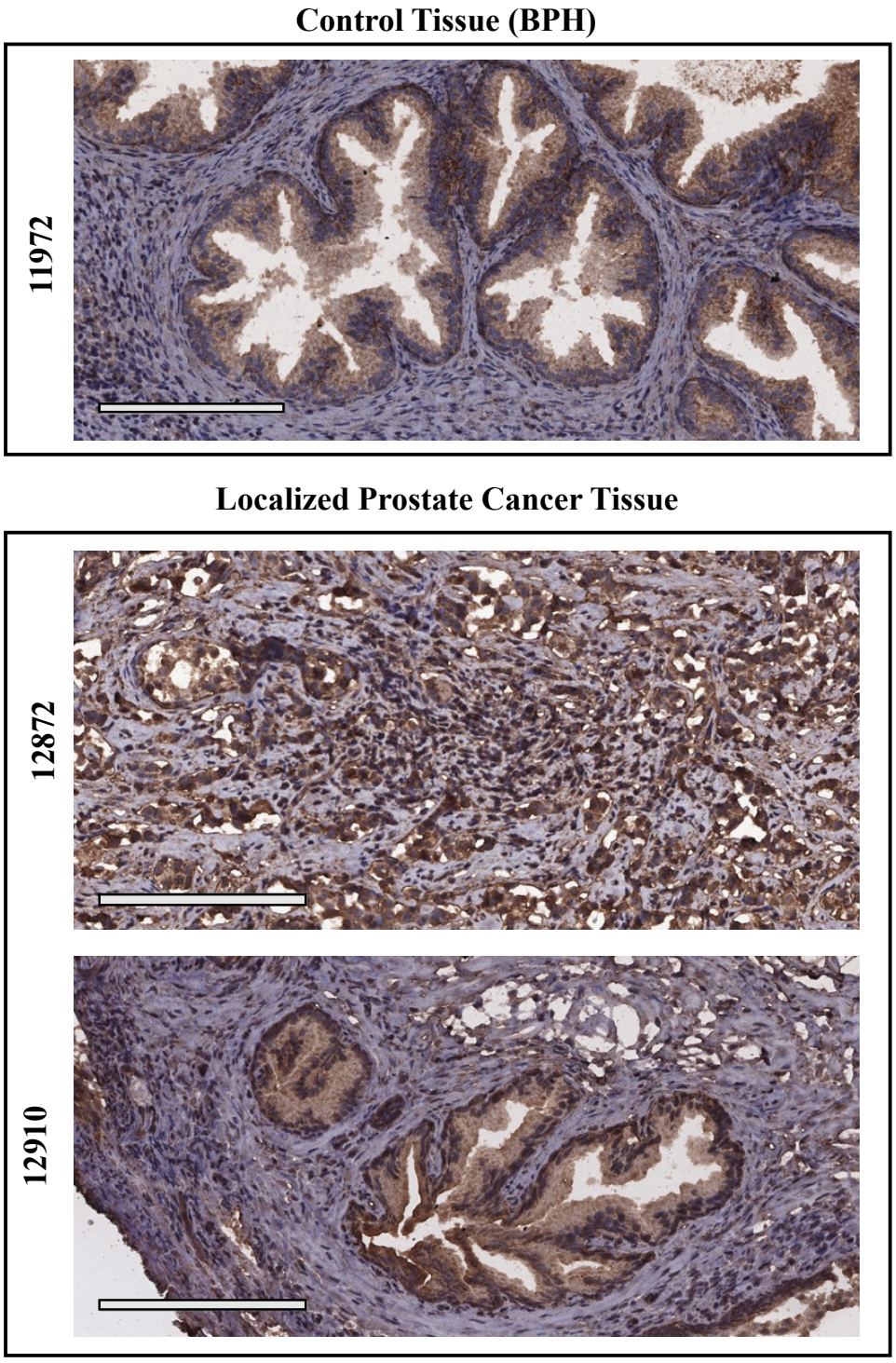

Figure 8.5. IHC analysis of PLOD3 expression in control and localized prostate cancer patients samples. Samples were stained with α- PLOD3 (1:50). Scale bars in the bottom left corner represent 200μm.

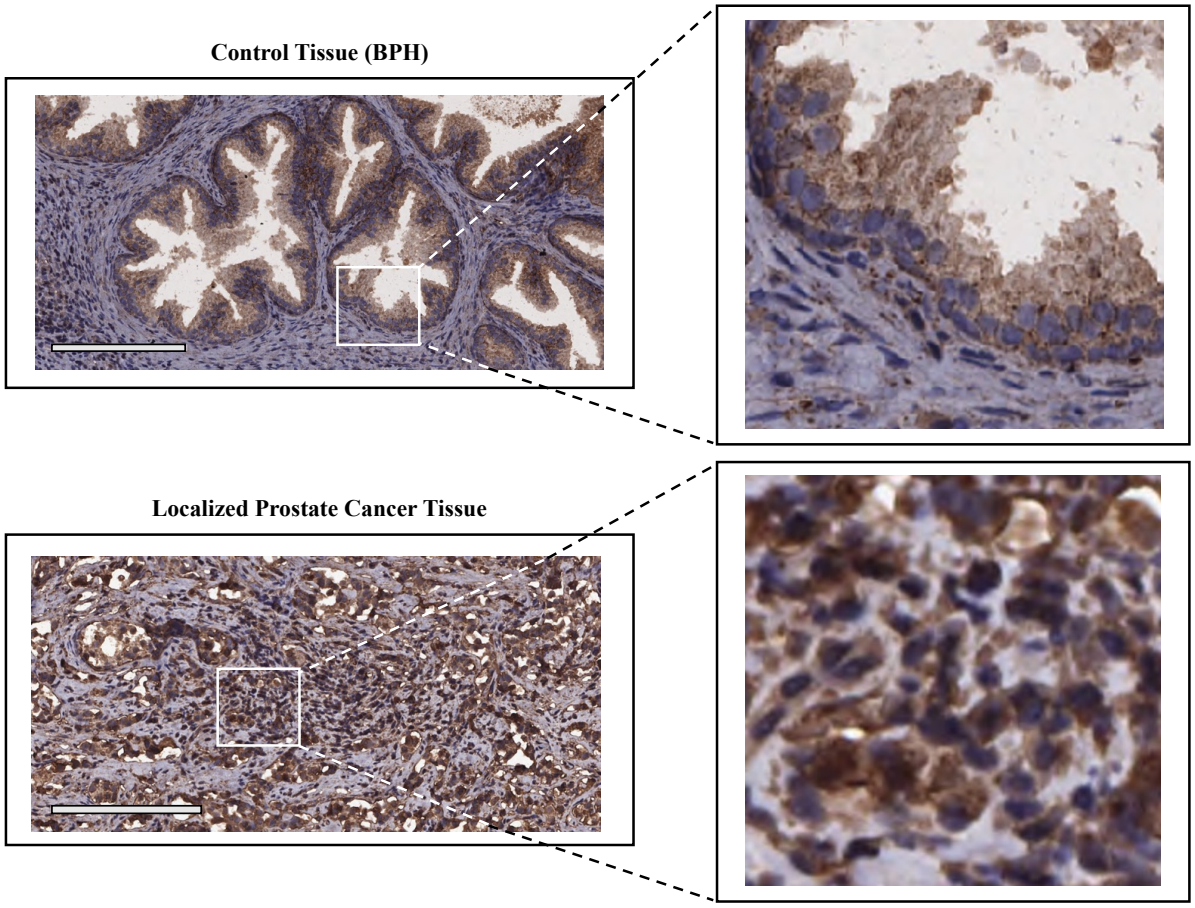

Figure 8.6. Nuclear expression of PLOD3 in control and localized prostate patient tissue samples. Enhanced images of IHC analysis show translocation of PLOD3 expression to the cell nucleus in cancer tissue samples. No PLOD3 staining in nuclei was observed in BPH controls. Scale bars in the bottom left corner represent 200μm.

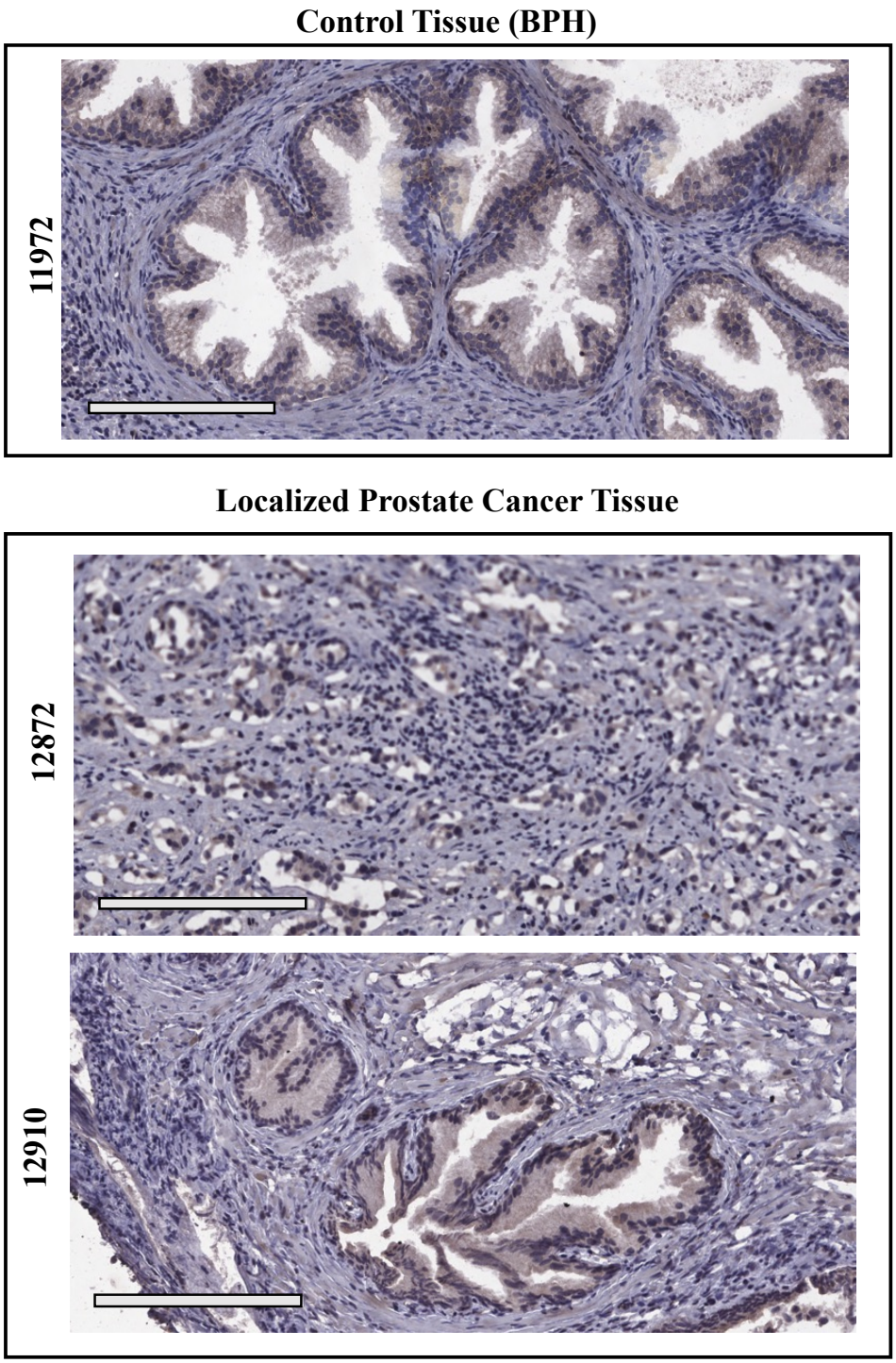

Figure 8.7. IHC analysis of TIMP1 expression in control and localized prostate cancer patients samples. Samples were stained with a α-TIMP1 (1:50). Scale bars in the bottom left corner represent 200μm.

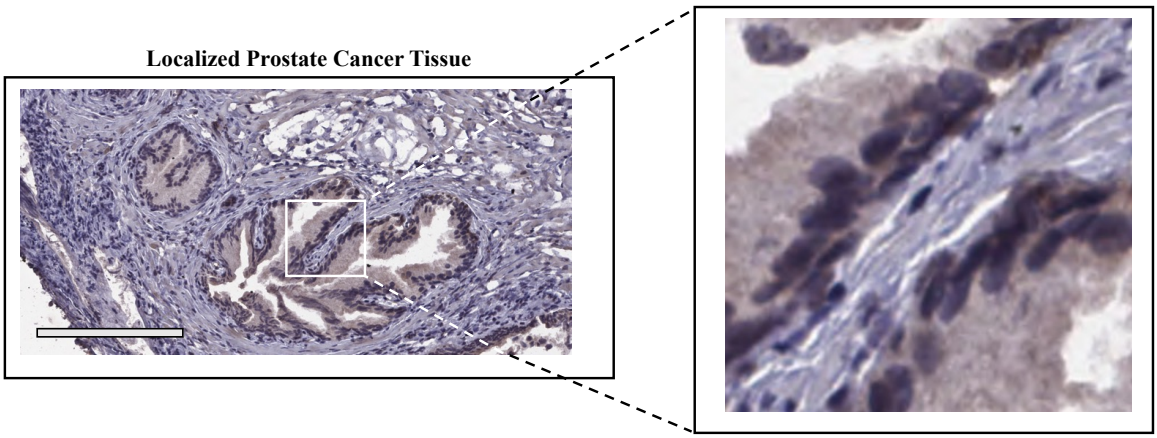

Figure 8.8. Nuclear expression of TIMP1 in localized prostate patient tissue samples. Enhanced images of IHC analysis show TIMP1 staining in cell nuclei in cancer tissue samples. Some level of nuclear staining was also observed in BPH controls. Scale bars in the bottom left corner represent 200μm.

Glypican 4 is highly expressed across all samples (*Figure 8.9*), with very dark staining in the cytoplasm of epithelial cells, basal cells and in the stroma. GPC4 is also found expressed in some nuclei in the BPH controls. The two localized prostate cancer samples differ slightly in their distribution of GPC4. The expression pattern in sample #12910 is consistent with that observed in BPH but GPC4 seems to have moved to the basal cells of the glands, as observed by a lighter staining in the cytoplasm of the epithelial cells and a darker pattern of the basal cells compared to controls. On the contrary, sample #12872 presents higher cytoplasmic expression in the remnants of the prostate glands, with a higher colocalization of GPC4 in the nucleus compared to controls samples.

8.3. Discussion

In summary, the results presented here have shown that all 4 genes of interest have conserved expression in prostate tissue samples, and both TIMP1 and GPC4 are also expressed in 3D definitive endoderm spheroids. SPARC, PLOD3, GPC4 and TIMP1 are expressed in the epithelial, basal and stromal cells in prostate tissue, indicating a wide-spread expression pattern of these proteins in different cell types. Prostate stem cells are thought to reside in the basal layer of the tissue (Taylor et al., 2010), and therefore, these results suggest that the stem cell-specific expression of all 4 proteins could be conserved between *Drosophila* and mammalian models.

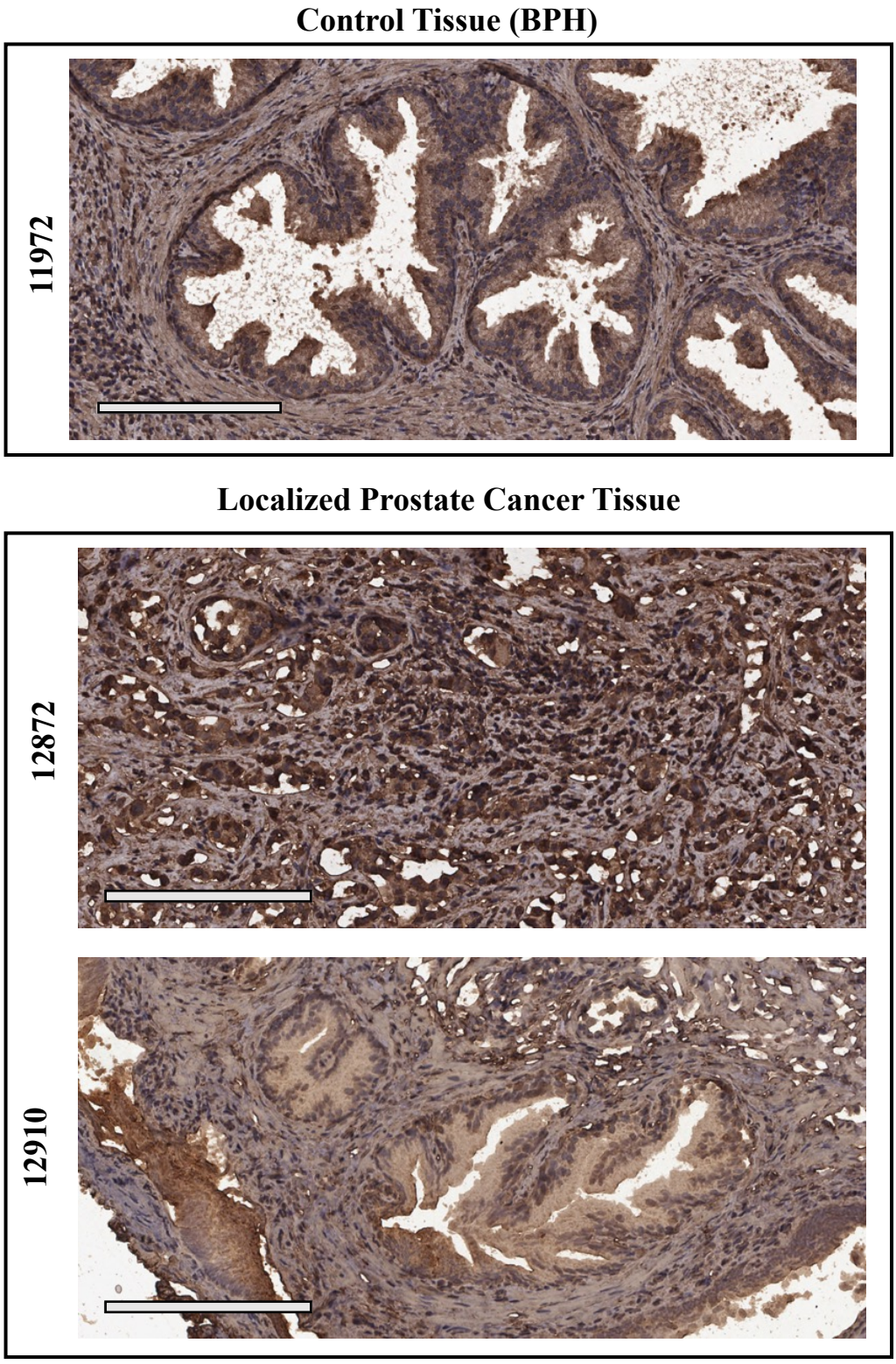

Figure 8.9. IHC analysis of glypican-4 (GPC4) expression in control and localized prostate cancer patients samples. Samples were stained with α-GPC4(1:50). Scale bars in the bottom left corner represents 200μm.

8.3.1. SPARC

Secreted protein acidic and rich in cysteine (SPARC) is a collagen-binding glycoprotein that plays important roles in the extracellular matrix (Hu et al., 2020). Both *Drosophila* and mammals present a single SPARC gene, with 30% protein sequence identity between them (Martinek et al., 2002), but the fly protein is functionally and structurally less complex than its mammalian ortholog. SPARC plays many roles within the tissue, including cell cycle control, differentiation and migration (Liu et al., 2020), but its most studied feature is its context-dependent role in tumour development, where SPARC can present oncogenic or tumour suppressor properties depending on the tissue type, the tumour characteristics and disease stage (reviewed by Ghanemi et al., 2020).

Characterization of SPARC expression in prostate tissue has revealed that this protein is found in the cytoplasm of glandular epithelial cells and in the basal cells, at moderate to low levels, with weaker staining in some stromal cells (Thomas et al., 2000). According to the Human Protein Atlas (HPA) database, SPARC is mainly found in connective tissue, i.e. the ECM, and it is enriched in the cytoplasm of fibroblasts in prostate tissue. Specifically, intracellular SPARC is found in cytoplasmic vesicles. This expression pattern was consistent in both healthy prostate tissue and in tumour samples, but elevated SPARC expression was observed in transformed cells, i.e. cells that have acquired a malignant phenotype, and in metastatic foci (Thomas et al. 2000). This expression pattern is consistent with our data, although it is worth noting that the data available in the HPA shows low or negative staining of SPARC in some prostate samples, indicating that the expression levels of SPARC in prostate tissue have high variability among patients.

The notion that SPARC localizes to the nucleus was first brought to light in 1999 by Gooden et al., where they demonstrated that SPARC was taken up into the nucleus of embryonic chicken cells, and proposed that SPARC might play similar roles in the nuclear matrix as it does in the extracellular matrix (ECM). In mouse epithelial cells, reduction of SPARC levels causes the protein to translocate to the nucleus through passive diffusion across the nuclear pores, therefore proposing the idea that SPARC is not only an extracellular protein, but that it also exists in an intracellular form that plays important roles in the maintenance of homeostasis (Yan et al., 2005). Since then, many other groups have shown expression of nuclear SPARC in a variety of cells. However, there is a gap in

the literature regarding the nuclear localization of SPARC in prostate cancer tissue, as proposed by our data.

As mentioned in Chapter 3, the function and regulation of SPARC is tissue- and context-dependent. The role of SPARC in prostate cancer, however, is well-characterized, and results across published literature are consistent in the oncogenic properties of SPARC in this tissue. DeRosa et al. showed that SPARC expression is increased in prostate cancer, where it forms a network with 12 associated genes that promote the formation of bone metastasis, thus highlighting the use of this protein as a marker of tumour aggressiveness. Increased SPARC expression in prostate cancer correlated with higher malignancy, increased invasive potential of cells and poor prognosis (Liang et al., 2010). Moreover, SPARC is enriched in endothelial cells and in some immune cells, including neutrophils, and can be found circulating in the blood (HPA).

SPARC is responsible for the regulation of markers such as E-cadherin, cytokeratin-18 and ZEB1, where their expression is inversely correlated, i.e. increased SPARC levels reduces the expression of epithelial markers in prostate tissue (López-Moncada et al., 2022). Thus, SPARC plays an important role in triggering epithelial to mesenchymal transition (EMT) in prostate cancer, and some reports have hypothesized that this is due to the SPARC-mediated triggering of the p38-MAPK signalling cascade (Wang et al., 2019). SPARC has also been proposed to regulate invasion of PCa cells through its interaction with integrin β1 (Shin et al., 2013). Recent results from a bioinformatics analysis of SPARC function in prostate cancer are consistent with published in vitro data that highlights SPARC as a useful biomarker of human prostate cancer aggressiveness (Chekhun et al., 2024).

In summary, the expression pattern of SPARC presented here correlates with that described in the literature and in online databases, and demonstrates the expression of this protein both in BPH and in localized prostate cancer. Moreover, the observations made here correlate with results presented in Chapter 3, where the SPARC expression pattern in the fly could be found through the tissue, in both the epithelial and stromal compartments.

8.3.2. PLOD3

PLOD (procollagen-lysine, 2-oxyglutarate, 5-dioxygenase) is an enzyme responsible for the post-translational modifications (PTMs) of collagen molecules (D'Aniello et al., 2021; Xu et al., 2021) with key roles in ECM deposition (Yamada et al., 2019; Zhang et al., 2021).

In mammals, the PLOD family consists of three genes: PLOD1, PLOD2 and PLOD3 (Zhang et al., 2021), whereas the fly *Drosophila melanogaster* only has one copy of the PLOD gene. The protein sequence of *Drosophila* PLOD is highly homologous to PLOD3, sharing 45% identity and 66% similarity, and both proteins have the same hydroxylase and glycotransferase activity (Bunt et al., 2011).

The expression pattern of PLOD3 presented in this chapter is consistent with that found in the HPA database, where PLOD3 localizes to the cytoplasm of the epithelial cells, as well as to some stromal cells, but in lower levels. According to the HPA database, PLOD3 is found in the cytoplasm of most tissues, as well as throughout the ECM. PLOD3 has low tissue and immune cell specificity, and, interestingly, immunoassays of PLOD3 did not detect the protein in the bloodstream.

The function of mammalian PLODs in the context of cancer has been extensively studied, and evidence in the literature demonstrates that all three mammalian PLODs carry out slightly different functions during tumour development, i.e. their functions are not fully redundant, but PLOD expression could be mutually exclusive in certain instances (Guo et al., 2021). A relationship between PLOD1 expression and prostate cancer has been established, with its overexpression correlating with poor prognosis (Ross et al., 2020), but the specific role of this molecule or PLOD2/3 in prostate tumours is yet to be elucidated. Analysis of pan-cancer data from The Cancer Genome Atlas (TCGA) by Shi et al. showed that PLOD3 expression is significantly increased in prostate adenocarcinoma compared to normal prostate tissue. Despite the significant gap in the literature regarding PLOD3 function in prostate cancer, the role of PLOD3 in the development of other epithelial cancers has been largely documented. PLOD3 is highly enriched in melanoma, and it is a prognostic biomarker in colorectal and cervical cancer, where increased PLOD3 expression correlates with poor patient survival (HPA). Similarly, PLOD3 expression increases in bladder cancer compared to normal tissue at both the mRNA and protein levels (Chen et al., 2023). Metastatic lesions of ovarian cancer present enhanced expression of PLOD2 and PLOD3, with high PLOD3 expression

correlating with worsened survival of patients (Guo et al., 2021). One key characteristic of PLOD3 is its association with gap junctions and its correlation with connexin-43 expression (Gou et al., 2021; Lyu and Feng, 2021), as well as its ability to bind to MMP-9 and remodel the ECM to facilitate migration of tumour cells (Baek et al., 2018)

In summary, the expression pattern of PLOD3 presented here correlates with that found in online databases, demonstrating this protein is present in prostate tissue. The accumulation of PLOD3 in the basal compartment of the prostate glands in BPH samples could indicate PLOD3 expression in stem cells, which correlates with the expression pattern suggested in the fly model. However, experimental limitations and a lack of evidence in published literature restrict the extent of the conclusion that can be drawn from this. In any case, PLOD expression is found in mammalian tissue and its roles in epithelial tissues correlate with those presented in Chapter 4 of this thesis, even if the evidence in prostate tissue is limited.

8.3.3. TIMP1

Tissue inhibitors of metalloproteinases (TIMPs) are important regulators of the ECM and tissue remodelling (Brew and Nagase, 2010). Besides their role as inhibitors of metalloproteinase activity, TIMPs are involved in cell migration, differentiation, and synaptic plasticity, as well as in many aspects of tumour development (Brew and Nagase, 2010).

While the *Drosophila* genome encodes a single TIMP gene (Hughes et al. 2020), mammals have 4 TIMP genes (TIMP1-4), which present 40% identity in their protein sequence (Nagase and Murphy, 2008), and extensive functional redundancy despite having independent regulatory mechanism (Murphy, 2011).

Selective TIMP1 expression has been documented in glandular cells in the prostate, according to data obtained from the HPA database. This is consistent with the observations from the IHC data presented in this chapter, although no expression in the basal or stromal cells is documented.

The role of TIMP1 in prostate cancer has been extensively studied over the last few decades. TIMP1, a negative regulator of matrix metalloproteinase-9 (MMP-9) activity (Reis et al., 2011), is expressed at low levels in the vast majority of prostate tumours (Pacheco de Moraes et al., 2021). TIMP1 is expressed at low levels in prostate cancer compared to benign prostatic hyperplasia (BPH) controls (Reis et al., 2011). In

BPH, TIMP1 is mainly found in granules in the epithelial cells, and the significant reduction in its expression has been demonstrated in prostate adenocarcinoma (Babichenko et al., 2014), as well as in an in vitro system (Dong et al., 2001). Brehmer et al. showed differential TIMP-1 expression between healthy and tumour epithelium in prostate tissue: benign prostate epithelium presented high intensity of TIMP-1 staining using IHC, whereas the tumour tissue had weak to no staining. TIMP-1 levels were also higher in the stromal cells compared to the prostate epithelium (Brehmer et al., 2003).

qRT-PCR analysis of TIMP1 expression showed that protein levels are significantly increased in BPH tissue samples when compared to LNCaP cells, indicating a significant reduction in TIMP1 in prostate cancer cells compared to healthy tissues, and suggesting a tumour suppressor role for TIMP1 in prostate cancer (Yang et al. 2021). This same study also demonstrated that TIMP1 reduces the migratory and invasive capacity of LNCaP cells (Yang et al., 2021). Loss of TIMP1 expression in prostate cancer correlates with increased aggressiveness and metastatic potential, and poor prognosis (Guccini et al., 2021). Interestingly, TIMP1 has been shown to control the senescence programme of prostate cancer cells, thus controlling the metastatic capacity of the tumour (Guccini et al., 2021). Reis et al. demonstrated that the reduction in TIMP1 expression in prostate cancer is accompanied by an increased expression of MMP-9 (Reis et al., 2011). Thus, the aggressive phenotype that has been widely associated with low TIMP1 expression in prostate tumours is not solely due to the decreased levels of the MMP inhibitor, but is rather a combination of this and the proportional increase it triggers in MMP9 activity.

No papers have described the translocation of TIMP1 to the nucleus in tumour cells, so further analysis is needed to confirm the observations made here regarding the presence of TIMP1 staining in the nuclei of localized prostate cancer tissue samples.

In summary, the expression pattern of TIMP described here in both BPH and prostate cancer samples correlates with that found in the literature: we identified TIMP1 expression in the cytoplasm of epithelial cells, as well as some expression in the surrounding stroma. However, we did not observe a difference in the intensity of staining, i.e. in the expression levels of TIMP1, between BPH and localized prostate samples, which is not consistent with published literature (Babichenko et al., 2014). Similarly to the other proteins studied here, TIMP1 is expressed in the basal cells of the tissue, where the stem cell population is thought to be located, and therefore, this suggests that the expression pattern of TIMP in the fly model is conserved in mammalian tissues. It is worth noting the limitations of this study that could account for this inconsistency: as

mentioned previously, time constraints prevented the analysis of multiple replicates for IHC, and therefore the observations described here are based on a single tissue section for each sample. Moreover, the TIMP1 antibody employed for our analysis was discontinued shortly after, preventing any comparison between this data and future analyses.

8.3.4. GPC4

Glypicans (GPCs) are members of the heparan sulfate proteoglycan (HSPG) family that are found tethered to the plasma membrane of cells through a glycosylphosphatidynositol (GPI) anchor (Filmus, 2001). Besides their expression on the cell surface, glypicans can also be found in the basement membrane of epithelial tissues and highly expressed throughout the extracellular matrix (Thota and Chignalia, 2022). In mammals, the glypican family is made up of 6 members (GPC1-6) (Filmus et al., 2008), whereas *D. melanogaster* only has two glypicans, Dally and dally-like (dlp) (Nakato et al., 2021). The mammalian orthologs for dlp are glypicans 1, 2, 4 and 6 (Filmus et al., 2008). Glypicans are important regulators of growth factor signalling, where they control the formation of morphogen gradients and thus play key roles during development (Li et al., 2020; Wang et al., 2021). Abnormal expression of the different glypican family members has been reported in multiple types of cancer and at different stages of tumour progression.

According to the HPA database, GPC-4 is found in glandular cells, in some basal cells, and in smooth muscle cells, but expression in stromal cells is significantly lower than those presented in this chapter. GPC-4 expression localizes to the plasma membrane but can also be found in the nucleoplasm of prostate cells. GPC-4 is also a favourable prognostic factor in renal and lung cancer.

In a prostate tissue context, GPC-4 is expressed in LNCaP and C4-2B cells, and its expression is increased 3-fold in PC3 cells (Murillo-Garzón et al. 2018). GPC4 is also increased in pancreatic and colorectal cancer, where it has oncogenic properties, whereas in breast and ovarian cancers, GPC4 acts as a tumour suppressor (Li et al., 2020; Munir et al., 2020; Muendlein et al. 2023). Grillo et al. showed that higher expression of GPC4 in breast cancer patients correlates with prolonged survival. However, in ER-negative breast cancer tissues, lower levels of GPC4 prolonged the remission-free survival rates of the patients (Grillo et al., 2021). These seemingly contradictory roles of GPC4 in prostate

cancer resemble the roles of dlp in the *Drosophila* gut, where the HSPG molecule acts as a morphogen that can adjust its function depending on its environment.

The main glypican associated with prostate cancer is glypican-1 (GPC-1), and its role has been widely studied. In healthy prostate tissue, GPC1 is found at low levels in epithelial cells, whereas in tumours samples epithelial expression was further decreased and accompanied by an increase in GPC-1 expression in the surrounding stroma (Suhovskih et al. 2013). This same paper demonstrated that GPC1 expression is enhanced in prostate cancer both at the mRNA and protein level. The aggressive PC3 cell line also shows increased expression of GPC-1, which promotes cell growth and migration (Quach et al., 2019). However, this glypican had the opposite effect on another prostate cancer cell line with a similar aggressive phenotype, suggesting a context- and tissue-dependent role of GPC1 in prostate tumour development (Quach et al., 2019). qRT-PCR analysis of GPC1 expression in healthy prostate tissue and BPH samples showed that no mRNA expression of GPC1 was detected in healthy prostate tissue whereas in BPH, GPC1 expression was weak and only found in 1 out of 4 cases (Suhovskih et al. 2013)

Interestingly, GPC5 has also been found in to be expressed in prostate tumours, where its expression is reduced compared to controls (Zhang et al. 2016). Here, GPC5 promotes epithelial-to-mesenchymal transition in the tumour cells by inhibiting the Wnt/Beta catenin pathway (Sun et al., 2018). GPC5 is the mammalian ortholog of the other *Drosophila* glypican, Dally (Filmus et al., 2008)

In summary, the results presented here showed very high expression of GPC4 in in epithelial cells, basal cells and in the stroma of BPH and localized prostate cancer tissue samples. Because of the overlapping and redundant roles of glypicans in tumours, and their seemingly morphogenetic properties, further in-depth analyses are needed to characterize the role of GPC4 in localized prostate cancer. The fly data presented in Chapter 6 also shows minimal changes to gut homeostasis when dlp expression levels are altered in the intestinal stem cells of the *Drosophila* gut. Taken together, these results indicate that perhaps both dlp/GPC4 have highly-specific context- and tissue-dependent roles. Thus, further studies are needed to characterize the function, expression pattern and regulation of GPC4 in localized prostate cancer.

8.4. Conclusions

In summary, the mammalian orthologs all four proteins of interest, SPARC, PLOD, dlp and TIMP are expressed in prostate tissue samples and in 3D definitive endoderm spheroid models. Moreover, the expression pattern seems to be conserved: all 4 proteins are expressed in the basal compartment of the prostate glands in tissue samples, which suggests the potential likelihood that the mammalian orthologs of the ISC-secreted proteins are also expressed in the stem cells in prostate tissue. All four proteins are also found in the stromal compartment, which is consistent with the ECM expression and ECM-related roles documented in the fly. This conserved expression pattern could suggest the conservation of their function within the tissue, but the presence of multiple mammalian orthologs for each fly proteins raises the possibility of overlapping functions in the mammalian systems. Thus, these results highlight the benefits of using *Drosophila* as a model system to study the roles and expression of these proteins in epithelial tissues, and confirms that these in vitro models are suitable for future work exploring the function of these proteins.

Chapter 9

Thesis Discussion and Future Perspectives

9.1. Summary of findings

The aim of this project was to determine if stem cell-secreted factors play key roles in the regulation of stem cell homeostasis, their potential contributions to the ISC niche, and to understand their functions to provide insight into the ISC dysregulation in disease. In order to do this, the project aimed to characterize the function, expression pattern and regulatory mechanisms of SPARC, PLOD, TIMP and dlp using Drosophila midgut ISCs as the model system. Furthermore, the characterization of their expression pattern and conservation in human intestinal tissue and in vitro mammalian models was the final aim of this PhD, to form the basis of future work.

The work presented here has demonstrated that SPARC, PLOD and TIMP play active roles in the regulation of intestinal stem cell homeostasis and the maintenance of the gut tissue, and insight into the signaling cascades the proteins are involved in has been provided. While a homeostatic role is lacking at the cellular level, it is possible that dlp does an effect in the gut tissue in specific contexts such as damage, which warrants further exploration.

SPARC has been shown to play a role in controlling the proliferation of midgut ISCs, as well as in the regulation of differentiation, as observed by an increase in EE cells when SPARC expression levels were elevated. Changes to SPARC expression in the intestinal and progenitor cells of the gut are accompanied in some cases by phenotypic changes in the gut tissue, which highlights a potential role in the maintenance of the homeostatic balance of the intestinal epithelium. The expression pattern of SPARC suggested here is not consistent with previous work that described this protein as specifically secreted by stem and progenitor cells of the tissue. Here, data shows that SPARC is expressed in a small subset of differentiated cells in the posterior midgut, but this project was not able to conclusively establish if SPARC is expressed in the absorptive enterocyte cells or the secretory enteroendocrine cells. SPARC plays key roles in collagen deposition and BM assembly in the epithelial tissue, and results presented here suggest that misregulation of SPARC could perhaps affect the actin filament network as well. SPARC has been shown to act upstream of the Ras/MAPK signaling pathway, and a potential upstream regulatory role of Notch signalling has been proposed, but the results were not robust enough to conclusively determine this.

PLOD plays an important role in the regulation of ISC homeostasis. Knocking down PLOD in the ISC and EBs in the *Drosophila* gut alters the distribution of cells in the posterior midgut, and seems to favour differentiation into EEs. The data shown here are consistent with the sequencing study (Doupé et al., 2018) that identified PLOD as an ISC/EB-specific protein, but the preliminary data obtained from use of a nuclear localization sequence tagged with GFP suggests that PLOD might also be expressed in absorptive ECs. PLOD is proposed to regulate a range of signalling pathways in the fly gut, including Ras/MAPK, TGF-β (through the SMAD proteins), and Notch, which is consistent with the data reported in the literature in other tissues and organisms.

TIMP also contributes to the maintenance of ISC homeostasis. Overexpression of TIMP in ISCs and EBs increases the number of EE cells in the posterior midgut, suggesting a role for TIMP in ISC differentiation. On the contrary, knockdown of TIMP increases proliferation in the gut epithelium and significantly reduces the lifespan of the fly, suggesting that a reduction in TIMP levels could lead to tissue hyperplasia and disrupt tissue homeostasis. Further characterization of the function, expression pattern and regulation of TIMP has proven difficult because the lack of reliable tools available for its study, but results from this project and published data suggest a role for MAPK signalling

in the regulation of TIMP in the *Drosophila* gut, but the location of the inhibitor within the signalling cascade is yet to be determined.

There is a lack of evidence to conclude dlp contributes to the ISC niche and the maintenance of homeostasis. Multiple independent knockdown and overexpression lines suggest dlp does not have a significant role in the ISCs and EBs of the posterior midgut in normal homeostasis, but despite the lack of a cellular phenotype, the data presented in this thesis suggests that dlp could act upstream of the Ras/MAPK signaling cascade.

Moreover, this project showed that the expression pattern of all four proteins was conserved in human prostate tissue samples, with expression of the mammalian orthologs of SPARC, PLOD, dlp and TIMP in the basal compartment of the tissue suggesting a potentially-conserved stem cell expression pattern in human tissues. This conservation in expression raises the possibility that the function of these proteins is also conserved between Drosophila and humans, highlighting the advantages of using the simpler Drosophila model system to study epithelial stem cell homeostasis.

Overall, this project has shown that SPARC, PLOD and TIMP may contribute to the regulation and maintenance of the ISC niche, and misregulation of their expression disrupts the intestinal epithelium in the fly. A summary of the main changes to gut morphology observed as a result of the overexpression and knockdown of the 4 genes of interests can be found in *Table 6*. The aim of this work was to provide evidence that the ISCs contribute to the regulation of their own niche, and that, although the surrounding microenvironment, ECM and other tissue cells contribute to ISC regulation, the stem cells themselves are capable of substantially contributing signals to their own niche.

9.2. Limitations and future perspectives

Any work comes with its limitations, and the work presented here is no exception. The limited number of samples available for some experiments prevented any statistical analysis to be carried out and therefore, the ability to draw conclusions from these data sets is restricted. Changes to the qRT-PCR sample preparation half-way through the project could have also translated in a small variability to the data obtained, and the quality of the dissections at early stages of the project should also be taken into account. In regards to the mammalian data shown here, time and facility access were big constraints, as shown by the single replicate for each experiment. This has bigger

implications, as the takeaways from this data set cannot be quantitatively compared to the fly model, and all observations are qualitative.

Moreover, issues beyond my control, including the temporary shut-down of the electron microscopy facility, administrative set-backs regarding the collaboration at Newcastle University, the many damages to the microscope, complications with the delivery of fly lines, and the restriction of lab access during the first 8 months of my PhD due to the Covid-19 pandemic, have had a big impact on the work presented here.

All of this has left gaps for future work to consider. The expression patterns for each protein described in this thesis provide an initial framework form which to build a clear picture of the distribution of these proteins in the intestinal tissue. The use of a specific EE cell driver, prosGal4^{TS}, was employed to understand if EE-specific manipulation of SPARC had an effect on midgut homeostasis, after some results suggested SPARC is expressed in EE cells in the tissue.

In regards to establishing a clear function and regulation of each of these proteins, the work presented here has shown the effects of knockdown and overexpression on protein expression in the gut tissue, but a lack of consistency between different knockdown lines and in comparisons between knockdown and overexpression phenotypes (*Table 6*) means additional tools required to solidify conclusions. An obvious next step would be to explore the effects of loss of function mutations in these proteins on the maintenance of homeostasis, particularly for SPARC and PLOD, which have provided the most solid evidence for future work. For example, the use of MARCM (Mosaic Analysis with a Repressible Cell Marker) would be valuable in this context, as it allows the labelling of cells derived from a common progenitor as well as the generation of homozygous mutations within these labelled cells (Lee and Luo, 2001; Wu and Luo, 2007). Moreover, the generation of functional gene knockouts, thought the use of single guide RNAs (sgRNAs) (Hiranniramol et al., 2020) would also provide additional information on protein function. These two additional approaches to manipulate gene expression would contribute to the understanding of the function and regulation of SPARC, PLOD, TIMP and dlp.

Some published data hints to the possibility that these 4 proteins, in their role in the regulation of ECM composition and mechanical properties, could be linked within the same network to regulate ISC and tissue homeostasis. Three of the proteins of interest studied as part of this project have important roles in BM formation and integrity: SPARC, PLOD and the HSPG dlp (reviewed in Isabella and Horne-Baldovinac, 2015; Pozzi et al.,

2017). Moreover, dlp can be found in a soluble form in the ECM when it is cleaved by the lipase Notum from the cell surface, raising the possibility that it has additional roles in the regulation of the ECM, much like SPARC, PLOD and TIMP. Therefore, the interplay between these four proteins in the maintenance of the ISC niche and gut homeostasis cannot be ruled out. Page-McCaw and colleagues reported that Dlp is a positive regulator of the germline stem cell niche, where proliferation is mediated by matrix metalloproteinases (Page-McCaw et al., 2014), thus suggesting the possibility that dlp and Timp act in consonance to regulate Wnt signaling and maintain its homeostatic balance in the niche. In a similar manner, SPARC and PLOD could be working in consonance to regulate collagen formation and distribution in epithelial tissues. Thus, future work should aim to characterize this further, through the generation of fly lines that allow for the the study of SPARC and PLOD expression with a collagen reporter in the background. Attempts to do this were started as part of this project, through the generation of a stable *5961GS,vkg::GFP* line, as well as a *vkg::GFP/SM6a,TIGS/TM6C* line, but the time limit prevented this from being taken further. These driver lines with the fluorescent vkg reporter could then be crossed to SPARC and PLOD overexpression and knockdown lines to directly study the effects of SPARC and PLOD manipulation on collagen.

All of this would provide a greater understanding of the roles of SPARC, PLOD, TIMP and dlp in the regulation of ISC homeostasis, their contributions to the stem cell niche and their involvement in the maintenance of tissue homeostasis. The hope is that this research can provide a solid rationale for the study of these proteins in the regulation of ISCs, for the use of Drosophila as a model to study epithelial stem cell homeostasis, and contribute to the identification of potential therapeutic targets for disease treatment, particularly for cancer development.

Table 6. Summary of results of *Drosophila* data. This table summarizes the main significant changes, presented in Chapters 3-6 of this thesis, as a results of the overexpression or knockdown of the 4 genes of interests in the ISC and EBs of the *Drosophila* midgut.

Gene of Interest	Genetic manipulation	*Drosophila* line	Total number of cells in the gut	EE cells	% EE cells/FOV	Cell Density	Number of proliferating cells
SPARC	Overexpression	77924	Decrease	Decrease	No difference	Decrease	Decrease
	Knockdown	40885	Decrease	No difference	No difference	No difference	Decrease
		16677	No difference	No difference	No difference	No difference	Increase
PLOD	Knockdown	67935	No difference	Increase	Increase	No difference	Increase
		34911	No difference	No difference	No difference	No difference	No difference
		454848	Increase	Decrease	Decrease	No difference	No difference
TIMP	Overexpression	58707	No difference	Increase	Increase	No difference	No difference
		58708	Increase	Increase	Increase	Increase	No data available
	Knockdown	61294	No difference	No difference	No difference	No difference	No difference
		15372	No difference	No difference	No difference	No difference	Increase
dlp	Overexpression	9160	No difference	No difference	No difference	No difference	No difference
	Knockdown	34089	No difference	No difference	No difference	No difference	No difference
		34091	No difference	No difference	No difference	No difference	No difference
		50540	No difference	No difference	No difference	No difference	No difference
		10299	No difference	Increase	No difference	No difference	No difference

References

Adams, M. D., Celniker, S. E., Holt, R. A., Evans, C. A., Gocayne, J. D., Amanatides, P. G., Scherer, S. E., Li, P. W., Hoskins, R. A., Galle, R. F., George, R. A., Lewis, S. E., Richards, S., Ashburner, M., Henderson, S. N., Sutton, G. G., Wortman, J. R., Yandell, M. D., Zhang, Q., Chen, L. X., … Venter, J. C. (2000). The genome sequence of Drosophila melanogaster. *Science (New York, N.Y.)*, *287*(5461), 2185–2195. https://doi.org/10.1126/science.287.5461.2185

Ahmed, A. S., Sheng, M. H., Wasnik, S., Baylink, D. J., & Lau, K. W. (2017). Effect of aging on stem cells. *World journal of experimental medicine*, *7*(1), 1–10. https://doi.org/10.5493/wjem.v7.i1.1

Akagi, K., Wilson, K. A., Katewa, S. D., Ortega, M., Simons, J., Hilsabeck, T. A., Kapuria, S., Sharma, A., Jasper, H., & Kapahi, P. (2018). Dietary restriction improves intestinal cellular fitness to enhance gut barrier function and lifespan in *D. melanogaster*. *PLoS genetics*, 14(11), e1007777. https://doi.org/10.1371/journal.pgen.1007777

Alam, R., Schultz, C. R., Golembieski, W. A., Poisson, L. M., & Rempel, S. A. (2013). PTEN suppresses SPARC-induced pMAPKAPK2 and inhibits SPARC-induced Ser78 HSP27 phosphorylation in glioma. *Neuro-oncology*, *15*(4), 451–461. https://doi.org/10.1093/neuonc/nos326

Alison, M. R., Poulsom, R., Forbes, S., & Wright, N. A. (2002). An introduction to stem cells. *The Journal of pathology*, *197*(4), 419–423. https://doi.org/10.1002/path.1187

Amcheslavsky, A., Jiang, J. and Ip, Y. T. (2009) 'Tissue Damage-Induced Intestinal Stem Cell Division in Drosophila', *Cell Stem Cell*, 4(1), pp. 49–61. doi: 10.1016/j.stem.2008.10.016.

Amcheslavsky, A., Song, W., Li, Q., Nie, Y., Bragatto, I., Ferrandon, D., Perrimon, N., & Ip, Y. T. (2014). Enteroendocrine cells support intestinal stem-cell-mediated homeostasis in Drosophila. *Cell reports*, *9*(1), 32–39. https://doi.org/10.1016/j.celrep.2014.08.052

Avellaneda, J., & Schnorrer, F. (2022). Tagging Drosophila Proteins with Genetically Encoded Fluorophores. *Methods in molecular biology (Clifton, N.J.)*, *2540*, 251–268. https://doi.org/10.1007/978-1-0716-2541-5_12

Babichenko, I. I., Andriukhin, M. I., Pulbere, S., & Loktev, A. (2014). Immunohistochemical expression of matrix metalloproteinase-9 and inhibitor of matrix metalloproteinase-1 in prostate adenocarcinoma. *International journal of clinical and experimental pathology*, *7*(12), 9090–9098.

Bach, S. P., Renehan, A. G., & Potten, C. S. (2000). Stem cells: the intestinal stem cell as a paradigm. *Carcinogenesis*, *21*(3), 469–476. https://doi.org/10.1093/carcin/21.3.469

Baeg, G. H., & Perrimon, N. (2000). Functional binding of secreted molecules to heparan sulfate proteoglycans in Drosophila. *Current opinion in cell biology*, *12*(5), 575–580. https://doi.org/10.1016/s0955-0674(00)00134-4

Baek, J. H., Yun, H. S., Kwon, G. T., Kim, J. Y., Lee, C. W., Song, J. Y., Um, H. D., Kang, C. M., Park, J. K., Kim, J. S., Kim, E. H., & Hwang, S. G. (2018). PLOD3 promotes lung metastasis via regulation of STAT3. *Cell death & disease*, *9*(12), 1138. https://doi.org/10.1038/s41419-018-1186-5

Baena-López, L. A., Rodríguez, I., & Baonza, A. (2008). The tumor suppressor genes dachsous and fat modulate different signalling pathways by regulating dally and dally-like. *Proceedings of the National Academy of Sciences of the United States of America*, *105*(28), 9645–9650. https://doi.org/10.1073/pnas.0803747105

Bankaitis, E. D., Ha, A., Kuo, C. J., & Magness, S. T. (2018). Reserve Stem Cells in Intestinal Homeostasis and Injury. *Gastroenterology*, 155(5), 1348–1361. https://doi.org/10.1053/j.gastro.2018.08.016

Barker, N., van de Wetering, M., & Clevers, H. (2008). The intestinal stem cell. *Genes & development*, *22*(14), 1856–1864. https://doi.org/10.1101/gad.1674008

Batlle, E., & Clevers, H. (2017). Cancer stem cells revisited. *Nature medicine*, 23(10), 1124–1134. https://doi.org/10.1038/nm.4409

Beaucher, M., Hersperger, E., Page-McCaw, A., & Shearn, A. (2007). Metastatic ability of Drosophila tumors depends on MMP activity. *Developmental biology*, *303*(2), 625–634. https://doi.org/10.1016/j.ydbio.2006.12.001

Beebe, K., Lee, W. C. and Micchelli, C. A. (2010) 'JAK/STAT signaling coordinates stem cell proliferation and multilineage differentiation in the Drosophila intestinal stem cell lineage', *Developmental Biology*, 338(1), pp. 28–37. doi: 10.1016/j.ydbio.2009.10.045.

Bellenghi, M., Talarico, G., Botti, L., Puglisi, R., Tabolacci, C., Portararo, P., Piva, A., Pontecorvi, G., Carè, A., Colombo, M. P., Mattia, G., & Sangaletti, S. (2022). SCD5-dependent inhibition of SPARC secretion hampers metastatic spreading and favors host immunity in a TNBC murine model. *Oncogene*, *41*(34), 4055–4065. https://doi.org/10.1038/s41388-022-02401-y

Beumer, J., & Clevers, H. (2016). Regulation and plasticity of intestinal stem cells during homeostasis and regeneration. *Development* (Cambridge, England), 143(20), 3639–3649. https://doi.org/10.1242/dev.133132

Bhoopathi, P., Chetty, C., Dontula, R., Gujrati, M., Dinh, D. H., Rao, J. S., & Lakka, S. S. (2011). SPARC stimulates neuronal differentiation of medulloblastoma cells via the Notch1/STAT3 pathway. *Cancer research*, *71*(14), 4908–4919. https://doi.org/10.1158/0008-5472.CAN-10-3395

Bianco, P., Robey, P. G. and Simmons, P. J. (2008) 'Mesenchymal Stem Cells: Revisiting History, Concepts, and Assays', *Cell Stem Cell*, 2(4), pp. 313–319. doi: 10.1016/j.stem.2008.03.002.

Biteau, B., Hochmuth, C. E., & Jasper, H. (2008). JNK activity in somatic stem cells causes loss of tissue homeostasis in the aging Drosophila gut. *Cell stem cell*, *3*(4), 442–455. https://doi.org/10.1016/j.stem.2008.07.024

Biteau, B. and Jasper, H. (2011). 'EGF signaling regulates the proliferation of intestinal stem cells in Drosophila', *Development*, 138(6), pp. 1045–1055. doi: 10.1242/dev.056671.

Biteau, B. and Jasper, H. (2014). 'Slit/Robo Signaling Regulates Cell Fate Decisions in the Intestinal Stem Cell Lineage of Drosophila', *Cell Reports*, 7(6), pp. 1867–1875. doi: 10.1016/j.celrep.2014.05.024.

Bjornson, C. R., Rietze, R. L., Reynolds, B. A., Magli, M. C., & Vescovi, A. L. (1999). Turning brain into blood: a hematopoietic fate adopted by adult neural stem cells in vivo. *Science (New York, N.Y.)*, *283*(5401), 534–537. https://doi.org/10.1126/science.283.5401.534

Böhm, J., Thavaraja, R., Giehler, S., & Nalaskowski, M. M. (2017). A set of enhanced green fluorescent protein concatemers for quantitative determination of nuclear localization signal strength. *Analytical biochemistry*, *533*, 48–55. https://doi.org/10.1016/j.ab.2017.06.015

Bongso, A. and Richards, M. (2004). 'History and perspective of stem cell research', *Best Practice and Research: Clinical Obstetrics and Gynaecology*, 18(6), pp. 827–842. doi: 10.1016/j.bpobgyn.2004.09.002.

Bornemann, D. J., Duncan, J. E., Staatz, W., Selleck, S., & Warrior, R. (2004). Abrogation of heparan sulfate synthesis in Drosophila disrupts the Wingless, Hedgehog and Decapentaplegic signaling pathways. *Development (Cambridge, England)*, *131*(9), 1927–1938. https://doi.org/10.1242/dev.01061

Bradshaw A. D. (2012). Diverse biological functions of the SPARC family of proteins. *The international journal of biochemistry & cell biology*, *44*(3), 480–488. https://doi.org/10.1016/j.biocel.2011.12.021

Brand, A. H., & Perrimon, N. (1993). Targeted gene expression as a means of altering cell fates and generating dominant phenotypes. *Development (Cambridge, England)*, *118*(2), 401–415. https://doi.org/10.1242/dev.118.2.401

Brehmer, B., Biesterfeld, S. & Jakse, G. (2003). Expression of matrix metalloproteinases (MMP-2 and -9) and their inhibitors (TIMP-1 and -2) in prostate cancer tissue. *Prostate Cancer Prostatic Dis* **6**, 217–222. https://doi.org/10.1038/sj.pcan.4500657

Brew K. (2019). Reflections on the evolution of the vertebrate tissue inhibitors of metalloproteinases. *FASEB journal : official publication of the Federation of American Societies for Experimental Biology*, *33*(1), 71–87. https://doi.org/10.1096/fj.201801262R

Brew, K., Dinakarpandian, D., & Nagase, H. (2000). Tissue inhibitors of metalloproteinases: evolution, structure and function. *Biochimica et biophysica acta*, *1477*(1-2), 267–283. https://doi.org/10.1016/s0167-4838(99)00279-4

Broadie, K., Baumgartner, S., & Prokop, A. (2011). Extracellular matrix and its receptors in Drosophila neural development. *Developmental neurobiology*, *71*(11), 1102–1130. https://doi.org/10.1002/dneu.20935

Buchon, N., Osman, D., David, F. P. A., Fang, H. Y., Boquete, J.-P., Deplancke, B., & Lemaitre, B. (2013). 'Morphological and Molecular Characterization of Adult Midgut Compartmentalization in Drosophila', *Cell Reports*, 3(5), pp. 1725–1738. doi: 10.1016/j.celrep.2013.05.019.

Buchon, N., & Osman, D. (2015). All for one and one for all: Regionalization of the Drosophila intestine. *Insect biochemistry and molecular biology*, *67*, 2–8. https://doi.org/10.1016/j.ibmb.2015.05.015

Bunt, S., Hooley, C., Hu, N., Scahill, C., Weavers, H., & Skaer, H. (2010). Hemocyte-secreted type IV collagen enhances BMP signaling to guide renal tubule morphogenesis in Drosophila. *Developmental cell*, *19*(2), 296–306. https://doi.org/10.1016/j.devcel.2010.07.019

Bunt, S., Denholm, B., & Skaer, H. (2011). Characterisation of the Drosophila procollagen lysyl hydroxylase, dPlod. *Gene expression patterns : GEP*, *11*(1-2), 72–78. https://doi.org/10.1016/j.gep.2010.09.006

Cai, C. X., Li, S. L., Lin, H. L., Wei, Z. H., Xie, L., Lin, L. R., Niu, J. J., & Yang, T. C. (2022). *Treponema pallidum* protein Tp0136 promoting MMPs/TIMPs imbalance via PI3K, MAPK and NF-κB signalling pathways in HDVSMCs. *Heliyon*, *8*(12), e12065. https://doi.org/10.1016/j.heliyon.2022.e12065

Cao, J., Ma, J., Sun, L., Li, J., Qin, T., Zhou, C., Cheng, L., Chen, K., Qian, W., Duan, W., Wang, F., Wu, E., Wang, Z., Ma, Q., & Han, L. (2018). Targeting glypican-4 overcomes 5-FU resistance and attenuates stem cell-like properties via suppression of Wnt/β-catenin pathway in pancreatic cancer cells. *Journal of cellular biochemistry*, *119*(11), 9498–9512. https://doi.org/10.1002/jcb.27266

Capo, F., Wilson, A., & Di Cara, F. (2019). The Intestine of *Drosophila melanogaster*: An Emerging Versatile Model System to Study Intestinal Epithelial Homeostasis and Host-Microbial Interactions in Humans. *Microorganisms*, *7*(9), 336. https://doi.org/10.3390/microorganisms7090336

Carriere, P., Calvo, N., Novoa Díaz, M. B., López-Moncada, F., Herrera, A., Torres, M. J., Alonso, E., Gandini, N. A., Gigola, G., Contreras, H. R., & Gentili, C. (2021). Role of SPARC in the epithelial-mesenchymal transition induced by PTHrP in human colon cancer cells. *Molecular and cellular endocrinology*, *530*, 111253. https://doi.org/10.1016/j.mce.2021.111253

Casali, A. and Batlle, E. (2009*). 'Intestinal Stem Cells in Mammals and Drosophila'*, *Cell Stem Cell*., 4(2), pp. 124–127. doi: 10.1016/j.stem.2009.01.009.

Casas-Vila, N., Bluhm, A., Sayols, S., Dinges, N., Dejung, M., Altenhein, T., Kappei, D., Altenhein, B., Roignant, J. Y., & Butter, F. (2017). The developmental proteome of *Drosophila melanogaster*. *Genome research*, *27*(7), 1273–1285. https://doi.org/10.1101/gr.213694.116

Chacón-Martínez, C. A., Koester, J., & Wickström, S. A. (2018). Signaling in the stem cell niche: regulating cell fate, function and plasticity. *Development (Cambridge, England)*, *145*(15), dev165399. https://doi.org/10.1242/dev.165399

Chakrabarti, S., Poidevin, M., & Lemaitre, B. (2014). The Drosophila MAPK p38c regulates oxidative stress and lipid homeostasis in the intestine. *PLoS genetics*, *10*(9), e1004659. https://doi.org/10.1371/journal.pgen.1004659

Chekhun, V., Borikun, T., Zadvornyi, T., Mushii, O., Stakhovsky, E., Vitruk, Y., & Lukianova, N. (2024). Osteonectin (SPARC) prognostic value in prostate cancer. *Pathology, research and practice*, *254*, 155053. https://doi.org/10.1016/j.prp.2023.155053

Chen, J., Wang, M., Xi, B., Xue, J., He, D., Zhang, J., & Zhao, Y. (2012). SPARC is a key regulator of proliferation, apoptosis and invasion in human ovarian cancer. *PloS one*, *7*(8), e42413. https://doi.org/10.1371/journal.pone.0042413

Chen, J., Xu, N., Huang, H., Cai, T., & Xi, R. (2016). 'A feedback amplification loop between stem cells and their progeny promotes tissue regeneration and tumorigenesis', *eLife*, 5, pp. 1–19. doi:10.7554/elife.14330.

Chen, J., Xu, N., Wang, C., Huang, P., Huang, H., Jin, Z., Yu, Z., Cai, T., Jiao, R., & Xi, R. (2018). Transient Scute activation via a self-stimulatory loop directs enteroendocrine cell pair specification from self-renewing intestinal stem cells. *Nature cell biology*, 20(2), 152–161. https://doi.org/10.1038/s41556-017-0020-0

Chen, R., Jiang, M., Hu, B., Fu, B., & Sun, T. (2023). Comprehensive Analysis of the Expression, Prognosis, and Biological Significance of PLOD Family in Bladder Cancer. *International journal of general medicine*, *16*, 707–722. https://doi.org/10.2147/IJGM.S399875

Chetty, C., Dontula, R., Ganji, P. N., Gujrati, M., & Lakka, S. S. (2012). SPARC expression induces cell cycle arrest via STAT3 signaling pathway in medulloblastoma cells. *Biochemical and biophysical research communications*, *417*(2), 874–879. https://doi.org/10.1016/j.bbrc.2011.12.065

Choi, N. H., Lucchetta, E. and Ohlstein, B. (2011). 'Nonautonomous regulation of Drosophila midgut stem cell proliferation by the insulin-signaling pathway', *Proceedings of the National Academy of Sciences of the United States of America*, 108(46), pp. 18702–18707. doi: 10.1073/pnas.1109348108.

Collier, J. R., Monk, N. A., Maini, P. K., & Lewis, J. H. (1996). Pattern formation by lateral inhibition with feedback: a mathematical model of delta-notch intercellular signalling. *Journal of theoretical biology*, *183*(4), 429–446. https://doi.org/10.1006/jtbi.1996.0233

Cordero, J. B., Stefanatos, R. K., Scopelliti, A., Vidal, M., & Sansom, O. J. (2012). Inducible progenitor-derived Wingless regulates adult midgut regeneration in Drosophila. *The EMBO journal*, *31*(19), 3901–3917. https://doi.org/10.1038/emboj.2012.248

D'Aniello, C., Cermola, F., Patriarca, E. J., & Minchiotti, G. (2017). Vitamin C in Stem Cell Biology: Impact on Extracellular Matrix Homeostasis and Epigenetics. *Stem cells international*, *2017*, 8936156. https://doi.org/10.1155/2017/8936156

Dear, M. L., Dani, N., Parkinson, W., Zhou, S., & Broadie, K. (2016). Two classes of matrix metalloproteinases reciprocally regulate synaptogenesis. *Development (Cambridge, England)*, *143*(1), 75–87. https://doi.org/10.1242/dev.124461

De Cat, B., & David, G. (2001). Developmental roles of the glypicans. *Seminars in cell & developmental biology*, *12*(2), 117–125. https://doi.org/10.1006/scdb.2000.0240

DeLeon-Pennell, K. Y., Barker, T. H., & Lindsey, M. L. (2020). Fibroblasts: The arbiters of extracellular matrix remodeling. *Matrix biology : journal of the International Society for Matrix Biology*, *91-92*, 1–7. https://doi.org/10.1016/j.matbio.2020.05.006

de Navascués, J., Perdigoto, C. N., Bian, Y., Schneider, M. H., Bardin, A. J., Martínez-Arias, A., & Simons, B. D. (2012). 'Drosophila midgut homeostasis involves neutral competition between symmetrically dividing intestinal stem cells', *EMBO Journal*, 31(11), pp. 2473–2485. doi: 10.1038/emboj.2012.106.

del Valle Rodríguez, A., Didiano, D., & Desplan, C. (2011). Power tools for gene expression and clonal analysis in Drosophila. *Nature methods*, *9*(1), 47–55. https://doi.org/10.1038/nmeth.1800

Desbordes, S. C., & Sanson, B. (2003). The glypican Dally-like is required for Hedgehog signalling in the embryonic epidermis of Drosophila. *Development (Cambridge, England)*, *130*(25), 6245–6255. https://doi.org/10.1242/dev.00874

Dong, Z., Nemeth, J. A., Cher, M. L., Palmer, K. C., Bright, R. C., & Fridman, R. (2001). Differential regulation of matrix metalloproteinase-9, tissue inhibitor of metalloproteinase-1 (TIMP-1) and TIMP-2 expression in co-cultures of prostate cancer and stromal cells. *International journal of cancer*, *93*(4), 507–515. https://doi.org/10.1002/ijc.1358

Doupé, D. P., Alcolea, M. P., Roshan, A., Zhang, G., Klein, A. M., Simons, B. D., & Jones, P. H. (2012). 'A single progenitor population switches behavior to maintain and repair esophageal epithelium', *Science*, 337(6098), pp. 1091–1093. doi: 10.1126/science.1218835.

Doupé, D. P., Marshall, O. J., Dayton, H., Brand, A. H., & Perrimon, N. (2018). *Drosophila* intestinal stem and progenitor cells are major sources and regulators of homeostatic niche signals. *Proceedings of the National Academy of Sciences of the United States of America*, *115*(48), 12218–12223. https://doi.org/10.1073/pnas.1719169115

Duffy J. B. (2002). GAL4 system in Drosophila: a fly geneticist's Swiss army knife. *Genesis (New York, N.Y. : 2000)*, *34*(1-2), 1–15. https://doi.org/10.1002/gene.10150

Duncan, S., Delage, S., Chioran, A., Sirbu, O., Brown, T. J., & Ringuette, M. J. (2020). The predicted collagen-binding domains of Drosophila SPARC are essential for survival and for collagen IV distribution and assembly into basement membranes. *Developmental biology*, *461*(2), 197–209. https://doi.org/10.1016/j.ydbio.2020.02.011

Dutta, D., Dobson, A. J., Houtz, P. L., Gläßer, C., Revah, J., Korzelius, J., Patel, P. H., Edgar, B. A., & Buchon, N. (2015). Regional Cell-Specific Transcriptome Mapping Reveals Regulatory Complexity in the Adult Drosophila Midgut. *Cell reports*, 12(2), 346–358. https://doi.org/10.1016/j.celrep.2015.06.009

Easwaran, S., Van Ligten, M., Kui, M., & Montell, D. J. (2022). Enhanced germline stem cell longevity in Drosophila diapause. *Nature communications*, *13*(1), 711. https://doi.org/10.1038/s41467-022-28347-z

Ehninger, A., Boch, T., Medyouf, H., Müdder, K., Orend, G., & Trumpp, A. (2014). Loss of SPARC protects hematopoietic stem cells from chemotherapy toxicity by accelerating their return to quiescence. *Blood*, *123*(26), 4054–4063. https://doi.org/10.1182/blood-2013-10-533711

Fang H.Y., Martinez-Arias A- and de Navascués J. (2016). Autocrine and paracrine Wingless signalling in the *Drosophila* midgut by both continuous gradient and asynchronous bursts of *wingless* expression, *F1000Research*, **5**:317,https://doi.org/10.12688/f1000research.8170.1

Ferraces-Riegas, P., Galbraith, A. C., & Doupé, D. P. (2022). Epithelial Stem Cells: Making, Shaping and Breaking the Niche. *Advances in experimental medicine and biology*, *1387*, 1–12. https://doi.org/10.1007/5584_2021_686

Fico, A., Maina, F., & Dono, R. (2011). Fine-tuning of cell signaling by glypicans. *Cellular and molecular life sciences : CMLS*, *68*(6), 923–929. https://doi.org/10.1007/s00018-007-7471-6

Filmus J. (2001). Glypicans in growth control and cancer. *Glycobiology*, *11*(3), 19R–23R. https://doi.org/10.1093/glycob/11.3.19r

Filmus, J., Capurro, M., & Rast, J. (2008). Glypicans. *Genome biology*, *9*(5), 224. https://doi.org/10.1186/gb-2008-9-5-224

Fischer, A., & Gessler, M. (2007). Delta-Notch--and then? Protein interactions and proposed modes of repression by Hes and Hey bHLH factors. *Nucleic acids research*, *35*(14), 4583–4596. https://doi.org/10.1093/nar/gkm477

Fonseca-Camarillo, G., Furuzawa-Carballeda, J., Razo-López, N., Barreto-Zúñiga, R., Martínez-Benítez, B., & Yamamoto-Furusho, J. K. (2021). Intestinal production of secreted protein acidic and rich in cysteine (SPARC) in patients with ulcerative colitis. *Immunobiology*, *226*(3), 152095. https://doi.org/10.1016/j.imbio.2021.152095

Foronda, D., Weng, R., Verma, P., Chen, Y. W., & Cohen, S. M. (2014). Coordination of insulin and Notch pathway activities by microRNA miR-305 mediates adaptive homeostasis in the intestinal stem cells of the Drosophila gut. *Genes & development*, *28*(21), 2421–2431. https://doi.org/10.1101/gad.241588.114

Gallet, A., Staccini-Lavenant, L., & Thérond, P. P. (2008). Cellular trafficking of the glypican Dally-like is required for full-strength Hedgehog signaling and wingless transcytosis. *Developmental cell*, *14*(5), 712–725. https://doi.org/10.1016/j.devcel.2008.03.001

Gao, Z. W., Liu, C., Yang, L., He, T., Wu, X. N., Zhang, H. Z., & Dong, K. (2021). SPARC Overexpression Promotes Liver Cancer Cell Proliferation and Tumor Growth. *Frontiers in molecular biosciences*, *8*, 775743. https://doi.org/10.3389/fmolb.2021.775743

Ghanemi, A., Yoshioka, M., & St-Amand, J. (2020). Secreted protein acidic and rich in cysteine and cancer: A homeostatic hormone?. *Cytokine*, *127*, 154996. https://doi.org/10.1016/j.cyto.2020.154996

Giráldez, A. J., Copley, R. R., & Cohen, S. M. (2002). HSPG modification by the secreted enzyme Notum shapes the Wingless morphogen gradient. *Developmental cell*, *2*(5), 667–676. https://doi.org/10.1016/s1534-5807(02)00180-6

Giudici, C., Raynal, N., Wiedemann, H., Cabral, W. A., Marini, J. C., Timpl, R., Bächinger, H. P., Farndale, R. W., Sasaki, T., & Tenni, R. (2008). Mapping of SPARC/BM-40/osteonectin-binding sites on fibrillar collagens. *The Journal of biological chemistry*, *283*(28), 19551–19560. https://doi.org/10.1074/jbc.M710001200
Godenschwege, T. A., Pohar, N., Buchner, S., & Buchner, E. (2000). Inflated wings, tissue autolysis and early death in tissue inhibitor of metalloproteinases mutants of Drosophila. *European journal of cell biology*, *79*(7), 495–501. https://doi.org/10.1078/0171-9335-00072

Golembieski, W. A., Thomas, S. L., Schultz, C. R., Yunker, C. K., McClung, H. M., Lemke, N., Cazacu, S., Barker, T., Sage, E. H., Brodie, C., & Rempel, S. A. (2008). HSP27 mediates SPARC-induced changes in glioma morphology, migration, and invasion. *Glia*, *56*(10), 1061–1075. https://doi.org/10.1002/glia.20679

Golic, K. G., & Lindquist, S. (1989). The FLP recombinase of yeast catalyzes site-specific recombination in the Drosophila genome. *Cell*, *59*(3), 499–509. https://doi.org/10.1016/0092-8674(89)90033-0

Gong, S., Schopow, N., Duan, Y., Wu, C., Kallendrusch, S., & Osterhoff, G. (2022). PLOD Family: A Novel Biomarker for Prognosis and Personalized Treatment in Soft Tissue Sarcoma. *Genes*, *13*(5), 787. https://doi.org/10.3390/genes13050787

Gong, X., Wang, A., & Song, W. (2022). Clinicopathological significances of PLOD2, epithelial-mesenchymal transition markers, and cancer stem cells in patients with esophageal squamous cell carcinoma. *Medicine*, *101*(34), e30112. https://doi.org/10.1097/MD.0000000000030112

Gooden, M. D., Vernon, R. B., Bassuk, J. A., & Sage, E. H. (1999). Cell cycle-dependent nuclear location of the matricellular protein SPARC: association with the nuclear matrix. *Journal of cellular biochemistry*, *74*(2), 152–167.

Grillo, P. K., Győrffy, B., & Götte, M. (2021). Prognostic impact of the glypican family of heparan sulfate proteoglycans on the survival of breast cancer patients. *Journal of cancer research and clinical oncology*, *147*(7), 1937–1955. https://doi.org/10.1007/s00432-021-03597-4

Guccini, I., Revandkar, A., D'Ambrosio, M., Colucci, M., Pasquini, E., Mosole, S., Troiani, M., Brina, D., Sheibani-Tezerji, R., Elia, A. R., Rinaldi, A., Pernigoni, N., Rüschoff, J. H., Dettwiler, S., De Marzo, A. M., Antonarakis, E. S., Borrelli, C., Moor, A. E., Garcia-Escudero, R., Alajati, A., … Alimonti, A. (2021). Senescence Reprogramming by TIMP1 Deficiency Promotes Prostate Cancer Metastasis. *Cancer cell*, *39*(1), 68–82.e9. https://doi.org/10.1016/j.ccell.2020.10.012

Guo, T., Gu, C., Li, B., & Xu, C. (2021). PLODs are overexpressed in ovarian cancer and are associated with gap junctions via connexin 43. *Laboratory investigation; a journal of technical methods and pathology*, *101*(5), 564–569. https://doi.org/10.1038/s41374-021-00533-5

Han, C., Belenkaya, T. Y., Wang, B., & Lin, X. (2004). Drosophila glypicans control the cell-to-cell movement of Hedgehog by a dynamin-independent process. *Development (Cambridge, England)*, *131*(3), 601–611. https://doi.org/10.1242/dev.00958

Han, C., Yan, D., Belenkaya, T. Y., & Lin, X. (2005). Drosophila glypicans Dally and Dally-like shape the extracellular Wingless morphogen gradient in the wing disc. *Development (Cambridge, England)*, *132*(4), 667–679. https://doi.org/10.1242/dev.01636

Han, H., Pan, C., Liu, C., Lv, X., Yang, X., Xiong, Y., Lu, Y., Wu, W., Han, J., Zhou, Z., Jiang, H., Zhang, L., & Zhao, Y. (2015). Gut-neuron interaction via Hh signaling regulates intestinal progenitor cell differentiation in Drosophila. *Cell discovery*, *1*, 15006. https://doi.org/10.1038/celldisc.2015.6

Hartley, P. S., Motamedchaboki, K., Bodmer, R., & Ocorr, K. (2016). SPARC-Dependent Cardiomyopathy in Drosophila. *Circulation. Cardiovascular genetics*, *9*(2), 119–129. https://doi.org/10.1161/circgenetics.115.001254

Harvey, A., Caretti, G., Moresi, V., Renzini, A., & Adamo, S. (2019). Interplay between Metabolites and the Epigenome in Regulating Embryonic and Adult Stem Cell Potency and Maintenance. *Stem cell reports*, *13*(4), 573–589. https://doi.org/10.1016/j.stemcr.2019.09.003

Hayashi, Y., Kobayashi, S., & Nakato, H. (2009). Drosophila glypicans regulate the germline stem cell niche. *The Journal of cell biology*, *187*(4), 473–480. https://doi.org/10.1083/jcb.200904118

Hepburn, A. C., Curry, E. L., Moad, M., Steele, R. E., Franco, O. E., Wilson, L., Singh, P., Buskin, A., Crawford, S. E., Gaughan, L., Mills, I. G., Hayward, S. W., Robson, C. N., & Heer, R. (2020). Propagation of human prostate tissue from induced pluripotent stem cells. *Stem cells translational medicine*, 9(7), 734–745. https://doi.org/10.1002/sctm.19-0286

Houtz, P., Bonfini, A., Liu, X., Revah, J., Guillou, A., Poidevin, M., Hens, K., Huang, H. Y., Deplancke, B., Tsai, Y. C., & Buchon, N. (2017). Hippo, TGF-β, and Src-MAPK pathways regulate transcription of the upd3 cytokine in Drosophila enterocytes upon bacterial infection. *PLoS genetics*, *13*(11), e1007091. https://doi.org/10.1371/journal.pgen.1007091

Hsu, Y. C., & Fuchs, E. (2012). A family business: stem cell progeny join the niche to regulate homeostasis. *Nature reviews. Molecular cell biology*, *13*(2), 103–114. https://doi.org/10.1038/nrm3272

Hsu, T. H., Yang, C. Y., Yeh, T. H., Huang, Y. C., Wang, T. W., & Yu, J. Y. (2017). The Hippo pathway acts downstream of the Hedgehog signaling to regulate follicle stem cell maintenance in the Drosophila ovary. *Scientific reports*, *7*(1), 4480. https://doi.org/10.1038/s41598-017-04052-6

Hu, Y., Flockhart, I., Vinayagam, A., Bergwitz, C., Berger, B., Perrimon, N., & Mohr, S. E. (2011). An integrative approach to ortholog prediction for disease-focused and other functional studies. *BMC bioinformatics*, *12*, 357. https://doi.org/10.1186/1471-2105-12-357

Hu, Y., Comjean, A., Perkins, L. A., Perrimon, N., & Mohr, S. E. (2015). GLAD: an Online Database of Gene List Annotation for Drosophila. *Journal of genomics*, *3*, 75–81. https://doi.org/10.7150/jgen.12863

Hu, J., Ma, Y., Ma, J., Chen, S., Zhang, X., Guo, S., Huang, Z., Yue, T., Yang, Y., Ning, Y., Zhu, J., Wang, P., Wang, X., Chen, G., & Liu, Y. (2020). Macrophage-derived SPARC Attenuates M2-mediated Pro-tumour Phenotypes. *Journal of Cancer*, *11*(10), 2981–2992. https://doi.org/10.7150/jca.39651

Huang, H., Li, J., Hu, L., Ge, L., Ji, H., Zhao, Y., & Zhang, L. (2014). Bantam is essential for Drosophila intestinal stem cell proliferation in response to Hippo signaling. *Developmental biology*, *385*(2), 211–219. https://doi.org/10.1016/j.ydbio.2013.11.008

Hughes, C. J. R., Turner, S., Andrews, R. M., Vitkin, A., & Jacobs, J. R. (2020). Matrix metalloproteinases regulate ECM accumulation but not larval heart growth in Drosophila melanogaster. *Journal of molecular and cellular cardiology*, *140*, 42–55. https://doi.org/10.1016/j.yjmcc.2020.02.008

Jennings, B. H. (2011). Drosophila – a versatile model in biology & medicine, Materials Today, 14(5), 190-195. https://doi.org/10.1016/S1369-7021(11)70113-4.

Jiang, H., Patel, P. H., Kohlmaier, A., Grenley, M. O., McEwen, D. G., & Edgar, B. A. (2009). Cytokine/Jak/Stat signaling mediates regeneration and homeostasis in the Drosophila midgut. *Cell*, *137*(7), 1343–1355. https://doi.org/10.1016/j.cell.2009.05.014

Jiang, H., Grenley, M. O., Bravo, M. J., Blumhagen, R. Z., & Edgar, B. A. (2011). EGFR/Ras/MAPK signaling mediates adult midgut epithelial homeostasis and regeneration in *Drosophila*. *Cell stem cell*, 8(1), 84–95. https://doi.org/10.1016/j.stem.2010.11.026

Jiang, H., & Edgar, B. A. (2009). EGFR signaling regulates the proliferation of Drosophila adult midgut progenitors. *Development* (Cambridge, England), 136(3), 483–493. https://doi.org/10.1242/dev.026955

Jiang, H. and Edgar, B. A. (2012). *'Intestinal stem cell function in Drosophila and mice'*, *Current Opinion in Genetics and Developmen*t. Elsevier Ltd, 22(4), pp. 354–360. doi: 10.1016/j.gde.2012.04.002

Jiang, H., Tian, A. & Jiang, J., (2016*).* 'Intestinal stem cell response to injury: lessons from Drosophila' *Cellular and Molecular Life Sciences*, 73(17), pp. 3337–3349. doi: 10.1007/s00018-016-2235-9.

Jiang, X., Liu, F. and Wang, Y. (2019) 'Secreted protein acidic and rich in cysteine promotes epithelial–mesenchymal transition of hepatocellular carcinoma cells and acquisition of cancerstem cell phenotypes,' *Journal of Gastroenterology and Hepatology*, 34(10), pp. 1860–1868. https://doi.org/10.1111/jgh.14692.

Jin, Y., Patel, P. H., Kohlmaier, A., Pavlovic, B., Zhang, C., & Edgar, B. A. (2017). *'Intestinal Stem Cell Pool Regulation in Drosophila'*, Stem Cell Reports. 8(6), pp. 1479–1487. doi: 10.1016/j.stemcr.2017.04.002.

John, B., Naczki, C., Patel, C., Ghoneum, A., Qasem, S., Salih, Z., & Said, N. (2019). Regulation of the bi-directional cross-talk between ovarian cancer cells and adipocytes by SPARC. *Oncogene*, *38*(22), 4366–4383. https://doi.org/10.1038/s41388-019-0728-3

Jones, P. H., & Watt, F. M. (1993). Separation of human epidermal stem cells from transit amplifying cells on the basis of differences in integrin function and expression. *Cell*, *73*(4), 713–724. https://doi.org/10.1016/0092-8674(93)90251-k

Jones, P. H., Harper, S., & Watt, F. M. (1995). Stem cell patterning and fate in human epidermis. *Cell*, *80*(1), 83–93. https://doi.org/10.1016/0092-8674(95)90453-0

Kapuria, S., Karpac, J., Biteau, B., Hwangbo, D., & Jasper, H. (2012). Notch-mediated suppression of TSC2 expression regulates cell differentiation in the Drosophila intestinal stem cell lineage. *PLoS genetics*, *8*(11), e1003045. https://doi.org/10.1371/journal.pgen.1003045

Karpowicz, P., Perez, J., & Perrimon, N. (2010). The Hippo tumor suppressor pathway regulates intestinal stem cell regeneration. *Development (Cambridge, England)*, *137*(24), 4135–4145. https://doi.org/10.1242/dev.060483

Ke, H., Feng, Z., Liu, M., Sun, T., Dai, J., Ma, M., Liu, L. P., Ni, J. Q., & Pastor-Pareja, J. C. (2018). Collagen secretion screening in Drosophila supports a common secretory machinery and multiple Rab requirements. *Journal of genetics and genomics = Yi chuan xue bao*, S1673-8527(18)30097-3. Advance online publication. https://doi.org/10.1016/j.jgg.2018.05.002

Khetan, K., Baloda, V., Sahoo, R. K., Vishnubhathla, S., Yadav, R., Saraya, A., Sharma, A., Gupta, S. D., & Das, P. (2019). SPARC expression in desmoplastic and non desmoplastic pancreatic carcinoma and cholangiocarcinoma. *Pathology, research and practice*, *215*(12), 152685. https://doi.org/10.1016/j.prp.2019.152685

Kim, W. T., & Ryu, C. J. (2017). Cancer stem cell surface markers on normal stem cells. *BMB reports*, *50*(6), 285–298. https://doi.org/10.5483/bmbrep.2017.50.6.039

Kirkpatrick, C. A., Dimitroff, B. D., Rawson, J. M., & Selleck, S. B. (2004). Spatial regulation of Wingless morphogen distribution and signaling by Dally-like protein. *Developmental cell*, *7*(4), 513–523. https://doi.org/10.1016/j.devcel.2004.08.004

Klein, A. M., & Simons, B. D. (2011). Universal patterns of stem cell fate in cycling adult tissues. *Development (Cambridge, England)*, *138*(15), 3103–3111. https://doi.org/10.1242/dev.060103

Klonisch, T., Wiechec, E., Hombach-Klonisch, S., Ande, S. R., Wesselborg, S., Schulze-Osthoff, K., & Los, M. (2008). Cancer stem cell markers in common cancers - therapeutic implications. *Trends in molecular medicine*, *14*(10), 450–460. https://doi.org/10.1016/j.molmed.2008.08.003

Knippenberg, M., Helder, M. N., Doulabi, B. Z., Bank, R. A., Wuisman, P. I., & Klein-Nulend, J. (2009). Differential effects of bone morphogenetic protein-2 and transforming growth factor-beta1 on gene expression of collagen-modifying enzymes in human adipose tissue-derived mesenchymal stem cells. *Tissue engineering. Part A*, *15*(8), 2213–2225. https://doi.org/10.1089/ten.tea.2007.0184

Köllmer, M., Buhrman, J. S., Zhang, Y., & Gemeinhart, R. A. (2013). Markers Are Shared Between Adipogenic and Osteogenic Differentiated Mesenchymal Stem Cells. *Journal of developmental biology and tissue engineering*, *5*(2), 18–25. https://doi.org/10.5897/JDBTE2013.0065

Koon, A. C., & Chan, H. Y. (2017). *Drosophila melanogaster* As a Model Organism to Study RNA Toxicity of Repeat Expansion-Associated Neurodegenerative and Neuromuscular Diseases. *Frontiers in cellular neuroscience*, *11*, 70. https://doi.org/10.3389/fncel.2017.00070

Korzelius, J., Azami, S., Ronnen-Oron, T., Koch, P., Baldauf, M., Meier, E., Rodriguez-Fernandez, I. A., Groth, M., Sousa-Victor, P., & Jasper, H. (2019). The WT1-like transcription factor Klumpfuss maintains lineage commitment of enterocyte progenitors in the Drosophila intestine. *Nature communications*, 10(1), 4123. https://doi.org/10.1038/s41467-019-12003-0

Kraushaar, D. C., Dalton, S., & Wang, L. (2013). Heparan sulfate: a key regulator of embryonic stem cell fate. *Biological chemistry*, *394*(6), 741–751. https://doi.org/10.1515/hsz-2012-0353

Kreuger, J., Perez, L., Giraldez, A. J., & Cohen, S. M. (2004). Opposing activities of Dally-like glypican at high and low levels of Wingless morphogen activity. *Developmental cell*, *7*(4), 503–512. https://doi.org/10.1016/j.devcel.2004.08.005

LaFever, K. S., Wang, X., Page-McCaw, P., Bhave, G., & Page-McCaw, A. (2017). Both Drosophila matrix metalloproteinases have released and membrane-tethered forms but have different substrates. *Scientific reports*, *7*, 44560. https://doi.org/10.1038/srep44560

Lakshmipathy, U., & Verfaillie, C. (2005). Stem cell plasticity. *Blood reviews*, *19*(1), 29–38. https://doi.org/10.1016/j.blre.2004.03.001

Laronha, H., & Caldeira, J. (2020). Structure and Function of Human Matrix Metalloproteinases. *Cells*, *9*(5), 1076. https://doi.org/10.3390/cells9051076

Lee, S. H., Park, J. S., Kim, Y. S., Chung, H. Y., & Yoo, M. A. (2012). Requirement of matrix metalloproteinase-1 for intestinal homeostasis in the adult Drosophila midgut. *Experimental cell research*, *318*(5), 670–681. https://doi.org/10.1016/j.yexcr.2012.01.004

Lee, P. T., Zirin, J., Kanca, O., Lin, W. W., Schulze, K. L., Li-Kroeger, D., Tao, R., Devereaux, C., Hu, Y., Chung, V., Fang, Y., He, Y., Pan, H., Ge, M., Zuo, Z., Housden, B. E., Mohr, S. E., Yamamoto, S., Levis, R. W., Spradling, A. C., … Bellen, H. J. (2018). A gene-specific *T2A-GAL4* library for *Drosophila*. *eLife*, *7*, e35574. https://doi.org/10.7554/eLife.35574

Lee, S. H., & Min, K. J. (2019). Drosophila melanogaster as a model system in the study of pharmacological interventions in aging. *Translational Medicine of Aging*, *3*, 98-103. https://doi.org/10.1016/j.tma.2019.09.004

Legier, T., Rattier, D., Llewellyn, J., Vannier, T., Sorre, B., Maina, F., & Dono, R. (2023). Epithelial disruption drives mesendoderm differentiation in human pluripotent stem cells by enabling TGF-β protein sensing. *Nature communications*, *14*(1), 349. https://doi.org/10.1038/s41467-023-35965-8

Leivonen, S. K., Lazaridis, K., Decock, J., Chantry, A., Edwards, D. R., & Kähäri, V. M. (2013). TGF-β-elicited induction of tissue inhibitor of metalloproteinases (TIMP)-3 expression in fibroblasts involves complex interplay between Smad3, p38α, and ERK1/2. *PloS one*, *8*(2), e57474. https://doi.org/10.1371/journal.pone.0057474

Lerner, D. W., McCoy, D., Isabella, A. J., Mahowald, A. P., Gerlach, G. F., Chaudhry, T. A., & Horne-Badovinac, S. (2013). A Rab10-dependent mechanism for polarized basement membrane secretion during organ morphogenesis. *Developmental cell*, *24*(2), 159–168. https://doi.org/10.1016/j.devcel.2012.12.005

Lewis, J. P., & Trobaugh, F. E., Jr (1964). Haematopoietic Stem Cells. *Nature*, *204*, 589–590. https://doi.org/10.1038/204589a0

Li, F., & Curry, T. E., Jr (2009). Regulation and function of tissue inhibitor of metalloproteinase (TIMP) 1 and TIMP3 in periovulatory rat granulosa cells. *Endocrinology*, *150*(8), 3903–3912. https://doi.org/10.1210/en.2008-1141

Li, H. and Jasper, H. (2016). 'Gastrointestinal stem cells in health and disease: From flies to humans', *DMM Disease Models and Mechanisms*, 9(5), pp. 487–499. doi: 10.1242/dmm.024232.

Li, L., and Xie, T. (2005). Stem cell niche: structure and function. *Annual review of cell and developmental biology*, *21*, 605–631. https://doi.org/10.1146/annurev.cellbio.21.012704.131525

Li, H., Qi, Y., & Jasper, H. (2016). Preventing Age-Related Decline of Gut Compartmentalization Limits Microbiota Dysbiosis and Extends Lifespan. *Cell host & microbe*, 19(2), 240–253. https://doi.org/10.1016/j.chom.2016.01.008

Li, S. S., Lian, Y. F., Huang, Y. L., Huang, Y. H., & Xiao, J. (2020). Overexpressing PLOD family genes predict poor prognosis in gastric cancer. *Journal of Cancer*, *11*(1), 121–131. https://doi.org/10.7150/jca.35763

Liang, J. F., Wang, H. K., Xiao, H., Li, N., Cheng, C. X., Zhao, Y. Z., Ma, Y. B., Gao, J. Z., Bai, R. B., & Zheng, H. X. (2010). Relationship and prognostic significance of SPARC and VEGF protein expression in colon cancer. *Journal of experimental & clinical cancer research : CR*, *29*(1), 71. https://doi.org/10.1186/1756-9966-29-71

Liang, Y., Häring, M., Roughley, P. J., Margolis, R. K., & Margolis, R. U. (1997). Glypican and biglycan in the nuclei of neurons and glioma cells: presence of functional nuclear localization signals and dynamic changes in glypican during the cell cycle. *The Journal of cell biology*, *139*(4), 851–864. https://doi.org/10.1083/jcb.139.4.851

Liang, J., Balachandra, S., Ngo, S., & O'Brien, L. E. (2017). Feedback regulation of steady-state epithelial turnover and organ size. *Nature*, *548*(7669), 588–591. https://doi.org/10.1038/nature23678

Lin, X., & Perrimon, N. (2000). Role of heparan sulfate proteoglycans in cell-cell signaling in Drosophila. *Matrix biology : journal of the International Society for Matrix Biology*, *19*(4), 303–307. https://doi.org/10.1016/s0945-053x(00)00073-1

Lin, G., Xu, N. & Xi, R., (2008). 'Paracrine Wingless signalling controls self-renewal of Drosophila intestinal stem cells', *Nature*, 455(7216), pp. 1119–1123. doi: 10.1038/nature07329.

Lin, G., Xu, N., & Xi, R. (2010). Paracrine unpaired signaling through the JAK/STAT pathway controls self-renewal and lineage differentiation of drosophila intestinal stem cells. *Journal of molecular cell biology*, *2*(1), 37–49. https://doi.org/10.1093/jmcb/mjp028

Lin, C. S., Xin, Z. C., Dai, J., & Lue, T. F. (2013). Commonly used mesenchymal stem cell markers and tracking labels: Limitations and challenges. *Histology and histopathology*, *28*(9), 1109–1116. https://doi.org/10.14670/HH-28.1109

Lin, G., Zhang, X., Ren, J., Pang, Z., Wang, C., Xu, N., & Xi, R. (2013). Integrin signaling is required for maintenance and proliferation of intestinal stem cells in Drosophila. *Developmental biology*, *377*(1), 177–187. https://doi.org/10.1016/j.ydbio.2013.01.032

Liu, Y., Feng, Y., Wang, X., Yang, X., Hu, Y., Li, Y., Zhang, Q., Huang, Y., Shi, K., Ran, C., Hou, J., Jiang, L., Li, J., & Wang, X. (2020). SPARC Negatively Correlates With Prognosis After Transarterial Chemoembolization and Facilitates Proliferation and Metastasis of Hepatocellular Carcinoma via ERK/MMP Signaling Pathways. *Frontiers in oncology*, *10*, 813. https://doi.org/10.3389/fonc.2020.00813

Llano, E., Adam, G., Pendás, A. M., Quesada, V., Sánchez, L. M., Santamariá, I., Noselli, S., & López-Otín, C. (2002). Structural and enzymatic characterization of Drosophila Dm2-MMP, a membrane-bound matrix metalloproteinase with tissue-specific expression. *The Journal of biological chemistry*, *277*(26), 23321–23329. https://doi.org/10.1074/jbc.M200121200

López-Moncada, F., Torres, M. J., Lavanderos, B., Cerda, O., Castellón, E. A., & Contreras, H. R. (2022). SPARC Induces E-Cadherin Repression and Enhances Cell Migration through Integrin αvβ3 and the Transcription Factor ZEB1 in Prostate Cancer Cells. *International journal of molecular sciences*, *23*(11), 5874. https://doi.org/10.3390/ijms23115874

Losick, V. P., Morris, L. X., Fox, D. T., & Spradling, A. (2011). 'Drosophila Stem Cell Niches: A Decade of Discovery Suggests a Unified View of Stem Cell Regulation', *Developmental Cell*, 21(1), pp. 159–171. doi: 10.1016/j.devcel.2011.06.018.

Lovell-Badge R. (2001). The future for stem cell research. *Nature*, *414*(6859), 88–91. https://doi.org/10.1038/35102150

Lum, L., Yao, S., Mozer, B., Rovescalli, A., Von Kessler, D., Nirenberg, M., & Beachy, P. A. (2003). Identification of Hedgehog pathway components by RNAi in Drosophila cultured cells. *Science (New York, N.Y.)*, *299*(5615), 2039–2045. https://doi.org/10.1126/science.1081403

Lyssenko, N. N., Hanna-Rose, W., & Schlegel, R. A. (2007). Cognate putative nuclear localization signal effects strong nuclear localization of a GFP reporter and facilitates gene expression studies in Caenorhabditis elegans. *BioTechniques*, *43*(5), 596–560. https://doi.org/10.2144/000112615

Lyu, Y., & Feng, C. (2021). Collagen synthesis and gap junctions: the highway for metastasis of ovarian cancer. *Laboratory investigation; a journal of technical methods and pathology*, *101*(5), 540–542. https://doi.org/10.1038/s41374-021-00546-0

Ma, J., Gao, S., Xie, X., Sun, E., Zhang, M., Zhou, Q., & Lu, C. (2017). SPARC inhibits breast cancer bone metastasis and may be a clinical therapeutic target. *Oncology letters*, *14*(5), 5876–5882. https://doi.org/10.3892/ol.2017.6925

Ma, H., Zhao, H., Liu, F., Zhao, H., Kong, R., Shi, L., Li, Z. (2019). 'Heparan sulfate negatively regulates intestinal stem cell proliferation in Drosophila adult midgut', *Biology Open*, 8(10), pp. 1–11. doi: 10.1242/bio.047126.

Ma, Y., Zhu, J., Chen, S., Ma, J., Zhang, X., Huang, S., Hu, J., Yue, T., Zhang, J., Wang, P., Wang, X., Rong, L., Guo, H., Chen, G., & Liu, Y. (2019b). Low expression of SPARC in gastric cancer-associated fibroblasts leads to stemness transformation and 5-fluorouracil resistance in gastric cancer. *Cancer cell international*, *19*, 137. https://doi.org/10.1186/s12935-019-0844-8

Maleki, M., Ghanbarvand, F., Reza Behvarz, M., Ejtemaei, M., & Ghadirkhomi, E. (2014). Comparison of mesenchymal stem cell markers in multiple human adult stem cells. *International journal of stem cells*, *7*(2), 118–126. https://doi.org/10.15283/ijsc.2014.7.2.118

Marianes, A. and Spradling, A. C. (2013). 'Physiological and stem cell compartmentalization within the Drosophila midgut', *eLife*, 2013(2), pp. 1–19. doi: 10.7554/eLife.00886.

Martin G. R. (1981). Isolation of a pluripotent cell line from early mouse embryos cultured in medium conditioned by teratocarcinoma stem cells. *Proceedings of the National Academy of Sciences of the United States of America*, *78*(12), 7634–7638. https://doi.org/10.1073/pnas.78.12.7634

Martinek, N., Zou, R., Berg, M., Sodek, J., & Ringuette, M. (2002). Evolutionary conservation and association of SPARC with the basal lamina in Drosophila. *Development genes and evolution*, *212*(3), 124–133. https://doi.org/10.1007/s00427-002-0220-9

Martinek, N., Shahab, J., Saathoff, M., & Ringuette, M. (2008). Haemocyte-derived SPARC is required for collagen-IV-dependent stability of basal laminae in Drosophila embryos. *Journal of cell science*, *121*(Pt 10), 1671–1680. https://doi.org/10.1242/jcs.021931

McCulloch, E. A., & Till, J. E. (2005). Perspectives on the properties of stem cells. *Nature medicine*, *11*(10), 1026–1028. https://doi.org/10.1038/nm1005-1026

McGuire, S. E., Mao, Z., & Davis, R. L. (2004). Spatiotemporal gene expression targeting with the TARGET and gene-switch systems in Drosophila. *Science's STKE : signal transduction knowledge environment*, *2004*(220), pl6. https://doi.org/10.1126/stke.2202004pl6

Melton, Douglas & Cowen, Chad. (2014). "Stemness": Definitions, Criteria, and Standards. E ssentials of Stem Cell Biology (Third Edition), Academic Press, 7-17. https://doi.org/10.1016/B978-0-12-409503-8.00002-0

Micchelli, C. A. and Perrimon, N. (2006). 'Evidence that stem cells reside in the adult Drosophila midgut epithelium', *Nature*, 439(7075), pp. 475–479. doi: 10.1038/nature04371.

Micchelli C. A. (2012). The origin of intestinal stem cells in Drosophila. *Developmental dynamics : an official publication of the American Association of Anatomists*, *241*(1), 85–91. https://doi.org/10.1002/dvdy.22759
Miguel-Aliaga, I., Jasper, H. & Lemaitre, B., (2018). 'Anatomy and Physiology of the Digestive Tract of Drosophila melanogaster', *Genetics*, 210(2), pp.357–396. doi: 10.1534/genetics.118.300224.

Mirzoyan, Z., Sollazzo, M., Allocca, M., Valenza, A. M., Grifoni, D., & Bellosta, P. (2019). 'Drosophila melanogaster: A model organism to study cancer', *Frontiers in Genetics*, 10, pp. 1–16. doi: 10.3389/fgene.2019.00051.

Morgan, T. H. (1910). Sex limited inheritance in Drosophila. *Science*, *32*(812), 120-122.

Morgan, T. H. (1910b). Chromosomes and heredity. *The American Naturalist*, *44*(524), 449-496.

Morgan, T. H. (1917). The theory of the gene. *The American Naturalist*, *51*(609), 513-544.

Morgner, J., Ghatak, S., Jakobi, T., Dieterich, C., Aumailley, M., & Wickström, S. A. (2015). Integrin-linked kinase regulates the niche of quiescent epidermal stem cells. *Nature communications*, *6*, 8198. https://doi.org/10.1038/ncomms9198

Morin, X., Daneman, R., Zavortink, M., & Chia, W. (2001). A protein trap strategy to detect GFP-tagged proteins expressed from their endogenous loci in Drosophila. *Proceedings of the National Academy of Sciences of the United States of America*, *98*(26), 15050–15055. https://doi.org/10.1073/pnas.261408198

Morrissey, M. A., Jayadev, R., Miley, G. R., Blebea, C. A., Chi, Q., Ihara, S., & Sherwood, D. R. (2016). SPARC Promotes Cell Invasion In Vivo by Decreasing Type IV Collagen Levels in the Basement Membrane. *PLoS genetics*, *12*(2), e1005905. https://doi.org/10.1371/journal.pgen.1005905

Muendlein, A., Heinzle, C., Brandtner, E. M., Leiherer, A., Drexel, H., Dechow, T., & Decker, T. (2023). Circulating Glypican-4 Is a Predictor of 24-Month Overall Survival in Metastatic Breast Cancer. *Oncology research and treatment*, *46*(4), 151–156. https://doi.org/10.1159/000529547

Munir, J., Van Ngu, T., Na Ayudthaya, P. D., & Ryu, S. (2020). Downregulation of glypican-4 facilitates breast cancer progression by inducing cell migration and proliferation. *Biochemical and biophysical research communications*, 526(1), 91–97. https://doi.org/10.1016/j.bbrc.2020.03.064

Murillo-Garzón, V., Gorroño-Etxebarria, I., Åkerfelt, M., Puustinen, M. C., Sistonen, L., Nees, M., Carton, J., Waxman, J., & Kypta, R. M. (2018). Frizzled-8 integrates Wnt-11 and transforming growth factor-β signaling in prostate cancer. *Nature communications*, *9*(1), 1747. https://doi.org/10.1038/s41467-018-04042-w

Murphy G. (2011). Tissue inhibitors of metalloproteinases. *Genome biology*, *12*(11), 233. https://doi.org/10.1186/gb-2011-12-11-233

Naba, A., Clauser, K. R., Ding, H., Whittaker, C. A., Carr, S. A., & Hynes, R. O. (2016). The extracellular matrix: Tools and insights for the "omics" era. *Matrix biology : journal of the International Society for Matrix Biology*, *49*, 10–24. https://doi.org/10.1016/j.matbio.2015.06.003

Nagarajan, A., Malvi, P., & Wajapeyee, N. (2018). Heparan Sulfate and Heparan Sulfate Proteoglycans in Cancer Initiation and Progression. *Frontiers in endocrinology*, *9*, 483. https://doi.org/10.3389/fendo.2018.00483

Nagase, H., & Woessner, J. F., Jr (1999). Matrix metalloproteinases. *The Journal of biological chemistry*, *274*(31), 21491–21494. https://doi.org/10.1074/jbc.274.31.21491

Nakato, E., Kamimura, K., Knudsen, C., Masutani, S., Takemura, M., Hayashi, Y., Akiyama, T., & Nakato, H. (2024). Differential heparan sulfate dependency of the Drosophila glypicans. *The Journal of biological chemistry*, *300*(1), 105544. https://doi.org/10.1016/j.jbc.2023.105544

Nászai, M., Carroll, L. R. and Cordero, J. B. (2015). 'Intestinal stem cell proliferation and epithelial homeostasis in the adult Drosophila midgut', *Insect Biochemistry and Molecular Biology,* 67, pp. 9–14. doi: 10.1016/j.ibmb.2015.05.016.

Ngo, S., Liang, J., Su, Y. H., & O'Brien, L. E. (2020). Disruption of EGF Feedback by Intestinal Tumors and Neighboring Cells in Drosophila. *Current biology : CB*, *30*(8), 1537–1546.e3. https://doi.org/10.1016/j.cub.2020.01.082

Nicastri, A., Gaspari, M., Sacco, R., Elia, L., Gabriele, C., Romano, R., Rizzuto, A., & Cuda, G. (2014). N-glycoprotein analysis discovers new up-regulated glycoproteins in colorectal cancer tissue. *Journal of proteome research*, *13*(11), 4932–4941. https://doi.org/10.1021/pr500647y

Nichols C. D. (2006). Drosophila melanogaster neurobiology, neuropharmacology, and how the fly can inform central nervous system drug discovery. *Pharmacology & therapeutics*, *112*(3), 677–700. https://doi.org/10.1016/j.pharmthera.2006.05.012

Noda, T., Yamamoto, H., Takemasa, I., Yamada, D., Uemura, M., Wada, H., Kobayashi, S., Marubashi, S., Eguchi, H., Tanemura, M., Umeshita, K., Doki, Y., Mori, M., & Nagano, H. (2012). PLOD2 induced under hypoxia is a novel prognostic factor for hepatocellular carcinoma after curative resection. *Liver international : official journal of the International Association for the Study of the Liver*, *32*(1), 110–118. https://doi.org/10.1111/j.1478-3231.2011.02619.x

Nurcombe, V., Helledie, T. & Cool, S. Regulation of embryonic stem cell fate by heparan sulfate proteoglycans. *Cell Res* **18** (Suppl 1), S53 (2008). https://doi.org/10.1038/cr.2008.143

Nybakken, K., & Perrimon, N. (2002). Heparan sulfate proteoglycan modulation of developmental signaling in Drosophila. *Biochimica et biophysica acta*, *1573*(3), 280–291. https://doi.org/10.1016/s0304-4165(02)00395-1

Ohlstein, B. and Spradling, A. (2006). 'The adult Drosophila posterior midgut is maintained by pluripotent stem cells', *Nature*, 439(7075), pp. 470–474. doi: 10.1038/nature04333.
Osterwalder, T., Yoon, K. S., White, B. H., & Keshishian, H. (2001). A conditional tissue-specific transgene expression system using inducible GAL4. *Proceedings of the National Academy of Sciences of the United States of America*, *98*(22), 12596–12601. https://doi.org/10.1073/pnas.221303298

Oszajca, K., & Szemraj, J. (2021). Assessment of the correlation between oxidative stress and expression of *MMP-2*, *TIMP-1* and *COX-2* in human aortic smooth muscle cells. *Archives of medical sciences. Atherosclerotic diseases*, *6*, e158–e165. https://doi.org/10.5114/amsad.2021.109255

Otsuki, L., & Brand, A. H. (2018). Cell cycle heterogeneity directs the timing of neural stem cell activation from quiescence. *Science (New York, N.Y.)*, *360*(6384), 99–102. https://doi.org/10.1126/science.aan8795

Pacheco de Moraes, R., Pimenta, R., Mori, F. N. C., Dos Santos, G. A., Viana, N. I., Guimarães, V. R., de Camargo, J. A., Leite, K. R. M., Srougi, M., Nahas, W. C., & Reis, S. T. (2021). Tissue expression of MMP-9, TIMP-1, RECK, and miR338-3p in prostate gland: can it predict cancer?. *Molecular biology research communications*, *10*(4), 149–156. https://doi.org/10.22099/mbrc.2021.40912.1646

Pan, L., Wang, H., Luo, J., Zeng, J., Pi, J., Liu, H., Liu, C., Ba, X., Qu, X., Xiang, Y., Boldogh, I., & Qin, X. (2019). Epigenetic regulation of TIMP1 expression by 8-oxoguanine DNA glycosylase-1 binding to DNA:RNA hybrid. *FASEB journal : official publication of the Federation of American Societies for Experimental Biology*, *33*(12), 14159–14170. https://doi.org/10.1096/fj.201900993RR

Park, J. S., Jeon, H. J., Pyo, J. H., Kim, Y. S., & Yoo, M. A. (2018). Deficiency in DNA damage response of enterocytes accelerates intestinal stem cell aging in *Drosophila*. *Aging*, *10*(3), 322–338. https://doi.org/10.18632/aging.101390

Pastor-Pareja, J. C., & Xu, T. (2011). Shaping cells and organs in Drosophila by opposing roles of fat body-secreted Collagen IV and perlecan. *Developmental cell*, *21*(2), 245–256. https://doi.org/10.1016/j.devcel.2011.06.026

Patel, P. H., & Edgar, B. A. (2014). Tissue design: how Drosophila tumors remodel their neighborhood. *Seminars in cell & developmental biology*, *28*, 86–95. https://doi.org/10.1016/j.semcdb.2014.03.012

Patel, P. H., Dutta, D., & Edgar, B. A. (2015). Niche appropriation by Drosophila intestinal stem cell tumours. *Nature cell biology*, *17*(9), 1182–1192. https://doi.org/10.1038/ncb3214

Paul, R., Dorsey, J. F., & Fan, Y. (2022). Cell plasticity, senescence, and quiescence in cancer stem cells: Biological and therapeutic implications. *Pharmacology & therapeutics*, *231*, 107985. https://doi.org/10.1016/j.pharmthera.2021.107985

Pearson, J. R., Zurita, F., Tomás-Gallardo, L., Díaz-Torres, A., Díaz de la Loza, M.del C., Franze, K., Martín-Bermudo, M. D., & González-Reyes, A. (2016). ECM-Regulator timp Is Required for Stem Cell Niche Organization and Cyst Production in the Drosophila Ovary. *PLoS genetics*, *12*(1), e1005763. https://doi.org/10.1371/journal.pgen.1005763

Peeney, D., Fan, Y., Gurung, S., Lazaroff, C., Ratnayake, S., Warner, A., Karim, B., Meerzaman, D., & Stetler-Stevenson, W. G. (2023). Whole organism profiling of the Timp gene family. *Matrix biology plus*, *18*, 100132. https://doi.org/10.1016/j.mbplus.2023.100132

Peng, D. H., Kundu, S. T., Fradette, J. J., Diao, L., Tong, P., Byers, L. A., Wang, J., Canales, J. R., Villalobos, P. A., Mino, B., Yang, Y., Minelli, R., Peoples, M. D., Bristow, C. A., Heffernan, T. P., Carugo, A., Wistuba, I. I., & Gibbons, D. L. (2019). ZEB1 suppression sensitizes KRAS mutant cancers to MEK inhibition by an IL17RD-dependent mechanism. *Science translational medicine*, *11*(483), eaaq1238. https://doi.org/10.1126/scitranslmed.aaq1238

Pérez-Oquendo, M., & Gibbons, D. L. (2022). Regulation of ZEB1 Function and Molecular Associations in Tumor Progression and Metastasis. *Cancers*, *14*(8), 1864. https://doi.org/10.3390/cancers14081864

Petersen, B. E., Bowen, W. C., Patrene, K. D., Mars, W. M., Sullivan, A. K., Murase, N., Boggs, S. S., Greenberger, J. S., & Goff, J. P. (1999). Bone marrow as a potential source of hepatic oval cells. *Science (New York, N.Y.)*, *284*(5417), 1168–1170. https://doi.org/10.1126/science.284.5417.1168

Phipps, D. N., Powell, A. M., & Ables, E. T. (2023). Utilizing the FLP-Out System for Clonal RNAi Analysis in the Adult Drosophila Ovary. *Methods in molecular biology (Clifton, N.J.)*, *2626*, 69–87. https://doi.org/10.1007/978-1-0716-2970-3_4

Poernbacher, I., Baumgartner, R., Marada, S. K., Edwards, K., & Stocker, H. (2012). Drosophila Pez acts in Hippo signaling to restrict intestinal stem cell proliferation. *Current biology : CB*, *22*(5), 389–396. https://doi.org/10.1016/j.cub.2012.01.019

Pohar, N., Godenschwege, T. A., & Buchner, E. (1999). Invertebrate tissue inhibitor of metalloproteinase: structure and nested gene organization within the synapsin locus is conserved from Drosophila to human. *Genomics*, *57*(2), 293–296. https://doi.org/10.1006/geno.1999.5776

Poirier, L., Shane, A., Zheng, J., & Seroude, L. (2008). Characterization of the Drosophila gene-switch system in aging studies: a cautionary tale. *Aging cell*, *7*(5), 758–770. https://doi.org/10.1111/j.1474-9726.2008.00421.x

Portela, M., Casas-Tinto, S., Rhiner, C., López-Gay, J. M., Domínguez, O., Soldini, D., & Moreno, E. (2010). Drosophila SPARC is a self-protective signal expressed by loser cells during cell competition. *Developmental cell*, *19*(4), 562–573. https://doi.org/10.1016/j.devcel.2010.09.004

Post, Y., & Clevers, H. (2019). Defining Adult Stem Cell Function at Its Simplest: The Ability to Replace Lost Cells through Mitosis. *Cell stem cell*, *25*(2), 174–183. https://doi.org/10.1016/j.stem.2019.07.002

Poulsom, R., Alison, M. R., Forbes, S. J., & Wright, N. A. (2002). Adult stem cell plasticity. *The Journal of pathology*, *197*(4), 441–456. https://doi.org/10.1002/path.1176

Prüßing, K., Voigt, A., & Schulz, J. B. (2013). Drosophila melanogaster as a model organism for Alzheimer's disease. *Molecular neurodegeneration*, *8*, 35. https://doi.org/10.1186/1750-1326-8-35

Qi, Y., & Xu, R. (2018). Roles of PLODs in Collagen Synthesis and Cancer Progression. *Frontiers in cell and developmental biology*, *6*, 66. https://doi.org/10.3389/fcell.2018.00066

Qiu, Q., Yang, M., Tsang, B. K., & Gruslin, A. (2004). EGF-induced trophoblast secretion of MMP-9 and TIMP-1 involves activation of both PI3K and MAPK signalling pathways. *Reproduction (Cambridge, England)*, *128*(3), 355–363. https://doi.org/10.1530/rep.1.00234

Quach, N. D., Kaur, S. P., Eggert, M. W., Ingram, L., Ghosh, D., Sheth, S., Nagy, T., Dawson, M. R., Arnold, R. D., & Cummings, B. S. (2019). Paradoxical Role of Glypican-1 in Prostate Cancer Cell and Tumor Growth. *Scientific reports*, *9*(1), 11478. https://doi.org/10.1038/s41598-019-47874-2

Ragab, A., Buechling, T., Gesellchen, V., Spirohn, K., Boettcher, A. L., & Boutros, M. (2011). Drosophila Ras/MAPK signalling regulates innate immune responses in immune and intestinal stem cells. *The EMBO journal*, *30*(6), 1123–1136. https://doi.org/10.1038/emboj.2011.4

Reis, S. T., Pontes-Junior, J., Antunes, A. A., de Sousa-Canavez, J. M., Dall'Oglio, M. F., Passerotti, C. C., Abe, D. K., Crippa, A., da Cruz, J. A., Timoszczuk, L. M., Srougi, M., & Leite, K. R. (2011). MMP-9 overexpression due to TIMP-1 and RECK underexpression is associated with prognosis in prostate cancer. *The International journal of biological markers*, *26*(4), 255–261. https://doi.org/10.5301/JBM.2011.8831

Ren, F., Wang, B., Yue, T., Yun, E. Y., Ip, Y. T., & Jiang, J. (2010). Hippo signaling regulates Drosophila intestine stem cell proliferation through multiple pathways. *Proceedings of the National Academy of Sciences of the United States of America*, *107*(49), 21064–21069. https://doi.org/10.1073/pnas.1012759107

Sakane, H., Yamamoto, H., Matsumoto, S., Sato, A., & Kikuchi, A. (2012). Localization of glypican-4 in different membrane microdomains is involved in the regulation of Wnt signaling. *Journal of cell science*, *125*(Pt 2), 449–460. https://doi.org/10.1242/jcs.091876

Sallé, J., Gervais, L., Boumard, B., Stefanutti, M., Siudeja, K., & Bardin, A. J. (2017). Intrinsic regulation of enteroendocrine fate by Numb. *The EMBO journal*, 36(13), 1928–1945. https://doi.org/10.15252/embj.201695622

Santos, A. J. M., Lo, Y. H., Mah, A. T., & Kuo, C. J. (2018). The Intestinal Stem Cell Niche: Homeostasis and Adaptations. *Trends in cell biology*, *28*(12), 1062–1078. https://doi.org/10.1016/j.tcb.2018.08.001

Scadden D. T. (2014). Nice neighborhood: emerging concepts of the stem cell niche. *Cell*, *157*(1), 41–50. https://doi.org/10.1016/j.cell.2014.02.013

Schulze-Osthoff, K., Ferrari, D., Riehemann, K., & Wesselborg, S. (1997). Regulation of NF-kappa B activation by MAP kinase cascades. *Immunobiology*, *198*(1-3), 35–49. https://doi.org/10.1016/s0171-2985(97)80025-3

Shahab, J., Baratta, C., Scuric, B., Godt, D., Venken, K. J., & Ringuette, M. J. (2015). Loss of SPARC dysregulates basal lamina assembly to disrupt larval fat body homeostasis in Drosophila melanogaster. *Developmental dynamics : an official publication of the American Association of Anatomists*, *244*(4), 540–552. https://doi.org/10.1002/dvdy.24243

Shaw, R. L., Kohlmaier, A., Polesello, C., Veelken, C., Edgar, B. A., & Tapon, N. (2011). The Hippo pathway regulates intestinal stem cell proliferation during Drosophila adult midgut regeneration. *Development (Cambridge, England)*, *137*(24), 4147–4158. https://doi.org/10.1242/dev.052506

Shi, J., Bao, M., Wang, W., Wu, X., Li, Y., Zhao, C., & Liu, W. (2021). Integrated Profiling Identifies *PLOD3* as a Potential Prognostic and Immunotherapy Relevant Biomarker in Colorectal Cancer. *Frontiers in immunology*, *12*, 722807. https://doi.org/10.3389/fimmu.2021.722807

Shilts, J., & Broadie, K. (2017). Secreted tissue inhibitor of matrix metalloproteinase restricts *trans*-synaptic signaling to coordinate synaptogenesis. *Journal of cell science*, *130*(14), 2344–2358. https://doi.org/10.1242/jcs.200808

Shiomi, T., Lemaître, V., D'Armiento, J., & Okada, Y. (2010). Matrix metalloproteinases, a disintegrin and metalloproteinases, and a disintegrin and metalloproteinases with thrombospondin motifs in non-neoplastic diseases. *Pathology international*, *60*(7), 477–496. https://doi.org/10.1111/j.1440-1827.2010.02547.x

Song, M., Liu, X., Li, T., Zhang, Y., Zhao, X., Sun, W., & Li, Z. (2022). Silencing PLOD2 attenuates cancer stem cell-like characteristics and cisplatin-resistant through Integrin β1 in laryngeal cancer. *Translational oncology*, *22*, 101460. https://doi.org/10.1016/j.tranon.2022.101460

Springer P. S. (2000). Gene traps: tools for plant development and genomics. *The Plant cell*, *12*(7), 1007–1020. https://doi.org/10.1105/tpc.12.7.1007

Staley, B. K., & Irvine, K. D. (2010). Warts and Yorkie mediate intestinal regeneration by influencing stem cell proliferation. *Current biology : CB*, *20*(17), 1580–1587. https://doi.org/10.1016/j.cub.2010.07.041

Staley, B. K., & Irvine, K. D. (2012). Hippo signaling in Drosophila: recent advances and insights. *Developmental dynamics : an official publication of the American Association of Anatomists*, *241*(1), 3–15. https://doi.org/10.1002/dvdy.22723

Stetler-Stevenson W. G. (2008). Tissue inhibitors of metalloproteinases in cell signaling: metalloproteinase-independent biological activities. *Science signaling*, *1*(27), re6. https://doi.org/10.1126/scisignal.127re6

Stewart, M. D., & Sanderson, R. D. (2014). Heparan sulfate in the nucleus and its control of cellular functions. *Matrix biology : journal of the International Society for Matrix Biology*, *35*, 56–59. https://doi.org/10.1016/j.matbio.2013.10.009

Su, T. Y., Nakato, E., Choi, P. Y., & Nakato, H. (2018). *Drosophila* Glypicans Regulate Follicle Stem Cell Maintenance and Niche Competition. *Genetics*, *209*(2), 537–549. https://doi.org/10.1534/genetics.118.300839

Suhovskih, A. V., Mostovich, L. A., Kunin, I. S., Boboev, M. M., Nepomnyashchikh, G. I., Aidagulova, S. V., & Grigorieva, E. V. (2013). Proteoglycan expression in normal human prostate tissue and prostate cancer. *ISRN oncology*, *2013*, 680136. https://doi.org/10.1155/2013/680136

Sun, T., Song, Y., Teng, D., Chen, Y., Dai, J., Ma, M., Zhang, W., & Pastor-Pareja, J. C. (2021). Atypical laminin spots and pull-generated microtubule-actin projections mediate Drosophila wing adhesion. *Cell reports*, *36*(10), 109667. https://doi.org/10.1016/j.celrep.2021.109667

Takashima, S., Mkrtchyan, M., Younossi-Hartenstein, A., Merriam, J. R., & Hartenstein, V. (2008). The behaviour of Drosophila adult hindgut stem cells is controlled by Wnt and Hh signalling. *Nature*, *454*(7204), 651–655. https://doi.org/10.1038/nature07156

Takemura, M., & Nakato, H. (2017). Drosophila Sulf1 is required for the termination of intestinal stem cell division during regeneration. *Journal of cell science*, *130*(2), 332–343. https://doi.org/10.1242/jcs.195305

Taylor, R. A., Toivanen, R., & Risbridger, G. P. (2010). Stem cells in prostate cancer: treating the root of the problem. *Endocrine-related cancer*, *17*(4), R273–R285. https://doi.org/10.1677/ERC-10-0145

Tetteh, P. W., Farin, H. F., & Clevers, H. (2015). Plasticity within stem cell hierarchies in mammalian epithelia. *Trends in cell biology*, 25(2), 100–108. https://doi.org/10.1016/j.tcb.2014.09.003

Termine, J. D., Kleinman, H. K., Whitson, S. W., Conn, K. M., McGarvey, M. L., & Martin, G. R. (1981). Osteonectin, a bone-specific protein linking mineral to collagen. *Cell*, *26*(1 Pt 1), 99–105. https://doi.org/10.1016/0092-8674(81)90037-4

Thomas, R., True, L. D., Bassuk, J. A., Lange, P. H., & Vessella, R. L. (2000). Differential expression of osteonectin/SPARC during human prostate cancer progression. *Clinical cancer research : an official journal of the American Association for Cancer Research*, *6*(3), 1140–1149.

Thomson, J. A., Itskovitz-Eldor, J., Shapiro, S. S., Waknitz, M. A., Swiergiel, J. J., Marshall, V. S., & Jones, J. M. (1998). Embryonic stem cell lines derived from human blastocysts. *Science (New York, N.Y.)*, *282*(5391), 1145–1147. https://doi.org/10.1126/science.282.5391.1145

Thota, L. N. R., & Chignalia, A. Z. (2022). The role of the glypican and syndecan families of heparan sulfate proteoglycans in cardiovascular function and disease. *American journal of physiology. Cell physiology*, *323*(4), C1052–C1060. https://doi.org/10.1152/ajpcell.00018.2022

Tian, A., Wang, B., & Jiang, J. (2017). Injury-stimulated and self-restrained BMP signaling dynamically regulates stem cell pool size during *Drosophila* midgut regeneration. *Proceedings of the National Academy of Sciences of the United States of America*, *114*(13), E2699–E2708. https://doi.org/10.1073/pnas.1617790114

Till, J. E., & McCulloch, E. A. (1980). Hemopoietic stem cell differentiation. *Biochimica et biophysica acta*, *605*(4), 431–459. https://doi.org/10.1016/0304-419x(80)90009-8

Till, J. E., Mcculloch, E. A., & Siminovitch, L. (1964). A Stochastic Model Of Stem Cell Proliferation, Based On The Growth Of Spleen Colony-Forming Cells. *Proceedings of the National Academy of Sciences of the United States of America*, *51*(1), 29–36. https://doi.org/10.1073/pnas.51.1.29

Trisnadi, N., & Stathopoulos, A. (2014). Ectopic expression screen identifies genes affecting Drosophila mesoderm development including the HSPG Trol. *G3 (Bethesda, Md.)*, *5*(2), 301–313. https://doi.org/10.1534/g3.114.015891

Uhlén, M., Fagerberg, L., Hallström, B. M., Lindskog, C., Oksvold, P., Mardinoglu, A., Sivertsson, Å., Kampf, C., Sjöstedt, E., Asplund, A., Olsson, I., Edlund, K., Lundberg, E., Navani, S., Szigyarto, C. A., Odeberg, J., Djureinovic, D., Takanen, J. O., Hober, S., Alm, T., … Pontén, F. (2015). Proteomics. Tissue-based map of the human proteome. *Science (New York, N.Y.)*, *347*(6220), 1260419. https://doi.org/10.1126/science.1260419

Uhlén, M., Zhang, C., Lee, S., Sjöstedt, E., Fagerberg, L., Bidkhori, G., Benfeitas, R., Arif, M., Liu, Z., Edfors, F., Sanli, K., von Feilitzen, K., Oksvold, P., Lundberg, E., Hober, S., Nilsson, P., Mattsson, J., Schwenk, J. M., Brunnström, H., Glimelius, B., … Ponten, F. (2017). A pathology atlas of the human cancer transcriptome. *Science (New York, N.Y.)*, *357*(6352), eaan2507. https://doi.org/10.1126/science.aan2507

Uhlirova, M., & Bohmann, D. (2006). JNK- and Fos-regulated Mmp1 expression cooperates with Ras to induce invasive tumors in Drosophila. *The EMBO journal*, *25*(22), 5294–5304. https://doi.org/10.1038/sj.emboj.7601401

Urbano, J. M., Torgler, C. N., Molnar, C., Tepass, U., López-Varea, A., Brown, N. H., de Celis, J. F., & Martín-Bermudo, M. D. (2009). Drosophila laminins act as key regulators of basement membrane assembly and morphogenesis. *Development (Cambridge, England)*, *136*(24), 4165–4176. https://doi.org/10.1242/dev.044263

Vaughan, L., Marley, R., Miellet, S., & Hartley, P. S. (2018). The impact of SPARC on age-related cardiac dysfunction and fibrosis in Drosophila. *Experimental gerontology*, *109*, 59–66. https://doi.org/10.1016/j.exger.2017.10.011

Vaz, J., Ansari, D., Sasor, A., & Andersson, R. (2015). SPARC: A Potential Prognostic and Therapeutic Target in Pancreatic Cancer. *Pancreas*, *44*(7), 1024–1035. https://doi.org/10.1097/MPA.0000000000000409

Visse, R., & Nagase, H. (2003). Matrix metalloproteinases and tissue inhibitors of metalloproteinases: structure, function, and biochemistry. *Circulation research*, *92*(8), 827–839. https://doi.org/10.1161/01.RES.0000070112.80711.3D

Wang, M. C., Bohmann, D., & Jasper, H. (2003). JNK signaling confers tolerance to oxidative stress and extends lifespan in Drosophila. *Developmental cell*, *5*(5), 811–816. https://doi.org/10.1016/s1534-5807(03)00323-x

Wang, C., Zhao, R., Huang, P., Yang, F., Quan, Z., Xu, N., & Xi, R. (2013). APC loss-induced intestinal tumorigenesis in Drosophila: Roles of Ras in Wnt signaling activation and tumor progression. *Developmental biology*, *378*(2), 122–140. https://doi.org/10.1016/j.ydbio.2013.03.020

Wang, X. and Page-McCaw, A. (2014). 'A matrix metalloproteinase mediates long-distance attenuation of stem cell proliferation', *Journal of Cell Biology*, 206(7), pp. 923–936. doi: 10.1083/jcb.201403084.

Wang, Q., Yang, Q., Zhang, A., Kang, Z., Wang, Y., & Zhang, Z. (2019). Silencing of SPARC represses heterotopic ossification via inhibition of the MAPK signaling pathway. *Bioscience reports*, *39*(11), BSR20191805. https://doi.org/10.1042/BSR20191805

Wang, J. Y., Wang, X. K., Zhu, G. Z., Zhou, X., Yao, J., Ma, X. P., Wang, B., & Peng, T. (2021). Distinct diagnostic and prognostic values of Glypicans gene expression in patients with hepatocellular carcinoma. *BMC cancer*, *21*(1), 462. https://doi.org/10.1186/s12885-021-08104-z

Watt F. M. (1998). Epidermal stem cells: markers, patterning and the control of stem cell fate. *Philosophical transactions of the Royal Society of London. Series B, Biological sciences*, *353*(1370), 831–837. https://doi.org/10.1098/rstb.1998.0247

Wei, S., Xie, Z., Filenova, E., & Brew, K. (2003). Drosophila TIMP is a potent inhibitor of MMPs and TACE: similarities in structure and function to TIMP-3. *Biochemistry*, *42*(42), 12200–12207. https://doi.org/10.1021/bi035358x

Wen, D., Chen, Z., Zhang, Z., & Jia, Q. (2020). The expression, purification, and substrate analysis of matrix metalloproteinases in Drosophila melanogaster. *Protein expression and purification*, *171*, 105629. https://doi.org/10.1016/j.pep.2020.105629

Williams, E. H., Pappano, W. N., Saunders, A. M., Kim, M. S., Leahy, D. J., & Beachy, P. A. (2010). Dally-like core protein and its mammalian homologues mediate stimulatory and inhibitory effects on Hedgehog signal response. *Proceedings of the National Academy of Sciences of the United States of America*, *107*(13), 5869–5874. https://doi.org/10.1073/pnas.1001777107

Wilmut, I., Schnieke, A. E., McWhir, J., Kind, A. J., & Campbell, K. H. (1997). Viable offspring derived from fetal and adult mammalian cells. *Nature*, *385*(6619), 810–813. https://doi.org/10.1038/385810a0

Winkler, J., Abisoye-Ogunniyan, A., Metcalf, K.J. *et al.* (2020). Concepts of extracellular matrix remodelling in tumour progression and metastasis. *Nature Communications,* 11, 5120. https://doi.org/10.1038/s41467-020-18794-x

Xiang, J., Bandura, J., Zhang, P., Jin, Y., Reuter, H., & Edgar, B. A. (2017). EGFR-dependent TOR-independent endocycles support Drosophila gut epithelial regeneration. *Nature communications*, *8*, 15125. https://doi.org/10.1038/ncomms15125

Xie, Y., Kuan, A. T., Wang, W., Herbert, Z. T., Mosto, O., Olukoya, O., Adam, M., Vu, S., Kim, M., Tran, D., Gómez, N., Charpentier, C., Sorour, I., Lacey, T. E., Tolstorukov, M. Y., Sabatini, B. L., Lee, W. A., & Harwell, C. C. (2022). Astrocyte-neuron crosstalk through Hedgehog signaling mediates cortical synapse development. *Cell reports*, *38*(8), 110416. https://doi.org/10.1016/j.celrep.2022.110416

Xu, N., Wang, S. Q., Tan, D., Gao, Y., Lin, G., & Xi, R. (2011). EGFR, Wingless and JAK/STAT signaling cooperatively maintain Drosophila intestinal stem cells. *Developmental biology*, *354*(1), 31–43. https://doi.org/10.1016/j.ydbio.2011.03.018

Xu, M., Fang, S., & Xie, A. (2021). Posttranscriptional control of *PLOD1* in adipose-derived stem cells regulates scar formation through altering macrophage polarization. *Annals of translational medicine*, *9*(20), 1573. https://doi.org/10.21037/atm-21-4978

Yamada, Y., Kato, M., Arai, T., Sanada, H., Uchida, A., Misono, S., Sakamoto, S., Komiya, A., Ichikawa, T., & Seki, N. (2019). Aberrantly expressed PLOD1 promotes cancer aggressiveness in bladder cancer: a potential prognostic marker and therapeutic target. *Molecular oncology*, *13*(9), 1898–1912. https://doi.org/10.1002/1878-0261.12532

Yamashita, Y. M., Fuller, M. T., & Jones, D. L. (2005). Signaling in stem cell niches: lessons from the Drosophila germline. *Journal of cell science*, *118*(Pt 4), 665–672. https://doi.org/10.1242/jcs.01680

Yan, Q., Weaver, M., Perdue, N., & Sage, E. H. (2005). Matricellular protein SPARC is translocated to the nuclei of immortalized murine lens epithelial cells. *Journal of cellular physiology*, *203*(1), 286–294. https://doi.org/10.1002/jcp.20226

Yan, D., Wu, Y., Feng, Y., Lin, S. C., & Lin, X. (2009). The core protein of glypican Dally-like determines its biphasic activity in wingless morphogen signaling. *Developmental cell*, *17*(4), 470–481. https://doi.org/10.1016/j.devcel.2009.09.001

Yan, D., Wu, Y., Yang, Y., Belenkaya, T. Y., Tang, X., & Lin, X. (2010). The cell-surface proteins Dally-like and Ihog differentially regulate Hedgehog signaling strength and range during development. *Development (Cambridge, England)*, *137*(12), 2033–2044. https://doi.org/10.1242/dev.045740

Yang, B., Zhao, Y., Wang, L., Zhao, Y., Wei, L., Chen, D., & Chen, Z. (2020). Identification of PLOD Family Genes as Novel Prognostic Biomarkers for Hepatocellular Carcinoma. *Frontiers in oncology*, *10*, 1695. https://doi.org/10.3389/fonc.2020.01695

Yang, Y., Feng, Q., Hu, K., & Cheng, F. (2021). Using CRISPRa and CRISPRi Technologies to Study the Biological Functions of ITGB5, TIMP1, and TMEM176B in Prostate Cancer Cells. *Frontiers in molecular biosciences*, *8*, 676021. https://doi.org/10.3389/fmolb.2021.676021

You, J. (2013) Functions of Heparan Sulfate Proteoglycans in Cell Signaling and Stem Cell Regulation during *Drosophila* Development. UMI Number: 3613401.

Zeng, X., & Hou, S. X. (2015). Enteroendocrine cells are generated from stem cells through a distinct progenitor in the adult Drosophila posterior midgut. *Development (Cambridge, England)*, *142*(4), 644–653. https://doi.org/10.1242/dev.113357

Zeng, X., Han, L., Singh, S. R., Liu, H., Neumüller, R. A., Yan, D., Hou, S. X. (2016). 'Genome-wide RNAi Screen Identifies Networks Involved in Intestinal Stem Cell Regulation in Drosophila', *Cell Reports*, 10(7), pp. 1226–1238. doi: 10.1016/j.celrep.2015.01.051.

Zhang, W., Thompson, B. J., Hietakangas, V., & Cohen, S. M. (2011). MAPK/ERK signaling regulates insulin sensitivity to control glucose metabolism in Drosophila. *PLoS genetics*, *7*(12), e1002429. https://doi.org/10.1371/journal.pgen.1002429

Zhang, Y., You, J., Ren, W., & Lin, X. (2013). Drosophila glypicans Dally and Dally-like are essential regulators for JAK/STAT signaling and Unpaired distribution in eye development. *Developmental biology*, *375*(1), 23–32. https://doi.org/10.1016/j.ydbio.2012.12.019

Zhang, C., Liu, Z., Wang, L., Qiao, B., Du, E., Li, L., Xu, Y., & Zhang, Z. (2016). Prognostic significance of GPC5 expression in patients with prostate cancer. *Tumour biology : the journal of the International Society for Oncodevelopmental Biology and Medicine*, *37*(5), 6413–6418. https://doi.org/10.1007/s13277-015-4499-3

Zhang, J., Tian, Y., Mo, S., & Fu, X. (2021). Overexpressing PLOD Family Genes Predict Poor Prognosis in Pancreatic Cancer. *International journal of general medicine*, *15*, 3077–3096. https://doi.org/10.2147/IJGM.S341332

Zhao, W., Ji, X., Zhang, F., Li, L., & Ma, L. (2012). Embryonic stem cell markers. *Molecules (Basel, Switzerland)*, *17*(6), 6196–6236. https://doi.org/10.3390/molecules17066196

Zhong, M. E., Chen, Y., Xiao, Y., Xu, L., Zhang, G., Lu, J., Qiu, H., Ge, W., & Wu, B. (2019). Serum extracellular vesicles contain SPARC and LRG1 as biomarkers of colon cancer and differ by tumour primary location. *EBioMedicine*, *50*, 211–223. https://doi.org/10.1016/j.ebiom.2019.11.003

Zhou, F., Rasmussen, A., Lee, S., & Agaisse, H. (2013). The UPD3 cytokine couples environmental challenge and intestinal stem cell division through modulation of JAK/STAT signaling in the stem cell microenvironment. *Developmental biology*, *373*(2), 383–393. https://doi.org/10.1016/j.ydbio.2012.10.023

Zhu, A., Yuan, P., Du, F., Hong, R., Ding, X., Shi, X., Fan, Y., Wang, J., Luo, Y., Ma, F., Zhang, P., Li, Q., & Xu, B. (2016). SPARC overexpression in primary tumors correlates with disease recurrence and overall survival in patients with triple negative breast cancer. *Oncotarget*, *7*(47), 76628–76634. https://doi.org/10.18632/oncotarget.10532

Zhu, J., Wang, L. Y., Li, C. Y., Wu, J. Y., Zhang, Y. T., Pang, K. P., Wei, Y., Du, L. Q., Liu, M., & Wu, X. Y. (2020). SPARC promotes self-renewal of limbal epithelial stem cells and ocular surface restoration through JNK and p38-MAPK signaling pathways. *Stem cells (Dayton, Ohio)*, *38*(1), 134–145. https://doi.org/10.1002/stem.3100